



**University of Liège**

Faculty of Sciences

Department of Life Sciences

Laboratory of Genetics and Physiology of Microalgae

**Vrije Universiteit Brussels**

Faculty of Sciences and Bioengineering Sciences

Department of Bioengineering Sciences

Research group Structural Biology Brussels

The role of ascorbate peroxidase 2 and protein cysteine  
modifications in the green alga *Chlamydomonas reinhardtii*

Thesis submitted in fulfilment of the requirements for the award of the degree of  
Doctor of Science and Doctor of Bioengineering Sciences

**Anna Caccamo**

Promoters: Prof. Dr. Claire Remacle and Prof. Dr. Joris Messens

Academic year 2023-2024

Alle rechten voorbehouden. Niets van deze uitgave mag worden vermenigvuldigd en/of openbaar gemaakt worden door middel van druk, fotokopie, microfilm, elektronisch of op welke andere wijze ook, zonder voorafgaande schriftelijke toestemming van de auteur.

All rights reserved. No part of this publication may be produced in any form by print, photoprint, microfilm, electronic or any other means without permission from the author.

Printed by  
Crazy Copy Center Productions  
VUB Pleinlaan 2, 1050 Brussel  
Tel : +32 2 629 33 44  
crazycopy@vub.be  
www.crazycopy.be

ISBN: 9789464948073  
NUR CODE: 923  
THEMA: PS

# Examination board

## **Chairman/Président/Voorzitter**

- Prof. Dr. Marc Hanikenne  
Faculty of Sciences  
Department of Life Sciences  
Translational Plant Biology  
Integrative Biological Sciences (InBioS)  
Université de Liège

## **Secretary/Secrétaire/Secretaris**

- Prof. Dr. ir. Geert Angenon  
Faculty of Sciences and Bioengineering Sciences  
Department of Bioengineering Sciences  
Plant Genetics Laboratory  
Vrije Universiteit Brussel

## **ULiège jury member**

- Dr. Frédéric Kerff  
Faculty of Sciences  
Department of Life Sciences  
Center for Protein Engineering (CIP)  
Faculty of Sciences  
Department of Chemistry (Sciences)  
Integrative Biological Sciences (InBioS)

## **VUB jury member**

- Prof. Dr. Joske Ruytinx  
Faculty of Sciences and Bioengineering Sciences  
Department of Bioengineering Sciences  
Microbiology research group  
Vrije Universiteit Brussel

## **External jury members**

- Dr. Didier Vertommen  
de Duve Institute  
Université Catholique de Louvain

- Prof. Dr. Michael Hippler  
WWU Münster  
Institute of Plant Biotechnology and Biology  
Plant Biochemistry and Biotechnology  
Universität Münster

## **Promoters**

- Prof. Dr. Claire Remacle  
Faculty of Sciences  
Department of Life Sciences  
Genetic and Physiology of Microalgae  
Integrative Biological Sciences (InBioS)  
Université de Liège

- Prof. Dr. Joris Messens  
Faculty of Sciences and Bioengineering Sciences  
Department of Bioengineering Sciences  
Structural Biology Brussels research group  
Redox Signaling Laboratory  
Vrije Universiteit Brussel



This work was funded by Fonds de la Recherche Scientifique—the Research Foundation Flanders—Excellence of Science project No. 30829584 – ReACTs - Retrograde Arabidopsis Chlamydomonas Thiol signaling. It was conducted under the supervision of Prof. Dr. Claire REMACLE at the Laboratory of Genetics and Physiology of Microalgae, Institute of Botany, University of Liège, Belgium and Prof. Dr. Joris MESSENS, at The Redox Signaling lab, VIB-VUB Center for Structural Biology, Vrije Universiteit Brussel, Belgium.

# List of publications

1. Patrice P. Hamel, Thalia Salinas-Giegé, Jonathan Przybyla-Toscano, **Anna Caccamo**, Nitya Subrahmanian, Nicolas Rouhier, Laurence Drouard, Pierre Cardol, Diego Gonzalez-Halphen, Claire Remacle. (2022) Chlamydomonas Sourcebook, volume 2, “Organellar and Metabolic Processes”, the mitochondrion: from genome to proteome (Chapter 11), editors Francis-André Wollman and Arthur Grossman, Elsevier
2. **Anna Caccamo**, Félix Vega de Luna, Khadija Wahni, Alexander N. Volkov, Jonathan Przybyla-Toscano, Antonello Amelii, Alexandre Kriznik, Nicolas Rouhier, Joris Messens and Claire Remacle. (2023) Ascorbate peroxidase 2 (APX2) of Chlamydomonas binds copper and modulates the copper insertion into plastocyanin. *Antioxidants*. 12, 1946. <https://doi.org/10.3390/antiox12111946>
3. **Anna Caccamo**, Félix Vega de Luna, Agnieszka E. Misztak, Sébastien Pyr dit Ruyt, Didier Vertommen, Pierre Cardol, Joris Messens, Claire Remacle. (2023) APX2, the ascorbate peroxidase-related protein, regulates the levels of plastocyanin in Chlamydomonas. *Plant Cell Physiol.* in revision

## Summary

H<sub>2</sub>O<sub>2</sub>, a reactive oxygen species (ROS), is known for causing oxidative damage during stress. However, it is now recognized as a signaling molecule, particularly in modifying protein cysteine residues, leading to cysteine sulfenylation in specific proteins. Cellular signaling can be anterograde, driven by the nucleus to other organelles such as chloroplast or mitochondria in the photosynthetic organisms, or retrograde, directed backwards from the organelles to the nucleus. Organisms that undergo photosynthesis, such as cyanobacteria, algae, and plants, primarily produce H<sub>2</sub>O<sub>2</sub> in the chloroplasts during photosynthesis and in the mitochondria during respiration.

In this study, we used the green alga *Chlamydomonas reinhardtii*. Specifically, our attention was directed towards the H<sub>2</sub>O<sub>2</sub>-scavenging enzyme ascorbate peroxidase 2 (APX2), recently classified as ascorbate peroxidase-related (APX-R), of which the function remains unclear. We investigated the cellular role of APX2 and we identified modified cysteines in their sulfenylated form (-SOH) in *Chlamydomonas* under oxidative stress.

With an explorative screening of mutants through molecular and genetic methods, employing <sup>1</sup>H-NMR, activity assays, and biophysical techniques with recombinantly expressed and purified APX2 and plastocyanin proteins, and utilizing structure predictions, we discovered that APX2 is most probably localized in the lumen of the chloroplasts and has an impact on plastocyanin. APX2, distinct from typical H<sub>2</sub>O<sub>2</sub> scavengers, also exhibited next to peroxidase activity copper binding in a typical metal binding MxxM sequence motif and is involved in regulating the cellular plastocyanin levels.

Through the refinement of a mass spectrometric sulfenome analysis technique applied to protein extracts from *Chlamydomonas* wild type with and without oxidative stress, we successfully pinpointed one sulfenylated peptide associated with three light-harvesting complexes of photosystem II and one sulfenylated peptide associated with the ATP/ADP carrier protein AAA1. This discovery serves as an initial indication that the regulation of these complexes and of the AAA1 carrier protein involves the modification of a cysteine residue.

All in all, our findings reveal a novel function for APX2 and offer insights into sulfenylation patterns in *Chlamydomonas*.

## Résumé

Le peroxyde d'hydrogène ( $H_2O_2$ ) est une espèce réactive de l'oxygène qui cause des dommages liés au stress oxydatif. Cette molécule est aussi impliquée dans les voies de signalisation car elle modifie les résidus cystéine de certaines protéines, en les sulfénylant. Les organismes photosynthétiques comme les cyanobactéries, les algues et les plantes produisent de l' $H_2O_2$  dans les chloroplastes lors de la photosynthèse et dans les mitochondries lors de la respiration.

Dans notre étude, nous avons utilisé la microalgue verte modèle *Chlamydomonas reinhardtii*. Nous avons d'une part analysé le rôle d'une ascorbate peroxydase de type R ('ascorbate-related protein'), APX2, et d'autre part identifié des protéines présentant des résidus cystéine sulfénylés. Concernant APX2, nous avons démontré que la protéine est chloroplastique et probablement adressée dans le lumen des thylacoïdes. Des mutants *apx2* déficients pour la protéine montrent un niveau réduit de plastocyanine, la protéine à cuivre majeure au sein du lumen des chloroplastes. Nous avons purifié la protéine recombinante à partir de *E. coli*. Nous avons démontré qu'elle n'utilise pas l'ascorbate pour réduire le  $H_2O_2$  en  $H_2O$ , ce qui valide son appartenance à la classe R des ascorbate peroxydases. De plus, cette enzyme lie le cuivre probablement grâce à la présence d'un motif de liaison aux métaux (MxxM). Nous avons également analysé l'interaction entre la plastocyanine et APX2 en utilisant des approches de  $^1H$ -NMR et proposé que APX2 occuperait un site proche de celui de l'insertion du cuivre au sein de la plastocyanine.

Nous avons établi un protocole de détection des peptides sulfénylés pour *Chlamydomonas* et avons identifié quelques protéines répondant au stress  $H_2O_2$  par la sulfénylation de résidus cystéine (protéines LHCII du système collecteur d'énergie du photosystème II et de l'ADP/ATP translocase chloroplastique).

En résumé, notre travail a révélé une nouvelle fonction pour la protéine APX2 de *Chlamydomonas* et apporté les premiers résultats concernant l'établissement du sulfénome de l'algue.



## Samenvatting

H<sub>2</sub>O<sub>2</sub>, een reactieve zuurstofsoort (ROS), staat erom bekend oxidatieve schade te veroorzaken bij stress, maar wordt nu ook erkend als signaalmolecuul voor het modificeren van cysteïnes in eiwitten, ook gekend als cysteïne-sulfenylatie. Cellulaire signaaloverdracht kan anterograad plaatsvinden, een signaal wordt dan door de kern naar andere organellen gestuurd zoals de chloroplasten of mitochondriën in fotosynthetische organismen, of retrograad, een signaal van de organellen gaat terug naar de kern. Organismen die aan fotosynthese doen, zoals cyanobacteriën, algen en planten, produceren H<sub>2</sub>O<sub>2</sub> voornamelijk in de chloroplasten tijdens de fotosynthese en in de mitochondriën tijdens de ademhaling.

In deze studie gebruikten we de groene alg *Chlamydomonas reinhardtii*. Onze aandacht ging specifiek uit naar het H<sub>2</sub>O<sub>2</sub>-afbrekende enzym ascorbaatperoxidase 2 (APX2), dat onlangs werd geclassificeerd als ‘ascorbate peroxidase-related’ (APX-R) en waarvan de functie nog onduidelijk is. Wij onderzochten de cellulaire rol van het H<sub>2</sub>O<sub>2</sub>-afbrekende enzym APX2 en identificeerden gemodificeerde cysteïnen in hun gesulfenyleerde vorm (-SOH) in *Chlamydomonas* gedurende oxidatieve stress.

Met een exploratieve screening van mutanten door middel van moleculaire en genetische methoden, gebruikmakend van <sup>1</sup>H-NMR, activiteitstests en biofysische technieken met recombinant geëxprimeerde en gezuiverde APX2 en plastocyanine eiwitten, en door middel van structuurvoorspellingen, ontdekten we dat APX2 zich hoogstwaarschijnlijk in het lumen van de chloroplasten bevindt en een invloed heeft op plastocyanine. Anders dan de typische H<sub>2</sub>O<sub>2</sub>-afbrekende enzymen, vertoonde APX2 naast peroxidase activiteit ook koperbinding in een typisch metaalbindend MxxM sequentiemotief en is APX2 betrokken bij het reguleren van de cellulaire plastocyanine niveaus.

Door een verfijning van een massaspectrometrische sulfenoom-analysetechniek, toegepast op eiwitextracten van *Chlamydomonas* wild-type onder zowel normale als oxidatieve stressomstandigheden, hebben we een gesulfenyleerd peptide geïdentificeerd dat geassocieerd is met drie ‘light-harvesting’ complexen van fotosysteem-II en met het ATP/ADP AAA1 dragereiwit. Deze ontdekking dient als een eerste aanwijzing dat de modificatie van een cysteïne betrokken is bij de regulatie van deze complexen en het AAA1 dragereiwit.

Onze resultaten onthullen een nieuwe functie voor APX2 en geven ons een inzicht in de sulfenyleringspatronen in Chlamydomonas.

# List of abbreviations

·OH	Hydroxyl radical
<sup>1</sup> Chl*	Singlet-state excitation of Chl <i>a</i> molecule
<sup>1</sup> O <sub>2</sub>	Singlet oxygen
2-Cys PRX	2-cys peroxiredoxin
<sup>3</sup> Chl*	Triplet state of Chl <i>a</i> molecule
<sup>3</sup> P680	Excited state of PSII
AAA1	ADP, ATP carrier protein
AOX	Alternative oxidase
APX-L	Ascorbate peroxidase-like
APX-R	Ascorbate peroxidase-related
APXs	Ascorbate peroxidases
AsA-GSH cycle	Ascorbate-glutathione cycle
AtOM66	Arabidopsis thaliana outer membrane of mitochondria 66
BCA	Bicinchoninic acid
BTD	1-(pent-4-yn-1-yl)-1h-benzo[c]-[1,2]-thiazin-4(3h)-one 2,2-dioxide
CATs	Catalases
CBB	Calvin-Benson-Bassham
CEF	Cyclic electron flow
ATPase	CF <sub>0</sub> -F <sub>1</sub> ATP synthase
Chl	chlorophyll
CLiP	Chlamydomonas library project
<i>Cytb<sub>6f</sub></i>	Cytochrome <i>b<sub>6f</sub></i>
<i>Cytf</i>	Cytochrome <i>f</i>
DCMU	3-(3,4-dichlorophenyl)-1,1-dimethylurea
DHR	Dehydroascorbate reductase
DYn-2	5,5-dimethyl-1,3-cyclohexanedione
ECS	Electrochromic shift
FCCP	Carbonyl cyanide 4-(trifluoromethoxy) phenylhydrazone
Fd	Ferredoxin
FLV	Flavodi-iron protein
FNR	Ferredoxin-NADP <sup>+</sup> -reductase
FQR	Ferredoxin-dependent plastoquinone reductase

Fv/Fm	Maximum quantum yield of PSII
GPXs	Glutathione peroxidases
GR	Glutathione reductase
GRXs	Glutaredoxins
GS·	Glutathione radical
GSH	Reduced form of glutathione
GSNO	S-nitrosoglutathione
GSNOR	GSNO reductase
GSOH	GSH sulfenic acid form
GSSG	Oxidized glutathione
GSTs	Glutathione-S-transferase
JTS	Joliot-Type-Spectrophotometer
LCA1	AAA-ATPase
LEF	Linear electron flow
LHCBM2/3/5	Major light harvesting complex of PSII 2/3/5
LHCIIs	Light harvesting complexes of PSII
MDHR	Monodehydroascorbate reductase
mt <sup>-</sup> , mt <sup>+</sup>	Mating type minus, mating type plus
NO	Nitric oxide
NPQ	Non-photochemical quenching
NRXs	Nucleoredoxins
NTR	NADPH-thioredoxin-reductase
O <sub>2</sub> <sup>-</sup>	Superoxide
ONOO·	Peroxynitrite
P680	Primary electron donor of PSII
P700	Primary electron donor of PSI
PC	Plastocyanin
PERs	Peroxidases
PGR5	Proton gradient regulator 5
PGRL1	Proton Gradient Regulator-Like 1
<i>pmf</i>	Proton motive force
PQ	Plastoquinone
PQH <sub>2</sub>	Plastoquinol
PRXs	Peroxiredoxins
PSI	Photosystem I

PSII	Photosystem II
PTMs	Post-translational modifications
PTOX	Plastoquinol or plastid terminal oxidase
qE	Light energy-dependent quenching
qI	Photoinhibitory quenching
qP	Photochemical quenching
qT	State transition quenching
RBO1	Respiratory burst oxidase 1
rETR	Relative electron transport rate
ROS	Reactive oxygen species
-SNO	Nitrosylated form of modified cysteine residue
-SO <sub>2</sub> H	Sulfinylation
-SO <sub>3</sub> H	Sulfonylation
SODs	Superoxide dismutases
-SOH	Sulfenylation
SRXs	Sulfiredoxins
-SSG	S-glutathionylated form of modified cysteine residue
STT7	Serine/threonine-protein kinase
TAP	Tris-acetate-phosphate
TCA	Tricarboxylic acid
THB5	Truncated hemoglobin 5
TMP	Tris-minimal-phosphate
TRXs	Thioredoxins
φPo	Maximum quantum yield of PSII
φPSII	Effective quantum yield of PSII

# List of Figures and Tables

## Figures

### Chapter I

<b>Figure 1:</b> Phylogenetic relation of the green lineage.	2
<b>Figure 2:</b> Anatomy of Chlamydomonas cell.	4
<b>Figure 3:</b> Scheme of one multiple-fission cycle of Chlamydomonas.	5
<b>Figure 4:</b> Chlamydomonas life cycle.	6
<b>Figure 5:</b> Photosynthetic electron transfer chain and ROS production sites.	11
<b>Figure 6:</b> Scheme of the four proposed pathways for cyclic electron flow (CEF) and the model of PGR5/PGRL1-dependent pathway.	14
<b>Figure 7:</b> Representation of the main photoprotective mechanisms of the NPQ to avoid photodamage.	16
<b>Figure 8:</b> Copper transporters in Chlamydomonas and their putative localization.	20
<b>Figure 9:</b> Scheme of intracellular ROS production sites under stress conditions and ROS scavenging systems.	22
<b>Figure 10:</b> Schematic processes of PTOX and Mehler reaction during photosynthetic electron transport.	25
<b>Figure 11:</b> Scheme of the cysteine oxidation mediated by H <sub>2</sub> O <sub>2</sub> .	30
<b>Figure 12:</b> Scheme of the experimental procedures to identify thioredoxin targets and their redox-regulated cysteines.	37
<b>Figure 13:</b> Scheme of the experiment of the <i>in vivo</i> identification of Arabidopsis sulfenome.	39
<b>Figure 14:</b> Scheme of the DYn-2 workflow to trap sulfenylated proteins.	41
<b>Figure 15:</b> Novel classes of nucleophile probes to trap sulfenylated cysteine residues.	42
<b>Figure 16:</b> Workflow for S-sulfenylation labelling and analysis in Arabidopsis cell cultures.	44
<b>Figure 17:</b> Physical properties and kinetic profile of the WYne probes.	45

### Chapter III

<b>Figure 1:</b> Scheme of the drop test set up.	51
<b>Figure 2:</b> Map of the plasmid and scheme of the <i>SRX2</i> gene construct used for transformation.	58
<b>Figure 3:</b> Scheme of the CIB1 cassette of the CLiP mutants, conferring resistance to paromomycin ( <i>AphVIII</i> ).	63
<b>Figure 4:</b> Drop tests of wt and mutants on agar plates did not show any phenotypical differences.	67
<b>Figure 5:</b> Maximum quantum yield of PSII and rETR of <i>srx2</i> and <i>apx2</i> mutants grown in acetate medium in control condition (TAP) and submitted to H <sub>2</sub> O <sub>2</sub> treatment did not show any significant differences compared to the wt.	72
<b>Figure 6:</b> Crossing between <i>srx2</i> and <i>apx2</i> shows paromomycin <sup>R</sup> cells.	73
<b>Figure 7:</b> Analysis of the <i>srx2</i> mutant co-transformants shows that the <i>SRX2</i> gene is expressed in one of the three co-transformants tested.	74
<b>Figure 8:</b> Maximum yield of PSII (Fv/Fm) and rETR of double mutant <i>d1</i> from <i>srx2</i> x <i>apx2</i> crossing reveals differences compared to its parental strains.	76
<b>Figure 9:</b> Measurements of NPQ and state transition at 77 K in cells grown in phototrophic conditions show difference in the photoprotective mechanism in the <i>apx2</i> mutant.	79
<b>Figure 10:</b> Measurements of wt and <i>apx2</i> low-light phototrophic cells at a temperature of 77 K shows that the <i>apx2</i> mutant displays a higher tendency to be in state I.	81
<b>Figure 11:</b> Photo-oxidation and re-reduction rate of P700 in low-light and high-light phototrophic cells show faster oxidation and slower re-reduction rate in low-light <i>apx2</i> mutant cells.	83

<b>Figure 12:</b> Re-reduction and photo-oxidizable P700 and cytochrome <i>f</i> of low-light and high-light phototrophic cells show differences in <i>apx2</i> low-light cells.	85
<b>Figure 13:</b> Electrochromic shift of phototrophic low-light and high-light cells reveals that the first ms of cyclic electron flow of the <i>apx2</i> mutant is low.	87
<b>Figure 14:</b> The growth and the PSII activity of the <i>apx2</i> are affected in fluctuating light growing condition.	88
<b>Figure 15:</b> ROS determination of wt and <i>apx2</i> cells stressed for 1 h under high light intensity shows no increase of H <sub>2</sub> O <sub>2</sub> in the <i>apx2</i> mutant.	89
<b>Figure S1:</b> Sequencing of all the mutants with their gene map and paromomycin resistant cassette position.	92

#### Chapter IV

<b>Figure 1:</b> Mutants of APX2 exhibit levels of the APX2 protein that are beyond detection.	122
<b>Figure 2:</b> <i>apx2</i> mutants display no defect in PSII activity but in electron transfer around PSI when grown in phototrophic conditions with low light.	124
<b>Figure 3:</b> The electron transfer to P700 was impaired in the <i>apx2</i> mutant cells, accompanied by a reduced level of plastocyanin.	126
<b>Figure 4:</b> Comparative proteomic analysis reveals variations in protein levels in the <i>apx2-1</i> mutant which are confirmed by immunoblot in both mutants.	128
<b>Figure 5:</b> Induction of cytochrome <i>c</i> <sub>6</sub> under copper-deficiency restores a wt phenotype in <i>apx2</i> mutants.	130
<b>Figure 6:</b> Transcriptomics analyses reveal post-transcriptional differences between wt and the <i>apx2-1</i> mutant in copper replete conditions and similar response to CRR1 master regulator in copper deficient conditions.	132



<b>Figure S1:</b> Uncropped gel images of the immunoblots showed in <b>Fig. 1</b> .	138
<b>Figure S2:</b> Wt and <i>apx2-1</i> exhibit comparable responses to copper deficiency, and the APX2 transcript remains unchanged in the presence of copper deficiency.	142
<b>Figure S3:</b> Alignment of Arabidopsis APX6 and Chlamydomonas APX2 reveals the absence of the AxA cleavage site of the TAT signal in APX6 but confirms the presence of the MxxM motif.	144

## Chapter V

<b>Figure 1:</b> APX2 is localized in the chloroplasts and present specific conserved motifs typical for lumen targeting and metal binding.	161
<b>Figure 2:</b> APX2 peroxidase activity relies on guaiacol instead of ascorbate and APX2 binds copper.	164
<b>Figure 3:</b> APX2 modulates copper binding in plastocyanin (PC).	167
<b>Figure S1:</b> Amino acid sequence alignment of APX and APX-R showing conserved residues in representatives from algae, plants and diatoms.	171
<b>Figure S2:</b> Chlamydomonas APX2 lacks the loop that faces the heme, and APX-R contains the MxxM/H sequence motif.	175
<b>Figure S3:</b> APX2 utilizes guaiacol, but not ascorbate, as electron donor.	177
<b>Figure S4:</b> Further analyses of APX2 and plastocyanin.	178

## Chapter VI

- Figure 1:** Schematic overview depicting the complete protocol for capturing modified cysteine residues. 189
- Figure 2:** Immunoblot analysis shows that the cell-wall-plus-strain is suitable for labelling Cys-modified proteins. 191
- Figure 3:** Immunoblot analyses show that cell and BTD concentrations are important for protein labelling. 192
- Figure 4:** Analysis of the identified peptides shows the conserved Cys. 195

## Chapter VII

- Figure 1:** Schemes of APX2 and SRX2 catalytic reaction mechanisms. 203
- Figure 2:** Model depicting hypotheses regarding the role of APX2, highlighting distinctions between the wildtype (wt) and *apx2* mutant. 213

## Tables

### Chapter III

- Table 1.** List of mutants defective in H<sub>2</sub>O<sub>2</sub>-signaling and stress responsive enzymes ordered from CLiP library 61
- Table 2.** Summary of the molecular and genetic screening of the 17 mutants. 64
- Table 3.** Maximum quantum yield of PSII (Fv/Fm) of the wt and mutant strains grown in continuous low light condition with and without H<sub>2</sub>O<sub>2</sub> for 15 min and 30 min showed some significant differences. 68
- Table 4.** Maximum quantum yield of PSII (Fv/Fm) of the wt and mutant strains in circadian cycle with and without H<sub>2</sub>O<sub>2</sub> exposed for 15 min, showed some significant differences. 69

<b>Table 5.</b>	Growth rate expressed in doubling time (hour) of <i>srx2</i> and <i>apx2</i> cells grown under continuous low light 50 $\mu\text{mol photons m}^{-2} \text{s}^{-1}$ in phototrophy are similar to the wt.	71
<b>Table 6.</b>	Summary of the <i>srx2</i> mutant co-transformation.	74
<b>Table S1.</b>	Primers used for sequencing, RT-PCR and transformation.	109

## Chapter IV

<b>Table 1.</b>	The growth rate of both wt and <i>apx2</i> mutants is comparable.	123
<b>Table S1.</b>	Confirmation of the presence of paromomycin cassette in the three <i>apx2</i> mutants.	145
<b>Table S2.</b>	Primers used for sequencing.	146
<b>Table S3.</b>	Significantly decreased protein from TMT labeling analysis with a $\log_2$ fold change $\leq -0.5$ and p-value $< 0.05$ .	146
<b>Table S4.</b>	Significantly increased protein from TMT labeling analysis with a $\log_2$ fold change $\geq 0.37$ and p-value $< 0.05$ .	148

## Chapter VI

<b>Table 1.</b>	Identified peptides with conserved sulfenylated cysteines of wt137C sample treated with 0.1 mM $\text{H}_2\text{O}_2$ .	196
<b>Table 2.</b>	Identified peptides with conserved sulfenylated cysteines of wt137C sample treated with 1 mM $\text{H}_2\text{O}_2$ .	197

# Table of contents

List of publications	iv
Summary	v
Résumé	vi
Samenvatting	vii
List of abbreviations	ix
List of Figures and Tables	xii
Chapter I: Introduction	
1.1 The model organism <i>Chlamydomonas reinhardtii</i>	1
1.2 The bad and the good of ROS	21
1.3 Identification of modified proteins	32
Chapter II	
Thesis objectives	46
Chapter III	
Redox signaling mutants in <i>Chlamydomonas</i> : a survey	48
Abstract	48
3.1 Introduction	49
3.2 Material and Methods	50
3.3 Results	60
3.4 Discussion	90
Supplementary materials	92
Chapter IV	
APX2, the ascorbate peroxidase-related protein, regulates the levels of plastocyanin in <i>Chlamydomonas</i>	111
Abstract	111
4.1 Introduction	112
4.2 Material and Methods	114
4.3 Results	121
4.4 Discussion	133
Supplementary materials	138

Chapter V	
Ascorbate Peroxidase 2 (APX2) of Chlamydomonas binds copper and modulates the copper Insertion into plastocyanin	150
Abstract	150
5.1 Introduction	151
5.2 Material and Methods	153
5.3 Results	159
5.4 Discussion	168
Supplementary materials	171
Chapter VI	
Refinement of the methodology for capturing cysteine-modified proteins: protocol and encountered challenges	180
Abstract	180
6.1 Introduction	181
6.2 Material and Methods	181
6.3 Results	187
6.4 Discussion	198
Chapter VII: General discussion and perspectives	200
7.1 General discussion	200
7.2 Perspectives	208
Acknowledgement	220
References	222
Curriculum vitae	253

# Chapter I: Introduction

## 1.1 The model organism *Chlamydomonas reinhardtii*

### 1.1.1 Major green photosynthetic eukaryotes and *Chlamydomonas*

Green algae and plants belong to the green lineage, or Viridiplantae, one of the major groups of oxygenic photosynthetic eukaryotes. The green lineage, together with the red lineage and the glaucophyte lineage, originated after a primary endosymbiotic event between a eukaryotic cell and a cyanobacterium which became an organelle called chloroplast. The symbiosis event is thought to have happened more than 1.5 billion years ago and yielded an ancestral flagellate (Keeling 2010). From the unicellular ancestor of the green lineage, two clades diverged; a) the Chlorophyta which include the majority of marine microalgae and the so-called core Chlorophytes; and b) the Streptophyta which house Charophyte green algae and land plants (**Fig. 1**) (Leliaert et al 2012). The division Chlorophyta is characterized by a large and morphologically diverse group of organisms, including motile and non-motile single cells, filaments, or colonies (Leliaert et al 2012). The core Chlorophyta is composed of three major classes: Ulvophyceae, Trebouxiophyceae, and Chlorophyceae (UTC). While the Trebouxiophyceae and Chlorophyceae are mostly found in the soil and freshwater, the Ulvophyceae are mostly present in the coastal environment (Leliaert et al 2012). The group of Streptophyta is one of the oldest branches of the green lineage (a billion years ago or more), and includes unicellular to more complex green algae forms, and land plants (Leliaert et al 2011). Within the Chlorophyceae group of green algae, we find Chlamydomonadales that include *Volvox* spp. and *Chlamydomonas* spp. These species have been used as model organisms for evolutionary and phylogenetic studies. In particular, *Chlamydomonas* spp. have been found suitable for genetic studies and investigations on photosynthesis and mitochondrial respiration (Harris 2001, Harris 2009). One of the species, *Chlamydomonas reinhardtii* (hereafter *Chlamydomonas*, Greek *chlamys*, a cloak; *monas*, solitary; (Harris 2001)) has been widely used for molecular and biochemical studies and is the model organism used for this project.

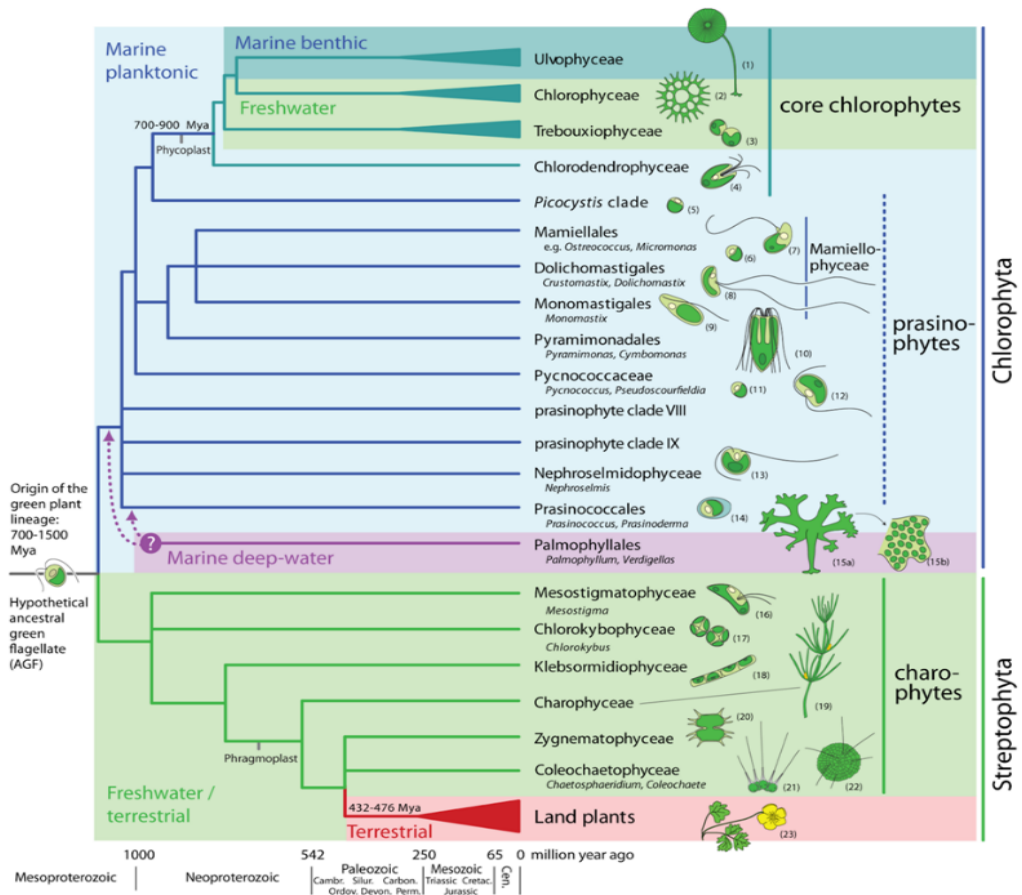


**Figure 1: Phylogenetic relation of the green lineage.** The phylogenetic tree displays widely accepted relations between the green lineage based on molecular evidence. *Chlamydomonas* belongs to the Chlorophyceae class in the core Chlorophyte (Leliaert et al 2011).

### 1.1.2 Exploring *Chlamydomonas*

#### 1.1.2.1 Inside *Chlamydomonas*: anatomy of a vegetative cell and cell cycle

Vegetative *Chlamydomonas* cells are haploid with a 5-10  $\mu\text{m}$  diameter (**Fig. 2**) and present a mating type designed as plus ( $\text{mt}^+$ ) or minus ( $\text{mt}^-$ ). The cells are embedded in a cell-wall and a periplasmic membrane. The cell-wall mainly consists of several layers of hydroxyproline-rich glycoproteins similar to the extensins of higher plants (Goodenough et al 2007, Harris 2001, Woessner 1994). The cilia structure is typical of the eucaryotes with 9+2 microtubules arrangement, which helps the cell swim and recognize its partner of the opposite

mating type during sexual reproduction (Harris 2001, Sasso et al 2018). The osmolarity of the cells is controlled by two contractile vacuoles (Komsic-Buchmann et al 2014) and a set of basal bodies that are responsible for ciliary assembly (Dutcher & O'Toole 2016).

*Chlamydomonas* is unique due to the presence of a single U-shape chloroplast where the machinery to capture and transform light into energy takes place. The chloroplast occupies two thirds of the entire cell volume (Harris 2001) and contains the pyrenoid and the eyespot. The pyrenoid is the site of the carbon fixation process and the carbon concentrating mechanism (CCM) used to accumulate inorganic carbon. Moreover, it is also the storage site of starch and Rubisco together with the molecular linker essential pyrenoid component 1 (EPYC1) (Mackinder et al 2016, Wang & Jonikas 2020). The eyespot (or stigma) appears bright orange due to the presence of carotenoids. It functions as an antenna for swimming cells to direct them to unidirectional light (Harris 2001). The presence of photoreceptors, called rhodopsins, helps the cell to absorb light and drive a cascade of reactions which direct the cell towards light sources for optimal conditions of photosynthesis (Thompson 2017). Two distinct photo-responses have been observed in *Chlamydomonas*, one towards the light called phototaxis, calcium dependent (Bennett & Golestanian 2015, Josef et al 2006) and the opposite called photophobic in which the cells move backwards in response to a sudden increase of light intensity changing from an asymmetric to a symmetric waveform (Dutcher 2020, Rochaix 1995).

Dispersed in the cytosol, several mitochondria are present with the typical elongated or branching structures (Harris 2001). These organelles serve as the cell energy machinery involved in several metabolic pathways. In mitochondrial matrix, the Krebs cycle, or also called the tricarboxylic acid (TCA) cycle, takes place and produces NADH used for respiration and ATP (Massoz 2017). The mitochondrial internal membrane houses the oxidative phosphorylation (OXPHOS) in which substrate oxidation drives the electron transfer along the chain together with ATP production through a transmembrane gradient. It is composed of four complexes and an ATP synthase. An alternative oxidase (AOX) is also associated to the electron transfer chain and its role is to regulate the electron flow and to protect the cells from oxidative damage (Hamel et al 2022).

Peroxisomes are present in the cytosol. These organelles are involved in the



oxidation of lipids and fatty acids and in H<sub>2</sub>O<sub>2</sub> scavenging due to the presence of several oxidases and catalase (Kong et al 2017). Additionally, they host the glyoxylate cycle, which supports growth in acetate medium (Durante et al 2019, Lauersen et al 2016, Plancke et al 2014).

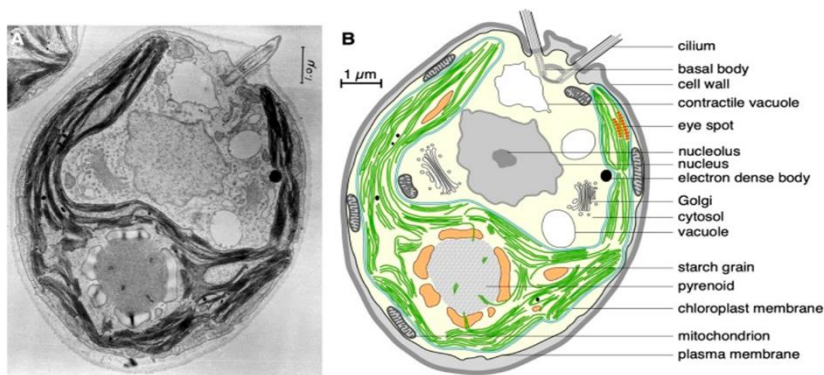


**Figure 2: Anatomy of Chlamydomonas cell.** A) Picture of Chlamydomonas cell realised with transmission electron micrograph (TEM) available on CellImage Library website (CIL:37252, *C. reinhardtii*. CIL. Data set: <https://doi.org/doi:10.7295/W9CIL37252>). B) Schematic illustration of a Chlamydomonas cell based on the TEM picture from A).

Another aspect that makes Chlamydomonas a successful model organism is its life cycle and the possibility to control it.

Haploid Chlamydomonas cells can reproduce either asexually and sexually. In the first case they can reproduce indefinitely via mitosis in which the cells require 24 h to grow when submitted to a 12 h dark/ 12 h light cycle. During the growth phase (G1 in **Fig. 3**) the mother cell can increase its size more than twice and divide in synthesis/mitosis (S/M) phase  $n$  times to release  $2^n$  daughter cells. The number of divisions depends on the volume reached by the mother cell at the commitment point when the division starts. For example, if the size of a mother cell increases three times during G1 phase, in the S/M phase it will produce eight daughter cells. Daughter cells then emerge from the mother cell and the cycle starts over again (**Fig. 3**) (Cross & Umen 2015, Jeanneret et al 2016).

In the second case, in condition of nitrogen limitation, Chlamydomonas cells differentiate into gametes, designed as plus and minus (considered as female and male respectively) (Goodenough et al 2007, Innami et al 2022). In laboratory conditions, this strategy is used to induce gametogenesis, leading

Chlamydomonas gametes to undergo cilia adhesion through plus and minus agglutinin glycoproteins. Cells of opposite mating-type fuse to form a quadriciliate cell ( $2n$ ) (**Fig. 4**) (Cross & Umen 2015, Jeanneret et al 2016). The nitrogen deprivation induces the up-regulation of some genes like nitrogen-starved gametogenesis (*NSG*) and gamete-specific (*GAS*) genes. From the quadriciliate cell, a zygote is formed and after zygote maturation, the addition of nitrogen favors cell division by meiosis and the release of 4 gametes, 2  $mt^+$  and 2  $mt^-$  (Goodenough et al 2007). It is possible to cross different strains of Chlamydomonas as described in (Jiang & Stern 2009). For example, a mutant and a wild type, to generate mutant cells harboring either the mating type plus or minus or double mutants by crossing two Chlamydomonas strains carrying different mutations.

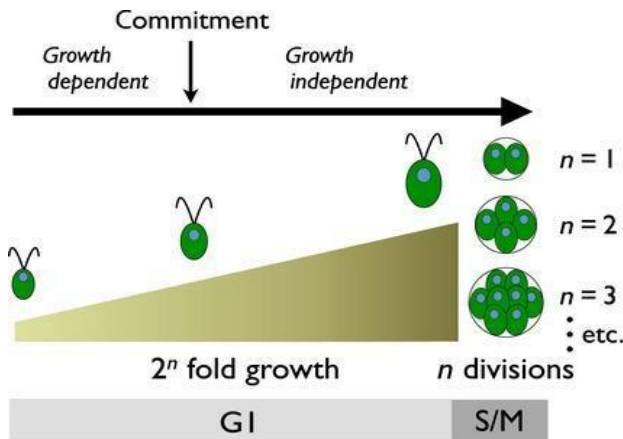


**Figure 3: Scheme of one multiple-fission cycle of Chlamydomonas.** (To read from left to the right). Cells are growing during the G1 phase reaching the same or a bigger volume than the one of the starting sizes. The division starts when the cells reach the commitment point, going to a series of alternating synthesis phases and mitosis (S/M) and producing  $2^n$  daughters. The cell division number  $n$  depends on the mother-cell size and typically ranges from one to three divisions, to produce two, four or eight daughter cells. After the S/M phase, daughter-cells prepare and re-enter the G1 phase to repeat the cycle. From (Cross & Umen 2015).

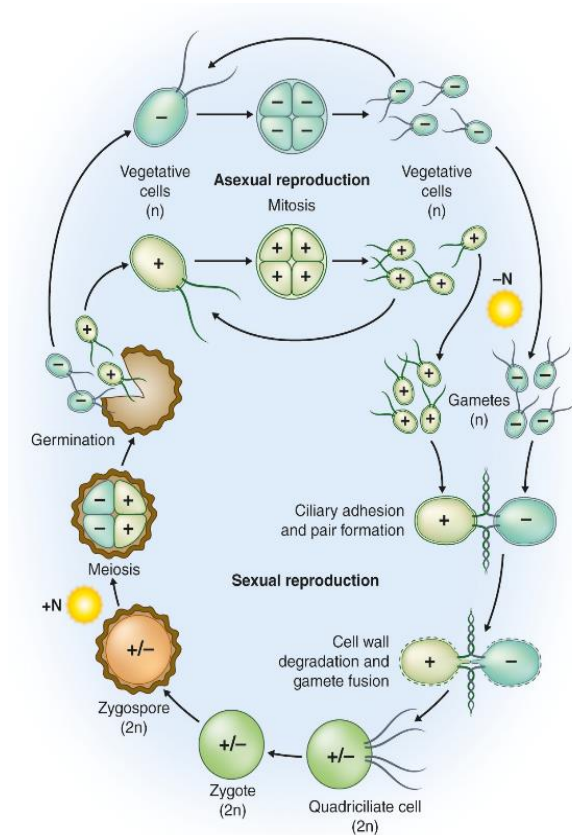


**Figure 4: Chlamydomonas life cycle.** During asexual reproduction, vegetative cells of  $mt^+$  or  $mt^-$ , divide by mitosis and from one cell, four daughter cells are generated (Goodenough et al 2007, Harris 2001). Gametogenesis can be induced in the light and under nitrogen starvation. When these two conditions are present, two cells of opposite mating types can fuse to generate a diploid zygote (sexual reproduction). Within a few days, the zygote becomes a resistant and dormant zygospore in which the chlorophyll is degraded (Goodenough et al 2007, Harris 2001). When environmental conditions improve, the zygospore undergoes meiosis yielding four daughter cells, two of each mating type (germination). In laboratory conditions, sexual reproduction can be induced by altering nitrogen (+/- N in photo) availability and light conditions (Harris 2001). Image from (Sasso et al 2018), credits to Debbie Maizels.

Thus, because of the easy genetic manipulation and the possibility to control the cell cycle, *Chlamydomonas* is a good model organism to work with. *Chlamydomonas* is a soil alga, but in laboratory conditions it can be cultivated in solid or liquid media as long as it is kept at constant temperature between 20°C and 25°C. It can grow phototrophically, relying only on a light source, heterotrophically in the dark with an additional carbon source like acetate, or adopt a mixotrophic approach (light and acetate) (Harris 2009). Under optimal

conditions of temperature, nutrient availability and light source, the algae grow at such a rapid rate that the cell number can double within 8 h (Harris 2001). White light is often used at  $100 \mu\text{mol photons m}^{-2} \text{s}^{-1}$ , but this intensity can be regulated according to the type of experiment to perform (Harris 2009). In photosynthetic organisms, light drives photosynthesis, one of the processes that fuels algal energy.

#### *1.1.2.2 Inside Chlamydomonas: laboratory strains, genome annotation and techniques of transformation*

The first isolation of a *Chlamydomonas* strain is dated to 1946 thanks to Gilbert Smith who was interested in studying sexual recombination and shared matched mating pairs to other interested researchers (Smith 1946, Smith & Regnery 1950). Each of these mating-matched pairs are considered the principal strains and they are referred to as Sager lineage (Sager 1955), Cambridge lineage and Ebersold-Levine lineage (Ebersold 1956). Because of that, it is assumed that the mating types within a lineage are isogenic and that each lineage differs from the others (Harris 2009). In addition, crosses have been performed within these lineages to obtain strains with desired phenotypes. The standard laboratory strains are maintained in a common repository known as the *Chlamydomonas* Resource Center (<https://www.chlamycollection.org/>) (Gallaher et al 2015). Due to the whole genome sequence, it was possible to re-sequence a wide range of laboratory strains. Each of these strains was aligned to the *Chlamydomonas* reference genome, a mating type plus ( $\text{mt}^+$ ) member of the Ebersold-Levine lineage (Merchant et al 2007). The comparison of these strains with the reference one showed genetic diversity that was distributed in a non-homogeneous manner in distinct and heritable patterns. Such pattern distribution represents a unique fingerprint for each strain that could be useful to identify new strains and inter-strain relatedness (Gallaher et al 2015).

Extensive work has been conducted to uncover and annotate the *Chlamydomonas* genome. The first draft of the *Chlamydomonas* genome, assembled from  $\sim 13\times$  coverage of Sanger-sequenced reads, was released in 2007 (Merchant et al 2007). The 121-megabase (Mb) nuclear genome is fully sequenced and annotated, consisting of 17 linkage groups and is rich in GC nucleotides (64%) (Merchant et al 2007). Later, with the development of next-generation sequencing (NGS), the more accurate v5 assembly was released in 2012 (described (Blaby et al 2014)). Recently, the newest v6 version was released in 2022 (Craig et al 2023).

Data of CC-4532 wild type strain v6 is available at Phytozome (<https://phytozome-next.jgi.doe.gov>). For this project, I have started to use the v5 assembly as reference coupled with the v6 at its release. In addition, mitochondrial and chloroplast genomes are also fully sequenced and annotated, respectively 15.8 kb (Vahrenholz et al 1993) and 203.8 kb long (Maul et al 2002).

The availability of the three sequenced genomes improved and supported studies on *Chlamydomonas*.

Currently, a library of *Chlamydomonas* mutants (CLiP library), generated via random mutagenesis carrying an insertional cassette which confers resistance to the antimicrobial paromomycin (Li et al 2019, Li et al 2016), is also available for reverse genomic studies (<https://www.chlamylibrary.org/>). Mutants of *Chlamydomonas* used in my study come from the CLiP library. Moreover, the development of comparative genomics led to the generation of a set of proteins called GreenCut (Heinnickel & Grossman 2013), with a new version available GreenCut2 which collects the photosynthetic nuclear-encoded proteins common in the green lineage (Grossman et al 2019). In this context *Chlamydomonas* is one of the most suitable organisms to study photosynthesis, as most of the proteins assembled are common among photosynthetic organisms.

The importance of using *Chlamydomonas* for biochemical and molecular studies derives from the possibility to transform the nucleus, mitochondria and chloroplast. Several techniques exist for nuclear transformation of *Chlamydomonas*. (i) The glass beads method, where beads are mixed and vortexed with exogenous DNA and cell-wall free *Chlamydomonas* cells, make breaks into the cell membrane, allowing exogenous DNA to be incorporated (Kindle 1990). (ii) The electroporation, in which the high voltage increases cell membrane permeability, enables incorporation of exogenous DNA (Shimogawara et al 1998). This method has been found more efficient than the glass beads when adapting voltage and endogenous DNA concentration (Zhang et al 2021). (iii) The biolistic (or gene-gun) method consists in bombarding *Chlamydomonas* cells with gold/tungsten coated with DNA (El-Sheekh et al 2019). In the gene-gun technique several variables can affect the transformation efficiency, such as the distance between the plate and the cells, as well as the size of the particles or particle diameter (Zhang et al 2021). (iv) The *Agrobacterium*-mediated method usually used for plants, consists in the insertion of the gene of

interest in the T-DNA of *Agrobacterium tumefaciens*. Bacteria and Chlamydomonas cells are co-cultivated and the bacterial plasmid is integrated in the algal cell by infection (Kumar et al 2004). Among them, the technique of biolistic transformation was successful for chloroplasts and mitochondria transformations (Boynton et al 1988, Remacle et al 2006).

### 1.1.3 Photosynthesis

#### 1.1.3.1 Photosynthetic electron transport chain

All green photosynthetic organisms conduct photosynthesis, a vital process for life on Earth. It involves light-driven electron transfer from water to CO<sub>2</sub>, leading to the release of O<sub>2</sub> and the formation of reduced carbon compounds (Kanazawa et al 2021). Through the photosynthetic electron transport chain, plants, algae and cyanobacteria convert solar energy into chemical energy. The core of the reactions of photosynthesis is called “linear electron flow” (LEF) and comprises a series of reactions resulting in light-dependent H<sub>2</sub>O oxidation, NADP<sup>+</sup> reduction, and ATP formation (**Fig. 5**). NADPH and ATP produced during the linear electron flow, are useful for the Calvin-Benson-Bassham (CBB) cycle. The photosynthetic machinery is located in the thylakoid membrane of the chloroplast and comprises four major multi-subunit protein complexes. Two of these are the photosystems I (PSI) and II (PSII). Each of these complexes harbor light-harvesting complexes (LHCs) which contain pigments to capture light and transfer the energy to the reaction center of both photosystems. Linear electron flow can be explained as light-energy absorbed by the light harvesting complex antennas which is subsequently transferred to the special chlorophyll *a* of PSII, P680 reaction center. This serves as the primary electron donor where charge separation occurs (Barber 2012, Gäbelein et al 2017, Le Moigne et al 2023). At P680, excited electrons are transferred towards a tightly bound plastoquinone (PQ) at the Q<sub>A</sub> site via the primary electron acceptor pheophytin. From the loosely bound plastoquinone at the Q<sub>B</sub> site, electrons enter the PQ pool by successive PQ reduction during two photochemical cycles involving the uptake of protons from the thylakoid stroma. The resulting electron gap at P680<sup>+</sup> provides the redox potential necessary to oxidize H<sub>2</sub>O, giving rise to O<sub>2</sub> evolution followed by proton release to the thylakoid lumen. This process is mediated by the Mn<sub>4</sub>CaO<sub>5</sub> cluster at the luminal side of the membrane (Gäbelein et al 2017, Vinyard et al 2013).

An intermediate complex, the cytochrome *b<sub>6</sub>f* complex (Cyt *b<sub>6</sub>f* complex), is responsible for connecting the electron transfer between both photosystems and uses the energy of this electron transfer to translocate protons (H<sup>+</sup>) to the thylakoid lumen, thus generating the proton motive force (*pmf*). Cyt *b<sub>6</sub>f* is a functional dimer with each monomeric unit made up of four major subunits cytochrome *f*, cytochrome *b<sub>6</sub>*, the Rieske iron-sulfur protein and subunit IV and four minor subunits (Malone et al 2021). During the activity of the Cyt *b<sub>6</sub>f*, plastoquinol is oxidized at the Q<sub>o</sub> site, involving the release of protons in the thylakoid lumen, generating the *pmf* (Gäbelein et al 2017). From Cyt *b<sub>6</sub>f* the electrons are driven through the cytochrome *f* subunit to the electron donor plastocyanin (Martinez et al 1994). Reduced plastocyanin transfer electrons to PSI through the N-terminal of the PsaF subunit of PSI (Caspy et al 2021, Hippler et al 1998). When light excites the P700 reaction center of PSI, the electron donation to one of two primary acceptors chlorophyll *a* A<sub>0</sub> is facilitated. Subsequently, electrons are transmitted towards the stromal side along two parallel branches via phylloquinone A<sub>1</sub>, rejoining at the iron-sulfur [4Fe-4S] clusters F<sub>X</sub>, F<sub>A</sub> and F<sub>B</sub>, where the reduction of the iron-sulfur [2Fe-2S] electron carrier ferredoxin occurs. At the downstream part of the linear electron flow, electrons are successively transferred within a ternary complex from ferredoxin to NADP<sup>+</sup> via the ferredoxin-NADP<sup>+</sup>-reductase (FNR) enzyme, consuming one proton H<sup>+</sup> per NADPH (Kurisu et al 2001). The resulting reducing equivalents facilitate assimilatory pathways, in particular the CBB cycle involved in CO<sub>2</sub> fixation (Gäbelein et al 2017). At the stromal side of the thylakoid membrane, the electrons are not only used in the CBB cycle, but they are involved in other metabolic pathways including nitrate metabolism, biosynthesis of lipids, amino acids, pigments, etc... (Cardol et al 2011).

One last complex, the chloroplast CF<sub>0</sub>-F<sub>1</sub> ATP synthase (ATPase) uses the electrochemical proton gradient generated with the proton pumping into the lumen, to synthesize ATP (Hahn et al 2018) (**Fig. 5**). ATP synthase is also a thiol enzyme which is subjected to thioredoxin regulation especially during periods of darkness (i.e., night-time) to avoid ATP hydrolysis waste (Hisabori et al 2013, Kohzuma et al 2017). This regulation occurs on the  $\gamma$  subunit which has a redox sensor that can form a disulfide bond to prevent ATP formation (Hahn (Hahn et al 2018, Hisabori et al 2013, Kohzuma et al 2017).

The ATP/NADPH ratio produced during linear electron flow is 1.5. This ratio must be maintained for CO<sub>2</sub> fixation to occur (Cardol et al 2011). Therefore, the cell cannot afford to fuel other metabolic pathways which require ATP like nitrogen metabolism or lipid, amino acid, and/or pigment biosynthesis at the same time as the CBB cycle (Behrenfeld et al 2008, Finazzi et al 2010). For ATP supply, alternative pathways are present like cyclic electron flow (CEF; section 1.1.3.2) (Alric 2010, Cardol et al 2011) or water-to-water cycle (section 1.2.1) (Asada 1999, Curien et al 2016).

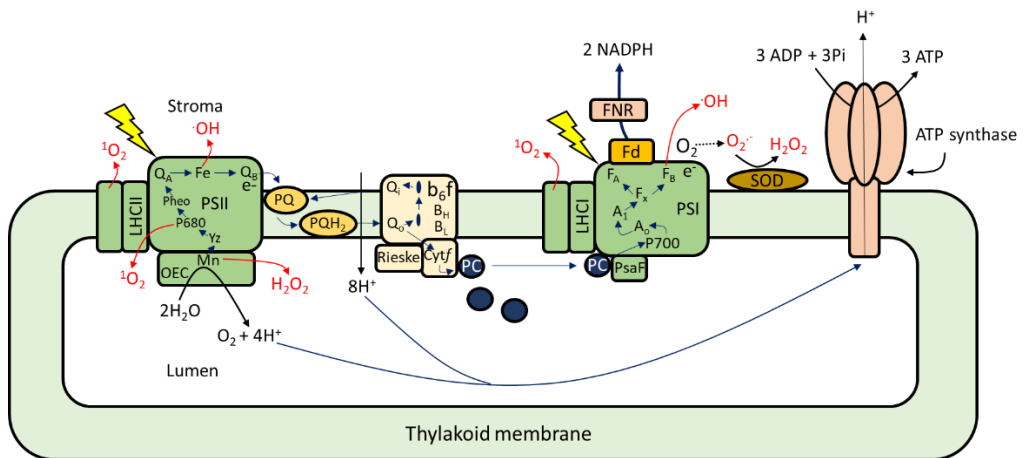


**Figure 5: Photosynthetic electron transfer chain and ROS production sites.** The photosynthetic electron transport chain is composed of the two photosystems (PSI and PSII) and cytochrome *b<sub>6</sub>f* complex. Extraction of electrons from water is catalyzed on the donor side of PSII by a cluster of four Mn ions. In addition, PSII contains two Fe atoms, a nonheme Fe on the acceptor side. Electrons are transferred from PSII to cytochrome *b<sub>6</sub>f* via plastoquinol molecules. Cytochrome *b<sub>6</sub>f* contains four b-type cytochromes (*b<sub>H</sub>*, *b<sub>L</sub>*, *b<sub>6</sub>*, and heme x), one c-type cytochrome *f*, and one 2Fe-2S cluster. Cytochrome *b<sub>6</sub>f* is the major proton pump that creates the potential gradient that is utilized by ATP synthase to produce ATP. Plastocyanin (PC), a Cu protein, transfers electrons from cytochrome *b<sub>6</sub>f* to PSI. In PSI, three 4Fe-4S clusters (*F<sub>X</sub>*, *F<sub>A</sub>*, and *F<sub>B</sub>*) participate in the electron transfer chain. Electrons from PSI are transferred to ferredoxin (Fd), a 4Fe-4S soluble protein. LHCII and LHCI are the light-harvesting complexes of PSII and PSI respectively. LEF is indicated by blue arrows, CEF is indicated with yellow arrows and ROS-generating reactions are indicated by red arrows. Adapted from (Shcolnick & Keren 2006).



### 1.1.3.2 Cyclic electron flow (CEF)

Besides the linear electron flow, alternative pathways are present to fulfil the demand of ATP for a proper ATP/NADPH ratio for carbon fixation. This mechanism is described as the return of the electrons to the PSI through Cyt *b<sub>6</sub>f* and via plastocyanin. Despite being still a matter of debate among the photosynthetic community, cyclic electron flow (CEF) has been explained through four different pathways (**Fig. 6**) (Kanazawa et al 2021).

The first one involves an NADH dehydrogenase-like (NDH) analogue to the mitochondrial complex I, which works as ferredoxin-dependent plastoquinone reductase (FQR). This enzyme is present in the thylakoid membrane of plants and it works as a proton-pump by coupling the pumping of two H<sup>+</sup> in the lumen with an electron transfer from ferredoxin (Fd) to plastoquinone (PQ) (Strand et al 2017).

Unicellular microalgae, like *Chlamydomonas*, instead present a type II NAD(P)H dehydrogenase-like (NDA2) which differs from the NDH of plants. It does not work as a proton-pump, but it directly interacts with NADPH, oxidizing it to NADP<sup>+</sup> and reducing the plastoquinone pool (Jans et al 2008, Peltier et al 2016).

Another pathway which is sensitive to antimycin A, involves plastocyanin, Cyt *b<sub>6</sub>f*, PSI and ferredoxin. For many years this pathway has been challenged due to the elusive mechanism behind the reinjection of the electron to the transport chain through reduced ferredoxin. In terrestrial plants, there is no binding between antimycin A and Cyt *b<sub>6</sub>f*. It has been hypothesized that a distinct antimycin A-sensitive enzyme, known as ferredoxin plastoquinone reductase (FQR), exists (Moss & Bendall 1984). However, attempts to identify this enzyme have been unsuccessful. Additionally, the thylakoid proteins Proton Gradient Regulator 5 (PGR5) (Munekage et al 2002) and Proton Gradient Regulator-Like 1 (PGRL1) (DalCorso et al 2008) play a role in antimycin A-sensitive cyclic electron flow (CEF). Both PGRL1 and PGR5 have the ability to accept electrons from ferredoxin and transfer them to plastoquinone, similar to the proposed function of FQR enzymes. Hence, they are suggested to be the elusive ferredoxin-dependent plastoquinone reductase (FQR) (DalCorso et al 2008, Hertle et al 2013). However, this concept has been challenged and the role of both PGRL1 and PGR5 has been redrawn. Recent studies have shown that the

contribution of PGRL1 is still controversial (Nawrocki et al 2019a), while it has been showed that PGR5 is essential for the Cyt *b<sub>6</sub>f* functioning during CEF activation in anoxic conditions (Buchert et al 2020). Moreover, a study on the Cyt *b<sub>6</sub>f* inhibition by antimycin A in CEF-favoring conditions, might rely on the activation of the serine/threonine kinase STT7 which regulates state transition (Buchert et al 2022). Despite these recent advances, CEF mechanism is still under debate. A common thought within the photosynthetic community, is the possibility of an alternate electron path during CEF directly at the Cyt *b<sub>6</sub>f* complex through its *c<sub>i</sub>* heme, following the formation of a supercomplex with the ferredoxin-NADP<sup>+</sup> reductase (FNR) (Kanazawa et al 2021, Nawrocki et al 2019b). In all these cases, the *pmf* produced during CEF is able to drive the formation of ATP without the reduction of NADP<sup>+</sup>, readjusting in this way the ATP/NADPH ratio required for carbon fixation. Moreover, the regulation of CEF is essential to prevent the excessive production of ATP beyond what is required in chloroplast metabolism (Kanazawa et al 2021). The regulation of CEF remains a topic of debate, however some studies have suggested the participation of the H<sub>2</sub>O<sub>2</sub> in some of the proposed CEF pathways in land plants (Kanazawa et al 2021).

It has been suggested that the mechanism involving NDH1 in plants, might be regulated by H<sub>2</sub>O<sub>2</sub> *in vivo* (Strand et al 2015). In this study the authors observed an increase of the NDH1-dependent pathway by external addition of H<sub>2</sub>O<sub>2</sub>, proposing that H<sub>2</sub>O<sub>2</sub> can directly activate CEF.

An *in vitro* study has shown that CEF is sensitive to the redox changes during the isolation process on spinach where the FQR-dependent pathway is dominant (Strand et al 2016). In the work presented, thylakoids were isolated in the presence of the reductant dithiothreitol (DTT) which preserved the CEF activity, normally lost during tissue disruption. Thus, the authors proposed that the FQR-CEF pathway *in vivo* might be regulated via thioredoxin-thiol reduction allowing this pathway to respond more rapidly to metabolic demands. On the contrary, under oxidative stress conditions, H<sub>2</sub>O<sub>2</sub> accumulates, promoting the activation of the NDH-CEF (Strand et al 2015). Therefore, it is likely that the two pathways are activated in response to the internal redox state of the chloroplast stroma (Strand et al 2016).

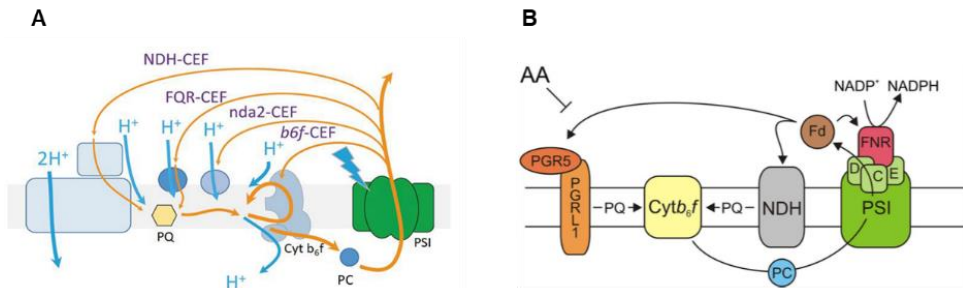


**Figure 6: Scheme of the four proposed pathways for cyclic electron flow (CEF) and the model of PGR5/PGRL1-dependent pathway. A)** The orange arrows indicate the four different CEF routes through NADH dehydrogenase-like (NDH), ferredoxin-dependent plastoquinone reductase (FQR), type II NAD(P)H dehydrogenase-like (*nda2*), cytochrome *b<sub>6</sub>f* (*b<sub>6</sub>f*), while with the blue arrows are indicated the proton  $H^+$  movement corresponding to each route. Adapted from (Kanazawa et al 2021). **B)** Model of the PGR5/PGRL1-dependent pathway of CEF sensitive to antimycin A (AA). In the image the pathway dependent by NDH is also illustrated. From (Labs et al 2016). Cyt *b<sub>6</sub>f*, cytochrome *b<sub>6</sub>f*; Fd, ferredoxin; FNR, ferredoxin-NADP<sup>+</sup> reductase; PQ, plastoquinone; PC, plastocyanin; PSI, photosystem I; PsaD/C/E, subunits of PSI are indicated as the proteins involved in CEF pathway. PGR5, proton gradient regulator 5; PGRL1, proton gradient regulator-like 1.

### 1.1.3.3 Non-photochemical quenching (NPQ)

On the other hand, when the photosynthetic electron transport rate becomes saturated and light excess is still absorbed, it can lead to photo-oxidation damage of protein and complexes of the photosynthetic chain (Erickson et al., 2015). When this is the case, excess light absorbed by pigments in the light harvesting complexes (LHCs) is transferred to their associated reaction centers at the photosystems. This results in a singlet-state excitation of chlorophyll (Chl) *a* molecule ( $^1Chl^*$ ), which can return to the ground state via one of several pathways described below. Part of the excitation energy transferred to reaction centers drives photochemistry and part of the excited Chl *a* can re-emit the energy as fluorescence, or it can be dissipated as heat. A less likely pathway involves the formation of the triplet state ( $^3Chl^*$ ) which can transfer the energy to the  $O_2$  and generate singlet oxygen ( $^1O_2$ ) a reactive oxygen species (ROS) molecule (discussed in the section 1.2.1). The formation of singlet oxygen  $^1O_2$  is limited by the high activity of photochemistry and thermal dissipation, thus protecting PSII from light-induced oxidative damage (Erickson et al 2015, Muller et al 2001). Thermal dissipation has been studied through the analysis of Chl *a*

fluorescence emission (Maxwell & Johnson 2000). A reduction in Chl *a* fluorescence yield, coupled with a decline in PSII photochemistry, is linked to the photoprotective ability, commonly referred to as non-photochemical quenching (NPQ; **Fig. 7**). NPQ comprises a series of photoprotective mechanisms to avoid photodamage, activated during the disbalance of the photosynthetic electron transport and the availability of ADP and NADP<sup>+</sup>. Such condition can trigger a highly reduced state of plastoquinone (PQ) and the acidification of the thylakoid lumen, thus activating NPQ mechanisms. These allow the capacity to dissipate light energy excess and redistributed it from the antennas to PSI and PSII (Eberhard et al 2008).

Acidification of the lumen pH (qE), constitutes the most rapidly responding mechanism of NPQ, manifested by a reduction in PSII fluorescence yield that corresponds to variations of pH within the thylakoid membrane. This process is often associated with the xanthophyll cycle, specifically involving the de-epoxidation of violaxanthin to zeaxanthin, activated by a low luminal pH. This process is reversible, but slower than the de-epoxidation. In *Chlamydomonas* the PsbS and the light harvesting complex stress related 3 (LHCSR3) proteins have been identified as associated regulators of qE (Bonente et al 2011, Redekop et al 2020).

The reduced state of PQ activates a serine/threonine kinase protein STT7 in *Chlamydomonas* (STN7 in *Arabidopsis thaliana*) which phosphorylates serine or threonine residues in the LHCII. *Chlamydomonas* presents a higher extent of state transition, reaching 85%, compared to *Arabidopsis thaliana* (hereafter *Arabidopsis*) which instead has only 20-25 %. This mechanism is known as state transition (qT) and it is linked with reversible phosphorylation of light antenna harvesting complexes (LHCII) attached to PSII. When phosphorylated, LHCII migrate towards PSI (state II), and dephosphorylation returns the LHCII protein to PSII (state I) (Minagawa 2013). Experimentally, this process can be chemically induced by using PSII inhibitor 3-(3,4-dichlorophenyl)-1,1-dimethylurea (DCMU) and the uncoupler carbonyl cyanide-p-trifluoromethoxyphenylhydrazone (FCCP) to force cells to reach full state I and full state II respectively, or by submitting the cells to different light exposure times (Finazzi et al 1999). Fluorescence of PSII and PSI can be measured at a low temperature of 77 K following the peaks corresponding to PSII (state I) and PSI (state II) Photoinhibition (qI) is connected to oxidative damage induced by

high light, wherein the D1 protein of the reaction center of PSII is degraded and replaced by a newly synthesized one (Aro et al 1993). Moreover, photoinhibition is proposed to control the electron transport to PSI, preventing irreversible damage that could result from exceeding the capacity of the electron acceptor. However, the exact mechanism is still unclear (Tikkanen et al 2014). Nonetheless, recent studies have shown that the qI is formed in the core of PSII. The authors elucidated its mechanism mainly during high light exposure and demonstrated that its depletion occurs through a gradual light-independent process caused by the degradation of PSII core subunits (Nawrocki et al 2021).

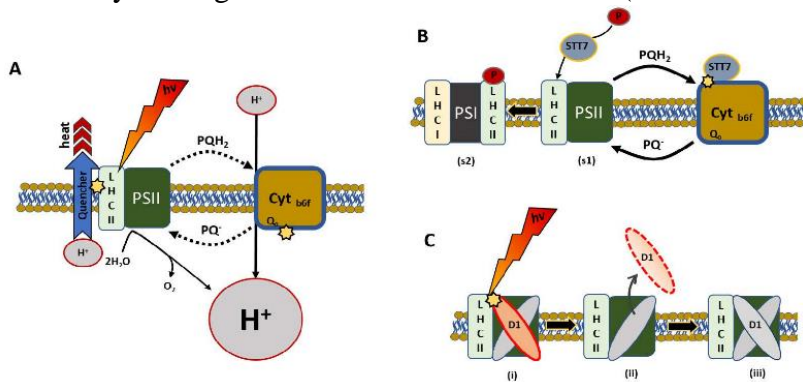


**Figure 7: Representation of the main photoprotective mechanisms of the NPQ to avoid photodamage.** **A)** Activation of the energy-dependent component (qE) due to the light-dependent acidification of the lumen which induces a decrease in Cyt *b<sub>6</sub>f* turnover (photosynthetic control). **B)** State transition (qT) component. Upon plastoquinone-pool (PQ) reduction, the thylakoid-associated protein kinase (STT7 in *Chlamydomonas*) phosphorylates the light harvesting complex (LHCII) antenna bounded to PSII (state I) inducing their migration and association with PSI (State II). **C)** Photoinhibition (qI) and repair cycle is illustrated. i) Photoinhibited PSII is in a quenched state (qI) and the D1 core subunit is damaged; ii) damaged D1 core subunit is disassembled and iii) replaced with a new copy of the protein. Figure taken from (Iacono 2023)

As mentioned above, reactive oxygen species (ROS) are generated during photosynthesis and participate in guiding some photosynthetic process, like CEF or water-water-cycle (described in 1.2.1 section) or regulate the action of some components, like the subunit  $\gamma$  of the ATP synthase. Before going into detail in the formation of the reactive oxygen species (ROS) and their specific role during photosynthesis, I would like to focus on one of the players of the LEF and CEF, the electron carrier plastocyanin, important in the context of the study of the

function of the APX2 enzyme. As a copper-containing protein, plastocyanin regulation is dependent on the availability of this micronutrient, crucial for photosynthesis. The next paragraph provides a concise overview of the information related to the copper-dependent plastocyanin regulation and copper distribution.

#### *1.1.4 On the regulation of the cupro-electron carrier plastocyanin and copper distribution*

One of the main actors of the linear and the cyclic electron flows is the cupro-protein electron carrier plastocyanin, which delivers electrons from Cyt *b<sub>6</sub>f* to PSI. Plastocyanin consists of an eight-stranded antiparallel  $\beta$ -barrel (about 100 residues) (Hill et al 1996) and it has been intensively studied in *Chlamydomonas*. A lot of information is available on its function and gene expression. Nevertheless, details about the proteins participating in its biogenesis remain unclear.

The synthesis of plastocyanin depends on the intracellular copper concentration, which in standard laboratory media conditions is 6  $\mu$ M (Hutner et al 1950). Pre-apoplastocyanin is imported into the chloroplast and then in the thylakoid lumen through a secretory pathway (SEC; (Smeekens et al 1986). Therefore, plastocyanin folding occurs inside the thylakoid, where it initially folds in the apo-form. Apoplastocyanin requires a cyclin for a trans-cis isomerization of two prolyl residues (P16 and P36), for the binding with a copper ion to attain its holo-form, as shown *in vitro* by Koide and coauthors (Koide et al 1993). In the study the authors demonstrated that the folding process of apoplastocyanin occurs in two slow steps with a formation of an unfolded intermediate with the mentioned proline residues cited above in trans or trans and cis. In presence of a cyclin, both steps accelerated with a factor of 2.1 for the first and 3.9 for the second step. In the first step P36 undergoes cis isomerization, while in the second step the isomerization of P16 is essential for the fully folded native form of apoplastocyanin. <sup>1</sup>D NMR, circular dichroism, and fluorescence of tyrosine techniques were used to monitor the folding process. As of now, there is no identified cyclin participating in the *in vivo* isomerization of apo-plastocyanin. The active site of plastocyanin, designed for one copper ion and responsible for redox function, comprises a cysteinyl thiolate, a methionyl sulfur, and two imidazole nitrogens of histidines (Hill et al 1996, Zhang et al 2023). Upon copper ligation, plastocyanin is ready to work as an electron carrier between Cyt *b<sub>6</sub>f* and

PSI. Plastocyanin is one of the most abundant proteins in *Chlamydomonas*, with  $\sim 8 \times 10^6$  molecules per cell (Kropat et al 2015). However, under conditions of copper deficiency in *Chlamydomonas* cells, defined as levels below 20 nM, plastocyanin undergoes a functional substitution by the iron-containing protein cytochrome  $c_6$  (Cyt  $c_6$ ) (Kropat et al 2005, Quinn & Merchant 1995). In this condition, the plastocyanin gene is still expressed, as its expression does not depend on copper concentration. Plastocyanin regulation occurs post-transcriptionally and in copper deficiency condition it is folded into its apo-form and degraded as the cell would not need it in copper deficient conditions (Hill & Merchant 1992).

Within the cell, copper can exist in two forms: cupric ( $\text{Cu}^{2+}$ ) and cuprous ( $\text{Cu}^+$ ). Copper, initially in the form of  $\text{Cu}^{2+}$ , undergoes reduction by cupric reductase localized in the cell surface (Georgatsou et al 1997, Hanikenne et al 2005), resulting in its insertion into the cell as  $\text{Cu}^+$ . The process of copper uptake has been extensively described in *Chlamydomonas* (Hill et al 1996). Given the toxicity of copper and its potential to generate harmful reactive oxygen species (ROS), various Cu-chaperones are present to mitigate oxidative stress. The chaperone antioxidant 1 (ATX1) has been identified (Pham et al 2022). It is localized in the cytosol and plays a role in distributing copper from copper transporters-like (CTR-like) and/or glutathione (GSH) at the plasma membrane to the secretory pathway. Additionally, there are other putative chaperones, such as the plastid copper chaperone (PCC1), structurally similar to ATX1 and downregulated under copper deficiency (Castruita et al 2011). Another candidate is plastid chaperone 1 (PCH1), derived from an alternative splicing of the copper transporter 2 (CTP2) (Blaby-Haas et al 2014). In *Arabidopsis*, PCH1 has been demonstrated to deliver copper to the  $\text{P}_{1\text{B}}$ -type ATPase PAA1, ortholog of CTP2, of the inner chloroplast membrane (Blaby-Haas et al 2014). The regulation of intracellular copper homeostasis and distribution involves a series of gene expressions dependent on the availability of copper (Merchant et al 2020). In eukaryotes, the transporters involved in copper reduction localized on the cell surface belong to the CTR family (Hanikenne et al 2005) (**Fig. 8**). *Chlamydomonas* presents four proteins belonging to the CTR family: copper transporter 1 (COPT1) and CTR1, CTR2 and CTR3. *Chlamydomonas* COPT1 might be localized in the plasma membrane and its homolog is the *Arabidopsis* COPT1. The expression of *COPT1* in *Arabidopsis* is regulated by copper

availability and in copper deficiency conditions, is up-regulated by SQUAMOSA PROMOTER-BINDING PROTEIN-LIKE 7 (SPL7), a central regulator for copper homeostasis (Hanikenne et al 2005, He et al 2023). COPT1 of *Chlamydomonas* is not regulated by copper availability and based on the mRNA abundance, does not seem to be quantitatively important in copper deficiency conditions (Page et al 2009).

The homolog of SPL7 in *Chlamydomonas* is copper response regulator 1 (CRR1), a global regulator of nutritional copper signaling which governs the expression of a series of 58 genes required in copper deficient conditions (Kropat et al 2015, Sommer et al 2010). One of the genes is Cyt  $c_6$ , which serves as functional substitute of plastocyanin in the absence of copper (Kropat et al 2015). CTR1/2/3, instead, form a distinct family and their function in *Chlamydomonas* is not yet well established, but they might be localized in the plasma membrane controlling copper import (Blaby-Haas & Merchant 2012, Hanikenne et al 2005). Another transporter family that has been described in *Chlamydomonas* and briefly mentioned above, is the P-type ATPase of the class IB (P<sub>IB</sub>-type-ATPase) which presents five members named CTP1, CTP2, CTP3 and CTP4 (copper transporters) and heavy-metal-associated 1 (HMA1) (Blaby-Haas & Merchant 2012, Hanikenne et al 2005). These pumps operate based on the hydrolysis of ATP, concentrating copper ions inside the cell or expelling them outside. CTP1 is the orthologous of the yeast cytosolic copper chaperone (Ccc2) and human P-type ATPase (ATP7A and ATP7B for Menkes and Wilson diseases respectively) that delivers copper in the secretory pathway where it is used to assembly proteins like ferroxidases and peptidylglycyl  $\alpha$ -amidating monooxygenase (PAM) (El Meskini et al 2003). CTP2 and CTP4 are homologous of the P-type ATPase transporters PAA1 and PAA2 in *Arabidopsis* respectively and they are localized in the chloroplast and thylakoid membranes respectively. They function to pump copper inside the thylakoid for plastocyanin assembly (Abdel-Ghany et al 2005). The role of CTP3 is not yet defined but it seems to be involved in pumping copper in endosomes or vacuoles, for copper detoxification (Merchant et al 2020). Lastly, *Chlamydomonas* HMA1 is the orthologous of the HMA1 in *Arabidopsis* localized in the chloroplast membrane. Previous study suggested that it is involved in the transport of copper into the stroma (Abdel-Ghany et al 2005). However, several studies have shown a wide ion specificity of this transporter for  $\text{Cu}^{2+}$ ,  $\text{Ca}^{2+}$ ,  $\text{Cd}^{2+}$  and  $\text{Zn}^{2+}$  whose function then it is still



under debate (Boutigny et al 2014, Kim et al 2009b, Moreno et al 2008, Seigneurin-Berny et al 2006).

Despite the comprehensive knowledge about copper metabolism and distribution, some questions are still to be answered (*e.g.* if other genes are CRR1 targets or how the copper signaling is regulated in other microorganisms), making this topic appealing for future investigations (Merchant et al 2020).

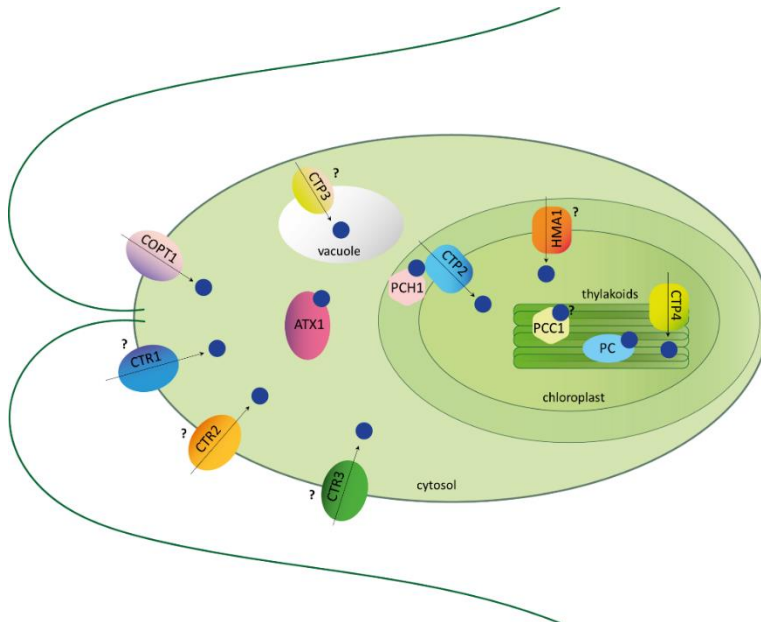


**Figure 8: Copper transporters in Chlamydomonas and their putative localization.** Scheme of Chlamydomonas cell with transporters of plasma membranes COPT1, CTR1, CTR2 and CTR3 which import  $\text{Cu}^+$ , indicated as blue sphere, in the cytosol; CTP3 transporter in the vacuole to import  $\text{Cu}^+$  for detoxification; CTP2 transporter deliver  $\text{Cu}^+$  in the chloroplast and CTP4 in the thylakoids; HMA1 might transport  $\text{Cu}^+$  inside the chloroplast or  $\text{Zn}$  outside chloroplast. ATX1 cytosol chaperone, PCH1 which delivers  $\text{Cu}^+$  to CTP2 and putative chaperone PCC plastid copper chaperones. PC is plastocyanin, blue dots are  $\text{Cu}^+$  and the white dot is the zinc  $\text{Zn}^{2+}$ . Question marks indicate the putative role and localization of the protein indicated. In the case of HMA1 and PCC1, studies have been conducted on the Arabidopsis counterpart, so related findings are hypothesized also for Chlamydomonas.

## 1.2 The bad and the good of ROS

### 1.2.1 ROS molecules and scavenging enzymes

Under unfavorable environmental conditions, green eukaryotic cells encounter abiotic or biotic stress. These stresses induce the generation of reactive oxygen species (ROS) that can be harmful for the cell by oxidizing proteins, lipids, DNA, RNA, and in the worst case, causing cell death. In photosynthetic organisms, chloroplast is one of the main sites of ROS production together with mitochondria (Foyer, 2018). To limit the damage caused by these molecules, cells have developed protection systems, which involve antioxidant enzymes and other defense processes (**Fig. 9**) (Foyer 2018, Foyer & Shigeoka 2011, Mittler 2017).

ROS molecules derive from the reduction or oxidation of the atmospheric oxygen  $O_2$  which can be converted as superoxide radical  $O_2^{\cdot-}$  or singlet oxygen  $^1O_2$ . Superoxide  $O_2^{\cdot-}$  is produced during the electron transport of the chloroplasts (**Fig 5, 9**) and mitochondria and in peroxisomes. It reacts with iron-sulfur (Fe-S) proteins, with nitric oxide (NO) to produce peroxynitrite ( $ONOO^{\cdot}$ ) and can be scavenged by ascorbate, flavonoids or superoxide dismutase (SOD) forming  $H_2O_2$ .

$H_2O_2$  (**Fig. 5, 9**) is produced in mitochondria, chloroplasts, peroxisomes, cytosol and apoplast and reacts with cysteine and methionine residues of proteins, with heme-containing proteins and DNA. It is scavenged by a set of enzymes like catalases (CATs), ascorbate peroxidases (APXs), peroxiredoxins (PRXs), glutathione peroxidase (GPXs), peroxidases (PERs), but also the ascorbate-glutathione cycle (Foyer-Halliwell-Asada) (Asada 1999, Foyer & Halliwell 1976, Mittler 2017).

$H_2O_2$  reacts with  $Fe^{2+}$  in the Fenton reaction to form hydroxyl radical  $\cdot OH$  (Foyer & Hanke 2022).

Hydroxyl radical  $\cdot OH$  (**Fig. 5, 9**) is very reactive with lipids, proteins, RNA and DNA. It is scavenged by ascorbate, sugars, flavonoids, and prolines. Singlet oxygen  $^1O_2$  is produced in the chloroplast at the level of PSII (**Fig. 5; 9**) and oxidizes lipids, proteins, targeting residues such as tryptophan, histidine, cysteine, tyrosine, and methionine, as well as guanine in DNA. Its scavenging system comprises carotenoids and  $\alpha$ -tocopherol.

Among all the ROS molecules,  $H_2O_2$  presents the longest half-life, more than 1

ms, and can travel across the organelles more than 1  $\mu\text{m}$  away. The other ROS molecules ( $\text{O}_2^{\cdot-}$ ,  $^1\text{O}_2$ ,  $\cdot\text{OH}$ ) have a half-life in the order of  $\mu\text{s}$  - ns and can travel at a maximum distance of 30 nm (Mittler 2017).

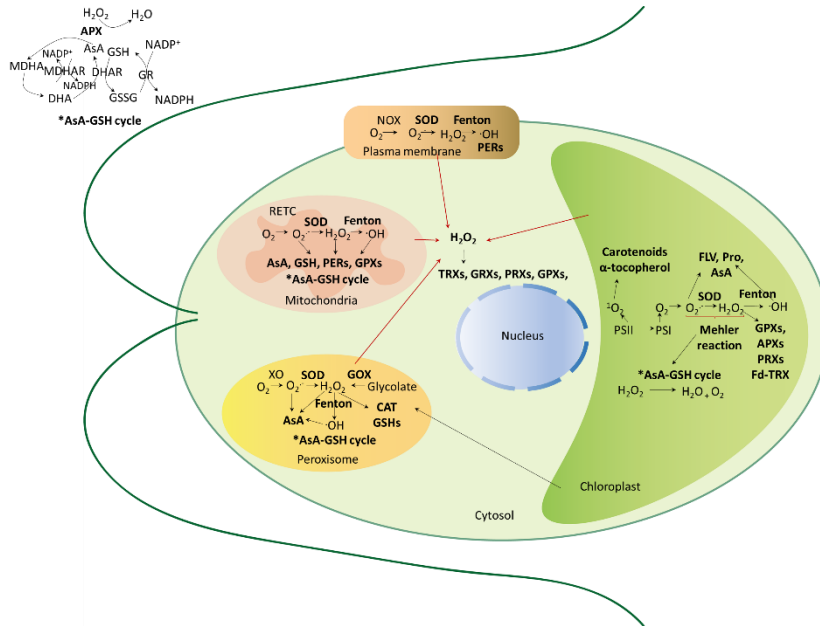


**Figure 9: Scheme of intracellular ROS production sites under stress conditions and ROS scavenging systems.** Plasma membrane:  $\text{O}_2^{\cdot-}$  is generated by NOX mediated oxidation of  $\text{O}_2$  and dismutates to  $\text{H}_2\text{O}_2$  with SOD. With the Fenton reaction  $\text{H}_2\text{O}_2$  generates  $\cdot\text{OH}$ , scavenged by PERs. Chloroplast:  $^1\text{O}_2$  is produced at the level of PSII and scavenged by carotenoids and  $\alpha$ -tocopherol.  $\text{O}_2^{\cdot-}$  is produced at the acceptor side of PSI and can be scavenged by FLV or AsA or dismutates to  $\text{H}_2\text{O}_2$  with SOD.  $\text{H}_2\text{O}_2$  is scavenged by the Mehler reaction using APX and AsA or by GPXs, APXs, PRXs, Fd-TRX. With the Fenton reaction  $\text{H}_2\text{O}_2$  generates  $\cdot\text{OH}$  that can be scavenged by FLV, Pro, Asa. Peroxisome:  $\text{O}_2$  is converted to  $\text{O}_2^{\cdot-}$  by XO and is scavenged by AsA or dismutates by SOD in  $\text{H}_2\text{O}_2$  or  $\text{H}_2\text{O}_2$  can be generated by GOX.  $\text{H}_2\text{O}_2$  can be scavenged by AsA, CAT, GSHs, PERs. With the Fenton reaction  $\text{H}_2\text{O}_2$  generates  $\cdot\text{OH}$  scavenged by AsA. Mitochondria:  $\text{O}_2^{\cdot-}$  is generated during RETC and dismutates with SOD to  $\text{H}_2\text{O}_2$ . With the Fenton reaction  $\text{H}_2\text{O}_2$  generates  $\cdot\text{OH}$ . All the ROS produced can be scavenged by AsA, GSH, PERs, GPXs. Cytosol: isoforms of TRXs, GRXs, PRXs and GPXs are implicated in  $\text{H}_2\text{O}_2$  detoxification. AsA-GSH cycle: APX converts  $\text{H}_2\text{O}_2$  into  $\text{H}_2\text{O}$  using AsA which oxidizes into MDHA. With MDHAR, MDHA gives an electron to reduce  $\text{NADP}^+$  into  $\text{NADPH}$ , thus becoming oxidized to DHA. DHA is re-converted into AsA with DHAR using GSH forming GSSG which is reduced again to GSH with GR and  $\text{NADPH}$ . APXs, ascorbate peroxidases; AsA, ascorbate; DHA, dehydroascorbate; DHAR, dehydroascorbate reductase; Fd-TRX, ferredoxin-thioredoxin system; FLV, flavodi-iron proteins; GOX, glucose oxidase; GPXs, glutathione peroxidases; GR, glutathione reductase; GSH, reduced glutathione; GSSG, oxidized glutathione; MDHA, monodehydroascorbate; MDHAR, monodehydroascorbate reductase; PERs, peroxidases; PETC, photosynthetic electron transport chain; PRXs, peroxiredoxins; RETC, respiratory electron transport chain; SOD, superoxide dismutase; XO, xanthine oxidase.

In photosynthetic organisms, excess of ROS production occurs due to photo-oxidation during light-driven processes including the electron transport (section 1.1.3.). ROS are specially produced at PSII and PSI levels (**Fig. 5**). PSII drives the oxidation of H<sub>2</sub>O to O<sub>2</sub> and the reduction of plastoquinone (PQ) to plastoquinol (PQH<sub>2</sub>) with a series of reactions that release four electrons to the lumen from the oxidation of two H<sub>2</sub>O molecules to O<sub>2</sub>. When the energy surpasses the threshold, the chlorophyll *a* within the light-harvesting complexes of PSII transitions to its excited triplet Chl *a* state (<sup>3</sup>Chl), which can be quenched by carotenoids. Alternatively, due to their increased lifespan, <sup>3</sup>Chl transfers the energy to the ground state of O<sub>2</sub>, forming <sup>1</sup>O<sub>2</sub> (Li & Kim 2022, Pospisil 2016). A group of carotenoids associated with the light harvesting complexes can quench and reduce the damage caused by <sup>1</sup>O<sub>2</sub> (Dogra et al 2018, Li & Kim 2022). <sup>1</sup>O<sub>2</sub> can be also formed via the excited state of P680 (<sup>3</sup>P680) when the electron transfer is over reduced (Li & Kim 2022).

Superoxide anion O<sub>2</sub><sup>-</sup>, instead, is formed through the one-electron reduction of O<sub>2</sub>, and it is spontaneously converted by dismutation into hydrogen peroxide H<sub>2</sub>O<sub>2</sub> which in turn produces hydroxyl radical ·OH via Fenton reaction (Pospisil 2016). A plastoquinol terminal oxidase enzyme (PTOX) is one of the actors responsible for scavenging ROS molecules by accepting electrons from PSII. This enzyme presents several functions that occur during the dark or light phase. In the dark, PTOX is involved in chloro-respiration, by catalyzing non-photochemical reactions to oxidize plastoquinol and limit overoxidation of plastoquinone to avoid oxidative damage. During the light, PTOX can play diverse roles, such as pigment biosynthesis, carotenoid biosynthesis which can scavenge the excess of absorbed light and/or ROS molecules (**Fig. 10**) (Curien et al 2016, Krieger-Liszky & Feilke 2015).

In the same condition of energy excess, at the acceptor side of PSI, O<sub>2</sub> is reduced to form O<sub>2</sub><sup>-</sup> where superoxide dismutase (SOD) converts O<sub>2</sub><sup>-</sup> into H<sub>2</sub>O<sub>2</sub>, in the so-called Mehler reaction (Mehler 1951). H<sub>2</sub>O<sub>2</sub> is scavenged by the ascorbate-glutathione cycle in which ascorbate peroxidase reduces H<sub>2</sub>O<sub>2</sub> into H<sub>2</sub>O and O<sub>2</sub> (process called water-water-cycle) by using ascorbate which is converted into monodehydroascorbate or dehydroascorbate (Asada 1999, Curien et al 2016). The enzyme monodehydroascorbate reductase (MDAR) regenerates ascorbate using NADPH (Hossain et al 1984), while dehydroascorbate reductase (DHAR) uses glutathione to regenerate ascorbate (Hossain & Asada 1984). Glutathione is regenerated by glutathione reductase (GR) and NADPH (Foyer & Shigeoka 2011). Moreover, in green algae, cyanobacteria and mosses, the presence of flavodi-iron (FLV) proteins at the stromal side of PSI catalyzes the NADPH-dependent reaction to reduce O<sub>2</sub> to H<sub>2</sub>O. The photoreduction of O<sub>2</sub> dependent from FLV proteins in *Chlamydomonas* is mainly present during dark-light

transition and these proteins are necessary in fluctuating light conditions (**Fig. 9**) (Chaux et al 2017). Other scavenging enzymes at the acceptor side of PSI that are working to limit the oxidative damage are 2-cys peroxiredoxins (2-Cys PRXs), whose activity depends on glutathione or glutaredoxin/thioredoxins (Dietz 2016). In plants it has been found that these enzymes are also involved in water-water-cycle by detoxifying H<sub>2</sub>O<sub>2</sub> into H<sub>2</sub>O and O<sub>2</sub>. Upon overoxidation, 2-Cys PRXs can change conformation and function, becoming chaperone proteins (Dietz 2016). Oxidized PRXs are regenerated by reduction via the thioredoxin (TRX) system (Dietz 2011, Nikkanen & Rintamäki 2019, Pascual et al 2011, Pulido et al 2010). Two main TRX systems exist in chloroplasts with different sources of reducing power. The ferredoxin-thioredoxin reductase (FTR), involved in the ferredoxin-thioredoxin (Fd-TRX) system activates the classical chloroplast TRXs (with the typical conserved motif WCG/PPC (Chibani et al 2021)) by receiving reducing equivalent from reduced ferredoxin (Schurmann & Buchanan 2008). Control under the Fd-TRX system prevails under constant illumination of growth and higher light intensities. The second system relies on a NADPH-dependent chloroplast thioredoxin reductase (NTRC) that is reduced by NADPH (Serrato et al 2004). These systems are known to regulate different processes, such as chloroplast biogenesis, plastid transcription, ATP synthesis, carbon fixation, ROS strictly related to photosynthesis (Nikkanen & Rintamäki 2019). Indeed, NTRC can also efficiently reduce chloroplast PRXs, by balancing chloroplast redox poise. NTRC is an important redox regulator of photosynthesis during the inductive period of dark–light and low–high light transitions and under light intensities that are lower than what plants are acclimated during the growth (Nikkanen & Rintamäki 2019). Recently, it has been shown that NTRC activity is regulated by a Ca<sup>2+</sup>-dependent thioredoxin (TRX) chloroplast-localized calredoxin (CRX) (Zinzius et al 2023). Calredoxin is present in the green algal lineage and some Dinophyceae, which was found to interact with the 2-cysteine peroxiredoxin PRX1 (2-Cys PRX1) in *Chlamydomonas* (Charoenwattanasatien et al 2020, Hochmal et al 2016). *In vitro* the Ca<sup>2+</sup>-binding domain of CRX controls the redox activity of the TRX domain (Hochmal et al 2016). CRX is involved in redox regulation and ROS scavenging after being induced by autotrophic and/or high light conditions (Hochmal et al 2016). Experiments conducted in *Chlamydomonas* mutants of CRX revealed severe decrease in growth under high light conditions, in addition to an impact on CO<sub>2</sub> fixation (Zinzius et al 2023). In the same study, the authors also showed that CRX inhibits electron transfer from NTRC to 2-Cys PRX1 under high light growing conditions, a mechanism dependent on the presence of Ca<sup>2+</sup>. The CRX-

dependent chloroplast redox regulation is essential for a robust and efficient photosynthesis in *Chlamydomonas*.

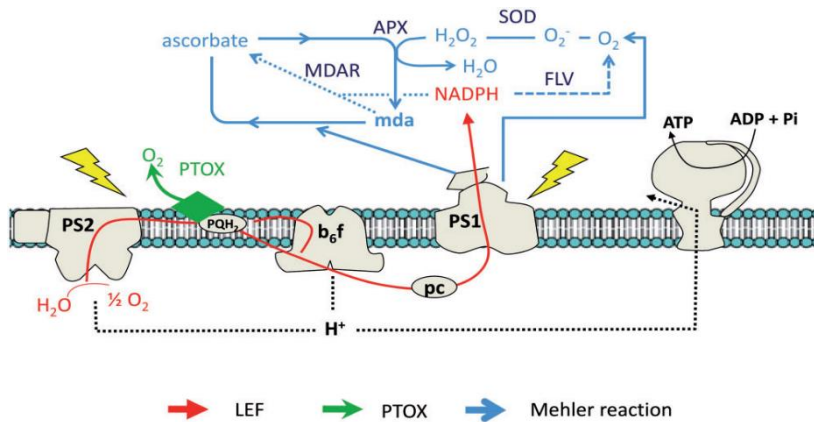


**Figure 10: Schematic processes of PTOX and Mehler reaction during photosynthetic electron transport.** Plastoquinol terminal oxidase (PTOX) reduces  $O_2$  by oxidizing plastoquinol ( $PQH_2$ ; green line). This reaction avoids over-reduction of plastoquinone and reduces the efficiency of linear electron flow (LEF) from  $H_2O$  to NADPH, competing with plastoquinol oxidation through Cyt  $b_6f$  (red line). In the Mehler reaction the reduction of the electron acceptor  $O_2$  at the stromal side of PSI generates  $O_2^-$  (blue solid line). With superoxide dismutase (SOD)  $O_2^-$  is dismutated to  $H_2O_2$  and  $O_2$ . Ascorbate peroxidase (APX) reduces  $H_2O_2$  using ascorbate to form  $H_2O$  and monodehydroascorbate (MDA; solid lines). MDA is an efficient electron sink that can be reduced either by electrons coming from PSI or in a reaction mediated by monodehydroascorbate reductase (MDAR; dotted lines) consuming NADPH. Flavodi-iron (FLV) proteins are involved in the  $O_2$  reduction using NADPH as electron donor (dashed lines). From (Curien et al 2016).

### 1.2.1.1 ROS scavenging enzyme isoforms

ROS scavenging enzymes exist in several isoforms which are distributed in different organelles and cell compartments like chloroplasts, mitochondria, peroxisome, cilia and plasma membrane. In *Chlamydomonas*, the superfamily of TRXs presents ten isoforms classified as TRXh1, TRXh2, putatively localized in the cytosol, TRXo putatively localized in the mitochondria, TRXm, TRXx, TRXy, TRXf1 and TRXf2 putatively localized in the chloroplast and dynein light chains (DLC14, DLC16) putatively localized in the cilia and most probably involved in the redox control of dynein activity (Lemaire & Miginiac-Maslow 2004). Within the TRX superfamily, there exist five isoforms of glutaredoxins

(GRXs) and fifteen isoforms of glutathione-S-transferases (GSTs). GRXs are classified in several groups with GRX1 and GRX2 having a CPYC active site (putatively localized in the cytosol), and GRX3 (Group III, putatively localized in mitochondria or chloroplast), GRX4 (Group I, putatively localized in the cytosol), GRX5 (Group II, putatively localized in mitochondria or chloroplast) and GRX6 (Group IV, putatively localized in the chloroplast) with CGFS active site sequence motif (Lemaire & Miginiac-Maslow 2004). GSTs presents fifteen isoforms named from GST1 to GST15. A study conducted on two of them, GST7 and GST10, showed that the GST enzymes might be useful for bioremediation and environmental application (Chatzikonstantinou et al 2017). Within the TRX family, there are also enzymes such as nucleoredoxin (NRXs) and sulfiredoxin (SRXs) enzymes (Kneeshaw et al 2017). *Chlamydomonas* possesses four isoforms of NRX, NRX1, NRX2, NRX3 and NRX4, whose localisation is not yet defined, and two isoforms of SRX, SRX1 and SRX2 from which SRX2 is putatively localized in the chloroplast (Blaby et al 2015). Regarding PRXs, *Chlamydomonas* possesses seven isoforms distributed as follows: two 2-Cys PRX (PRX1 and PRX2, putatively localized in the chloroplast and cytosol/cilia respectively), type II PRX (PRX3, PRX4, PRX5 putatively localized in cytosol/cilia, mitochondria and chloroplast respectively), PRX-Q (PRX6, putatively localized in chloroplast) and 2 Cys PRX/TRX fusion (PRX7, putatively localized in mitochondria) (Dayer et al 2008). Five isoforms of GPXs are present, distributed in chloroplast and/or mitochondria and cytosol (Dayer et al 2008). GPX1 and GPX2 putatively localized in mitochondria and/or chloroplast, GPX3 in mitochondria or chloroplast, GPX4 in cytosol or plasma membrane, and GPX5 in cytosol (short form) and chloroplast (long form) (Dayer et al 2008). *Chlamydomonas* has six genes encoding for superoxide dismutase (SOD), comprising five manganese SOD (MnSOD) and one iron SOD (FeSOD). MnSOD2 is putatively mitochondrial, while MnSOD3 together with FeSOD are chloroplastic. The sequence analysis of the remaining MnSOD enzymes (MnSOD1, MnSOD4, and MnSOD5) indicates potential specialized functions. For instance, MnSOD3 is induced under low iron and manganese concentrations as well as in the presence of H<sub>2</sub>O<sub>2</sub>. It plays a crucial role in conserving metals under conditions of metal limitation (Page et al 2012). However, it is conceivable that MnSOD4 and MnSOD5 could be localized in the secretory pathway (Blaby et al 2015).

Two CATs isoforms have been identified in *Chlamydomonas*, CAT1 in peroxisome and CAT2 (annotated as catalase/oxidase) in the endoplasmic reticulum (Kato et al 2021). The extensive PERs family comprises two major protein families distinguished by the presence or absence of heme. Heme-containing peroxidases encompass the non-animal peroxidases superfamily, constituting the most diverse group in terms of taxonomic distribution. There are three classes: Class I, II, III. Class I is the largest peroxidase class found in plants and algae. This class is divided in four subgroups: (i) catalase/oxidases (CAT2 in *Chlamydomonas*), which are mainly found in bacteria but also in other organisms due to the horizontal gene transfer; (ii) ascorbate peroxidases (APX1, APX2, APX4 in *Chlamydomonas*) mainly found in green eukaryotes; (iii) cytochrome *c* peroxidases (CcP, one isoform in *Chlamydomonas*) found in all organisms within mitochondria except plants; and (iv) hybrid APX-CcP (so far no evidence of presence of this enzyme in *Chlamydomonas*) mostly found in eukaryotes except plants. Class II has been described only in fungi able to degrade wood and includes lignin peroxidases (LiPs), manganese peroxidases (MnPs), and versatile peroxidases (VPs). Class III has been found in plants and has been described as potential multifunctional proteins that might be involved in different pathways like auxin metabolism, cell wall elongation and stiffening, and protection against pathogens. Enzymes of this class have been detected in some Streptophyta, but absent in Chlorophyta (Mbadinga Mbadinga et al 2020).

#### *1.2.1.2 Class I peroxidase: APX2*

Among the ROS scavenging enzymes described, my attention is focused on the recent classification of the APXs included in Class I of peroxidases. From the Mehler reaction it is known that APX converts  $H_2O_2$  into  $H_2O$  and  $O_2$  using ascorbate as reductant (Mehler 1951). However, recent studies have reclassified APXs enzymes according to differences in their sequences, in particular considering the absence of the amino acids responsible for ascorbate binding, heme binding, and peroxidase activity present in the classic APX (Granlund et al 2009, Lazzarotto et al 2021a). For this reason, APXs have been categorized into (classic) APX, APX-related (APX-R), which lacks only the amino acid responsible for binding ascorbate and APX-like (APX-L), which instead lacks all the amino acids responsible for ascorbate and heme binding, and those for peroxidase activity (Lazzarotto et al 2021a). To date, information on APX-L is



available for both *Arabidopsis* and *Chlamydomonas*. In *Arabidopsis*, it has been shown that the APX-L (AtAPX4) is associated with PSII and most probably is involved in PSII photoprotection (Granlund et al 2009), while in *Chlamydomonas*, APX-L (CrAPX4) is important under very high light conditions for protecting the cell (Kuo et al 2020a). Concerning the APX-R, the information available is related to land plants. In *Arabidopsis* (AtAPX6) it has been found that the enzyme might be involved in photomorphogenesis, senescence, or seed germination (Chen et al 2021, Chen et al 2014, Lazzarotto et al 2021b). Moreover, it has been proposed that its expression might be regulated by copper deficiency and in particular being suppressed by miR398 regulated by SPL7, general copper regulator in *Arabidopsis* (Chen et al 2021). In addition, *in vitro* experiments on purified protein have confirmed that the APX-R does not utilize ascorbate to reduce H<sub>2</sub>O<sub>2</sub>, but other compounds like guaiacol or pyrogallol (Lazzarotto et al 2021b). Mutants in *Oryza sativa* that were impacted in APX-R exhibited a growth delay. The expression of APX-R was observed under various stress conditions, revealing an up-regulation in response to cold, drought, or the presence of aluminum (Lazzarotto et al 2011). In *Triticum aestivum* and *Brassica rapa*, APX-R expression was modulated under different stress conditions during cold, heat, drought stress, salt stress showing down or up regulation of the enzyme in different tissues and at different time points after stress induction (Tyagi et al 2020, Verma et al 2022). However, the exact mechanism of APX-R is not yet known and the *in vivo* substrate is yet to be identified. The specific properties of this new classified APX-R enzyme, makes it challenging and interesting to study, particularly as it retains peroxidase activity without binding ascorbate. More and exhaustive information about our new findings on the APX-R of *Chlamydomonas* (APX2) are described in **chapters III, IV, V**.

Although there are various processes for scavenging reactive oxygen species (ROS), it doesn't rule out the possibility that ROS can also be beneficial for the cell. In physiological conditions, in the absence of a stressful environment, ROS can serve as signaling molecules, modifying proteins, altering their function, and triggering gene expressions.

### *1.2.2 ROS as signaling molecules: a sight on H<sub>2</sub>O<sub>2</sub>-dependent modifications*

Recent findings demonstrate that ROS also contribute positively to cell physiology. Indeed, they can act as messenger molecules participating in cell metabolism by modifying proteins and changing their function. For instance, ROS participate in intra-organelles crosstalk via anterograde signaling (from nucleus to the organelles) or via retrograde signaling (from organelles to the nucleus). The most studied signaling molecule is the H<sub>2</sub>O<sub>2</sub>, due to its extended lifespan and longer migration distance (Mittler 2017).

H<sub>2</sub>O<sub>2</sub> modifies sulfur-containing cysteine and methionine residues of proteins in their oxidized form. Such modification leads proteins to change both their conformation and function, allowing them to participate in different physiological and metabolic processes. These modifications can also trigger signals to activate or deactivate a specific gene inside the nucleus (Roos & Messens 2011).

In cysteine residues, the thiol group (-SH) is highly nucleophilic and highly reactive. These properties increase when the thiol is deprotonated (-S<sup>-</sup>) and the oxidation of two deprotonated thiols forms a disulfide bond (S-S). This oxidation state can be reverted back again to the thiol form through the action of glutaredoxins or thioredoxins. In presence of H<sub>2</sub>O<sub>2</sub>, a two-electron oxidant, thiols are oxidized to their sulfenylated form (-SOH). This modification exhibits both nucleophilic and electrophilic properties, rendering it highly unstable and reactive. It can be spontaneously reduced and reverted to the original thiol state or sulfenic acid can be further oxidized to its sulfinylated -SO<sub>2</sub>H or sulfonylated -SO<sub>3</sub>H forms which are irreversible. The highest oxidation form might also lead to protein aggregation or degradation (**Fig. 11**) (Roos & Messens 2011).

Nonetheless, the sulfinylated form of 2-cys peroxiredoxins can be reduced back to its sulfenylated form thanks to sulfiredoxin enzyme, working together with ATP. On the other hand, overoxidation leads to 2-cys peroxiredoxin changing its conformation and function as chaperone (Dietz 2011).

Sulfenic acid can also react with an amine or amide to form sulfenilamide (S-N) or with another sulfenic acid to form a thiosulfinate (RS(O)SR) (**Fig. 11**) (Roos & Messens 2011).

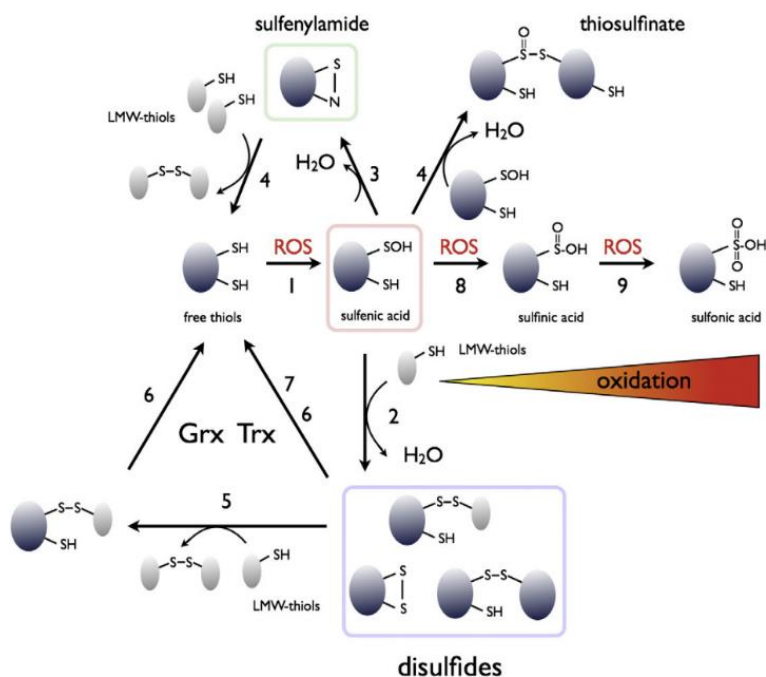


**Figure 11: Scheme of the cysteine oxidation mediated by H<sub>2</sub>O<sub>2</sub>.** 1) Free thiols are oxidized by ROS to their sulfenic form (-SOH). 2) Reaction between a low-molecular-weight thiols (LMW-thiols) and the sulfenic acid leads to the formation of disulfides. 3) Sulfenic acid can react with a nitric oxide (NO) to form a sulfenylamide which in presence of LMW-thiols (4) can release disulfide and free thiols again. 5, 6, 7) Disulfides can react with glutaredoxin (Grx) or thioredoxin (Trx) and LMW-thiols to regenerate free thiols. In conditions of overoxidation, sulfenic acid can be oxidized in its sulfinic form (-SO<sub>2</sub>H; 8) or sulphonic form (-SO<sub>3</sub>H; 9). From (Roos & Messens 2011).

The biological meaning of these modifications results in adjustment of physiology and metabolic processes within the cell. As mentioned above ROS can act as messengers or in the specific case of H<sub>2</sub>O<sub>2</sub>, can also travel across the membrane reaching different organelles. Such communication helps the cell to respond to diverse stimuli (*e.g.* growth, abiotic and biotic stresses, solute transport, autophagy...) and contributes to organelle biogenesis and photosynthesis. Redox control in the chloroplast involves numerous pathways which include ROS sensing proteins whose role is transmitting the information regarding the energy status to the nucleus. This depends on the environmental conditions, but the way in which this transmission occurs is not yet well understood. Moreover, chloroplasts are rich in cysteine-containing proteins that

can undergo modifications, regulating signals dependent on H<sub>2</sub>O<sub>2</sub> oxidation. Plants can tolerate abiotic stress by increasing the expression of antioxidants enzymes. However, this mechanism does not eliminate ROS produced in the chloroplast, but mainly prevent uncontrolled overoxidation and damage (Foyer & Hanke 2022, Li & Kim 2022, Wakao & Niyogi 2021).

Moreover, recent studies have advanced the idea that the H<sub>2</sub>O<sub>2</sub> produced in the chloroplast, is quite stable and can act as a messenger outside the chloroplast by regulating nuclear gene expressions modifying redox sensitive transcription factors (Exposito-Rodriguez et al 2017).

Several pathways have been demonstrated to generate H<sub>2</sub>O<sub>2</sub> along the photosynthetic electron transport chain, but the common thought suggests that the acceptor side of PSI generates enough H<sub>2</sub>O<sub>2</sub> for retrograde signaling (Lima-Melo et al 2021).

## 1.3 Identification of modified proteins

Post-translational modifications (PTMs) regulate the structure and the function of proteins, impacting cellular signaling and physiology (Corpas et al 2022). Among the various mechanisms of ROS sensing in cells, their reactivity with cysteine residues of proteins, seems to be the major oxidative post-translational modification (OxPTMs) (Mukherjee 2021). Cysteine thiols can be oxidized into their sulfenylated form (-SOH) by H<sub>2</sub>O<sub>2</sub>, or to their nitrosylated form (-SNO) by nitric acid (NO). Sulfenic acid or thiol-disulfide can react with reduced or oxidized form of glutathione, respectively, in a mechanism called S-glutathionylation to form -SSG.

Cysteine-associated PTMs have been studied to identify the related proteome patterns upon stress conditions. In *Chlamydomonas*, several techniques have been used to define such mentioned sets of modified proteins which are summarized below.

### 1.3.1 Glutathionylation

Glutathione is a tripeptide with the sequence  $\gamma$ -l-glutamyl-l-cysteinyl-glycine. It can exist in reduced form (GSH) and in oxidized form (GSSG), which is constantly reduced by glutathione reductase, using electrons coming from NADPH (Zaffagnini et al 2012). Glutathione is present in high abundance within the cell, reaching concentrations in the millimolar range, and is distributed across various compartments (Rouhier et al., 2008). In plants, it is involved in maintaining the redox balance, but also in xenobiotic detoxification, heavy metal detoxification and in general in cell signaling (Rouhier et al 2008). Glutathione can participate in a process called S-glutathionylation. This process is formed via ROS-mediated pathways, including (i) GSH reacting with the unstable oxidized sulfhydryl intermediates (R-SOH and thiyl radical S) induced by ROS; (ii) GSSG participating in a thiol-disulfide exchange with protein thiols; (iii) protein thiols reacting with GSH sulfenic acid form (GSOH) or glutathione radical (GS $\cdot$ ) (Li et al 2022). Initially, the role of S-glutathionylation was considered to serve protection to thiols from over-oxidation (sulfenylation – SOH and sulfinylation -SO<sub>2</sub>H). Recently, it has also increasingly been recognized as involved in cellular signaling (Li et al 2022). The study of S-glutathionylation has been conducted either in non-photosynthetic organisms like *Plasmodium falciparum* where 493

targets of S-glutathionylation were identified by affinity-purification of biotin-maleimide-tagged proteins (Kehr et al 2011), and photosynthetic organisms like *Arabidopsis* and *Chlamydomonas*. In two *in vitro* studies conducted on *Arabidopsis* cells suspension by using biotinylated glutathione, only two proteins in the first one (Ito et al 2003) and 79 proteins in the second one (Dixon et al 2005) were identified. The ones identified in the first study are involved in sugar metabolism (a cytosolic triose-phosphate isomerase and a putative chloroplastic aldolase), while in the second study are mostly involved in protein turnover, metabolism and glutathione transferase superfamily.

Two studies were also conducted in *Chlamydomonas*. In the first one, 25 glutathione targets were identified by radiolabelling [<sup>35</sup>S] cysteine. *Chlamydomonas* cell cultures were incubated with [<sup>35</sup>S] cysteine for 3 h and treated with diamide for 15 min. Proteins were extracted by two freeze/thaw cycles, precipitated with trichloroacetic acid, detected by two-dimensional gel electrophoresis and digested proteins were identified with matrix-assisted laser desorption ionization time-of-flight analysis (MALDI-TOF mass spectrometry). The identified proteins are involved in CBB cycle, stress related proteins, chaperones, amino acid, lipid and energy metabolism, acetate assimilation, translation, pentose phosphate pathway and flagella associated proteins (Michelet et al 2008).

In the second work, 225 glutathionylated sites were identified by biotinylated glutathione performed *in vivo* upon addition of H<sub>2</sub>O<sub>2</sub> or diamide and streptavidin affinity chromatography (Zaffagnini et al 2012). *Chlamydomonas* cell cultures were treated with the biotinylated form of glutathione N,N'-biotinyl glutathione disulfide (BioGSSG) for 1 h at room temperature in presence of H<sub>2</sub>O<sub>2</sub> or diamide (between 5 and 60 min). Three procedures were used to detect and identify S-glutathionylated proteins and cysteine glutathionylation sites. In the first one, glutathionylated proteins (R-SSGBiotin) were enriched with streptavidin, eluted with DTT analyzed by one- or two-dimensional electrophoresis and identified by MALDI-TOF and nanoLC-MS mass spectrometry. In the second one, glutathionylated proteins were alkylated and detected by immunoblot labelled with anti-biotin antibodies. In the third one, alkylated glutathionylated proteins were digested with trypsin, peptides were enriched with streptavidin, eluted with DTT and cysteine glutathionylation sites identified by tandem mass spectrometry. From the results obtained it has been suggested that

glutathionylation mostly regulates proteins involved in the CBB cycle under stress conditions.

### 1.3.2 Nitrosylation

Nitrosylation occurs in the presence of nitric oxide (NO) also involved in redox signaling guided by nitric oxide species (NOS). NO can directly nitrosylate protein thiols, but also react with GSH to form S-nitrosoglutathione (GSNO). GSNO is considered the main mobile actor of NO source and a major trans-nitrosylating agent. GSNO concentration is controlled by the enzyme GSNO reductase (GSNOR) which catalyzes the reduction of GSNO to oxidized glutathione (GSSG) and ammonia, modulating indirectly the intracellular level of nitrosylated proteins (Liu et al 2001). Nitrosylation has been more widely studied in mammalian cells than photosynthetic organisms. In plants such as in *Arabidopsis*, *Brassica juncea*, citrus, and maize, several studies have been conducted to identify nitrosylated sites, after abiotic or biotic stress. Altogether, within these studies about 200 S-nitrosylated proteins and putative sites have been identified. In *Chlamydomonas*, 492 nitrosylated proteins and 392 nitrosylated sites have been identified *in vivo* in cells submitted to a nitrosative stress (Morisse et al 2014). In this work, *Chlamydomonas* cells were subjected to GSNO incubation, after which modified proteins were identified either with a biotin switch technique (BST) (Jaffrey & Snyder 2001), or with S-nitrosiothiol-site identification (Hao et al 2006), or both. The first method consists out of three steps in which first the free cysteines residues of proteins are blocked with alkylating agents, secondly the S-nitrosylated proteins are reduced with ascorbate and thirdly labelled with a N-[6-(Biotinamido)hexyl]-3'- (2'-pyridyldithio)propionamide (HPDP-biotin), a thiol-specific dithiothreitol (DTT)-reducible biotinylation agent. Biotinylation of proteins were then purified by streptavidin-agarose affinity chromatography. The second method is based on the same principle as BST, but a tryptic digestion step is included before the affinity chromatography step. This method was useful to cover more deeply the S-nitrosylated proteins *in vivo* and identify S-nitrosiothiol-sites that could not be detected with the first method. The identified proteins are involved in a variety of metabolic and cellular pathways which involve photosynthesis, carbohydrate metabolism, amino acid metabolism, cell motility and stress response and 17% with a non-identified function. Most of them were also identified in plants and

some of them are established to be nitrosylation targets like cytosolic aldolase, mitochondrial glycine decarboxylase or cytosolic glyceraldehyde-3-phosphate dehydrogenase Others are specific to *Chlamydomonas*, for example the enzymes involved in the CBB cycle or iron assimilation (Morisse et al 2014).

Moreover, among the 239 putative glutathionylated proteins identified in *Chlamydomonas* (Michelet et al 2008, Zaffagnini et al 2012), 125 were also found nitrosylated, reinforcing the crosstalk between these two PTMs and their importance in cell metabolism.

### 1.3.3 Thioredoxome

Thioredoxins (TRXs) are proteins involved in the thiol-based redox PTMs like glutathionylation or nitrosylation. They contain a disulfide active site (-WCG(P)PC-) which is responsible for their oxidoreductase activity (Perez-Perez et al 2017). These proteins have been discovered in *Escherichia coli* (Laurent et al 1964), and since then have been studied in mammalian cells and found to be involved in cellular processes and human diseases. Non-photosynthetic organisms present only a small number of genes encoding TRX proteins, mainly localized in the cytosol and mitochondria. In photosynthetic organisms, TRXs constitute a large protein family which regulate the CBB cycle, the light dependent ATP-production, different carbon metabolism pathways. They are also involved in the regeneration of other antioxidant enzymes like peroxiredoxins or methionine sulfoxide reductases. Their action is mainly ascribed to the reduction of disulfide bonds. In the last 20 years, several groups have been working to develop techniques to identify putative TRX-targets proteins. The first approach is based on the reaction occurring between reduced TRX and its oxidized target protein. The most reactive cysteine at the N-terminal of the TRX active site first acts as nucleophile on the disulfide bond of its target, forming a transient mixed disulfide. A second step resolves this attack by involving an active cysteine at C-terminal TRX which releases the oxidized TRX protein and its reduced target. A strategy used to identify TRX targets consists of mutating the second active cysteine into serine or alanine, which allows stabilization of the mixed-disulfide dimeric form. Such TRX variants can be used to trap covalently bound targets, as they will not be released (Perez-Perez et al 2017). This strategy was used to purify Trx targets *in vivo* in yeast (Verdoucq et al 1999) in human cells (Wu et al 2014), and in *Escherichia coli* (Arts et al 2016).



The mutated TRX can also be attached on a chromatographic resin to trap TRX targets that are eluted by adding specific chemical reductants as DTT, and identified proteins by mass spectrometry. The second strategy is instead based on the *in vitro* reconstitution of the enzymatic TRX system with NADPH, NTR (NADPH-thioredoxin-reductase), and TRX in cell-free extracts. TRX-regulated cysteines are labelled with thiol-specific probes and their reduction with TRX mix system, allow the detection of TRX-target proteins and their identification with mass spectrometry. This approach was applied to various total or subcellular extracts in both plants and Archaea, using fluorescent, radioactive, or biotinylated probes (described in (Perez-Perez et al 2017)). Other adaptation included isotopic labelling with cleavable isotope-coded affinity tag reagents (cICAT) (Hagglund et al 2014, Hagglund et al 2008) or with cysteine-reactive tandem mass tag (Cys-TMT) (Zhang et al 2016). Both reagents (cICAT and Cys-TMT) specific to cysteine facilitated the identification of cysteines targeted by TRX. In *Chlamydomonas*, 55 putative targets were identified by coupling the first strategy of modified TRX with protein separation on 2D gels and proteins were identified with MALDI-TOF MS (Lemaire & Miginiac-Maslow 2004). With the last advances of the technique, by combining qualitative and quantitative mass spectrometry analyses, more than 1000 targets have been identified (Perez-Perez et al 2017). Both approaches are summarized in the **Fig. 12**. The identified TRX putative targets cover a variety of metabolic pathways and cellular processes such as metabolic functions, genetic information processing, cellular processes, stress response, redox homeostasis, and a portion of unknown functions. When comparing the TRX-targets identified with the glutathionylated and nitrosylated sites, it becomes evident that there exists a substantial interconnection between these post-translational modifications (PTMs). This underscores the significance of these mechanisms in enabling cells to regulate information through redox signaling.

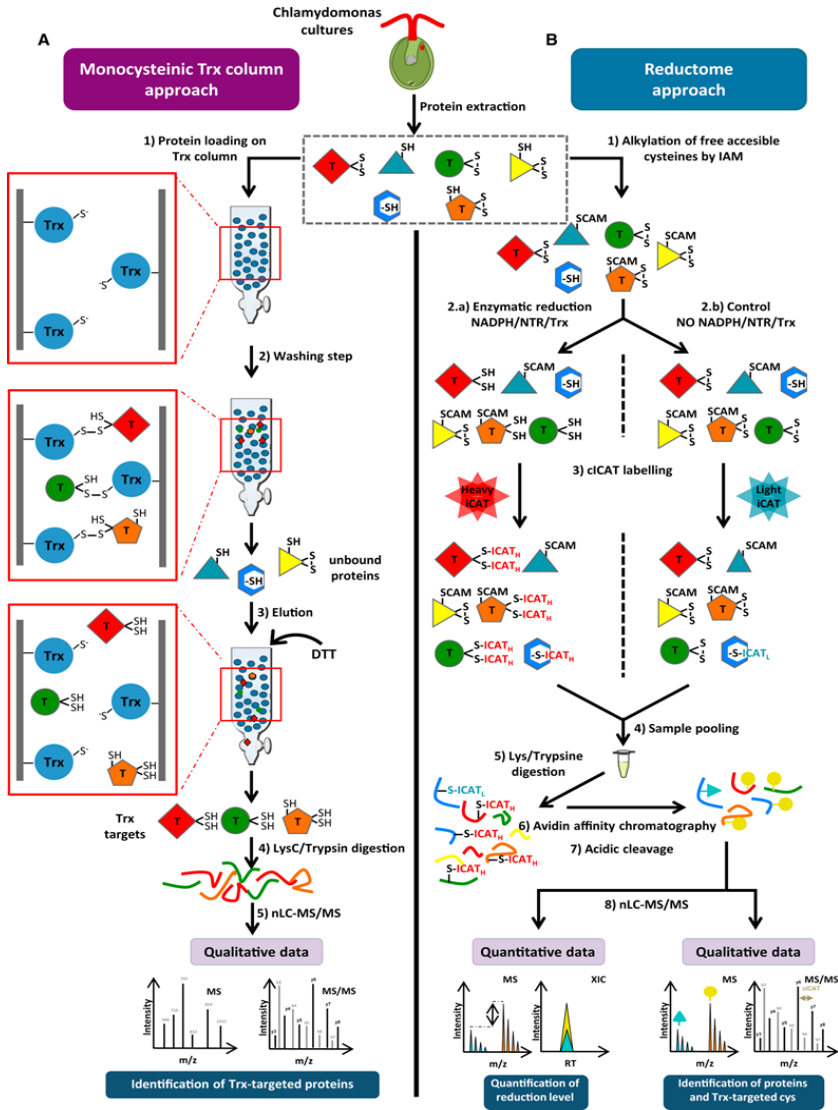


**Figure 12: Scheme of the experimental procedures to identify thioredoxin targets and their redox-regulated cysteines.** A) Monocysteine Trx column approach: identification of Trx targets using the affinity chromatography. B) Reductome approach: identification of the redox-regulated cysteines of Trx targets iCAT labelling approach after an *in vitro* reduction (in the study case mediated by cytosolic CrTrxh1. From (Perez-Perez et al 2017).

### 1.3.4 Sulfenylation

Another important PTM is the H<sub>2</sub>O<sub>2</sub>-mediated sulfenylation, already described in the section 1.2.2. Over the past few years, various techniques employing genetic and chemical methodologies have undergone advancements and enhancements to identify sulfenylated proteins and conserved cysteines in both mammalian cells and plants.

#### 1.3.4.1 Genetic approach

One of the first approaches used was based on the genetic construct obtained by fusing the C-terminal domain of the yeast *Saccharomyces cerevisiae* activator protein AP-1-like (YAP1) transcription factor and a tandem purification tag (Van Leene et al 2008). In *Saccharomyces cerevisiae* the H<sub>2</sub>O<sub>2</sub> sensor oxidant receptor peroxidase 1 (ORP1/glutathione peroxidase 3) and the transcription factor YAP1 (yeast AP-1-like) control a mechanism dependent on a sulfenic acid/thiol-disulfide exchange. The peroxidatic cysteine of ORP1 reacts with H<sub>2</sub>O<sub>2</sub>, undergoing oxidation to sulfenic acid. This sulfenic acid then reacts with a cysteine of the YAP1 C-terminal cysteine-rich domain (cCRD), forming a disulfide (Delaunay et al 2002). This mechanism forms the basis for the development of a YAP1-based probe to trap sulfenylated proteins (Takanishi et al 2007). With this technique almost 100 sulfenylated proteins of Arabidopsis cell suspension, have been identified upon incubation with and without H<sub>2</sub>O<sub>2</sub> (Waszczak et al 2014). In this study, two constructs were generated, YAP1C and YAP1A. In the first one, two of the three cysteines were mutated allowing the third one to form the mixed disulfides with sulfenylated proteins, while in the second one, all three cysteines were mutated. YAP1A was used as control (**Fig. 13**). Among the 97 quantified proteins, 66 were identified covering signal perception and transduction, protein degradation, RNA-binding and translation, in primary metabolism, hormone homeostasis, protein transport, amino acid metabolism, redox related enzymes, and some unknown functions. Some of them were also identified as glutathionylated and TRX-target or nitrosylated, for example dehydroascorbate reductase 2 (DHAR2) or thioredoxin-dependent peroxidase 1 (PRX1).

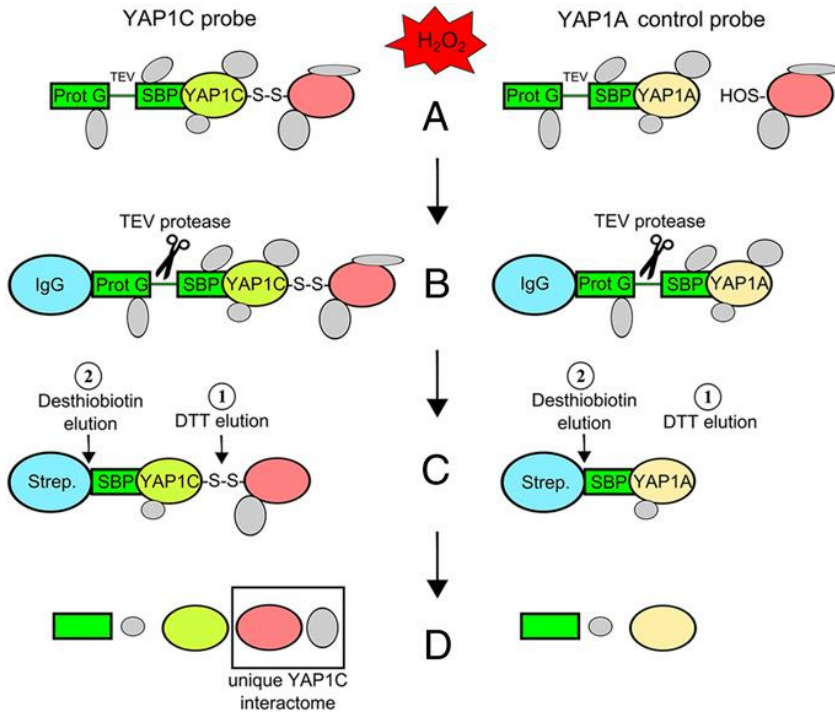


**Figure 13: Scheme of the experiment of the *in vivo* identification of Arabidopsis sulfenome.** A) Arabidopsis cells were transformed to over-express the YAP1C/YAP1A probes and treated with  $H_2O_2$ . (B, C) Proteins were isolated with a two-step purification based on the immunoglobulin G tag (IgG-tag) and the streptavidin-binding peptide (SBP) affinity. The numbers indicate the order of the elution step. D) Last step of the analysis of eluted sulfenylated proteins with LC-MS/MS with a comparison between YAP1C and the negative YAP1A. From (Waszczak et al 2014).

The same genetic approach was used to identify the sulfenome in plastid organelles of Arabidopsis cell culture transgenic lines expressing YAP1C and YAP1A in the chloroplast with and without  $H_2O_2$  (De Smet et al 2019). In this study the authors identified 132 putative sulfenylated proteins. Most of them are involved in amino acid, lipid and nucleotide metabolisms, glycolysis, CBB cycle, redox related proteins. A development of the YAP1C-probe technique applied in Arabidopsis, led to increase the number of sulfenylated sites *in situ* up to more than 1000 proteins with and without  $H_2O_2$  treatment (Wei et al 2020). The improved steps were related to the nucleophilic attack and the subsequent formation of a mixed disulfide bond by the active cysteine of YAP1C and the sulfenylated cysteine (Cys-SOH) residue in oxidized target proteins. Another

improvement was a second enrichment of YAP1C-probe after proteome digestion, which enhanced the amounts of modified proteins identified. Most of the identified proteins are localized in the cytosol in accordance with the YAP1C probe localization. Moreover, a variety of proteins involved in various stress-related adaptive processes (cadmium, salt, heat, and cold), metabolism, and RNA processes showed significant enrichment. This aligns with previous findings (Huang et al 2018, Huang et al 2019) providing confirmation that enzymes participating in essential carbon metabolic pathways, such as glycolysis, amino acid metabolism, and carbon fixation, were prone to S-sulfenylation. In addition, among the proteins identified, 55% of them were also found being glutathionylated or nitrosylated, as described in (Wei et al 2020), highlighting the significance of the interplay between the mentioned PTMs in the context of oxidative stress.

#### *1.3.4.2. Chemical approach*

Beside the genetic approach to identify sulfenylated proteins, chemical approaches have also been developed and their properties are described in (Gupta & Carroll 2016, Gupta et al 2017). The majority of molecules and immunochemical probes used to identify sulfenylated proteins are 5,5-dimethyl-1,3-cyclohexanedione (dimedone, DYn-2)-based, which is selective but presents low reactivity ( $10 \text{ M}^{-1} \text{ s}^{-1}$ ). However, several studies have been conducted using the DYn-2 probe in mammalian cells and plants. Herein, I will focus on photosynthetic organisms. In plants, DYn-2 was used in cell suspension of *Arabidopsis* with and without  $\text{H}_2\text{O}_2$  (Akter et al 2015). With this method 226 sulfenylated proteins have been identified in the presence of  $\text{H}_2\text{O}_2$  residing in the cytosol, nucleus, mitochondria, chloroplast, endoplasmic reticulum, Golgi apparatus and plasma membrane. Among them, 123 modified proteins were for the first time reported as redox sensitive proteins and 16 of them were found in common with the ones identified with YAP1C (Waszczak et al 2014). The workflow of DYn-2 trapping proteins is shown in **Fig. 14**. In brief, upon  $\text{H}_2\text{O}_2$  treatment, cysteine residue of proteins undergo oxidation and only sulfenylated proteins are trapped (Cys-SOH) (**Fig. 14 A**). Next, a “click” reaction (Gonzalez-Lainez et al 2022, Kolb et al 2001) is performed to link biotin to the DYn-2 of the protein (**Fig. 14 B**). Such biotinylated molecules can be visualized by immunoblotting with streptavidin antibodies or enriched with avidin for mass

spectrometry analyses (**Fig. 14 C**). This study was another step forward on the identification of the sulfenome in plants, even though it did not give any information about the mechanism behind the signaling dependent on the sulfenylated proteins upon oxidative stress (Akter et al 2015).

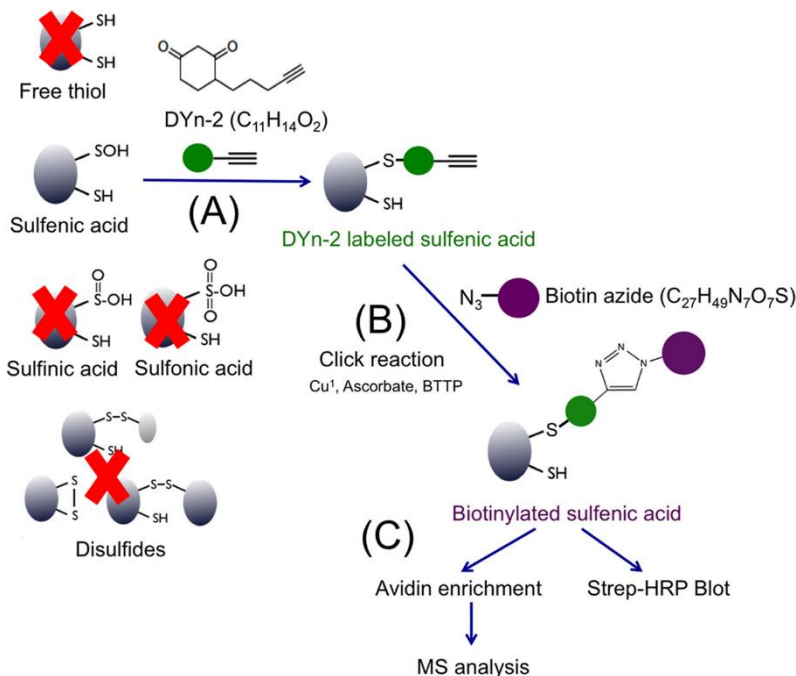


**Figure 14: Scheme of the DYn-2 workflow to trap sulfenylated proteins.** **A)** DYn-2 is specific to detect only sulfenic modification. **B)** DYn-2 are biotinylated via “click” reaction. **C)** Once DYn-2 tagged proteins are biotinylated they can be visualized by streptavidin-HRP (Strep-HRP) blot, or alternatively, after enrichment on avidin beads, proteins are identified by mass spectrometry analysis. From (Akter et al 2015).

Considering the low reactivity of the DYn-2 probe, Carroll’s lab (Scripps Research Institute, Florida) has been working on improving the dione-based probe with a generation of a collection of cyclic and linear C-nucleophiles that showed diverse reactivity profiles toward Cys-SOH. Among the almost 100 C-nucleophiles of the collection, some of them were selected and divided into eight scaffolds: cyclohexane-1,3-diones (1), (thio)barbituric acids (2), different sized  $\beta$ -dicarbonyl rings (3), dihydrothiophen-3(2H)-one 1,1-dioxides/2-substituted isothiazolidin-4-one 1,1-dioxides (4) pyrrolidine-2,4-diones (5), 1,3-indandiones(6), piperidine-2,4-5(6H)-one (7), 1,2-thiazinan-5-one1,1-

dioxides/2H-1,2-thiazin-5(6H)-one,1,1-dioxides/1H-benzo-[c][1,2]thiazine-4(3H)-one 2,2-dioxides (8) (**Fig. 15 A**). From this pool of eight scaffolds, five of the molecules were selected with different structure and different reactivity, as shown in **Fig. 15 B**. To these nucleophiles an alkyne was incorporated to improve the enrichment and the detection of modified trapped proteins. The already mentioned dimedone (DYN-2) with a modest reaction rate of  $10 \text{ M}^{-1} \text{ s}^{-1}$ , followed by nucleophiles with increasing reaction rates like thiazolidin-4-one 1,1-dioxide-based (TD)  $20 \text{ M}^{-1} \text{ s}^{-1}$ , pyrrolidine-2,4-dione-based (PYD) with a reaction rate  $330 \text{ M}^{-1} \text{ s}^{-1}$ , piperidine-2,4-dione-based (PRD) with a reaction rate of  $1155 \text{ M}^{-1} \text{ s}^{-1}$ , benzo[c][1,2]thiazine-based (BTD) with a reaction rate of  $1700 \text{ M}^{-1} \text{ s}^{-1}$ . As expected, the highest number of proteins detected was proportional to the reaction rate, aligning with the characteristics of the BTD probe (Gupta et al 2017). The workflow for capturing and identifying modified proteins adheres to the same steps outlined above, as illustrated **Fig. 14**. The key variation occurs in the “click” chemistry step, where a biotin linker with UV light-tag is employed for the photo-cleavable release of the modified peptides, subsequently analyzed by mass spectrometry.

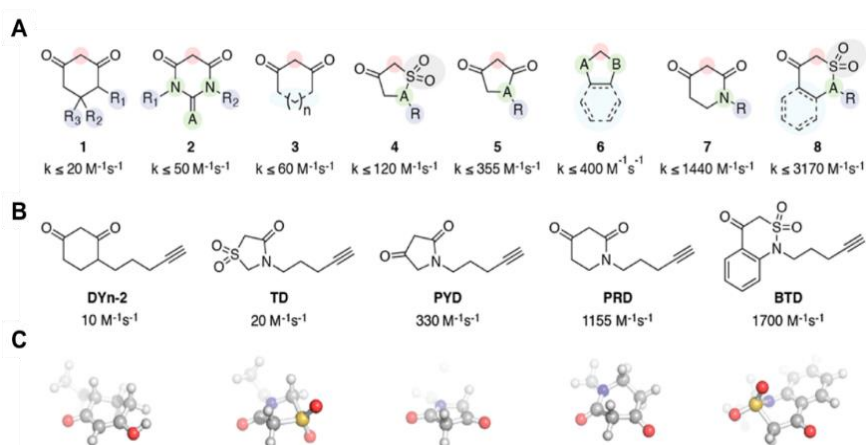


**Figure 15: Novel classes of nucleophile probes to trap sulfenylated cysteine residues. A)** Structural classes of cyclic C-nucleophiles (1–8). In each structure the nucleophilic carbon is highlighted in the red circle. The rate constant indicated is described in Gupta and Carroll, 2016. **B)** Selection of DYN-2 and four new C-nucleophiles from the cyclic C-nucleophiles collection, based on a range of reaction rate constants and scaffold diversity. **C)** Energy-minimized 3-dimensional representation of the probes. From (Gupta et al 2017).

Considering the high reactivity of the BTD probe, investigations on the sulfenome profile of Arabidopsis cells after cell lysis were carried out (**Fig. 16**) (Huang et al 2019). The workflow used for this study was adapted from (Fu et al 2019) and follows the same principle as mentioned before (**Fig. 14**), with and without H<sub>2</sub>O<sub>2</sub> incubation. With BTD the authors could map 1537 sulfenylated sites on more than 1000 proteins of Arabidopsis cell cultures. Many of the identified proteins are associated with RNA homeostasis and metabolism. When comparing the sulfenylated sites, 155 of them were found to be common with those in human cells. Examples include mitogen-activated protein kinase 4 (AtMAPK4), which holds a crucial role in plant signaling (Liu & He 2017). This comparative analysis confirmed the importance of these proteins as redox sensing actors and provides a fresh perspective on the mediation of CysSOH-signaling in plants.



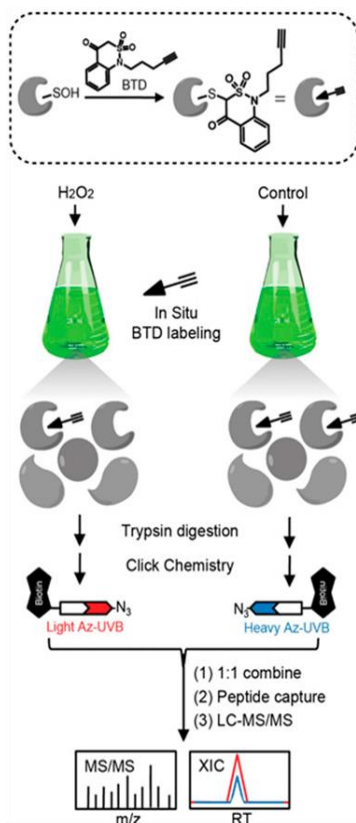


**Figure 16: Workflow for S-sulfenylation labelling and analysis in Arabidopsis cell cultures.** The BTD-based probe is represented as an arrow (chemical warhead) followed by 3 lines indicating the alkyne handle. Arabidopsis cell cultures were incubated with and without  $\text{H}_2\text{O}_2$  in the presence of BTD probe. The pool of proteins was extracted and digested with trypsin. Modified peptide were linked to a biotin moiety through click chemistry with light biotin azide carrying the tag for UV-light (Light Az-UVB) and heavy biotin azide carrying a tag for UV-light (Heavy Az-UVB) for treated and control samples respectively. The two pools of peptides with light and heavy Az-UVB biotin were combined in 1:1 ratio, the modified peptides were isolated using the UV light to release the UV-tag from the biotin and the samples were prepared and analyzed with LC-MS/MS to identify modified peptides and compared the two conditions with and without  $\text{H}_2\text{O}_2$ -mediated stress. From (Huang et al 2019).

Recently, a new method based on triphenylphosphonium (TPP) ylides, known as Wittig reagents (**Fig. 17 A**), among the most commonly used tools in synthetic chemistry, has been developed (Shi et al 2021). Wittig based probes (WYne probes, WYneC, WYneO and WYneN, **Fig. 17 B**) exhibited a 10-fold increase in kinetics compared to a benzo[c][1,2]thiazine-based sulfenic acid probe, BTD and was roughly 1,500-times faster than the 1,3-cyclohexanedione-based DYn-2 probe. Despite differences in the kinetics (**Fig.17 B**), WYne probes were successfully reacted with the dipeptide sulfenic acid with rate constants ranging

from 160 to 15,000  $M^{-1}s^{-1}$  at physiological pH. The workflow to trap sulfenylated proteins follows the same steps as previously described (**Fig. 16**). Using WYneN probe, more than 2000 S-sulfenylated sites labelled *in situ* in mammalian cells were identified. Moreover, in the same study the authors conducted investigation on enhancing organelle specificity in WYne probes, especially to mitochondria, as one of the main ROS production organelles. Thanks to the high selectivity and biocompatibility of the WYne probes, future investigations are directed on improving their specific action in mitochondria and their use as carrier to deliver small molecules (*e.g.* drugs, antioxidants...) to mitochondria.

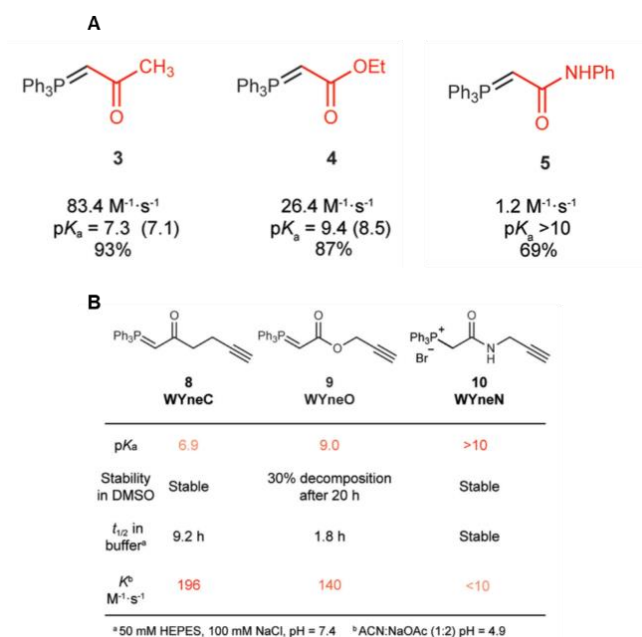


**Figure 17: Physical properties and kinetic profile of the WYne probes.** A) Wittig reagents used to synthesized WYne probes. (3) methoxymethylenetriphenylphosphine; (4) triphenylcarbethoxymethylenephosphorane; (5) diphenyl carbamoylmethyl enetriphenylphosphorane with the rate constant after screening for reaction with a dipeptide-SOH model compound. B) WYne probes WYneC, WYneO and WYneN synthesized by using Wittig reagent (3), (4), (5), respectively. Adapted from (Shi et al 2021).

## Chapter II

### Thesis objectives

The nucleus of a cell is the original source for creating anterograde signaling, leading to regulation by activation, overexpression, reduction of essential pathways such as photosynthesis or respiration. A signal can also travel backwards from organelles to its original source, the nucleus. Such a mechanism is known as retrograde signaling, and it may involve  $H_2O_2$  molecules. In recent years, there has been an increasing recognition of the significance of  $H_2O_2$  as a signaling molecule. Studying the redoxome of an organism can help to define new mechanisms of sensing ROS molecules and to identify new redox related proteins with a specific function. In photosynthetic organisms, chloroplast is one of the major sources of  $H_2O_2$  generated during photosynthesis in stress conditions. To define *in vivo* new redox related proteins involved in oxygenic photosynthesis, we used the unicellular green microalga *Chlamydomonas reinhardtii* (hereafter Chlamydomonas). The advantage to use Chlamydomonas is the existence of a singular chloroplast that dominates the majority of the cell volume, maximizing the chance to see potential modifications at the level of chloroplast proteins. This organism is also convenient to handle and manipulate. Moreover, the genomes of nucleus, chloroplast and mitochondria are fully sequenced, and genetics and physiology are well established and useful to support our investigation. **The objectives of this project were twofold: firstly, to characterize *in vivo* mutants of Chlamydomonas deficient in  $H_2O_2$ -scavenging enzymes, and secondly, to identify previously unexplored redox-sensing proteins by examining the altered cysteine protein patterns within selected  $H_2O_2$ -scavenging enzymes mutants.**

To answer the **first** objective, we used molecular, genetic, and physiological approaches to study insertional mutants of diverse  $H_2O_2$ -scavenging enzymes or stress responsive proteins. The loss of one of those scavengers could help to define new redox dependent regulations.

In **chapter III**, I describe the analysis of 17 Chlamydomonas mutants from the CLiP library harbouring a paromomycin cassette in genes encoding enzymes implicated in  $H_2O_2$  scavenging enzymes. Molecular and genetic approaches were used to confirm the presence of the cassette. A preliminary evaluation of the

photosynthetic efficiency was conducted on all the mutants to identify any phenotype that differed from that of the wild type. Initially, the photosynthetic measurements were conducted as an explorative step to identify the most promising mutant(s) for further investigation and to elucidate the function of the disrupted enzyme (section 3.3.1). After several attempts, based on the first results obtained and on careful literature research, we selected mutants of genes for sulfiredoxin 2 (SRX2) and ascorbate peroxidase 2 (APX2) (sections 3.3.2, 3.3.3, 3.3.4). The former is able to reduce sulfinylated proteins to their sulfenylated form, while the latter belongs to a newly classified type of ascorbate peroxidase enzymes named ascorbate peroxidase-related proteins.

Upon further examination of its photosynthetic machinery, intriguing findings emerged regarding the *apx2* mutant, leading us to concentrate our efforts on investigating this particular enzyme (first insight in section 3.3.5). As a result, we deviated somewhat from our original objective and began to focus on elucidating the function of the recently classified ascorbate peroxidase-related protein. The results obtained have been submitted and published and reported in **chapters IV and V**.

To answer the **second** objective, we used biochemical and proteomic approaches to define the sulfenome of *Chlamydomonas* by using a new synthesised 1-(pent-4-yn-1-yl)-1H-benzo[c]-[1,2]-thiazin-4(3H)-one 2,2-dioxide (BTD)-based probe designed in the lab of Kate Carroll (Scripps Research Institute, U. of Florida) able to specifically recognize the sulfenylated cysteine residue of a protein. Our aim was to adapt the protocol used in mammalian cells and plant cell cultures for use in *Chlamydomonas*, both in the wild-type strain with and without the addition of H<sub>2</sub>O<sub>2</sub>, and then to apply it to selected mutants. However, optimising the protocol for *Chlamydomonas* proved to be quite challenging, likely due to the presence of chlorophyll, which limited the yield of initial material in some steps of the procedure. Despite our efforts and assistance from experts in proteomic approaches, we were unable to fully identify the modified proteins.

In **chapter VI**, I describe the final version of the optimised protocol with which we could identify only a few modified proteins involved in photosynthesis and the challenges we faced to get through all the steps.

## Chapter III

### Redox signaling mutants in *Chlamydomonas*: a survey

Anna Caccamo<sup>1,2,3,4</sup>, Pierre Cardol<sup>1</sup>, Joris Messens<sup>2,3,4</sup>, Claire Remacle<sup>1</sup>

<sup>1</sup>Genetics and Physiology of Microalgae, InBios/Phytosystems research unit, University of Liège, 4000 Liège, Belgium

<sup>2</sup>VIB-VUB Center for Structural Biology, 1050 Brussels, Belgium

<sup>3</sup>Brussels Center for Redox Biology, 1050 Brussels, Belgium

<sup>4</sup>Structural Biology Brussels, Vrije Universiteit Brussel, 1050 Brussels, Belgium

My contribution on this first part of the results covered the bibliographic investigation, the molecular, genetic and physiological characterization of the selected mutant strains, the transformation of *srx2* mutant strain and generation of double mutants between *srx2* and *apx2* strains and the photosynthetic measurements.

#### *Abstract*

This section describes the first analyses performed on selected mutants affected in H<sub>2</sub>O<sub>2</sub> scavenging enzymes to define the redox signaling in *Chlamydomonas*, which was the first objective of our project. After a bibliographic investigation and a comparative analysis with the H<sub>2</sub>O<sub>2</sub> scavenging enzymes machinery of *Arabidopsis*, 17 *Chlamydomonas* mutants were selected and ordered from the CLiP library. The initial part of the project was focused on the confirmation of the mutants by molecular and genetic approaches concomitantly with a wide phenotypical screen of the mutants in different growing conditions. With this explorative research we did not find any phenotype in stress conditions compared to the wild-type strain (wt). This could be attributed to potential compensatory upregulation of alternative H<sub>2</sub>O<sub>2</sub> scavenging enzymes. As a result, we transitioned towards a more meticulous selection of mutants, considering optimal molecular and genetic attributes to ensure greater result reliability. Motivated by this and a desire to enhance the understanding of two specific enzymes, we directed our attention towards sulfiredoxin 2 (SRX2) and ascorbate peroxidase 2 (APX2).

### 3.1 Introduction

*Chlamydomonas* is a green alga model organism that has long been used to study genetics and biological processes (*i.g.* photosynthesis and respiration). The utility of *Chlamydomonas* as model organism has been limited by the difficulty to obtain mutants of specific genes. Different techniques have been developed to generate mutants of *Chlamydomonas*. Homologous recombination for gene disruption is not a viable tool for *Chlamydomonas*, due to the low frequency of random insertion of the exogenous DNA (Slaninová et al 2008). The zinc-finger nucleases method has not been demonstrated practical due to the time-consuming required for screening zinc finger arrays with high specificity for sequence of interest (Sizova et al 2013). The RNA silencing through the use of artificial microRNA has been developed for *Chlamydomonas*, but the suppression of transcript levels is usually incomplete (Molnar et al 2009, Zhao et al 2009). Insertional mutagenesis has been well established in *Chlamydomonas*, but has been mainly used for forward genetics screens (Galvan et al 2007). Moreover, methods for isolating mutants with insertions in specific target genes require large number of PCRs to identify genes of interest (Gonzalez-Ballester et al 2011, Pootakham et al 2010). Target mutagenesis with CRISPR-Cas9 in microalgae like *Chlamydomonas* has been challenging (Jiang et al 2014). The CRISPR-Cas9 technique on *Chlamydomonas* has been subjected to several improvements to finally reach successful results (Dhokane et al 2020, Kelterborn et al 2022, Kim et al 2020).

To facilitate fundamental studies on *Chlamydomonas*, the group of Martin Jonikas (Princeton University, USA) developed the *Chlamydomonas* Library project (CLiP) which generated a collection of 60,000 insertional mutants covering 83% of nuclear protein-coding genes, and available to the community (Li et al 2019, Li et al 2016). Mutants were obtained by transformation through electroporation of haploid cells with a DNA cassette that randomly inserts into the genome, disrupting and inactivating the gene into which the cassette inserts (Li et al 2019). As random inserted, the cassette may undergo different rearrangements, for example deletions of genomic DNA, cassette truncation, insertion of more than one cassette, or presence of genomic DNA from distant loci inserted next to mutagenic cassette (Li et al 2019, Li et al 2016, Zhang et al 2014b). The cassette harbours the resistance to the antimicrobial paromomycin for cell selection. Paromomycin inhibits cell growth through inhibition of the 16S

ribosomal RNA (Davies & Wright 1997). Mutants were screened with the *Chlamydomonas MmeI*-based insertion site sequencing (ChlaMmeSeq), based on massively parallel sequencing of 20- to 21-bp sequences immediately flanking the insertion cassettes (Zhang et al 2014b). The screening method was then optimized with Linear and Exponential Amplification of insertion site sequence coupled with Paired-end Sequencing (LEAP-Seq) based on deep sequence of the bar codes and the flanking sequences together on the entire mutant library or in six separated pools (Li et al 2019). With this method longer flanking sequences were obtained to confirm cassette insertion sites.

For this project we chose to work on CLiP mutants affected in H<sub>2</sub>O<sub>2</sub>-scavenging enzymes to study H<sub>2</sub>O<sub>2</sub>-mediated signaling and analysed their physiological responses to stress conditions by photosynthetic measurements. The role of the enzymes potentially impaired in the chosen mutants are described in section 3.3.

## 3.2 *Material and Methods*

### 3.2.1 *Phenotypical characterization*

#### 3.2.1.1 *Drop tests*

Phenotypical screening of the selected mutants was carried out on agar plates in mixotrophy (acetate medium and light (TAP)-agar plate) and phototrophy (minimal medium and light (TMP)-agar plate). The plates were exposed under different light intensities: to continuous low (50  $\mu\text{mol photons m}^{-2} \text{ s}^{-1}$ ) or high light (500  $\mu\text{mol photons m}^{-2} \text{ s}^{-1}$ ), circadian cycles with 12 h of light at 50  $\mu\text{mol photons m}^{-2} \text{ s}^{-1}$  and 12 h of darkness, and continuous darkness for those mutants plated on acetate medium plates at 25 °C. Cells were normalized to the same concentration of 10<sup>6</sup> cells/ml and prepared by serial dilutions of factor of 10. 10  $\mu\text{l}$  of samples were pipetted on agar plates as shown in **Fig. 1**. After three days and one week, pictures were taken to monitor cells growth.

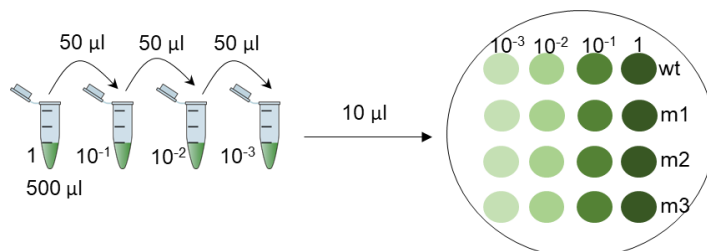


**Figure 1: Scheme of the drop test set up.** Cells were prepared in Eppendorf tubes in serial dilution of factor of 10, starting from  $10^6$  cells/ml to have  $10^5$  cells/ml ( $10^{-1}$  dilution),  $10^4$  cells/ml ( $10^{-2}$  dilution),  $10^3$  cells/ml ( $10^{-3}$  dilution). Each sample was mixed and  $10 \mu\text{l}$  per each dilution was pipetted on agar plates to monitor cells growth under different light intensities.

### 3.2.2 Photosynthetic measurements

#### 3.2.2.1 Fluorescence of PSII with SpeedZen Camera

In order to analyse the *in vivo* activity of PSII, the changes in chlorophyll *a* fluorescence level, in response to light pulses at room temperature, were obtained with a SpeedZen camera (Beambio, France (Johnson et al 2009)). With this imaging system we pictured 96-well microplates (Greiner®, 655075) with  $200 \mu\text{l}$  of liquid culture, and agar plates of 10 cm of diameter. Samples were incubated in the darkness for 15 min to let the photosynthetic redox components to be in the basal oxidized state. Chlorophyll *a* was excited by an array of blue LEDs (450 - 470 nm), filtered with a long-pass red filter and finally recorded with a CCD camera (UI324xCP-NIR 4103350683). In darkness, the lowest fluorescence level is referred as  $F_0$ , after a saturating light pulse the fluorescence level reaches its maximum, referred as  $F_m$ , and the maximum quantum yield of PSII was calculated ( $\phi_{Po} = F_v/F_m = (F_m - F_0)/F_m$ ). Measurements were followed by increasing light intensities to record the steady fluorescence level,  $F_s$ , and the maximum fluorescence level after light acclimation,  $F_m'$ , specific for each light intensity. The effective quantum yield of PSII then is calculated for every specific light intensity ( $\phi_{PSII} = (F_m' - F_s)/F_m'$ ) (Maxwell & Johnson 2000). The yield of PSII at each light intensity (photosynthetic photon flux density, PPFD) was then multiplied by the corresponding light intensity to calculate the relative electron transfer rate ( $rETR = \phi_{PSII} * PPFD$ ). Non-photochemical quenching (NPQ) induction was measured in the same way and calculated considering the  $F_m$  and the  $F_m'$  at each step of light to investigate the dissipation of energy ( $NPQ = (F_m - F_m')/F_m'$ ) (Maxwell & Johnson 2000). From the values obtained we



could also calculate the fraction of state transition (qT) by considering the last point measured in the dark phase (Fd) of the NPQ relaxation and the last one measured after illumination with far-red light for 10 min (Fm'') to oxidize the PQ pool ( $qT = (Fm'' - Fd)/Fd$ ) (Eberhard et al 2008).

### 3.2.2.2 Fluorescence of PSII and PSI at a temperature of 77 K

To quantify the fluorescence of photosystem I (PSI), a VIS-NIR spectrometer was used to conduct measurements at a temperature of 77K (-196°C) (Ocean Insight<sup>®</sup>). Liquid culture samples were obtained directly from their growth environments or subjected to light or chemical treatment to induce state transition (section 1.1.3.3) and subsequently frozen at a temperature of 77 K in liquid nitrogen within 1 cm cuvettes prior to measurement. Frozen samples were placed in a cuvette holder in the dark and submerged in liquid nitrogen. Spectra were recorded between 600 nm and 800 nm with an integration time of 1 s. Each value was then normalised to the level of fluorescence at 685 nm, corresponding to the PSII reaction centre (Andrizhiyevskaya et al 2005). State I, induced by the oxidized state of the PQ pool, was induced with a far-red light at 720 nm for 10 min, or by incubating the cells in 10 µM 3-(3,4-dichlorophenyl)-1,1-dimethylurea (DCMU) for 20 min under culturing light conditions (Finazzi et al 1999). State II, induced by the reduced state of the PQ pool, was induced by 10 min of darkness in samples that were previously exposed to 10 min of actinic light (660 nm) of high intensity ( $750 \mu\text{mol photons m}^{-2} \text{s}^{-1}$ ), or by adding 5 µM of carbonyl cyanide 4-(trifluoromethoxy) phenylhydrazone (FCCP) and incubating the cells for 20 min in culturing light conditions (Finazzi et al 1999).

### 3.2.2.3 Activity of PSI and cytochrome b<sub>6</sub>f

PSI activity was measured with a Joliot-Type-Spectrophotometer (JTS-10, BioLogic, France) by monitoring changes of absorption of the primary electron donor at the PSI reaction centre, P700. Photo-oxidation and re-reduction of P700 were monitored at 705 nm and corrected with identical measurements at 740 nm, to remove interferences from other components like ferredoxin and plastocyanin (Heinnickel et al 2016). To evaluate the photo-oxidation of P700 in the first 5 ms in relation to the maximum oxidizable P700 value (P<sub>m</sub>) achieved in the presence of 10 µM DCMU, cells were exposed to increasing light intensities. The

comparison between two different light intensities ( $345 \mu\text{mol photons m}^{-2} \text{s}^{-1}$ ) and saturating light ( $6000 \mu\text{mol photons m}^{-2} \text{s}^{-1}$ ) at different times (50 ms or 6 s) was executed in the same way. Oxidation and re-reduction of cytochrome *f*, the electron donor of cytochrome *b<sub>6</sub>f* to plastocyanin, was measured by monitoring changes of absorption at 546 nm with a baseline drawn with 520 nm and 573 nm readings (Malnoe et al 2011) in presence of 10  $\mu\text{M}$  DCMU. Re-reduction was calculated as rate ( $\text{s}^{-1}$ ), considering the half time that the electrons take to reduce P700 or cytochrome *f*.

#### 3.2.2.4 Electrochromic shift

The maximum activity of cyclic electron flow (CEF, section 1.1.3.2) was evidenced by monitoring the initial photochemical rate, in the presence of PSII inhibitors, by analysing the electrochromic shift. This method is used to monitor the electric field of the thylakoid membranes in response to the photosynthetic activity (Bailleul et al 2010). Cells of wt and *apx2* mutant grown under continuous low light  $50 \mu\text{mol photons m}^{-2} \text{s}^{-1}$  and continuous high light  $500 \mu\text{mol photons m}^{-2} \text{s}^{-1}$  were collected and brought to the same total chlorophyll content of 10  $\mu\text{g}$ . The cells were resuspended in fresh medium supplemented with 10% Ficoll to avoid cell sedimentation when placed in a 1 cm cuvette. To prevent electron transfer from PSII, samples were treated with 10  $\mu\text{M}$  DCMU prior measurements. Subsequently, the cells were exposed to saturating light of  $2000 \mu\text{mol photons m}^{-2} \text{s}^{-1}$  for increasing time periods of 5 ms, 20 ms, 50 ms, 100 ms, and 500 ms. Absorption changes were monitored at 520 nm, and the signal was corrected by identical readings at 546 nm (Nawrocki et al 2019a). These values were normalised to the extent of ECS originated by the activity of PSI, this was achieved by applying a single turnover flash (Nd-YAG laser Minilite II, Continuum) to samples containing 10  $\mu\text{M}$  DCMU and 1 mM hydroxylamine, preventing charge separations at PSII. The photochemical rate was determined by the difference in the slope of the last two milliseconds of the light phase minus the slope of the first five milliseconds of the following dark phase.

### 3.2.3 Molecular and genetics approaches

#### 3.2.3.1 Total DNA extraction and PCR amplification

DNA extraction was performed by following the protocol described in (Newman et al 1990). Cultures of wt and all the mutants were grown in mixotrophy condition under  $50 \mu\text{mol photons m}^{-2} \text{ s}^{-1}$  low light intensity until the mid-exponential phase. 2 ml of cultures were harvested, and the pellet was resuspended in 0.5 ml of 10 mM tris(hydroxymethyl)aminomethane-chloridric acid pH 8.0 (Tris-HCl), 10 mM ethylenediaminetetraacetic acid pH 8.0 (EDTA), 150 mM sodium chloride (NaCl) and centrifuged at 1500 g for 2 min, 25°C. The pellet was resuspended in 0.150 ml of cold H<sub>2</sub>O and 0.3 ml of 2% sodium dodecyl sulphate (SDS), 400 mM NaCl, 40 mM EDTA, 100 mM Tris HCl pH 8.0 was added. The extraction was performed by adding 0.175 ml phenol and 0.175 ml chloroform:isoamyl alcohol (24:1) to the samples, vortexing them 20-30 s and transferring them in a shaker at 4°C for 5 min. Hereafter, the samples were centrifuged 5 min at 15000 g and the aqueous phase (0.420 ml) was transferred in a new Eppendorf tube. The extraction was then carried out by adding 0.3 ml of chloroform:isoamyl alcohol (24:1), treating the samples as before and transferring the aqueous phase (0.370 ml) in a new tube. Then, two volumes of iced ethanol 100% were added and the samples were shaken until seeing fibres. Finally, they were incubated at -20°C O/N. The day after, the samples were centrifuged for 15 min at 15000 g, 4°C and the supernatant discarded. The pellet was washed with 0.300 ml of ethanol 70%, vortexed and centrifuged for 15 min at 15000 g at 4°C. The supernatant was discarded and the pellet dried for 15 min at 25°C. The pellet was resuspended with 50  $\mu\text{l}$  sterile distilled H<sub>2</sub>O, let 5 min at 25°C and stocked at -20 °C.

The DNA was used for PCR amplifications to confirm the presence of the paromomycin cassette in all the mutants. PCR amplifications were performed using the primers listed in **Table S1**.

#### 3.2.3.2 Total RNA extraction

Total RNA was extracted using the NucleoSpin® RNA Plant and Fungi, Macherey-Nagel. Wt, *srx2* mutant and complemented strains of *srx2* were grown in mixotrophy under continuous low light  $50 \mu\text{mol photons m}^{-2} \text{ s}^{-1}$ .  $1.5 - 2 \times 10^7$

total cell were collected at mid-exponential phase and the pellet was resuspended in 0.5 ml 2% SDS, 400 mM NaCl, 40 mM EDTA, 100 mM Tris-HCl pH 8.0 and dimethyl pyrocarbonate (DEPC) water to lyse the cells, followed by the addition of 0.5 ml of PFL (lysis buffer provided by the kit with guanidine hydrochloride 36-50%) and 20 µl of PFR (reduction buffer sodium sulfite 10-20%). The samples were centrifuged for 1 min at 14000 g and 25°C. To filter the lysate, NucleoSpin® RNA Plant and Fungi column (green ring) was inserted into a Collection tube (2 ml, provided) and the clear lysates were loaded onto the column and then centrifuged for 1 min at 14000 g. The RNA binding conditions were adjusted by adding 0.5 ml PFB binding buffer (lithium chloride 40-70%) to the flowthrough which was mixed by pipetting and incubated for 5 min at 25°C. The RNA was then bound in the NucleoSpin® RNA Plant and Fungi column (light blue ring) pre-assembled with a Collection Tube. First, 0.650 ml were added, followed by a centrifuge of 30 s at 14000 g, 25°C. The flowthrough was discarded, and the collection tube reused for the rest of the volume (approx. 0.2 ml) which was centrifuged for 30 s at 14000 g, 25°C. The collection tube with the flowthrough was discarded and the column was inserted into a fresh collection tube (2 ml, provided) for the following washing steps. 0.5 ml of PFW1 washing buffer were added and centrifuged for 1 min at 14000 g, 25°C. The flowthrough was discarded and 0.5 ml of PFW2 washing buffer were added onto the column and centrifuged for 1 min at 14000 g and 25°C (x2). An additional centrifuge step was added to remove the residue of the PFW2 buffer. The RNA was finally eluted by inserting the column into a fresh collection tube (1.5 ml, provided), by adding 50 µl of RNase-free H<sub>2</sub>O onto the column and incubated for approximately 1 min at 25°C. The RNA was collected by centrifuge for 1 min at 14000 g, 25°C. The concentration and the purity (260/280 ratio 2.0-2.1) of RNA was checked with the NanoDrop (Gen5 Spectrophotometer) and with gel electrophoresis. The RNA extracted was used for cDNA synthesis to confirm the presence of the *SRX2* transcripts in the complemented strains.

### 3.2.3.3 *cDNA synthesis and RT-PCR*

Total RNA was treated with DNase (Promega, M6101) to remove any traces of DNA, prior synthesis of cDNA. Samples (1.5 µg total RNA) were incubated with 1.5 µl of 10X DNase buffer (400 mM Tris-HCl pH 8.0, 100 mM magnesium sulfate (MgSO<sub>4</sub>), 10 mM calcium chloride (CaCl<sub>2</sub>)), 1.5 µl RQ1 Dnase (1 u) and

Nuclease-free H<sub>2</sub>O up to 15 µl for 30 min at 37 °C. The reaction was stopped by adding 1 µl of DNase stop solution and incubating the samples 5 min at 65 °C and then chilling them on ice. The RNA was directly used for cDNA synthesis by using Thermo Scientific RevertAid H Minus First Strand cDNA Synthesis Kit (K1632). 5 µl (500 ng) of treated RNA were taken and mixed with 1 µl of Random primers and 6 µl of Nuclease-free H<sub>2</sub>O up to 12 µl. The mix was incubated for 5 min at 65 °C as the RNA-template of *Chlamydomonas* is rich in GC content. Then, the rest of the products were added in the following order: 4 µl of 10X Reaction buffer, 1 µl of RiboLock RNase inhibitor (20U/µl), 2 µl of 10 mM dNTP mix, 1 µl of RevertAid H Minus M-MuLV Reverse Transcriptase (200 U/L) up to total 20 µl. The mix was incubated for 5 min at 25 °C, 60 min at 45°C and 5 min at 70 °C. The synthesised cDNA was directly used for PCR. The presence of the mature transcripts corresponding to *SRX2* gene in the wt and the complemented strains of *srx2* mutant was confirmed by using the primers listed in **Table S1**.

#### 3.2.3.4 Crossing of mutants

Crossing between each mutant *mt*<sup>-</sup> (listed in **Table 1**) and a *mt*<sup>+</sup> wt strain from the laboratory collection were performed to confirm the presence of one paromomycin cassette in the mutants. Firstly, gametogenesis was induced by inoculating each mutant cell in 0.5 ml in M-N minimal N-free medium (Sager & Granick 1953) for 8 h. Further, gametes of *mt*<sup>+</sup> and *mt*<sup>-</sup> cells were mixed in a 15-ml tube and let under continuous light for 16 h to let them fuse and form zygotes. The zygotes were plated on nitrogen-deficient solid medium containing acetate (agar 3%). After five days under continuous light, zygotes were encrusted into the agar, while the vegetative cells were on the surface. With the help of a microscope and a sterile razor blade, a thin piece of agar was cut and placed on a fresh acetate solid medium plate to rehydrate the cells. Any vegetative cells remaining were removed by exposing the plate to chloroform for 45 s. After 12 h, 0.5 ml of sterile water was added to the plates to allow germination of the zygotes and the meiotic progeny was spread by plating. After two weeks, 120 single colonies per each mutant were randomly picked and placed in acetate solid medium. Four days later single colonies were then “printed” by using filter paper, on acetate solid medium plate and in acetate plus paromomycin solid medium plate to check the segregation of the cassette. After five days the colonies

resistant to paromomycin were counted. The results are reported as percentage in **Table 2**.

The same procedure was performed to generate double mutants between *srx2* mt<sup>-</sup> and *apx2* mt<sup>+</sup>.

### 3.2.3.5 Transformation of *srx2* mutant

Transformation of the *srx2* mutant was performed according to the method reported by (Shimogawara et al 1998). Cells of *srx2* mutant were cultivated in 100 ml acetate liquid medium and incubated in continuous low light (50  $\mu\text{mol photons m}^{-2} \text{s}^{-1}$ ) until the mid/late-exponential phase.

Before the transformation, the *SRX2* target gene and the hygromycin B resistant cassette for colony selection, were amplified. The *SRX2* gene was amplified using specific primers including the sequences of the restriction enzymes *NdeI*, *EcoRI* (**Table S1**). The hygromycin B resistant cassette (APHVII; 1710 bp) from the plasmid pHyg3 (4376 bp) (**Fig. 2**) was amplified with APH7-F and APH7-R (**Table S1**). The PCR products were purified with Wizard® SV Gel and PCR Clean Up System Promega kit (#A9282). 25 ml of *srx2* mutant culture was collected at a cell density of  $7 \times 10^6$  cells/ml and centrifuged for 5 min at 2000  $\times g$  and 25°C. Cells were gently resuspended in 1.5 ml of acetate medium plus 40 mM of sucrose to reach a cell density of  $10^8$  cells/ml. Samples were then prepared in a sterile 4 mm gap cuvette containing 250  $\mu\text{l}$  of culture at  $10^8$  cells/mL (to have  $2.5 \times 10^7$  cells per transformation), 2.5  $\mu\text{l}$  herring sperm DNA (10 mg/ml in water), 10  $\mu\text{l}$  of gene of interest (500 ng of purified *SRX2* gene) and 3  $\mu\text{l}$  of purified plasmid hygromycin B resistant (total 1  $\mu\text{g}$ ). Positive and negative controls were also included. The positive control was prepared by adding 250  $\mu\text{l}$  of culture, 2.5  $\mu\text{l}$  herring sperm DNA 10 mg/ml and 3  $\mu\text{l}$  of the resistance cassette to hygromycin B (1  $\mu\text{g}$ ), while the negative control contained 250  $\mu\text{l}$  culture and 2.5  $\mu\text{l}$  herring sperm DNA. The samples were gently homogenised and submitted to electroporation following the standard parameters 800 V, 800  $\Omega$ , 25  $\mu\text{F}$ . Electroporated cells were placed in a sterile glass tube with 3 ml of fresh acetate medium shaking O/N at 25 °C under low continuous light 50  $\mu\text{mol photons m}^{-2} \text{s}^{-1}$ . The next day, cells were harvested by centrifugation at 900  $g$  for 5 min at 25°C and resuspended in the residual supernatant. The cells were gently plated on acetate solid medium plates containing hygromycin B (25  $\mu\text{g/ml}$ ) and cells

were grown under continuous low light  $50 \text{ photons } \mu\text{mol m}^{-2} \text{ s}^{-1}$ . The cells were screened by PCR using primers *srx2\_F2* and *srx2\_R2*.

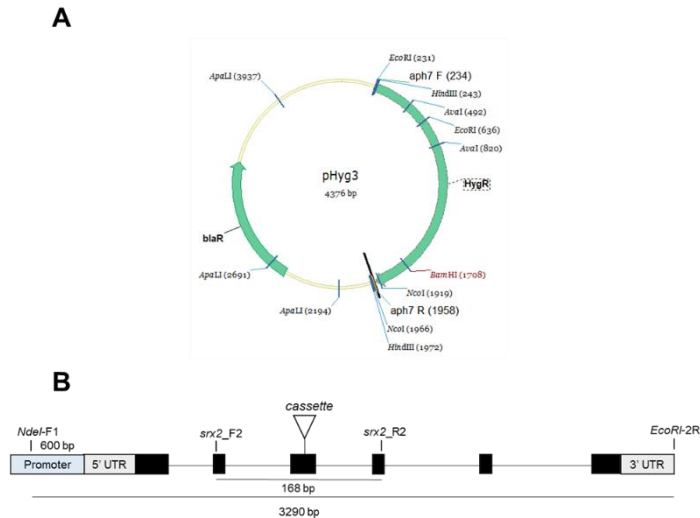


**Figure 2: Map of the plasmid and scheme of the *SRX2* gene construct used for transformation.** **A)** Map of the pHyg3 plasmid containing the hygromycin B resistant cassette (*HygR*) used as selection marker. **B)** Scheme of the *SRX2* gene, showing the size of the *NdeI-F1* and *EcoRI-2R* amplified fragment (3290 bp) for the transformation, and the size of the *srx2\_F2* and *srx2\_R2* amplified fragment (168 bp, without the cassette insertion) for transformant screening.

### 3.2.4 ROS measurements

#### 3.2.4.1 $H_2O_2$ measurement (*AmplexRed*)

Cultures of wt and *apx2* mutant were grown in triplicate in continuous low light ( $50 \text{ } \mu\text{mol photons m}^{-2} \text{ s}^{-1}$ ) in phototrophic condition until the mid-exponential phase. The day before the measurement, the reaction buffer was made ready by introducing  $150 \text{ } \mu\text{M}$  diethylenetriamine pentaacetate (DTPA) used to chelate divalent metals dissolved in the cultivation medium (minimal medium - TMP). Before starting the measurements, the stock solutions were prepared as described in the *AmplexRed* kit (Invitrogen, A22188). A stock of the *Amplex Red* probe at  $10 \text{ mM}$  in dimethyl sulfoxide (DMSO) was prepared, a stock solution of horseradish peroxidase at  $10 \text{ U/ml}$  in  $0.25 \text{ M}$  sodium phosphate buffer pH 7.4

(NaPO<sub>4</sub>) was prepared and 0.2 mM H<sub>2</sub>O<sub>2</sub> working solution was prepared by diluting 30% H<sub>2</sub>O<sub>2</sub> (9.8 M, Fluka, 31642) in the appropriate volume of reaction buffer. The stock solution of H<sub>2</sub>O<sub>2</sub> was used to prepare the standard curve.

The experiment was carried out in 1.5-ml Eppendorf tubes by mixing 250 µl of each cell replicate (30 µg chlorophyll/ml) with 250 µl of reaction mix (for 5 ml: 50 µl from 10 mM Amplex Red, 100 µl from 10 U/ml horseradish peroxidase and 4.85 ml TMP + DTPA). Samples were then placed under the same growing light (50 µmol photons m<sup>-2</sup> s<sup>-1</sup>) or under high light (500 µmol photons m<sup>-2</sup> s<sup>-1</sup>) for 1 h, covered by a “Rose pink” filter (Lee Filters, Andover, UK) as the Amplex Red probe is sensitive to the green/blue light range. Positive (reaction mix with probe + cells) and negative (reaction buffer without probe + cells) controls were also run in tandem in the dark and in the light only for positive controls. At the end of exposure time, samples were centrifuged for 5 min at 2300 g, 25°C and 100 µl of the supernatant were transferred into a flat black 96-well microplate (Greiner, 655087) together with the H<sub>2</sub>O<sub>2</sub> standard curve. Before measuring the absorbance, 20 µl of Amplex Red stop reagent (Invitrogen, A33855) was added to each well. The absorbance was measured with the Gen5 software (SynergyMX, BioTek) at an excitation wavelength of 530 nm and at an emission wavelength of 590 nm. Concentration of H<sub>2</sub>O<sub>2</sub> in the samples was calculated considering the absorbance of the standard curve and normalising the values to the chlorophyll content.

#### 3.2.4.2 H<sub>2</sub>O<sub>2</sub> measurement (CM-H<sub>2</sub>DCFDA probe)

Cultures of wt and *apx2* mutant were grown in triplicate in phototrophy under continuous low light intensity (50 µmol photons m<sup>-2</sup> s<sup>-1</sup>) until mid-exponential phase. Cells were harvested and chlorophyll concentration was set to 2.25 µg/ml in the same cultivation medium (TMP). Samples were then collected by centrifugation; the supernatant was discarded, and the pellet resuspended in fresh medium containing 150 µM diethylenetriamine pentaacetate (DTPA). 10 µM probe (stock of 1 mM dissolved in dimethyl sulfoxide) was added. Samples were then incubated 20 min in the dark to allow the probe to penetrate the cells. Meanwhile, cells for negative control (without probe) were prepared. At the end of the 20 min incubation, cells were washed once to remove excess of probe and resuspended in fresh medium. For each replicate, 1 ml was transferred into a 24-



well plate (Greiner®, 662150). For each plate, negative and positive controls were included. The positive control was made of 500  $\mu\text{M}$  of menadione sodium bisulphite (MSB), from a stock solution of 10 mM dissolved in  $\text{H}_2\text{O}$ . The positive control produced constant levels of ROS. Each of the controls and the sample replicates were prepared in triplicate. Baseline of fluorescence was determined before the light incubation with the Gen5 software (SynergyMX, BioTek) with excitation fluorescence at 492 nm and emission at 530 nm. Considering that the CM- $\text{H}_2\text{DCFDA}$  probe (Invitrogen, C6827) is sensitive to blue light, to avoid any interferences, the plates were placed in the SpeedZen camera as it uses red light (700 nm), for 1 h at continuous low light ( $45 \mu\text{mol photons m}^{-2} \text{s}^{-1}$ ) and high light ( $570 \mu\text{mol photons m}^{-2} \text{s}^{-1}$ ). After 1 h of incubation, the fluorescence was measured once more. The fold increase of ROS was then calculated by taking the fluorescence of the negative control and subtracting it from that of both the wt and *apx2* mutant samples. This value was then normalised per  $\mu\text{g}$  of chlorophyll.

### 3.3 Results

#### 3.3.1 Screening of mutants defective in $\text{H}_2\text{O}_2$ -signaling and stress responsive enzymes

To investigate the  $\text{H}_2\text{O}_2$ -signaling in *Chlamydomonas*, a comprehensive search of the literature was conducted to identify key redox enzymes that play a direct or indirect role in ROS detoxification and are found within organelles such as chloroplasts and mitochondria, as well as in the cytosol and secretory pathway. Following an initial *in silico* analysis of the putative localization of redox enzymes and a comparison with *Arabidopsis* sequences, we ordered 17 mutants corresponding to 10 genes (**Table 1**) encoding  $\text{H}_2\text{O}_2$ -scavenging enzymes and stress-responsive proteins from the CLiP library (Li et al 2019). Ascorbate peroxidases (selected APX1 and APX2), catalases (selected CAT2), glutathione peroxidases (selected GPX3), peroxiredoxins (selected PRX4) were chosen as they are the most important representative of  $\text{H}_2\text{O}_2$  scavengers as they transform this molecule into  $\text{H}_2\text{O}$  and  $\text{O}_2$  (Caverzan et al 2012). Nucleoredoxins (selected NRX1 and NRX2) and sulfiredoxins (selected SRX2) belong to the thioredoxin (TRX) family and they are indirectly involved in ROS detoxification. Nucleoredoxins protect antioxidant enzymes from ROS-induced oxidation like catalase (Kneeshaw et al 2017) (Kang et al 2020) or enhancing antioxidant enzymes expression upon heat stress such as in tomato (Cha et al 2022).

Sulfiredoxins decrease oxidation power of 2-cys peroxiredoxins by reducing the sulfinylated form (-SO<sub>2</sub>H) back to sulfenylated form (-SOH), thus avoiding 2-cys peroxiredoxin overoxidation (Dietz 2011). Glutathione-S-transferases (selected GST13) might be potentially involved in bioremediation as they are involved in detoxification of reactive electrophiles (Chatzikonstantinou et al 2017). Truncated hemoglobins (selected THB5, previous identifier PRX according to Phytozome <https://phytozome-next.jgi.doe.gov/>, in CLiP library still indicated as PRX) are involved in nitric oxide (NO) stress-mediated which influence and interact with ROS molecules during signaling process upon abiotic stress like drought, salinity and thermal stress (Farnese et al 2016). Respiratory burst oxidases (selected RBO1, previous identifier RBOL1 according to Phytozome <https://phytozome-next.jgi.doe.gov/>) are also regulating NO stress-mediated (Kuo et al 2020b) and are generating ROS molecules (Mittler 2017) involved in which is localised in the outer membrane of mitochondria in Arabidopsis and involved in pathogen defence, salicylic acid production and ROS signaling (Zhang et al 2014a). This suggests a possible role of promoting ROS signaling regulation also in Chlamydomonas.

**Table 1.** List of mutants defective in H<sub>2</sub>O<sub>2</sub>-signaling and stress responsive enzymes ordered from CLiP library (Li et al 2019). Putative localisation of the enzyme was predicted by using Predalgo prediction tool (Tardif et al 2012).

Enzyme name	Gene symbol	Gene identifier	Putative localization	CLiP reference	References
Ascorbate peroxidase 1	APX1	Cre02.g087700	Chloroplast	LMJ.RY040 2.208295	(Blaby et al 2015)
Ascorbate peroxidase 2	APX2	Cre06.g285150	Chloroplast	LMJ.RY040 2.180063	(Blaby et al 2015)
Catalase 2	CAT2	Cre01.g045700	Cytosol	LMJ.RY040 2.051905 LMJ.RY040 2.133009	(Blaby et al 2015)

Glutathione peroxidase 3	GPX3	Cre03.g 197750	Chloroplast	LMJ.RY040 2.196379 LMJ.RY040 2.229175	(Blaby et al 2015)
Glutathione-S-transferase 13	GST13	Cre17.g 721350	Other	LMJ.RY040 2.216443	(Chatzikonstantinou et al 2017)
Nucleoredoxin 1	NRX1	Cre02.g 094100	Other	LMJ.RY040 2.211911	(Blaby et al 2015)
Nucleoredoxin 2	NRX2	Cre02.g 093750	Other	LMJ.RY040 2.046208 LMJ.RY040 2.197028	(Blaby et al 2015)
Truncated hemoglobin	THB5 (PRX)	Cre07.g 351100	Other	LMJ.RY040 2.193060 LMJ.RY040 2.054490	(Hemschmeier et al 2013)
Peroxiredoxin 4	PRX4	Cre02.g 080900	Mitochondrion	LMJ.RY040 2.039746	(Blaby et al 2015)
Respiratory burst oxidase	RBO1	Cre03.g 188300	Secretory pathway	LMJ.RY040 2.245260	(Mittler 2017)
Sulfiredoxin 2	SRX2	Cre17.g 729950	Chloroplast	LMJ.RY040 2.082299	(Blaby et al 2015)
ATP-ase-AAA	LCA1	Cre02.g 106450	Secretory pathway	LMJ.RY040 2.045556 LMJ.RY040 2.108723	(Zhang et al 2014a)

The CLiP library counts 60,000 insertional mutants which makes difficult to prior screen all of them and subsequent select mutants which display interesting phenotype under H<sub>2</sub>O<sub>2</sub>-mediated stress. Indeed, the selection of CLiP mutants was carried out based on the genetic profile described on the webpage for each mutant. A short DNA sequence corresponding to the junctions (5' and 3' ends) of the cassette is provided, and a confidence score is attributed to the sequence, a 95% confidence score represents the most reliable mutants. Therefore, we chose these mutants because the presumed resistance cassette was situated within the gene coding region, with a 95% confidence level regarding the DNA sequence. The resistance cassette is described in **Fig. 3**.

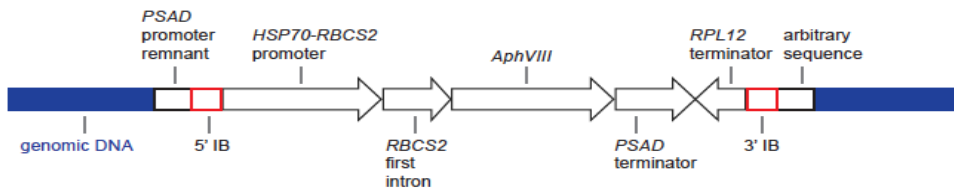


**Figure 3: Scheme of the CIB1 cassette of the CLiP mutants, conferring resistance to paromomycin (*AphVIII*).** CIB1 is a DNA cassette with two random regions of 22-bp called internal barcode (IB). For mutants generated with this cassette (those starting with LMJ.RY0402 in their IDs), there is a unique IB corresponding to each insertion junction, which is indicated in the description page of the selected mutant.

The first part of the study was focused on the analysis of the mutant strains using molecular and genetic approaches. Single cell colonies of the mutants were picked up to extract the DNA for sequencing analyses (**Fig. S1**) to confirm the presence of the cassette. Out of the 17 mutants, seven could be confirmed showing the correct localization of the cassette at both sides of the insertion (**Table 2**). In addition, the presence of a single cassette insertion in the strains was analysed by crossing (Goodenough et al 2007) the mt<sup>-</sup> mutant with an mt<sup>+</sup> wt from the laboratory collection. If a single cassette is inserted in the nuclear genome of the mutant, 50% of the meiotic progeny should inherit it. If two cassettes are inserted at different localizations, 75% of the meiotic progeny should inherit it. As shown in **Table 2** some of the mutants (*e.g. apx1* or *rbol1*) present a segregation which does not follow the expected inheritance and crosses should be repeated. Despite that, mutants located in *apx2*, *srx2*, *gpx3-1* and *lca1-2* could be correctly localised in the corresponding genes and present only one cassette as shown by the crosses (considered as ‘clean’ mutants).

**Table 2.** Summary of the molecular and genetic screening of the 17 mutants.

Gene name	Molecular characterization	Genetic characterization
	Confirmation of the cassette insertion – junction (sequencing data)	Confirmation of the presence of a single cassette (%)  Cross mutant (mt <sup>-</sup> ) x wt (mt <sup>+</sup> )
Ascorbate peroxidase 1 ( <i>apx1</i> )	5' and 3' sides	67
Ascorbate peroxidase 2 ( <i>apx2</i> )	5' and 3' sides	57
Catalase 2 ( <i>cat2-1</i> )	5' and 3' sides	60
Catalase 2 ( <i>cat2-2</i> )	X (different gene)	X
Glutathione peroxidase 3 ( <i>gpx3-1</i> )	5' and 3' sides	48
Glutathione peroxidase 3 ( <i>gpx3-2</i> )	5' side	86
Nucleoredoxin 1 ( <i>nrx1</i> )	5' and 3' sides	70
Nucleoredoxin 2 ( <i>nrx2-1</i> )	3' side	54
Nucleoredoxin 2 ( <i>nrx2-2</i> )	no cassette	X
Glutathione – S – transferase 13 ( <i>gst13</i> )	no cassette	X

Truncated hemoglobin ( <i>thb5-1</i> )	5' and 3' sides*	50
Truncated hemoglobin ( <i>thb5-2</i> )	5' and 3' sides*	50
Peroxiredoxin 4 ( <i>prx4</i> )	X (different gene)	X
Respiratory burst oxidase ( <i>rbo1</i> )	5' and 3' sides	64
Sulfiredoxin 2 ( <i>srx2</i> )	5' and 3' sides	56
ATP-ase-AAA ( <i>lca1-1</i> )	Not found	X
ATP-ase-AAA ( <i>lca1-2</i> )	5' and 3' sides	46

\*Not 100% matching with the reference sequence.

In parallel, a phenotypical characterization was performed by drop test screenings of all the mutant strains in minimal medium (TMP)- or acetate (TAP)-agar plate. The plates were exposed to continuous low ( $50 \mu\text{mol photons m}^{-2} \text{s}^{-1}$ ) or high light ( $500 \mu\text{mol photons m}^{-2} \text{s}^{-1}$ ), circadian cycles with 12 h of light at  $50 \mu\text{mol photons m}^{-2} \text{s}^{-1}$  and 12 h of darkness, and continuous darkness for those mutants plated on acetate medium plates (some examples in **Fig. 4**). The drop tests did not give any clear visible phenotype, even for the mutants considered 'clean' (*apx2*, *gpx3.1*, *srx2* and *lca1.2*), probably due to a compensation of other ROS enzymes different from the disrupted one or to not enough ROS production to trigger any responses affecting the growth. The study of the phenotype was then carried out in liquid cultures by checking the maximum quantum yield of PSII (Fv/Fm) in those cells grown in mixotrophy under continuous low light ( $50 \mu\text{mol photons m}^{-2} \text{s}^{-1}$ ) or in circadian cycle (12h dark/12h low light  $50 \mu\text{mol photons m}^{-2} \text{s}^{-1}$ ). The Fv/Fm parameter indicates the maximum efficiency of PSII to perform photochemical reactions, and it is widely used to identify structural

and functional changes in the overall photosynthetic activity of photosynthetic organisms. This experiment allowed us to check the cell acclimation in different light exposure and their response to stress by adding 1 mM or 5 mM H<sub>2</sub>O<sub>2</sub> for 15 min or 30 min (**Table 3** and **Table 4**). The effect of H<sub>2</sub>O<sub>2</sub> in the mutants compared to the wt was analysed by considering the difference of the Fv/Fm value in control conditions without H<sub>2</sub>O<sub>2</sub> in comparison with the treatment with 1 mM and 5 mM H<sub>2</sub>O<sub>2</sub>. Some differences between the control and treated conditions are observed. For example, in some mutants like *apx2*, *tbh5-1* and *rbo1* from low light growing conditions, the Fv/Fm in presence of 1 mM H<sub>2</sub>O<sub>2</sub> is slightly higher between 4 and 9% than in control conditions (0 mM) (**Table 3**). In the circadian cycle, some effects were observed in the presence of 5 mM H<sub>2</sub>O<sub>2</sub>. For *nrx1*, *tbh5-2*, *lca1-1*, the Fv/Fm decreased in presence of H<sub>2</sub>O<sub>2</sub> between 5 and 9 % more compared to the decrease observed in the wt, suggesting a higher damage on the PSII (**Table 4**). On the other hand, other mutants, *nrx2-1*, *prx4*, *srx2* and *lca1-2*, displayed a decrease of Fv/Fm value in the presence of H<sub>2</sub>O<sub>2</sub>, with less extent than the decrease of the wt, between 5 and 9%, suggesting instead, a possible higher tolerance of the stress. The effect of H<sub>2</sub>O<sub>2</sub> on Fv/Fm should be tested in cells at the mid exponential phase of growth. Our cells most likely were not in this phase and it might have influenced the Fv/Fm value, which is typically reported to be 0.6-0.7 in *Chlamydomonas* (Bonente et al 2012). Nevertheless, this exploratory search helped us to conclude that the addition of H<sub>2</sub>O<sub>2</sub> to cells in these growing conditions do not show a clear and straightforward phenotype. For future experiments, other conditions can be tested to induce a stronger stress, like fluctuating light or circadian cycle with high light intensity, either with or without addition of H<sub>2</sub>O<sub>2</sub>. Another possibility would be to repeat

it in minimal medium to maximise the use of photosynthesis, thus including another stress layer in the mutants.

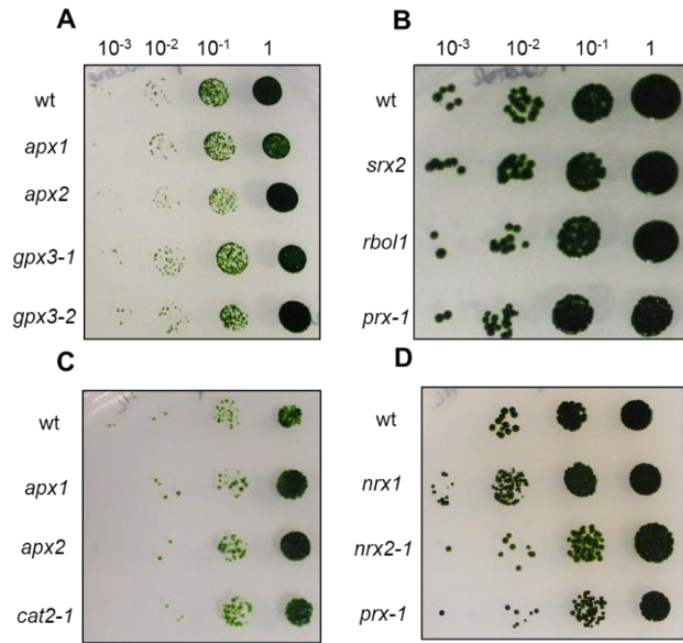


**Figure 4: Drop tests of wt and mutants on agar plates did not show any phenotypical differences.** A) and B) drop tests in continuous low light in phototrophy and mixotrophy respectively. C) and D) drop tests in continuous high light in phototrophy and mixotrophy respectively.



**Table 3.** Maximum quantum yield of PSII (Fv/Fm) of the wt and mutant strains grown in continuous low light condition with and without H<sub>2</sub>O<sub>2</sub> for 15 min and 30 min showed some significant differences. The percentages (%) are calculated by subtracting the value of Fv/Fm measured in the presence of H<sub>2</sub>O<sub>2</sub> to the control value. Average of 2 biological replicates per each strain with standard deviation. Statistical analyses with ANOVA One-Way, Dunnett's test, p-value < 0.0001\*\*\*\*, p-value < 0.01\*\*, p-value < 0.05\*, p-value > 0.05 ns relative to wt.

Strain	Fv/Fm control	15 min		30 min	
		ΔFv/Fm 0 mM – 1 mM (%)	ΔFv/Fm 0 mM – 5 mM (%)	ΔFv/Fm 0 mM – 1 mM (%)	ΔFv/Fm 0 mM – 5 mM (%)
wt	0.568 ± 0.007	3 ± 2	37 ± 3	1 ± 4	31 ± 4
<i>apx1</i>	0.621 ± 0.022	-1 ± 1	22 ± 2*	-2 ± 2	27 ± 3
<i>apx2</i>	0.579 ± 0.006	-7 ± 1**	25 ± 8	-4 ± 2	31 ± 2
<i>gpx3-1</i>	0.543 ± 0.006	5 ± 2	27 ± 5	3 ± 0	14 ± 4
<i>gpx3-2</i>	0.422 ± 0.008****	-1 ± 3	36 ± 2	-12 ± 2*	22 ± 7
<i>nrx1</i>	0.580 ± 0.016	6 ± 3	40 ± 4	7 ± 4	31 ± 0
<i>nrx2-1</i>	0.521 ± 0.002	-4 ± 0*	26 ± 0	1 ± 1	12 ± 3
<i>thb5-1</i>	0.489 ± 0.007**	-9 ± 2**	29 ± 0	-12 ± 2*	18 ± 1
<i>thb5-2</i>	0.528 ± 0.032	-2 ± 0	26 ± 0	-1 ± 5	19 ± 1
<i>prx4</i>	0.512 ± 0.003*	-8 ± 2**	48 ± 5	-5 ± 2	35 ± 5
<i>rbo1</i>	0.531 ± 0.018	-6 ± 2*	29 ± 0	-5 ± 1	18 ± 1

<i>srx2</i>	0.509 ± 0.011*	7 ± 4	38 ± 3	6 ± 3	32 ± 3
<i>lca1-1</i>	0.449 ± 0.027****	-1 ± 5	21 ± 7*	5 ± 9	16 ± 10
<i>lca1-2</i>	0.506 ± 0.032*	1 ± 1	19 ± 5**	4 ± 5	17 ± 1

**Table 4.** Maximum quantum yield of PSII (Fv/Fm) of the wt and mutant strains in circadian cycle with and without H<sub>2</sub>O<sub>2</sub> exposed for 15 min, showed some significant differences. The percentages (%) are calculated by subtracting the value of Fv/Fm measured in the presence of H<sub>2</sub>O<sub>2</sub> to the control value. Average of 2 biological replicates per each strain with standard deviation. Statistical analyses with ANOVA One-Way, Dunnett's test, p-value < 0.0001\*\*\*\*, p-value < 0.001\*\*\*, p-value < 0.01\*\*, p-value < 0.05\*, p-value > 0.05 ns relative to wt.

Strain	Fv/Fm control	15 min	
		ΔFv/Fm 0 mM – 1 mM (%)	ΔFv/Fm 0 mM – 5 mM (%)
wt	0.525 ± 0.027	4 ± 1	29 ± 3
<i>apx1</i>	0.529 ± 0.015	-3 ± 2*	24 ± 1**
<i>apx2</i>	0.517 ± 0.012	3 ± 0	34 ± 0**
<i>gpx3-1</i>	0.540 ± 0.002	2 ± 3	30 ± 0
<i>gpx3-2</i>	0.516 ± 0.010	3 ± 1	27 ± 1
<i>nrx1</i>	0.524 ± 0.019	7 ± 0	38 ± 0****
<i>nrx2-1</i>	0.532 ± 0.026	3 ± 1	24 ± 0*
<i>thb5-1</i>	0.553 ± 0.004	7 ± 1	35 ± 0**

<i>thb5-2</i>	$0.532 \pm 0.002$	$23 \pm 5^{*****}$	$27 \pm 0$
<i>prx4</i>	$0.493 \pm 0.004$	$-1 \pm 0$	$20 \pm 1^{***}$
<i>rbo1</i>	$0.483 \pm 0.021^*$	$1 \pm 2$	$32 \pm 2$
<i>srx2</i>	$0.543 \pm 0.013$	$4 \pm 0$	$24 \pm 3^{**}$
<i>lca1-1</i>	$0.522 \pm 0.009$	$5 \pm 0$	$34 \pm 1^{**}$
<i>lca1-2</i>	$0.509 \pm 0.006$	$5 \pm 1$	$20 \pm 1^{*****}$

At that point of my thesis, it was decided to focus the research on two mutants that would show interesting characteristics based on the literature. According to (Blaby et al 2015), the expression of *SRX2* increases upon  $H_2O_2$  addition, while that of *APX2* does not, making the comparison between these two genes interesting to understand  $H_2O_2$ -signaling. The reason why they were chosen is also related to their function. The former is involved in the reversible oxidation from sulfinylation to sulfenylation of protein cysteines (Liu et al 2006). *APX2*, on the other hand, has been classified as an ascorbate peroxidase-related protein (Lazzarotto et al 2021a), whose ortholog in Arabidopsis has been proven to not bind ascorbate *in vitro* and whose role *in vivo* is still to be clarified.

### 3.3.2 Exploring the phenotype of the *srx2* and the *apx2* mutants

First, we evaluated the growth rates of the *srx2* and *apx2* mutants compared to the wt, under continuous low light ( $50 \mu\text{mol photons m}^{-2} \text{s}^{-1}$ ) in mixotrophic and phototrophic conditions (**Table 5**). As these enzymes are putatively localized in the chloroplast, investigation was performed on the photosynthetic parameters with and without  $H_2O_2$  treatment. The maximum quantum yield of PSII of cells grown in acetate medium did not show any differences (**Fig. 5 A**). In addition, we measured the relative electron transfer rate (rETR) at increasing light intensities using the Joliot-Type-Spectrophotometer (JTS-10 BioLogic, France) in control condition with a pre-treatment of 0.5 mM of  $H_2O_2$  for one hour or six hours, and with a second addition of  $H_2O_2$  up to 1.5 mM right before the measurement (**Fig. 5 B, C, D, E**) as described in (Murik et al 2014). In their work, the authors explained that during the pre-treatment time, the cells activate various antioxidant defence mechanisms resulting in more sensitivity of the cells

to the second addition of H<sub>2</sub>O<sub>2</sub>. In the specific case of the *srx2* and *apx2* mutants we could observe some significant differences in the electron transport after one or six hours of H<sub>2</sub>O<sub>2</sub> exposure (**Fig. 5 B, C, D, E**). The rETR of *srx2* was higher than the wt in control condition and in treatment condition with H<sub>2</sub>O<sub>2</sub> after 1 and 6 hours, for light intensities higher than 100 μmol photons m<sup>-2</sup> s<sup>-1</sup>. In the *apx2*, the rETR was lower than the wt in all conditions tested after 6 hours. Such an experimental setup confirmed the hypothesis regarding the compensatory impact of H<sub>2</sub>O<sub>2</sub> scavenging enzymes, as the presence of H<sub>2</sub>O<sub>2</sub> had no influence on the tested mutants.

**Table 5.** Growth rate expressed in doubling time (hour) of *srx2* and *apx2* cells grown under continuous low light 50 μmol photons m<sup>-2</sup> s<sup>-1</sup> in phototrophy are similar to the wt. Average of at least 3 biological replicates per each strain with standard deviation. Statistical analyses with ANOVA One-Way, Dunnett’s test, p-value < 0.05\*, p-value > 0.05 ns relative to wt. ND, not determined.

Strain	Mixotrophy	Phototrophy
wt	8 ± 1	38 ± 8
<i>srx2</i>	ND	42 ± 4
<i>apx2</i>	9 ± 1	38 ± 5

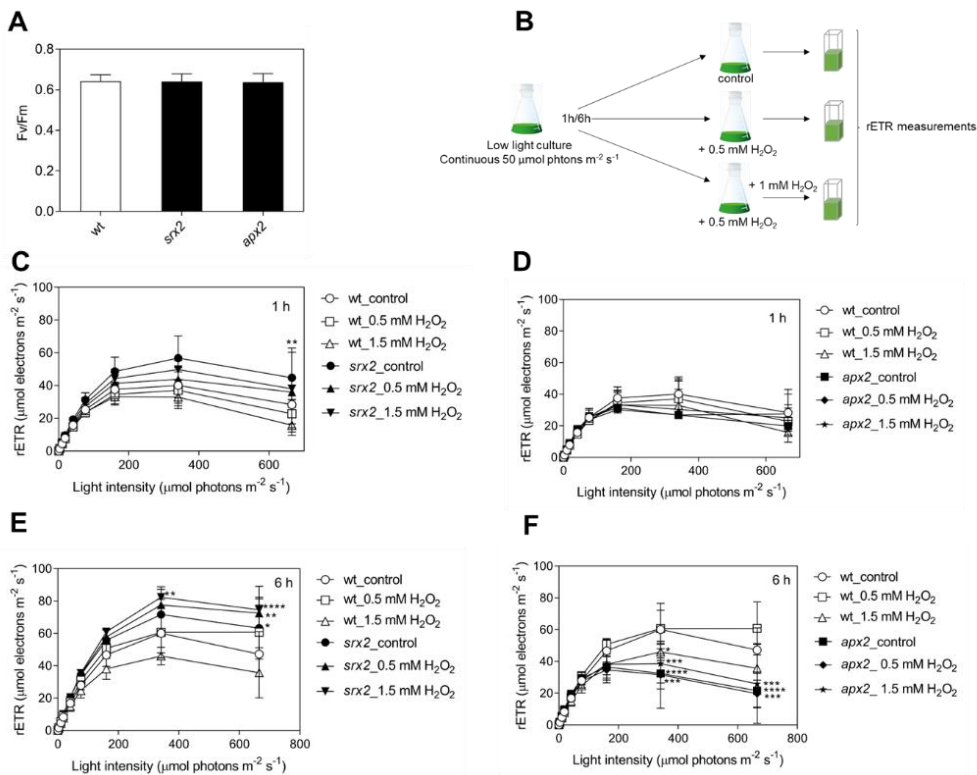


**Figure 5: Maximum quantum yield of PSII and rETR of *srx2* and *apx2* mutants grown in acetate medium in control condition (TAP) and submitted to H<sub>2</sub>O<sub>2</sub> treatment did not show any significant differences compared to the wt. A)** Fv/Fm of wt, *srx2* and *apx2* cells grown in low light. **B)** Scheme of the experiment set up. **C)** and **D)** rETR of wt and *srx2* and *apx2* mutants in control condition and during the pre-treatment with 0.5 mM H<sub>2</sub>O<sub>2</sub>. **E)** and **F)** rETR of wt and *srx2* and *apx2* after a second addition of H<sub>2</sub>O<sub>2</sub> up to 1.5 mM. Average of at least 3 biological replicates per each strain with standard deviation. Statistical analyses with ANOVA One-Way or ANOVA Two-Ways, Dunnett's test, p-value < 0.0001\*\*\*\*, p-value < 0.001\*\*\*, p-value < 0.01\*\*, p-value < 0.05\*, p-value > 0.05 ns.

### 3.3.3 Isolation of *srx2 apx2* double mutants and complemented strains of the *srx2* mutant

To increase the possibility of having a strain more susceptible to oxidative stress and to activate a response to H<sub>2</sub>O<sub>2</sub>, we generated double mutants by crossing *srx2* and *apx2* mutants. A cross between *srx2* paromomycin<sup>R</sup> (resistant) mt<sup>-</sup> and *apx2* paromomycin<sup>R</sup> mt<sup>+</sup> was made. From the crossing shown in **Fig. 6**, 33 meiotic products out of 120 were paromomycin<sup>S</sup> (sensitive), which was the expected ratio (25%) since the two paromomycin cassettes segregate independently. The

screening of the double mutants *srx2 apx2* was assessed by PCR on the paromomycin<sup>R</sup> progeny where 1/3 of the meiotic products displayed both cassettes.

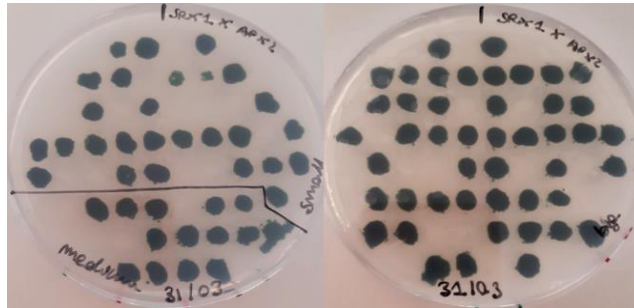


**Figure 6:** Crossing between *srx2* and *apx2* shows paromomycin<sup>R</sup> cells.  $\frac{3}{4}$  progeny positive on paromomycin plates.

Complemented strains of the *srx2* mutant were generated by transforming the mutant according to (Shimogawara et al 1998). For the complementation, *SRX2* gene was amplified from wt DNA in a region of 3290 bp starting 600 bp before the start codon in the promoter region and ending at the end of the 3' UTR (**Fig. 7 A**) with primers *NdeI*-1F and *EcoRI*-2R (**Table S1**). A co-transformation was performed using the *SRX2* gene fragment and a PCR fragment which amplifies the gene conferring resistance to hygromycin B (Berthold et al 2002). The presence of the *SRX2* in the hygromycin<sup>R</sup> transformants was assessed by PCR using primers *srx2\_F2* and *srx2\_R2* (**Table S1**). As shown in **Fig. 7 A**, the position of the primers covers the exon where the paromomycin cassette is inserted, so in the wt strain the expected size of the wild-type *SRX2* fragment of 168 bp, while in the *srx2* mutant it would be 2 kb. Among 395 hygromycin<sup>R</sup> transformants, 91 were analysed and only three of them exhibited the *SRX2* fragment (**Table 6**). To assess the presence of the transcript, RT-PCR was performed on these three transformants and one of them clearly presented the *SRX2* mature transcript (**Fig 7 B**). Unfortunately, this complemented *srx2* strains could not be used in the physiological experiments described below because they were not yet obtained at that time.

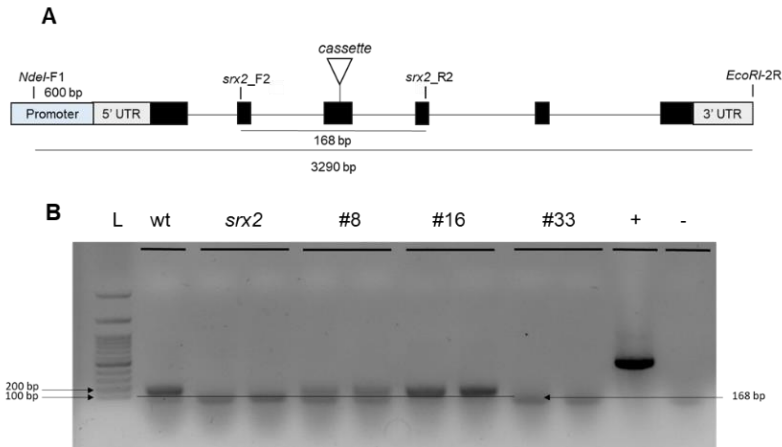


**Figure 7: Analysis of the *srx2* mutant co-transformants shows that the *SRX2* gene is expressed in one of the three co-transformants tested.** A) Scheme of *SRX2* gene shows the size of the amplified gene 3290 bp with *NdeI*-F1 and *EcoRI*-2R primers used for the transformation, the size of the *SRX2* gene fraction 168 bp with *srx2*\_F2 and *srx2*\_R2 primers without cassette insertion and the position of the cassette in the *srx2* mutant. B) PCR on cDNA of wt, *srx2*, complemented strains 8, 16, 33, positive control (+) provided by the kit (section 3.1.2.3.3) is the glyceraldehyde-3-phosphate dehydrogenase RNA (GAPDH RNA) and negative control (-). The strain 16 presented a PCR fragment of 168 bp, which is the size expected after amplification on cDNA using primers *srx2*\_F2 and *srx2*\_R2 as shown in A.

**Table 6.** Summary of the *srx2* mutant co-transformation.

	Numbers
Hygromycin resistant transformants	395
Hygromycin resistant transformants tested	91
Positive colonies by PCR for <i>SRX2</i> gene	3
Positive colonies by RT-PCR for <i>SRX2</i> transcript	1

Despite multiple attempts, the isolation of complemented strains of the *apx2* mutant was unsuccessful. To verify its phenotype, two additional mutants were ordered from the CLiP library (see the submitted publications in section 3.2).

#### 3.3.4 Investigating the phenotype of the *srx2*, *apx2* and double mutant strains

The cells were cultivated in minimal medium, to maximise the photosynthetic activity, under continuous low light ( $50 \mu\text{mol photons m}^{-2} \text{s}^{-1}$ ) and continuous high light ( $450 \mu\text{mol photons m}^{-2} \text{s}^{-1}$ ). One of the double *apx2 srx2* mutants, named *d1*, was included and the Fv/Fm value and the rETR were obtained. Compared to the wt and the *srx2* and *apx2* mutants, in the *d1* mutant we could observe an increase of 17% and 16% of Fv/Fm in cells grown under low light and high light respectively (**Fig. 8 A, B**). We observed a higher rETR in *srx2* and a lower rETR in *apx2* above  $100 \mu\text{mol photons m}^{-2} \text{s}^{-1}$  (**Fig. 8 C**). The rETR of the *d1* mutant was similar to the *apx2* in cells grown under low light and it was higher compared to the wt and *srx2* and *apx2* mutants in cells grown under high light (**Fig. 8 D**). These results opened more questions regarding the function of SRX2 and APX2 during photosynthesis. This led us to expand this search with other photosynthetic parameters and in particular about photoprotection mechanism, one of the reasons that could explain the lower rETR observed in the *apx2* mutant.



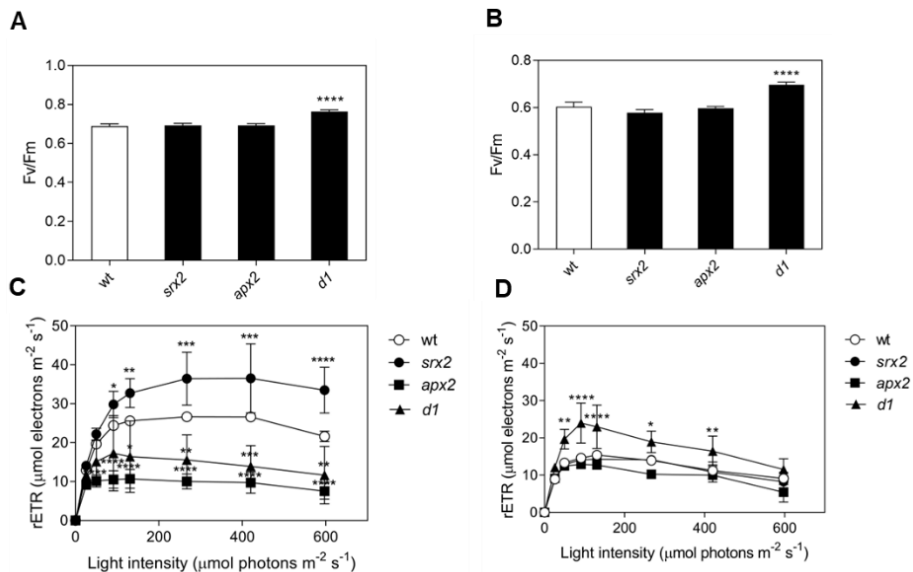


**Figure 8: Maximum yield of PSII (Fv/Fm) and rETR of double mutant *d1* from *srx2* x *apx2* crossing reveals differences compared to its parental strains.** A) and B) Fv/Fm of cells growing in phototrophy at low light condition show that the Fv/Fm of the double mutant *d1* is higher than the wt and its parental strains *srx2* and *apx2* mutants. C) and D) rETR at increasing light intensity of cells growing under continuous low light and continuous high light respectively show differences in all the mutants compared to the wt, especially in low-light cells. Average of 3 biological replicates per each strain with standard deviation. Statistical analyses with ANOVA One-Way or ANOVA Two-Ways, Dunnett's test, p-value < 0.0001\*\*\*\*, p-value < 0.001\*\*\*, p-value < 0.01\*\*, p-value < 0.05\*, p-value > 0.05 ns relative to wt.

Photoprotection was examined by measuring the non-photochemical quenching (NPQ) of *in vivo* chlorophyll *a* fluorescence, focusing on the PSII-antenna state transitions (qT) component (section 1.1.3.3) to better understand the energy balance. The measurements were performed together with a mutant of a serine/threonine-protein kinase *stt7* (Depege et al 2003) as control for a null qT phenotype. The *stt7* obtained by insertional mutagenesis is deficient for the kinase responsible for the light harvesting complexes (LHCII) antennas phosphorylation (Fleischmann et al 1999). In this mutant, the antennas do not detach from PSII, remaining insensitive to plastoquinone (PQ) redox changes (Lemeille & Rochaix 2010). The strategy to bring cells to state I consisted in the illumination during 10 min with far-red light (730 nm). This light is preferentially absorbed by PSI, bringing the PQ pool to the oxidized state, and having as a consequence the transition to state I (antennas remaining attached to PSII). These

cells were then illuminated during 10 min with actinic red light (660 nm) of 265  $\mu\text{mol photons m}^{-2} \text{s}^{-1}$ , and followed by 15 min of dark period, when it is possible to follow the induction of state II (antennas detaching from PSII) due to the reduction of the PQ pool (Lemeille & Rochaix 2010). Another phase of illumination with far-red light induced the cells back to state I, confirming that this fraction of fluorescence change was due to qT (**Fig. 9 A and B**). The induction of NPQ during the actinic light exposition was similar in the wt, *srx2* and *apx2*, while it was found to be higher in the *stt7* and *d1* mutants in the low light, but only higher in the *stt7* in the high light condition (minute 10 to 20 in **Fig. 9 A and B**). In the following period of dark exposure (minute 20 to 35 in **Fig. 9 A and B**), all the strains (except *apx2* in low light condition) exhibited an initial rapid decline in NPQ, attributed to the dissipation of the proton gradient along the thylakoid membrane (so called light energy-dependent quenching or qE) (Eberhard et al 2008). This change was followed by a gradual rise in NPQ, attributed to the transition to state II (Roach & Na 2017) (**Fig. 9 A and B**), while the *stt7* mutant did not perform any state transition as expected (**Fig. 9 A and B**). The mutants *apx2* and *d1* of the low light condition exhibited a lower change in NPQ than the wt during the dark phase (**Fig. 9 A**), indicated by no decline of NPQ after the light phase and no rise of NPQ attributed to state transition. On the contrary, cells grown in high light did not show any differences in the NPQ change during the dark period (**Fig. 9 B**). Accordingly, the fraction of the NPQ corresponding to state transition qT in low-light cells, the *apx2* and *d1* mutants are similar to the *stt7* mutant, while in the high-light cells only *stt7* had low qT. The fractions of qT to NPQ in the *apx2* and *d1* are similar in both growing conditions compared to the wt (**Fig. 9 C, D**).

To confirm the state transitions observed by *in vivo* chlorophyll *a* fluorescence, the samples were analysed by spectroscopy at low temperature (77 K). This technique allows recording the fluorescence of the PSI whose contribution is low at room temperature. The state I was induced by using the same sequence used previously for PSII fluorescence (**Fig. 9 A, B**), by transferring the cells under far-red light for 10 min and then freezing them at 77 K. The spectra were recorded in darkness with a blue light source as excitation light (470 nm). The transition to state II was triggered using the same method, which involved exposing the cells to 10 min of high light with an intensity increased to 750  $\mu\text{mol photons m}^{-2} \text{s}^{-1}$  to induce more extent of state II, and a subsequent 10-min dark period. The

only variation was that the dark period was reduced to 10 min instead of the previous 15-min duration. The spectra reported in **Fig. 9 E** and **Fig. 9 F** correspond to high light-cells in state I and state II respectively, and are normalised to the fluorescence value of 685 nm attributed to the fluorescence of PSII (Roach & Na 2017). Unfortunately, data of fluorescence taken at 77 K of low-light cells are lost, and I could not introduce them here. The measurements revealed a noteworthy distinction between the spectrum of state I and state II acclimated cells. In the wt in state I, the fluorescence value at 715 nm attributed to PSI (Roach & Na 2017) is lower (0.7 r.u.) than that of PSII, while in state II the fluorescence value at 715 nm is higher (1.2 r.u.) than the one of PSII. On the contrary, *stt7* is not able to perform state transitions, as the value of fluorescence at 715 nm remained unchanged upon state I and state II conditions (0.6 - 0.7 r.u.). The *apx2* mutant displayed a set of differences, in state I the fluorescence value at 715 nm of PSI was higher than the one of the wt with a fluorescence level equal to the one of 686 nm. In state II, the *apx2* mutant had a higher fluorescence level (2 r.u.) than the wt.

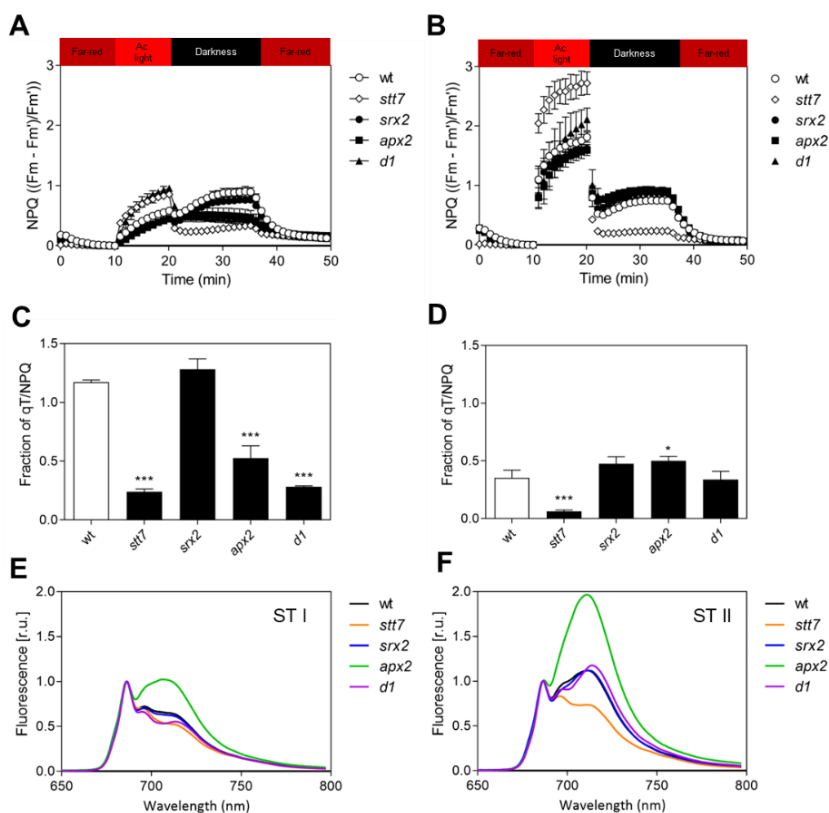


**Figure 9: Measurements of NPQ and state transition at 77 K in cells grown in phototrophic conditions show difference in the photoprotective mechanism in the *apx2* mutant. A) and B) induction of NPQ of low-light and high-light cells. C) and D) fraction of qT (calculated considering the last point measured in the dark phase (Fd) of relaxation and the last one measured after illumination with far-red light for 10 min (Fm'') to oxidize the PQ pool (qT = (Fm'' - Fd)/Fd) (Eberhard et al 2008), over non-photochemical quenching in low-light and high-light cells. E) and F) spectra of PSI and PSII fluorescence of high light-cells measured at 77 K by inducing the state I and state II respectively with 10 min of far-red light and 10 min with far red light, 10 min with 750  $\mu\text{mol m}^{-2} \text{s}^{-1}$  and 10 min of dark. Fluorescence values were normalised to 685 nm, attributed to PSII. Measurements of NPQ were taken with SpeedZen camera. Average of at least 2 biological replicates with standard deviation. Statistical analyses with ANOVA One-Way, Dunnett's test, p-value < 0.001\*\*\*, p-value < 0.05\*, p-value > 0.05 ns relative to wt.**

In conclusion, the absence of SRX2 appears to have no impact on the cell's fitness or its photosynthetic machinery, as indicated by NPQ measurements that resemble those of the wt. On the contrary the *apx2* mutant gave more interesting results: a lower rETR and a higher state II than the wt, suggesting impairment in state transition with possible higher portion of antennas attached to PSI. The double mutant *dl* presents some similarity with both *apx2* and *srx2* mutants in qT fractions and state transition measured at 77 K respectively. We therefore decided to focus on defining the APX2 function in *Chlamydomonas*. Considering the double *srx2 apx2* mutant, there exists a prospective foundation for future work, serving as a tool to elucidate the function of SRX2 together with APX2.

### 3.3.5 Characterization of the *apx2* mutant phenotype: first insights

Since the antennas of the *apx2* mutant could not reach the state I level of the wt with far-red light induction, we made use of 10  $\mu$ M 3-(3,4-dichlorophenyl)-1,1-dimethylurea (DCMU), a PSII inhibitor (Finazzi et al 1999) and 5  $\mu$ M of the uncoupler carbonyl cyanide *p*-(trifluoromethoxy)phenylhydrazone (FCCP) (Finazzi et al 1999) to chemically induce the oxidized and reduced state of the PQ pool (**Fig. 10 A**). These conditions bring the cells respectively to state I and state II. The cells were incubated for 20 min under growing light intensity prior measurements. **Fig. 10** shows that the *apx2* cells can reach the full state I (orange line in **Fig. 10 B**) to the same degree as the wt (green line in **Fig. 10 B**) when stimulated with the addition of DCMU. However, as previously observed for high light-cells, the *apx2* mutant (grey line in **Fig. 10 B**) displays a greater tendency to be in state II during continuous low light phototrophic growth, as indicated by the peak fluorescence relative to PSI at 715 nm. Moreover, in presence of FCCP, both wt (pink line in **Fig. 10 B**) and *apx2* (blue line in **Fig. 10 B**) mutant reach the full state II at similar extent (2.8 - 3 r.u.), but it is still a bit higher for the *apx2* mutant.

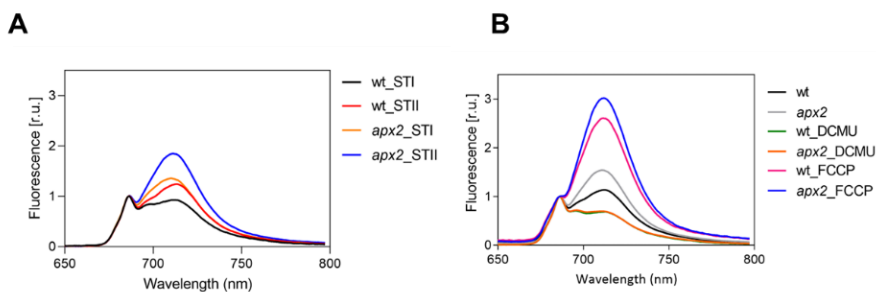


**Figure 10: Measurements of wt and *apx2* low-light phototrophic cells at a temperature of 77 K shows that the *apx2* mutant displays a higher tendency to be in state I. A)** Spectra of PSI and PSII fluorescence of low light-cells measured at 77 K by inducing the state I and state II respectively with 10 min of far-red light and 10 min with far red light, 10 min with 750  $\mu\text{mol photons m}^{-2} \text{s}^{-1}$  and 10 min of dark. Fluorescence values were normalised to 685 nm, attributed to PSII. **B)** Spectra of PSI and PSII fluorescence of low light-cells measured at 77 K. Full state I was reached by adding 10  $\mu\text{M}$  of DCMU and incubating the cell for 20 min under growing light; full state II was reached by adding 5  $\mu\text{M}$  of FCCP and incubating the cells for 20 min under growing light. Spectra were normalised to 685 nm attributed to PSII. Average of 3 biological replicates.

From these data we can conclude that the absence of the APX2 results in higher tendency of the cells to remain in state II with a fraction of the LHCII antennas attached to PSI. The fact that the *apx2* mutant responds in a similar way to the wt with chemical treatments, indicates that the PQ pool redox state is the one responsible for these differences. This, potentially indicates a disbalance in the activity of PSII and PSI.

To better understand the activity of PSI and the role of the APX2 at the downstream level of the photosynthetic chain, we monitored the photo-oxidation of P700, the primary electron donor of PSI, using JTS-10 spectrophotometer. Changes in absorption of P700 were followed upon illumination at increasing light intensities (**Fig. 11 A**), and compared to the maximum absorption change in DCMU inhibited samples, (Pm) (**Fig. 11 B**). Cells grown in two conditions, phototrophic low light and high light, were tested. The initial slope of the absorption changes of P700 were then compared for each light intensity (**Fig. 11 C**). From the **Fig. 11 C** we observed that the photo-oxidation rate of P700 (during light phase) is higher in the *apx2* mutant cells grown in phototrophic low light conditions compared to the wt. The photo-oxidation rate decreased for the *apx2* cells grown under phototrophic high light conditions, while it did not change in wt cells. This aligns with the results obtained by state transitions measurements

(**Fig. 11 E, F**), likely attributable to an increased absorption cross section in PSI. We also obtained the P700 re-reduction rate in the dark period after illumination of the cells with two different actinic light intensities: saturating light ( $6000 \mu\text{mol photons m}^{-2} \text{s}^{-1}$ ) for 50 ms (**Fig. 11 D**), and high light ( $345 \mu\text{mol photons m}^{-2} \text{s}^{-1}$ ) (**Fig. 11 E**) for 6 s. The re-reduction rate was lower in the *apx2* low-light mutant cells than in the wt. Conversely, no differences were observed in high-light cells for both durations of light exposure.

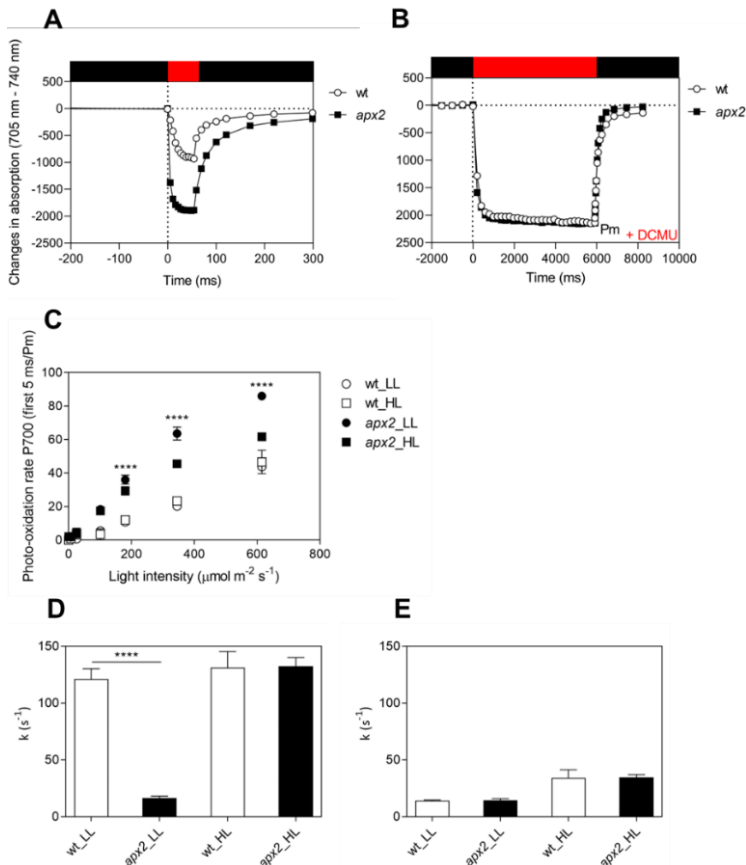


**Figure 11: Photo-oxidation and re-reduction rate of P700 in low-light and high-light phototrophic cells show faster oxidation and slower re-reduction rate in low-light *apx2* mutant cells.** **A)** Example of changes of absorption of P700 of wt and *apx2* mutant upon saturating light flash ( $6000 \mu\text{mol photons m}^{-2} \text{s}^{-1}$ ) of 50 ms (red bar) to evaluate the initial P700 oxidation, followed by the dark phase to evaluate the re-reduction of P700. **B)** Example of changes of absorption of P700 of wt and *apx2* mutant upon light flash of  $345 \mu\text{mol photons m}^{-2} \text{s}^{-1}$  of 6 s (red bar) to reach the maximum oxidation value (Pm) in presence of  $10 \mu\text{M}$  DCMU until the end of the light period when the light is off and P700 is re-reduced again until reaches 0. **C)** Photo-oxidation rate of P700 at increasing light intensities. Values are changes of absorption spectra of P700 ( $705 \text{ nm} - 740 \text{ nm}$ ). Rates of photo-oxidation of P700 are ratios of the first 5 ms of the spectra without DCMU normalised on the maximum P700 oxidisable (Pm) obtained by adding  $10 \mu\text{M}$  DCMU. **D)** Re-reduction rate of P700 during 50 ms of saturating light ( $6000 \mu\text{mol photons m}^{-2} \text{s}^{-1}$ ). Values are normalised to the Pm measured in presence of  $10 \mu\text{M}$  DCMU. **E)** Re-reduction rate of P700 during 6 s of high light  $345 \mu\text{mol photons m}^{-2} \text{s}^{-1}$ . Values are normalised to the Pm measured in presence of  $10 \mu\text{M}$  DCMU. Measurements performed with JTS-10 spectrophotometer. Average of 6 biological replicates with standard deviation. Statistical analyses with ANOVA One-Way, Šidák's test,  $p\text{-value} < 0.0001$ \*\*\*\*,  $p\text{-value} > 0.05$  ns relative to wt.



Based on these results, we hypothesised that the PSI donor side is limited in the *apx2* mutant. To prove this hypothesis and to confirm the lower re-reduction rate of P700 previously seen under saturating light for the *apx2* mutant, we decided to monitor the redox changes of cytochrome *f* and P700 after a light exposure of 50 ms or 6s with the light intensity of 345  $\mu\text{mol photons m}^{-2} \text{s}^{-1}$ . The results showed that the re-reduction rate of P700 is slower in the mutant after 50 ms of illumination in low light, but not after 6 s of illumination. Interestingly, the re-reduction rates remained proportional between P700 and cytochrome *f* in the cells tested (**Fig. 12 A**). No differences in the re-reduction rates were observed in the high-light cells nor after 50 ms nor after 6 s of illumination (**Fig. 12 B**). A comparison between the re-reduction of P700 and cytochrome *f* is shown in panels **C, D, E, F** of **Fig. 12** expressed in percentage. The only difference is observed in low-light cells submitted to 50 ms of light, where the *apx2* mutant reaches the highest P700 oxidisable value faster than that one of the wt. These results align with the one reported in **Fig. 12 C** where the photo-oxidation rate of *apx2* is faster than the wt, meaning that a higher fraction of P700 was oxidized in the mutant compared to the wt in 50 ms of light exposure. From these results, we could exclude the hypothesis that the faster oxidation of P700 is caused by cytochrome *f* limitation. Investigation were then directed to measure the plastocyanin pool size.

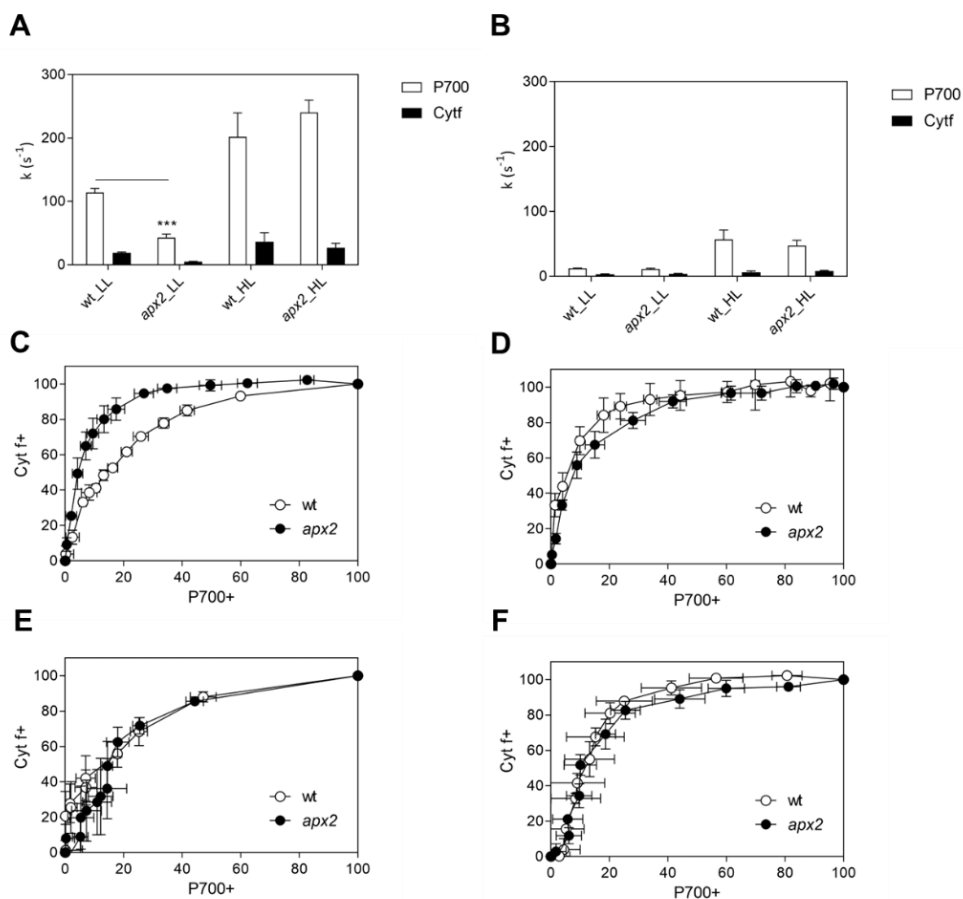


**Figure 12: Re-reduction and photo-oxidizable P700 and cytochrome *f* of low-light and high-light phototrophic cells show differences in *apx2* low-light cells.** **A)** Re-reduction rate of P700 and cytochrome *f* after 50 ms of  $345 \mu\text{mol photons m}^{-2} \text{s}^{-1}$  light intensity. **B)** Re-reduction rate of P700 and cytochrome *f* during 6 s of  $345 \mu\text{mol photons m}^{-2} \text{s}^{-1}$  light intensity. **C)** and **E)** Photo-oxidisable P700 and cytochrome *f* of low-light and high-light cells during 50 ms of  $345 \mu\text{mol photons m}^{-2} \text{s}^{-1}$  light intensity. **D)** and **F)** Photo-oxidisable P700 and cytochrome *f* of low-light and high-light cells during 6 s of  $345 \mu\text{mol photons m}^{-2} \text{s}^{-1}$  light intensity. Values of P700 are changes in absorption spectra of the differences between 705 nm and 740 nm, values of cytochrome *f* are changes in absorption of deconvolution of wavelengths 520 nm, 546 nm and 573 nm. All measurements were recorded in presence of  $10 \mu\text{M}$  DCMU. Measurements performed with JTS-10 spectrophotometer. Average of 3 biological replicates with standard deviation. Statistical analyses with ANOVA Two-Way, Šidák's test,  $p\text{-value} < 0.001$ \*\*\*,  $p\text{-value} > 0.05$  ns relative to wt.

Due to the faster photo-oxidation rate of P700 in the *apx2* mutant, we hypothesized that it might have been affected in one of the main photosynthetic

alternative electron pathways where PSI is involved, the cyclic electron flow (CEF). The cyclic electron flow (Nawrocki et al 2019b) involves PSI and cytochrome *b<sub>6</sub>f* and contributes to ATP supply for the Calvin-Benson-Bassham (CBB) cycle (Nawrocki et al 2019b). One way to evidence the maximum activity of cyclic electron flow is by monitoring the initial photochemical rate by electrochromic shift (ECS) in samples inhibited by DCMU (Nawrocki et al 2019a), having only the cytochrome *b<sub>6</sub>f* as electron source for PSI, where it is cycled. This measurement allows us to retrieve the maximum capacity of CEF at different periods of illumination (Nawrocki et al 2019b). According to this method, during the first milliseconds of illumination, the electrons can be cycled, but eventually are accepted by other components (*i.e.* CBB proteins) (Nawrocki et al 2019b). In the wt the initial photochemical rate of the maximum CEF-capacity in the first 5 ms is high as previously observed (Nawrocki et al 2019a). On the contrary, in *apx2* cells the initial photochemical rate is lower than that one of the wt, suggesting a lower CEF-capacity in the first 5ms of illumination.

Overall, considering the results obtained from the wide exploration of the photosynthetic apparatus of the *apx2* mutant, we can hypothesise a role for APX2 during photosynthesis especially when the cells are growing in low light in minimal medium. Indeed, we could exclude that its absence affects PSII as the Fv/Fm is not decreased compared to the wt (**Fig. 8 A, 8 A, B**), while it seems to play an important role during electron transport as shown by the lower rETR (**Fig. 8 C**). This might be due to the higher tendency of the *apx2* mutant cells to be in state II (**Fig. 9 E, F and 10**), which would let the PQ in its reduced form. In addition, considering the faster oxidation of P700 and its slower re-reduction rate, we may think that the role of APX2 is important for the electron transport to the PSI. Moreover, the *apx2* mutant showed a slower initial photosynthetic rate when measuring the ECS, suggesting a possible implication of the APX2 in CEF (**Fig. 13 A, B**). Considering that all these measurements were taken by transferring low light acclimated cells under sudden high light flash, we wondered if the APX2 might be also involved in the early acclimation from low light to high light intensity.

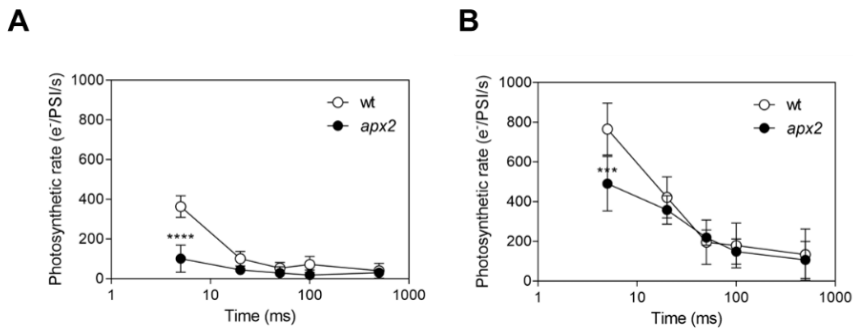


**Figure 13: Electrochromic shift of phototrophic low-light and high-light cells reveals that the first ms of cyclic electron flow of the *apx2* mutant is low.** **A)** Electrochromic shift of low-light cells in presence of PSII inhibitor, DCMU. **B)** Electrochromic shift of high-light cells in presence of PSII inhibitor, DCMU. Measurements performed with JTS-10 spectrophotometer. Average of 6 biological replicates with standard deviation. Statistical analyses with ANOVA Two-Way, Šidák's test, p-value < 0.0001 \*\*\*\*, p-value < 0.001 \*\*\*, p-value > 0.05 ns relative to wt.

Therefore, we decided to grow the cells under fluctuating light with cycles of 5 min of low light intensity ( $50 \mu\text{mol photons m}^{-2} \text{s}^{-1}$ ) followed by 1 min of high light intensity ( $600 \mu\text{mol photons m}^{-2} \text{s}^{-1}$ ) (**Fig. 14 A**). Interestingly, it was noted that the growth of *apx2* cells was inferior to that of wt (**Fig. 14 B**). Additionally, the Fv/Fm and the maximum rETR values were significantly decreased in the *apx2* mutant. (**Fig. 14 C, D**). Thus, we could confirm that the APX2 might be also important for the early acclimation from the low light to high light, as previously seen during the redox state measurements of P700.

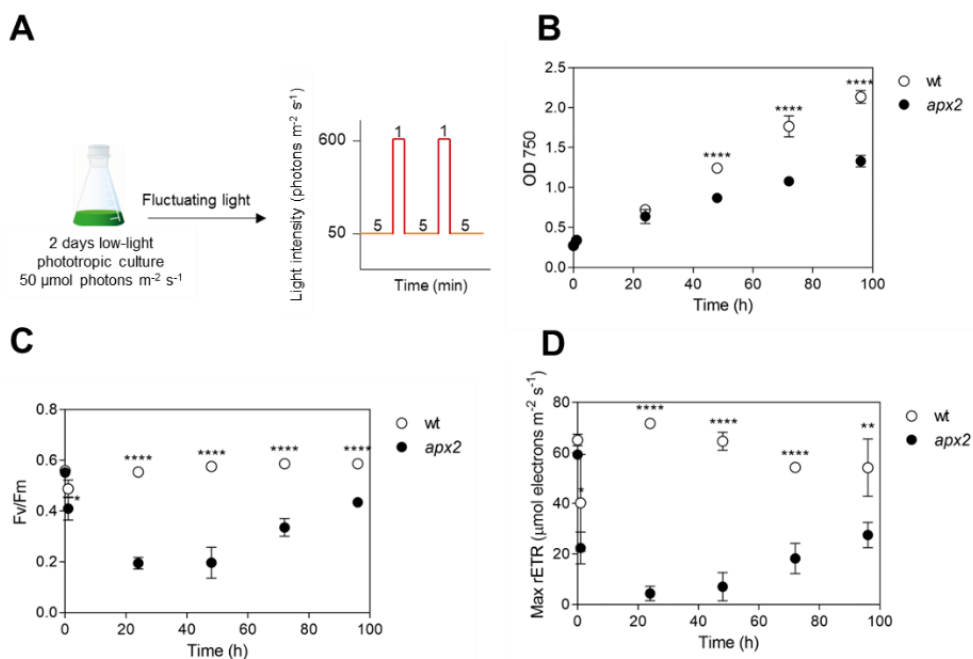


**Figure 14: The growth and the PSII activity of the *apx2* are affected in fluctuating light growing condition.** **A)** Scheme of fluctuating light condition growth set-up with several cycles of 5 min of low light 50  $\mu\text{mol photons m}^{-2} \text{s}^{-1}$  and 1 min of high light 600  $\mu\text{mol photons m}^{-2} \text{s}^{-1}$ . **B)** Growth of wt and *apx2* cells (based on the OD at 750 nm). **C)** Maximum yield of PSII of wt and *apx2* cells during the time. **D)** Maximum relative electron transfer rate value of wt and *apx2* cells during the time. Measurements taken with JTS-10 spectrophotometer. Average of 3 biological replicates with standard deviation. Statistical analyses with ANOVA Two-Way, Šidák's test, p-value < 0.0001\*\*\*\*, p-value < 0.01\*\*, p-value < 0.05\*, p-value > 0.05 ns relative to wt.

In addition, we evaluated the oxidative stress by measuring the  $\text{H}_2\text{O}_2$  in wt and *apx2* cells after growing them under continuous low light (50  $\mu\text{mol photons m}^{-2} \text{s}^{-1}$ ) and transferring them for 1 h under high light (450  $\mu\text{mol photons m}^{-2} \text{s}^{-1}$ ). We used the CM- $\text{H}_2\text{DCFDA}$  (**Fig. 15 A**) and the Amplex Red (**Fig. 15 B**) fluorescence probes to measure the  $\text{H}_2\text{O}_2$  concentration inside the cells and in the cultivation medium respectively. Unexpectedly, in the *apx2* mutant we did not observe any  $\text{H}_2\text{O}_2$  increase when the low-light cells were transferred to high light intensity. This could be explained by the slower re-reduction rate of P700 and the consequent slower delivery of the electrons to the acceptor side of PSI. It is also conceivable that other  $\text{H}_2\text{O}_2$ -scavenging enzymes could compensate for the

absence of APX2 in the *apx2* mutant. APX4, another isoform of ascorbate peroxidase that is anticipated to be present in the chloroplast of *Chlamydomonas* and is highly expressed in high light, could potentially serve for photoprotection in this context (Kuo et al 2020a).

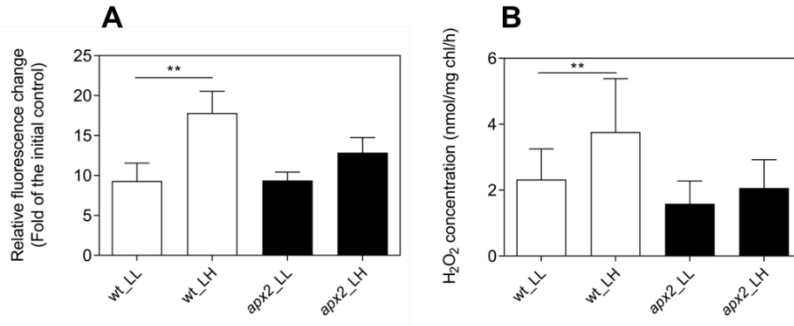


**Figure 15: ROS determination of wt and *apx2* cells stressed for 1 h under high light intensity shows no increase of H<sub>2</sub>O<sub>2</sub> in the *apx2* mutant.** **A)** Determination of total intracellular ROS with CM-H<sub>2</sub>DCFDA probe by measuring fluorescence with excitation wavelength of 492 nm and emission at 530 nm. **B)** Determination of H<sub>2</sub>O<sub>2</sub> in cells medium with AmplexRed probe by measuring fluorescence with excitation wavelength of 560 nm and emission at 590 nm. (wt\_LL: wt under low light intensity for 1 h and used it as control; wt\_HL: wt under high light intensity stress for 1 h; *apx2*\_LL: wt under low light intensity for 1 h and used it as control; *apx2*\_HL: wt under high light intensity stress for 1 h). Average of 3 biological replicates with standard deviation. Statistical analyses ANOVA One-Ways with Šidák’s Test, p-value < 0.01\*\*, p-value > 0.05 ns.

### 3.4 Discussion

In this chapter, I described the molecular, genetic and phenotypical characterization of the selected mutants. The methods utilized for the phenotypical screening, drop tests and measurements of maximum efficiency of PSII (Fv/Fm), are usually used as fast and easy tools to get information about the cell physiology. In my work, they served to compare the response of each mutant to different light intensities and stress conditions. In other works, in mutants of stromal ascorbate peroxidase (sAPX) and the ascorbate peroxidase located in the thylakoid membrane (tAPX) of *Arabidopsis*, the PSII activity showed no differences compared to the wt in the conditions tested, in control and in presence of methyl viologen after 48 h (Maruta et al 2009). Methyl viologen is an herbicide which accepts electron from PSI, enhancing the production of superoxide  $O_2^{\cdot-}$  with the consequent dismutation in  $H_2O_2$  (Miyagawa et al 2000). Mutant lines of *Oryza sativa* lacking the ascorbate peroxidase 4 (APX4) enzyme showed an increase of the Fv/Fm compared to the wt in presence of the inhibitor of catalase (CAT) 3-amino-1,2,4-triazole (3-AT). This was due to the up-regulation of some enzymes involved in cellular signaling (*i.e.* thioredoxin h1, TRXh1 and monodehydroascorbate reductase, MDHAR) and photosynthetic related proteins (*i.e.* ferredoxin-NADP reductase, FNR and the light-harvesting complexes subunits LHCB2 and LHCB4) (Sousa et al 2018). In another study on a *Chlamydomonas* mutant lacking glutathione peroxidase 5 (GPX5), the Fv/Fm in control condition was similar to that one of the wt. Transcriptomic analyses in control conditions were also conducted to compare gene expressions between the *gpx5* and the wt. Mutant cells revealed up-regulation of other antioxidant enzymes, such as nucleoredoxin 2 and 3 (NRX2, NRX3) and sulfiredoxin 2 (SRX2) (Ma et al 2020b). The responses of mutants to the lack of ROS-scavenging enzymes comprise the increase of other antioxidant enzymes and photosynthetic-related proteins and reveal that compensatory mechanisms are involved in cell protection even in non-stressed conditions. Similar scenario would be present in our mutants, which display comparable or higher PSII activity than the wt, with and without the addition of  $H_2O_2$  (**Table 3** and **Table 4**). Moreover, the presence of compensatory mechanisms would allow the mutants to grow at similar rates than the wt, as observed by drop tests in **Fig. 4**. Additional experiments on the selected mutants *srx2* and *apx2* revealed similar PSII activity and similar response to the addition of  $H_2O_2$  within the cells, as the

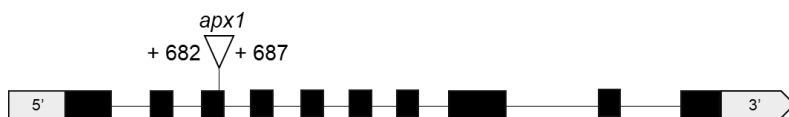
wt (**Fig. 5**). A double mutant (*dl*) obtained from a cross between the *srx2* and *apx2* mutants (**Fig. 6**) showed an increase of the PSII activity, probably due to the up-regulation of enzymes involved in cellular signaling and photosynthesis-related proteins. However, questions remain on the function of the two enzymes. The lower rETR of the *apx2* mutant (**Fig. 8 C**) and its impairment in state transition (movement of the light harvesting complex between PSII and PSI) with a tendency to be in state II (antennas attached to PSI, **Fig. 9E, F** and **10 A**), captured our attention on the function of this enzyme and the reason behind the defect of its photosynthetic machinery. Similar phenotype was observed in mutants lacking phylloquinone, an essential electron carrier in PSI (Emonds-Alt et al 2017). In this study, the lower rETR and the higher state II of the mutants tested were a consequence of the decrease in amount of the PSI presenting a bigger PSI antenna size. Although the *apx2* mutant does not have a higher PSI antenna, as shown by the 77 K measurements in presence of DCMU in which the cells can reach full state I (antennas attached to PSII, **Fig. 10 A**), the results of that study suggest that the *apx2* phenotype might be link to a disruption of the electron transport around PSI. Indeed, this is demonstrated by the faster oxidation and slower re-reduction of P700, primary electron donor of PSI, compared to the wt (**Fig. 11, 12**) and the lower initial photosynthetic rate of cyclic electron flow (**Fig. 13**). We attributed this to a limitation of the donor side of PSI that could be cytochrome *b<sub>6</sub>f* or plastocyanin. We have proved that the cytochrome *b<sub>6</sub>f* content is not different than in the wt (**Fig. 12**), which prompted us to hypothesis a limitation of the plastocyanin pool size. Moreover, no increase of H<sub>2</sub>O<sub>2</sub> and ROS in general have been detected in the *apx2* mutant compared to the wt when the cells were transferred from low light to high light (**Fig. 15**). Limitation of ROS production at the acceptor side of PSI is a consequence of the P700 oxidation due to the quenching of excess light energy to protect PSI from photoinhibition (Shimakawa & Miyake 2018). Despite in the *apx2* mutant, low ROS production depends on the limitation of the donor side of PSI, this would explain the absence of ROS increase when mutant cells are transferred to high light compared to the wt. This would also suggest that the main phenotype observed is not strictly related to the H<sub>2</sub>O<sub>2</sub>-mediated signaling, but mainly a consequence of the slower electron transport to PSI.



## Supplementary materials

**Figure S1.** Sequencing of all the mutants with their gene map and paromomycin resistant cassette position.

*apx1*



**CLiP:** LMJ.RY0402.208295

([https://www.chlamylibrary.org/showInsertion?insertionName=LMJ.RY0402.208295\\_1](https://www.chlamylibrary.org/showInsertion?insertionName=LMJ.RY0402.208295_1))

**Internal bar code of the cassette:** AACGTTGTGCTGTACATGGCTC

PCR amplification of 3' of the cassette (*apx1*\_R1 and OMJ944)

**Sequence with *apx1*\_R1**

CGGGAAAAAGAATGCTTCGGCTGTCGCCACGCCCCGCGCTAAACGT  
TGTGCTGTACATGGCTC ACTGACGTCGAGCCTTCTGGCAGACTAGTT  
GCTCCTGAGTCCAAGCCGGAGATTGACCATGGCGCCAACAAGGGTG  
CGGAAGGGGCTGTTATTGAATGGCGCTGGAGGCGCGGGGCCGCAGC  
GAGCAAGTAAACAGCACAGCAGGCGACACGCAACCAGCAGTGT  
AGAAGCATCATGCTCAGCTCTAAACTTGCATGTGAA

In grey is highlighted the *APX1* sequence and in pink is highlighted the paromomycin resistant cassette (CIB1, <https://www.chlamylibrary.org/showCassette?cassette=CIB1>)

In yellow is highlighted the bar code specific to the *apx1* mutant according to the link above.

**CLiP:** LMJ.RY0402.208295

([https://www.chlamylibrary.org/showInsertion?insertionName=LMJ.RY0402.208295\\_2](https://www.chlamylibrary.org/showInsertion?insertionName=LMJ.RY0402.208295_2))

**Internal bar code of the cassette:** TAACTAATCGGTGCCGAGGGCT

PCR amplification of 5' of the cassette (*apx1*\_F1 and OMJ913)

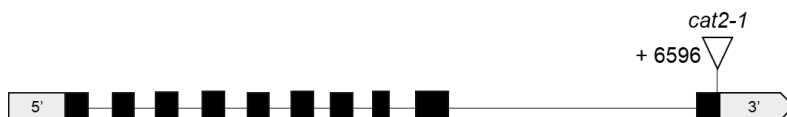
**Sequence with *apx1*\_F1 (reverse complement)**

TCTATGTGCTTTGTGTCTGTGCGACTGGAATGCGCAGGCTGCAACCCC  
 ATTTCTGTGCGCCTGGGCTGGCACGATTCCGGCACCTACGACAAGGT  
 GCGGCACTCGGGTGTTCGCCCCGCGTCATTCAGGACGCGCAGTGCCT  
 GCATGCACACGTGTGTGCGCACGTGCGAATTACACGGCGCATAGAG  
 CTGCAGCCCCTGCAATCTACGTGAGCTGTAGATAACGGCGGTGGC  
 AACTTAAGGGTTAACGGACCTTGTCACCTGCAGAACATCGCTGAGTT  
 CCCGGCCCGTGGCGGGCGCCAACGGCAGCATTGCTTGGACTCACTA  
 GTCACACGAGCCCTCGTCAGAAACACGTCTCCAGCCCTC

In grey is highlighted the *APX1* sequence and in pink is highlighted the paromomycin resistant cassette (CIB1, <https://www.chlamylibrary.org/showCassette?cassette=CIB1>)

In yellow is highlighted the bar code specific to the *apx1* mutant according to the link above.

*cat2-1*



CLiP: LMJ.RY0402.051905

([https://www.chlamylibrary.org/showInsertion?insertionName=LMJ.RY0402.051905\\_1](https://www.chlamylibrary.org/showInsertion?insertionName=LMJ.RY0402.051905_1))

**Internal bar code of the cassette:** CGTTCTTACTGATCTCATAAGC

PCR amplification of 5' of the cassette (*cat2-1\_F* and OMJ913)

**Sequence with *cat2.1\_F***

TTGC CGTTCTTACTGATCTCATAAGC GGAGACGTGTTTCTGACGAGG  
 GCTCGTGTGACTAGTGAGTCCAAC TCCTCCTCCACCCTGGCGGCAGC  
 CCCATACGACGCCTCCAGCACAAAGCTGAACCACCGCAGCCGCCTTC  
 TCGCTCGCAGCCCTCGCGCCCTCCTCTGCCGCAACAGCGGCAGCACC  
 CAGCAGTGCGCCAGCCAGCTCGCCGCCTTCGTGTCGTTACACAGGT  
 TGCCGTCGGGGCCGTCGAACCGGTCTGCATTCATCAATCGTGA

In grey is highlighted the *CAT2-1* sequence and in pink is highlighted the paromomycin resistant cassette (CIB1, <https://www.chlamylibrary.org/showCassette?cassette=CIB1>)

In yellow is highlighted the bar code specific to the *cat2-1* mutant according to the link above.

**CLiP:** LMJ.RY0402.051905

([https://www.chlamylibrary.org/showInsertion?insertionName=LMJ.RY0402.051905\\_2](https://www.chlamylibrary.org/showInsertion?insertionName=LMJ.RY0402.051905_2))

**Internal bar code of the cassette:** TAAACTTTGGGCTTTAATTCCC

PCR amplification of 5' (strand -) of the cassette (*cat2-1\_R* and OMJ944)

### Sequence with *cat2-1\_R*

```
GGCTCCATCTAAATAGGCGCTAGATGCTCGCGTCGGCTCCACAACG
GCGTGAGAGCTTTTACGTTTCAAGCAAGTAATATATATGTGAGGCGC
TGAGCGTGCGGCTCTCCCGAAGGGCGGAGGTCATTTTGTAGTGACGG
ACACAAATCGCGCGAGCCAGCGCTACGCCGGAGAGTGGGGCCCGG
AGGCACACGTAATGCGTCGCCGGGGCAGCTTAGGCCGGGAGTGTAGA
CCTTACAGCCGCTGTGTCGTTACGCCATCCCGAACAAGGACAATTCA
AAAGAGCCGTCTGTGTATATCATTGTCCTGCAATCATCCGATCC
```

The part sequenced corresponds to the 3'UTR of the *CAT2* gene. Not 100% identity with the *CAT2* reference gene.

Internal bar code and the cassette could not be identified.

### *cat2-2*

**CLiP:** LMJ.RY0402.133009

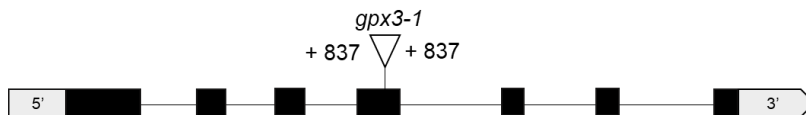
([https://www.chlamylibrary.org/showInsertion?insertionName=LMJ.RY0402.133009\\_1](https://www.chlamylibrary.org/showInsertion?insertionName=LMJ.RY0402.133009_1))

([https://www.chlamylibrary.org/showInsertion?insertionName=LMJ.RY0402.133009\\_2](https://www.chlamylibrary.org/showInsertion?insertionName=LMJ.RY0402.133009_2))

### Different gene

THO complex subunit 2 (THOC2)

### *gpx3-1*



**CLiP:** LMJ.RY0402.196379

([https://www.chlamylibrary.org/showInsertion?insertionName=LMJ.RY0402.196379\\_1](https://www.chlamylibrary.org/showInsertion?insertionName=LMJ.RY0402.196379_1))

**Internal bar code of the cassette:** **GTTCCCTGGCTCGCCAAGGAGC**

PCR amplification of 3' of the cassette (*gpx3-1*\_R1 and OMJ944)

**Sequence with *gpx3-1*\_R1**

GCGCTA**GTTCCCTGGCTCGCCAAGGAGC**ACTGACGTCGAGCCTTCTG  
 GCAGACTAGTTGCTCCTGAGTCCACGTCCAACACTACGGCGTGACCTTC  
 CCCCTCATGTCCAAGGTCGACGTGAACGGGCCCGGCGGTGAGCGGA  
 TAAGAGGAGGCTATGTTTGAACCCACCCCA**A**TTAGATAATAA

In grey is highlighted the *GPX3* sequence and in pink is highlighted the paromomycin resistant cassette (CIB1, <https://www.chlamylibrary.org/showCassette?cassette=CIB1>)

In yellow is highlighted the bar code specific to the *gpx3-1* mutant according to the link above.

The A base highlighted in red is a G in the sequence of *GPX3* gene.

**CLiP:** LMJ.RY0402.196379

([https://www.chlamylibrary.org/showInsertion?insertionName=LMJ.RY0402.196379\\_2](https://www.chlamylibrary.org/showInsertion?insertionName=LMJ.RY0402.196379_2))

**Internal bar code of the cassette:** **CATAGAGTTGGTTCGCTGGGAT**

PCR amplification of 5' of the cassette (*gpx3-1*\_F1 and OMJ913)

**Sequence with *gpx3-1*\_F1 (reverse complement)**

**A**TGGCAAG**G**ACTTTAAGCTATCGTCCCTCAAGGACAAGGCGGTTCT  
 GGTCGTGAACCTGGCCAGTGCTTGC GGCTTACCCCCCAGGTAAGA  
 CCAAGCGTCCAAACCTTTCGAACCTGTCGAAGGACCCGCCACGACA  
 CCACCTGCGGCTTCTTACACACACACACACACCCTCCGCCGCCCCCA  
 TGTCTATAGTACGCCGAGCTTCAGGACCTGCAAGACAAGTACGGCA  
 AGCAGGGCTTTGTGGTCTTGGGCTTCCCCTGCAACCAGTTCGGCGCG



Bases highlighted in red are the ones not matched with the reference sequence of *GPX3* gene.

*nrx1*



CLiP: LMJ.RY0402.211911

([https://www.chlamylibrary.org/showInsertion?insertionName=LMJ.RY0402.211911\\_1](https://www.chlamylibrary.org/showInsertion?insertionName=LMJ.RY0402.211911_1))

**Internal bar code of the cassette: CCGTTTTTTTGATCGGGAGAGC**

PCR amplification of 5' of the cassette (*nrx1\_F1* and OMJ913)

**Sequence with *nrx1\_F1* (reverse complement)**

TTTTTTTGGCAGGGGAGCCTAAAAAGAGACAAGAATGGGTGTTGCG  
TAAAGTTTCTTTGTGGTAACGCGGTGGAAAGGGTTTGC AACATCACT  
TCAATAGGCCCGAGCACTACCCGTGAAATGTGCCAAAACCGACTT  
GCTCGTCTCTCGACAATACGCGCTCACCCGCGATCGGGCGCTTGGAG  
ATGAAGGGCATCCCCACTCTGGAGGTGATGGACGAGCAGTTCATGG  
TCATCAACACGGTTGGCACGGCTGCCGTTTTTGGACTCGCTAATCAC  
TCGAGCCCTGGTCAGAAAACGTCTCCGCTCTACCGATCAAAGTACA  
CGC

In grey is highlighted the *NRX1* sequence and in pink is highlighted the paromomycin resistant cassette (CIB1, <https://www.chlamylibrary.org/showCassette?cassette=CIB1>)

In yellow is highlighted the bar code specific to the *nrx1* mutant according to the link above.

The TGG, A and G bases highlighted in red are GAT, G and A in the sequence of the internal bar code.

CLiP: LMJ.RY0402.211911

([https://www.chlamylibrary.org/showInsertion?insertionName=LMJ.RY0402.211911\\_2](https://www.chlamylibrary.org/showInsertion?insertionName=LMJ.RY0402.211911_2))

**Internal bar code of the cassette: GGGTCCGCCTGAAGGGTGGAAA**

PCR amplification of 3' of the cassette (*nrx1\_R1* and OMJ944)

### Sequence with *nrx1\_R1*

```
ATGGATATTGCAGCCCCGCGCTA GGGTCCGCTGAAGGGTGGAAA
CTGACGTTCGAGCCTTTTGGCAGACTAGTTGCTCCTGAGTCCAGTCTG
ACGCCGAGGCCGCGCGCTTCCCCTGGCGCCCACAGCCCCTGGAGGC
GCTCAGCCCTTTCACCGCCGGCCGCATCAACTCGGGGCCAACGCTGT
TGCTGATTGTGGACATGGGCGATGACGACGCCGCTGAGGGCCTTTCG
CAAGGAAGTGCTGCTGGGCGTGGCCACCGCCACCAAGGCTGCGCCC
GGCGGCAGGACTGGGCCTTCCTGTGGGCGCGCCGTGGCAACGAGA
TCGCGCAGAGCGTGCTGGCGTTTACGGGTTTCATCAAGGACGAGGA
GGCGGAGGCGCCCGCAGGGCACCTGGCGGTCACTACTGACGTGCC
CAGCAGGCGATGTGGGACCTGAAGGCCACGGGTGTGGAGGTCAGCG
CCGTGGGGCTGGGCAT TTGTGGTGTCCGGAC ATCAAG AT
```

In grey is highlighted the *NRX1* sequence and in pink is highlighted the paromomycin resistant cassette (CIB1, <https://www.chlamylibrary.org/showCassette?cassette=CIB1>)

In yellow is highlighted the bar code specific to the *nrx1* mutant according to the link above.

The T and the 2 A bases highlighted in red are G, T and G in the sequence of *NRX1* gene respectively.

### *nrx2-1*



CLiP: LMJ.RY0402.046208

([https://www.chlamylibrary.org/showInsertion?insertionName=LMJ.RY0402.046208\\_2](https://www.chlamylibrary.org/showInsertion?insertionName=LMJ.RY0402.046208_2))

**Internal bar code of the cassette:** **GTGGAGGCCATCGCGAGTTTAA**

PCR amplification of 3' of the cassette (*nrx2-1\_F1* and OMJ944)

### Sequence with *nrx2-1\_F1*

GCGCTA **GTGGAGGCCATCGCGAGTTTAA** ACTGACGTCGAGCCTTCT  
GGCAGACTAGTTGCTCCTGAGTCGCCAAGAATCTGGAAGACCTTGG  
GCTCCTCGGCCGCAGCAGGAGCGGGGAGGCGGCAGCTGCGGCCTC  
CTCAGCGTCCACCTGAAGTCATACGCCAACCGAATGGCCGGTCAGC  
GCGAAGTCTAACAACTTTAGCCCCGGCCGGGTGGCATGCGCAAAG  
GACACGTGGGCATGAACACGAACCTGAGATGCGTGCAGCTTACCTT  
GCGGCACACGTCCCCATCGCAGACCACGGCAGGCGCCATGCTGTTG  
GGTGTCTGGACTAGGTAAGAGAAGCTGAACACGGTTCGGCTTTGAAG  
GCCCGCCCAATAGGCTGGAGAACAAGGGACGATCGCTCTAGA

In grey is highlighted the *NRX2* sequence and in pink is highlighted the paromomycin resistant cassette (CIB1, <https://www.chlamylibrary.org/showCassette?cassette=CIB1>)

In yellow is highlighted the bar code specific to the *nrx2-1* mutant according to the link above, but not found in the sequencing.

**CLiP:** LMJ.RY0402.046208

([https://www.chlamylibrary.org/showInsertion?insertionName=LMJ.RY0402.046208\\_1](https://www.chlamylibrary.org/showInsertion?insertionName=LMJ.RY0402.046208_1))

**Internal bar code of the cassette:** **ACAACGCATATACTAGATTAAG**

PCR amplification of 5' of the cassette (*nrx2-1\_R1* and OMJ913)

**Sequence with *nrx2-1\_R1***

ACAGTATATAAGGGGATTGGTTTTACAAGGATTCTGTTAAAAAGGT  
CCACGCTCCACCTTGCCATGCCTTGCTCGACATCAAATACCCAGGCC  
CAGACAAGGCGGCTGCGCTCTACTTCTATGCGGCTGATCCCGCCTTG  
CCTGCACTTCAAGCCCCACAGACCTCCATCTACCCCAATTAAGA  
AGGATCACGCACCTAAGGCTGACTGGCAGGTGGTATTTGTGACCAT  
GTAACCGGTATAAGGACTCGTTTAAGGAGTACTTTGGCGAGATGCC  
TTGTTACCGCCCTGCCCTACGGCAAGCGTGAGGCCAAAG

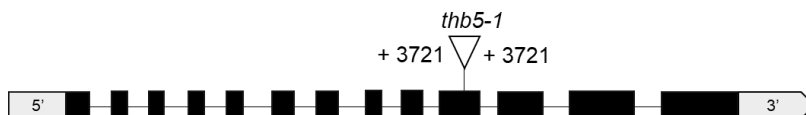
In grey is highlighted the *NRX2* sequence and in pink is highlighted the paromomycin resistant cassette (CIB1, <https://www.chlamylibrary.org/showCassette?cassette=CIB1>)

Internal bar code was not found.

Not 100% identity of the sequencing with the reference gene *NRX2*.

*thb5-1* (previous identifier on Phytozome PRX)





**CLiP:** LMJ.RY0402.193060

([https://www.chlamylibrary.org/showInsertion?insertionName=LMJ.RY0402.193060\\_1](https://www.chlamylibrary.org/showInsertion?insertionName=LMJ.RY0402.193060_1))

**Internal bar code of the cassette:** **ATGACGCGCCCGTTTATGCTCG**

PCR amplification of 3' of the cassette (*thb5-1\_F1* and OMJ944)

**Sequence with *thb5-1\_F1***

GCGCTA**ATGACGCGCCCGTTTATGCTCG**ACTGACGTCGAGCCTTCTG  
 GCAGACTAGTTGCTCCTGAGTCCAACCAGCTCGTACGCCGCCTCTGG  
 GCCGCCACACGCCGCACCAGACCCGTGGGAGGGCCGCGCTGCTCC  
 CCGTCCTGCTCCTGCGGCTGGCCGGGCAGGCCGCCGCCGCCGCT  
 TTCCTTATGTTCCGCCAATCGCGCCGCTCCTCGGACTCGAGTGCCG  
 CGAGCTCGGCCTCGAACTCCTCGCGGCTCATCAGCTCGTCCGGGCCG  
 GGCGTGAAGATAGCCTGCGGGACATAGACGTCGGGACATGCCACGG  
 AGAGAATTAT

In grey is highlighted the *PRX* sequence and in pink is highlighted the paromomycin resistant cassette (CIB1, <https://www.chlamylibrary.org/showCassette?cassette=CIB1>)

In yellow is highlighted the bar code specific to the *thb5-1* mutant according to the link above.

*thb5-1*

**CLiP:** LMJ.RY0402.193060

([https://www.chlamylibrary.org/showInsertion?insertionName=LMJ.RY0402.193060\\_2](https://www.chlamylibrary.org/showInsertion?insertionName=LMJ.RY0402.193060_2))

**Internal bar code of the cassette:** **CGCTCAAACGGCAGTGTTACGT**

PCR amplification of 5' of the cassette (*thb5-1\_R1* and OMJ913)

**Sequence with *thb5-1\_F1***

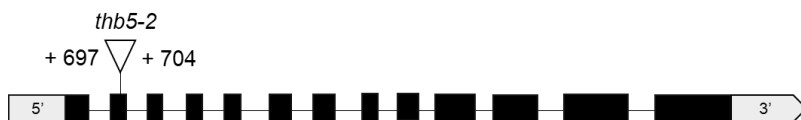
**CAGTGTTACGT**GGAGACGTGTTTCTGACGAGGGCTCGTGTGACTAGT  
 GAGTCCAACGTTTCGGCGGCTGTATTTCGCGGCTGTTTCGCGGACGAGG

TGCTCAAGGGCTTCTTCGCCGGCCTAAGCGTGGAGCGACTCAAGAC  
 CAAGCAGGTGAGGGAACGAGGGGGAGGGGTGGGTGTGAGGTTGAG  
 GAAGTGGGGCAGCGTGC GGATGCAGGATGGGCCATGGGTGGGTGTG  
 CGATAACAGCAGGAAAGCGGCGGCTGAGTGGTGGTGGATGTCAAG  
 GATCA

In grey is highlighted the *PRX* sequence and in pink is highlighted the paromomycin resistant cassette (CIB1, <https://www.chlamylibrary.org/showCassette?cassette=CIB1>)

In yellow is highlighted the bar code specific to the *thb5-1* mutant according to the link above.

*thb5-2*



CLiP: LMJ.RY0402.054490

([https://www.chlamylibrary.org/showInsertion?insertionName=LMJ.RY0402.054490\\_1](https://www.chlamylibrary.org/showInsertion?insertionName=LMJ.RY0402.054490_1))

**Internal bar code of the cassette:** TGGTGACGCACCTTGAATAACT

PCR amplification of 5' of the cassette (*thb5-2\_R1* and OMJ913)

**Sequence with *thb5-2\_R1***

GACGCACCTTGAATAACTGGAGACGTGTTTCTGACGAGGGCTCGTG  
 TGACTAGTGAGGTCCGCGGTCCGCTCCGCCAGCCGCTCCACAATGC  
 CGCCAGCGTGGTTGAGGTCGTTGGTGGCCTTTTTGAAGCTGTCCTTG  
 CGGACCGTCTTCAGAGCCTGTGGAGATCAATTTGGTTGTGGTGGTGA  
 GTGGAGGGGAATGCCCATGTGCTCAAAGTTGCTGCAGCCAGGGGCA  
 GCGCGGGAGGGTGAAGCGCACTGAAGGACTGCTAGCAGGTGGAC  
 GTGGCGTGAACTTTTGCTGGGGATAACCAGTGGACCCTCCGTTTCGCA  
 TATGTACTGTCCTTCAATTCAGGCTCTGAGAATGCCCGAAGCCGCGT  
 GTAGGGGACGCGGTCAAGCGCATGCAGCGAATGACTCAGCTGTGCT  
 TCTCCCTTGCGTAGACACACTATCGTTCCGGGGTGAATTCGTGTGCA  
 AGACACGCGTAAAGCTGCTCGCCTGAACGCTCTACGCCCCCGCAAC  
 TTTGCTTCTCGATGGCCCGGAAGCCGCACTCCGAGCCCCGAGCAGA  
 AAGGTAGGCCTGGGCGGTCAAGCAGCTCCGCCATTGATGTCATGAA

CCATTCAGGCGCTGTAGTCTTTCAAGCGAGCCTACCTGTGTGGTCTT  
TTGGGAGGCTTTTTGGGCGTCTTCCAGTCTGTGATAGCCTGGACTG  
CGGCTCGCACTTCGTCCTCCGTTACCATGTCACA

In grey is highlighted the *PRX* sequence and in pink is highlighted the paromomycin resistant cassette (CIB1, <https://www.chlamylibrary.org/showCassette?cassette=CIB1>)

In yellow is highlighted the bar code specific to the *thb5-2* mutant according to the link above.

**CLiP:** LMJ.RY0402.054490

([https://www.chlamylibrary.org/showInsertion?insertionName=LMJ.RY0402.054490\\_2](https://www.chlamylibrary.org/showInsertion?insertionName=LMJ.RY0402.054490_2))

**Internal bar code of the cassette:** GCCGAAGTGGCCGTTGTTGAGG

PCR amplification of 3' of the cassette (*thb5-2\_F1* and OMJ944)

### Sequence with OMJ944

GGAGACTGACACAATCCTTTGGCTATAGTTCCTCCTGAGTCCACAC  
CTCATCGGCTGTTGCCCTCGAACAGCGCAAAAATTCGCAGTGTAGGT  
GATAGTTTATGCCACGTGGTGCCCGGCTTTGGCGTGAGTTCTATGC  
CATATTGCCATGTGCTTTGTTTGTGACATACTGTTGGGTTGACAAAC  
TGTTGGGTTGCCGACATCACCGGAATATACGTGCTAACTGGTGAAGT  
GGTGTTGCCGCCTCCTTAAAAGCCAGTTGCCCTCCACCGCGCCTCAA  
ACCTACAGGCGTTTTAGCCCAAGTTGTTGCAGAATGCCATGGTGC GG  
CACTACTTCGATACCCTGTCCAGCGACCGCTTGAGGTCCAAACGGAT  
GAAGGTGAGCACCTTCTGCTGTATGCATGCGGCGGCGGTGGGTAGG  
GCGACAGGGCCGGCGGGTTATCGTGCCTATTCCTTGAAGGAGGTTT  
ATGGGTGAGGGAGCTCCCTGGCTATGTTGCGCATGCTGGCAACCTA  
AGGCTCTCTTCTGAAGCCTTAAAGATGGCCTGTCAGTTCTGCATACG  
GCTATGTCCC GTTGAGTGACCTCTTCTAACCTCTGCTCCAGAGTTC  
ATGCGCCCTATCAGTT

In grey is highlighted the *PRX* sequence and in pink is highlighted the paromomycin resistant cassette (CIB1, <https://www.chlamylibrary.org/showCassette?cassette=CIB1>)

Internal bar code of the cassette was not found.

No 100% identity with the reference gene of *PRX*.

*prx4*

**CLiP** : LMJ.RY0402.039746

([https://www.chlamylibrary.org/showInsertion?insertionName=LMJ.RY0402.039746\\_1](https://www.chlamylibrary.org/showInsertion?insertionName=LMJ.RY0402.039746_1))

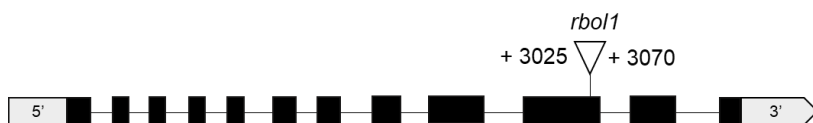
**CLiP**: LMJ.RY0402.039746

([https://www.chlamylibrary.org/showInsertion?insertionName=LMJ.RY0402.039746\\_2](https://www.chlamylibrary.org/showInsertion?insertionName=LMJ.RY0402.039746_2))

### Different gene

Cytosolic 80S ribosomal protein L12

*rbol1*



**CLiP**: LMJ.RY0402.245260

([https://www.chlamylibrary.org/showInsertion?insertionName=LMJ.RY0402.245260\\_1](https://www.chlamylibrary.org/showInsertion?insertionName=LMJ.RY0402.245260_1))

**Internal bar code of the cassette:** **AGCGTGACACCAGGCCATCTT**

PCR amplification of 3' of the cassette (*rbol1*\_F1 and OMJ944)

### Sequence with *rbol1*\_F1

**AGCGTGACACCAGGCCATCTT**ACTGACGTCGAGCCTTCTGGCAGACT  
AGTTGCTCCTGAGTCCAACGAGAAGTCCGTTGCTATGAAGTCGTCAC  
TTCCC GCCGTCCC GCCACGCCGTGCC CAGCACGGCGTCTGCCCGC  
TCCAAATCTGCCAATGCGGACGTCGAGGCCACCTTGGCCATCGGCG  
CGAGCGCACCGCCGCCAACGGCCGCGGCAGCAGCTGAGGTTGCGGA  
AGAAGGTGTGGGCGGCGCGTAGGGCGCCGGCTCTGCCGCGAGGCAG  
GCGCCTTCTTGGAGAGGTTGGGA

In grey is highlighted the *RBOLI* sequence and in pink is highlighted the paromomycin resistant cassette (CIB1, <https://www.chlamylibrary.org/showCassette?cassette=CIB1>)

In yellow is highlighted the bar code specific to the *rbol1* mutant according to the link above.

The G and AGA bases highlighted in red are T and GAT in the reverse complement sequence of *RBOLI* gene respectively.

**CLiP:** LMJ.RY0402.245260

([https://www.chlamylibrary.org/showInsertion?insertionName=LMJ.RY0402.245260\\_2](https://www.chlamylibrary.org/showInsertion?insertionName=LMJ.RY0402.245260_2))

**Internal bar code of the cassette:** ACAGGCTTGGAATTTGTTATCT

PCR amplification of 5' of the cassette (*rboli*\_R1 and OMJ913)

**Sequence with *rboli*\_R1**

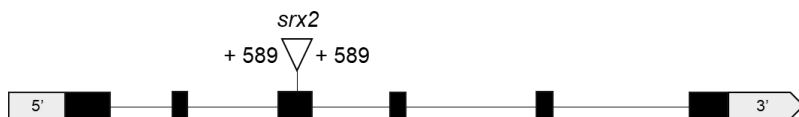
```
GCCACAGGCTTGGAATTTGTTATCTGGAGACGTGTTTCTGACGAGGG
CTCGTGTGACTAGTCTTCTAGGAGGGGGCTAAGGGGGAAGCACCTG
ACGCGGGGGCGGGTGGGTGGAAACCTGCTGGGGGGCGGCGCTCCTG
AGTCTCCTTGTGCACCCCTGCGTTGTGCACGCCCTCACGCAGCCTGA
CGCATTTCGCACCCTTACGAACCTTGCCCTTGCATCAGGCCCGGGACA
ACGACCGCACAAAGGCCAACATCAGGCCGGAGCTGCAGCCGGCGCT
GCGCCTGGGCCCGCCCCGACCTGCCGCAGCTGTTCATGGACACGGCG
CGGCGGGCGGAGAGCCTGCGGGAGCGGGAGGTGGCAGTGTTCGTGT
GCGGGTGAGTGACCAGCAGAACACCTAGGTCGCGGCAGCGTGTGGC
TTACAATGGATGGATTCGC
```

In grey is highlighted the *RBOLI* sequence and in pink is highlighted the paromomycin resistant cassette (CIB1, <https://www.chlamylibrary.org/showCassette?cassette=CIB1>)

In yellow is highlighted the bar code specific to the *rboli* mutant according to the link above.

The GA and TCG bases highlighted in red are AT and CGC in the sequence of *RBOLI* gene respectively.

*srx2*



CLiP: LMJ.RY0402.082299

([https://www.chlamylibrary.org/showInsertion?insertionName=LMJ.RY0402.082299\\_1](https://www.chlamylibrary.org/showInsertion?insertionName=LMJ.RY0402.082299_1))

**Internal bar code of the cassette:** **AAGTCTAGAAGCTTGCGGAGAG**

PCR amplification of 3' of the cassette (*srx2*\_F1 and OMJ944)

**Sequence with *srx2*\_F1**

**GTCTAGAAGCTTGCGGAGAG** ACTGACGTCGAGCCTTCTGGCAGACT  
AGTTGCTCCTGAGTCCAACAAATCTGTCCCGTTGCTAGCTGCACC  
CGAGGACTTATCTGCGTGCCGCCAAACACAAGACACGTTACGCCG  
GCACACGCAAATGCAGAACAGTACGATTGCC

In grey is highlighted the *SRX1* sequence and in pink is highlighted the paromomycin resistant cassette (CIB1, <https://www.chlamylibrary.org/showCassette?cassette=CIB1>)

In yellow is highlighted the bar code specific to the *srx2* mutant according to the link above.

CLiP: LMJ.RY0402.082299

([https://www.chlamylibrary.org/showInsertion?insertionName=LMJ.RY0402.082299\\_2](https://www.chlamylibrary.org/showInsertion?insertionName=LMJ.RY0402.082299_2))

**Internal bar code of the cassette:** **ATCCTCCATCATGCGATCTGGT**

PCR amplification of 5' of the cassette (*srx2*\_R1 and OMJ913)

**Sequence with *srx2*\_R1**

**ATCATGCGATCTGGT** GGAGACGTGTTTCTGACGAGGGCTCGTGTGAC  
TAGTGAGTCCAAC TTTGGA ACTACCGGTTGCGGCCATCCGCAGGCC  
GCTGGGCCGCACGCGCGGCAATGGTGCGTTTCTGCTGTCTTGCTGCA  
GTGTGCGTTGCTTTATCCGCTACTTGCGATGATCTCTGGGCTGGTGT  
GGGGCGAATGGGATGGTCGTTGGGCCGGCAGTTGTACGGGCAGTTA  
CACAGGTCGTTACTTACCGCGTCACACGATGCACGGGAGCTCTCAC

ACGTCGGCCGGGTGTGCCCGTTATCAGCCCCAAAATCCATCCGCACC  
ACGCCGCCACAAACACACACGCCTGATGCACAAAAAGAACACAA

*lca1-1*

**CLiP:** LMJ.RY0402.045556

([https://www.chlamylibrary.org/showInsertion?insertionName=LMJ.RY0402.045556\\_1](https://www.chlamylibrary.org/showInsertion?insertionName=LMJ.RY0402.045556_1))

**Not found**

**CLiP:** LMJ.RY0402.045556

([https://www.chlamylibrary.org/showInsertion?insertionName=LMJ.RY0402.045556\\_2](https://www.chlamylibrary.org/showInsertion?insertionName=LMJ.RY0402.045556_2))

**Not found**

*lca1-2*



**CLiP:** LMJ.RY0402.108723

([https://www.chlamylibrary.org/showInsertion?insertionName=LMJ.RY0402.108723\\_1](https://www.chlamylibrary.org/showInsertion?insertionName=LMJ.RY0402.108723_1))

**Internal bar code of the cassette:** **CCTCCCGGGACTGTCTGGGCC**

PCR amplification of 5' of the cassette (*lca1-2\_R1* and OMJ913)

**Sequence with *lca1-2\_R1***

**ACTGTCTGGGCC**GGAGACGTGTTTCTGACGAGGGCTCGTGTGACTA  
GTGAGTCCAACCTGGCGCCGCCGGTGC GG GTGTGGCAGGAGCTGGG  
CAATGGAGTCGAGTGAGTTGTTTGTGGGTGGGGTCTTTTGC GTGCAA  
AGGCCAAAGGGGGCGGGGTGCGAAGGGCGTAACGGGGCCGCCAAA  
GAAGGTAGGAGCCGCGCCCGCTGCTCGCCCCGAGCCTGATCATG  
CTGCCTCTGCTGCCTGCTGTGTTGCAGGTTTATGCGCTACACGTACA  
CGCACGACAGCAGCACCGAGAAGCGCCGCCGCATCGCCTCCGTCAT  
CAAGCTGCGCAGCCGCGCACCCGACGGCGCCCCGCGTGTGTCTGAC  
CTCATCACCGCGGCCCTGCAGGTCCGTAGCGGCAGCTGCGTACGGG

GCAGGAGCAGGGGCAGGAGCAGAGGCATGGGAAGGGGAAGGGGC  
AGGCGCTTGCCTGTCATATGGTTGCCTGTGTTCCGTGACGTTTTCAA  
TTACCCTGCAGCCGCGTTGAAAGCTTGTGGCCGTGAAACAGCGACT  
GAGGTCACCTGGCCCCCGCCGCGCCCTGCTGCCGTGCGCAGGACCA  
CCGTGAGCAGAAGGCCGCGCGCCCCGCCGACCGCCACCGCTACCTC  
TCGTCCCCACCTA

In grey is highlighted the *LCAI* sequence and in pink is highlighted the paromomycin resistant cassette (CIB1, <https://www.chlamylibrary.org/showCassette?cassette=CIB1>)

In yellow is highlighted the bar code specific to the *lca1.2* mutant according to the link above, but not found in the sequencing.

The CGT bases highlighted in red are ACG in the sequence of *LCAI* gene.

**CLiP:** LMJ.RY0402.108723

([https://www.chlamylibrary.org/showInsertion?insertionName=LMJ.RY0402.108723\\_2](https://www.chlamylibrary.org/showInsertion?insertionName=LMJ.RY0402.108723_2))

**Internal bar code of the cassette:** CGAGTGA ACTCAATCGAACACC

PCR amplification of 3' of the cassette (*lca1-2\_F1* and OMJ944)

**Sequence with *lca1-2\_R1***

GCGCTA CGAGTGA ACTCAATCGAACACC ACTGACGTCGAGCCTTCT  
GGCAGACTAGTTGCTCCTGAGTCAGCCCGTAGGCCGCCGCTCAGC  
CTGCTTGGCCGCGCCCACTGAGCTACCGCAGTCGCTGCTTTTGCTAC  
TGCTGCCTGCCGCCGAATCCTCATCGCCCGAGTCTGAATCAGCATCA  
CCGCCAGCTGCTGCGAGCCGCCGGCGCCGCTTCTCCAGGGAAAGGT  
ACGCCGTAGTCATGTCTCTAAGGAGCTTCGCGGGGGACTGGGCAGT  
CGCGGGAGCGGCGGCGCGGATGGCGGTGGGGGTGATGGCAGAGAT  
GCAGGCAGAGGCTGTGGCAGCGGGTCTCCGGCGCAATTGTTGACG  
TAGGCCAACAGTGCTCGCTGCAGGATGGCGTTCGCGGGCTGGCCGT  
CGGGGTCGTAGCTGCAAGTAGCAAATAGAAGGGCAGGCGGCGAGG  
GAGGGGCTTTGTTGAGGTTGGTGCTTGTCTGCTTGCACACCACACTA  
GCGGTGAACCACTGTGCGAGGGCCACGGTCGAGGGCCGAGTCCCTC  
GGCCCTGGCAAGTGGCCCCAGCGTACAACACGCAACCGCACACGGC  
GCTTCACGCCGCGCGGACGCGCCATACGTTCCCCCTCCGGCTCTCCG  
CTGATGTAGCCCCAGCCACCGCTAGCCGCCGACACTCCCGCTCCT



GCACCCCGCTGCCGTGCCAGGCACTCACACGGACCCCTTCGCACACT  
TCGCGCACTCACTAGTATC

In grey is highlighted the *LCA1* sequence and in pink is highlighted the paromomycin resistant cassette (CIB1, <https://www.chlamylibrary.org/showCassette?cassette=CIB1>)

In yellow is highlighted the bar code specific to the *lca1-2* mutant according to the link above, but not found in the sequencing.

Supplementary table

**Table S1.** Primers used for sequencing, RT-PCR and transformation.

Mutants	Primer name	Orientation 5' -> 3'
<i>apx1</i>	<i>apx1_F1</i>	CTATGTGCTTTGTGTCTGTC
	<i>apx1_R1</i>	CACATGCAAGTTTAGAGCTG
<i>apx2</i>	<i>apx2-0_F</i>	TTCCCTGTCTGAATTGCAC
	<i>apx2-0_R1</i>	CGAGACCACACATATCAAGG
<i>cat2-1</i>	<i>cat2-1_F</i>	CACGATTGATGAATGCAGAC
	<i>cat2-1_R</i>	CAATGATGAGCTATGGACGA
<i>cat2-2</i>	<i>cat2-2_F1</i>	CATGAAAGATGTTGCCGC
	<i>cat2-2_R1</i>	GAAGTGTAGAGAAGTAGGCG
<i>gpx3-1</i>	<i>gpx3-1_F1</i>	ACGGCAAGAACTTTAAGCTA
	<i>gpx3-1_R1</i>	TATTATCTAACGGGTGGGT
<i>gpx3-2</i>	<i>gpx3-2_F1</i>	ACGGCAAGAACTTTAAGCTA
	<i>gpx3-2_R1</i>	TATTATCTAACGGGTGGGT
<i>nrx1</i>	<i>nrx1_F1</i>	TGCAACATCACTTCAGTAGG
	<i>nrx1_R1</i>	CTTGAAGTCCGACACCAC
<i>nrx2-1</i>	<i>nrx2-1_F1</i>	CTAGAGCGATCGTCCCTTTG
	<i>nrx2-1_R1</i>	GCATAGCTTCTCCATAGCCG
<i>nrx2-2</i>	<i>nrx2-2_F1</i>	GCGTATGACTTCAGGTGGAC
	<i>nrx2-2_R1</i>	GGCTGTGGTACTCGTTCATC
<i>gst13</i>	<i>gst13_F1</i>	GTCTCTATCTTGTGGTTGGG
	<i>gst13_R1</i>	CTTGTCGTCTGAAGTTGGAT
<i>prx-1</i>	<i>prx-1_F1</i>	ATAATTCTCTCCGTGGCATG
	<i>prx-1_R1</i>	GATCCTTGACATCCACCAC
<i>prx-2</i>	<i>prx-2_F1</i>	AGCGGCAAGTTTGTGGAC
	<i>prx-2_R1</i>	TGGAACTTGGCTTTGTCC
<i>prx4</i>	<i>prx4_F1</i>	CCCAGACACGATTAGGTTTG
	<i>prx4_R1</i>	CTCCTTGGTTAGCGCAAGAC
<i>rbol1</i>	<i>rbol1_F</i>	CCCAACCTCTACCAAGAAG
	<i>rbol1_R</i>	GCGAATCATCCATTGTAAGC
<i>srx2</i>	<i>srx2_F1</i>	AGGCAATCGTACTGTTCTG
	<i>srx2_R1</i>	TGTGTTCTTTTGTGCATCAG
<i>lca1-1</i>	<i>lca1-1_F1</i>	GACCTTTCCTCCTTCTTC
	<i>lca1-1_R1</i>	AACTCCAAGGCTGTTGAAAA
<i>lca1-2</i>	<i>lca1-2_F1</i>	CTTAGAGACATGACTACGGC
	<i>lca1-2_R1</i>	GCTCCTACCTTCTTTGGC
cassette	OMJ913	GCACCAATCATGTCAAGCCT
cassette	OMJ944	GACGTTACAGCACACCCTTG

	Primer name (RT-PCR)	Orientation 5'-> 3'
<i>srx2</i>	<i>srx1_F2</i> <i>srx1_R2</i>	CAAGTACA ACTGGACCTTCG CGGTGATACTCTCCATCAG
		Tranformation
<i>srx2</i>	<i>NdeI</i> -F1 <i>EcoRI</i> -R2	ggtCATATGTGTTGGTCGCAGA GTGAATC ggtGAATTCCACCTTCCGGCGT TACAGC
pHyg3	APH7-F APH7-R	TCGATATCAAGCTTCTTTCTTG C AAGCTTCCATGGGATGACG

## Chapter IV

### APX2, the ascorbate peroxidase-related protein, regulates the levels of plastocyanin in *Chlamydomonas*

Anna Caccamo<sup>1,2,3,4</sup>, Félix Vega de Luna<sup>1</sup>, Agnieszka E. Misztak<sup>1</sup>, Sébastien Pyr dit Ruys<sup>5,6</sup>, Didier Vertommen<sup>5</sup>, Pierre Cardol<sup>1</sup>, Joris Messens<sup>2,3,4,\*</sup>, Claire Remacle<sup>1,\*</sup>

<sup>1</sup>Genetics and Physiology of Microalgae, InBios/Phytosystems research unit, University of Liège, 4000 Liège, Belgium

<sup>2</sup>VIB-VUB Center for Structural Biology, 1050 Brussels, Belgium

<sup>3</sup>Brussels Center for Redox Biology, 1050 Brussels, Belgium

<sup>4</sup>Structural Biology Brussels, Vrije Universiteit Brussel, 1050 Brussels, Belgium

<sup>5</sup>SSS/DDUV/PHOS, de Duve Institute and MASSPROT platform, UCLouvain, 1200 Brussels, Belgium

<sup>6</sup>SSS/LDRI/PMGK, Faculty of Pharmacy and Louvain Drug Research Institute, UCLouvain, 1200 Brussels, Belgium

In this publication, my involvement encompassed conducting the molecular, genetic, and physiological analysis of the *apx2* mutants. I actively engaged in assessing growth rate curves, immunoblots, photosynthetic parameters, protein extraction for proteomics experiments and data sets analyses, and RNA extraction for RNASeq analyses. This work has been submitted to *Plant and Cell Physiology* in 2023.

Mailing address: Genetics and Physiology of Microalgae, InBios/Phytosystems, University of Liège, 4000 Liège, Belgium.

\*Emails for correspondence: [c.remacle@uliege.be](mailto:c.remacle@uliege.be) and [joris.messens@vub.be](mailto:joris.messens@vub.be)

#### *Abstract*

The function of ascorbate peroxidase-related (APX-R) proteins, present in all green photosynthetic eukaryotes, remains unclear. This study focuses on APX-R from *Chlamydomonas reinhardtii*, namely ascorbate peroxidase 2 (APX2). We showed that *apx2* mutants exhibited a faster oxidation of the PSI primary electron donor, P700, upon sudden light increase and a slower re-reduction rate compared to the wild type, pointing to a limitation of plastocyanin. Spectroscopic, proteomic, and immunoblot analyses confirmed that the phenotype was a result of lower levels of plastocyanin in the *apx2* mutants. The redox state of P700 did

not differ between wild type and *apx2* mutants when the loss of function in plastocyanin was nutritionally complemented by growing *apx2* mutants under copper deficiency. In this case, cytochrome *c<sub>6</sub>* functionally replaces plastocyanin, confirming that lower levels of plastocyanin was the primary defect caused by absence of APX2. Overall, the results presented here shed light on an unexpected regulation of plastocyanin level under copper replete conditions, induced by ascorbate peroxidase 2 in *Chlamydomonas*.

Keywords: APX2, *Chlamydomonas*, plastocyanin, P700, cytochrome *c<sub>6</sub>*, copper-deficiency

#### 4.1 Introduction

Ascorbate peroxidases (APXs) (EC 1.11.1.11) are heme *b*-containing enzymes belonging to class I peroxidases and catalyse the reduction of H<sub>2</sub>O<sub>2</sub> into H<sub>2</sub>O using ascorbate as electron donor. Several nucleus-encoded APXs are present in the different compartments of plants and algae (Caverzan et al 2012). In chloroplasts, for example, APXs protect cells against oxidative damage (Foyer & Noctor 2011, Shigeoka et al 2002). Their primary function is carried out on the stromal side of the chloroplasts, where the superoxide anion produced by photoreduction of O<sub>2</sub> at the level of photosystem I (PSI) is converted into H<sub>2</sub>O<sub>2</sub> by superoxide dismutase (Asada 1999).

Beside the classic APXs, a new class of ascorbate peroxidase-related (APX-R) enzymes was identified (Lazzarotto et al 2021a). This class is present in all the green photosynthetic eukaryotes (Lazzarotto et al 2015) and typically encoded by a single locus (Dunand et al 2011). It is characterized by the absence of the amino acids typical for ascorbate binding while the amino acids for heme binding and catalysis are conserved (Lazzarotto et al 2021a). Most of the information regarding APX-Rs comes from studies in *Arabidopsis thaliana* (hereafter *Arabidopsis*), where the chloroplast localization of the APX-R enzyme (APX6) has been observed (Lazzarotto et al 2021b). *In vitro* studies showed that APX6 does not use ascorbate to reduce H<sub>2</sub>O<sub>2</sub> (Lazzarotto et al 2021b). *In vivo*, APX6 expression is increased during seed maturation, germination, and leaf senescence (Chen et al 2021, Chen et al 2014) and responds to stresses, such as high light combined with high temperature (Giraud et al 2008). In over-expressing transgenic plant lines, APX6 follows a degradative path from chloroplast

plastoglobuli to cytoplasm during photomorphogenesis (Lazzarotto et al 2021b). APX-R expression was also studied in a few other plants. In *Triticum aestivum*, expression of APX-R is down- or up-regulated during drought, heat stress or their combination (Tyagi et al 2020). In *Brassica rapa*, the expression of APX-R is differentially expressed according to stress exposure to drought and heat (Verma et al 2022). In *Oryza sativa*, the expression is up-regulated during drought or cold stress, and in presence of aluminium and UV-light. In addition, mutant lines defective for APX-R display a growth delay (Lazzarotto et al 2011).

Overall, no detailed information regarding the physiology and the photosynthetic activity of the above-mentioned land plants has been provided so far.

Previous work from our groups recently showed that the APX-R of the green alga *Chlamydomonas*, namely APX2, is chloroplast-localized, exhibits a twin arginine motif (TAT signal) for targeting to the lumen of the thylakoids and a MxxM motif, typical of metal binding. In addition, the recombinant protein does not use ascorbate as electron donor for reduction of H<sub>2</sub>O<sub>2</sub>, confirming its classification to the APX-R family. Additionally, it binds both copper and heme, and it modulates the copper-binding capabilities of plastocyanin *in vitro* (Caccamo et al 2023).

With the aim to elucidate the link between APX2 and plastocyanin, we decided to investigate the physiology of *apx2* insertional mutants. Our detailed analysis of the photosynthetic machinery revealed that the mutants were not affected at the level of photosystem II (PSII). However, when transferred from low light to a sudden increase of light, *apx2* mutants exhibited a different redox state of P700, the PSI primary electron donor. This defect was caused by reduced levels of the photosynthetic electron carrier, plastocyanin. This phenotype was rescued under copper-deficient conditions, in which cytochrome *c<sub>6</sub>* functionally replaces plastocyanin, confirming that plastocyanin deficiency was the sole responsible for the mutant phenotype. Overall, these results provide support for the role of APX2 in regulating plastocyanin levels under copper-replete conditions in *Chlamydomonas*.

## 4.2 Material and Methods

### 4.2.1 Strains and culture media

Wt (CC-4533 *cw15* mt-), *apx2* mutants of *Chlamydomonas* (*APX2* Cre06g.285150) have been ordered from the *Chlamydomonas* library (<https://www.chlamylibrary.org/>, **Li et al., 2019**) (Li et al., 2019). We will refer to them, respectively as wt, *apx2-1* (LMJ.RY0402.180063), *apx2-2* (LMJ.RY0402.095128). Wild-type and mutant strains were grown at 25°C under phototrophic minimal condition in Tris-minimal-phosphate (TMP) medium, or under mixotrophic condition in Tris-acetate phosphate (TAP) medium in standard copper concentration (6 µM CuSO<sub>4</sub>) (Hutner et al., 1950) or in copper-low condition [TMP + 1nM CuSO<sub>4</sub>], under continuous low light (30 µmol photons.m<sup>-2</sup>.s<sup>-1</sup>) and with gentle shaking (Harris 2009).

### 4.2.2 Growth measurements

Algal growth was determined two times per day by measuring the optical density (OD) at 750 nm until the stationary phase was reached, using a LAMBDA™ 265 UV/Vis spectrophotometer (PerkinElmer). The growth rate  $\mu$  (h<sup>-1</sup>) of the cell cultures was calculated as in (Jia et al., 2015).

$$\mu \text{ (h}^{-1}\text{)} = [\ln (\text{OD}2) - \ln (\text{OD}1)] / (t2 - t1)$$

an equation in which  $\mu$  is the growth rate (h<sup>-1</sup>), OD = Optical density of cells at the end (OD2) and beginning (OD1) of the exponential phase, t2 = time in h at the end of the exponential phase, t1 = time in h at the beginning of the exponential phase.

The doubling time was calculated as  $t_d = \ln (2) / \mu$  (h<sup>-1</sup>)

### 4.2.3 Total DNA extraction and PCR amplification

DNA extraction was performed by following the protocol described in (Newman et al 1990). The DNA was used for PCR amplifications to confirm the presence of the paromomycin cassette in *apx2* mutants. PCR amplifications were performed as suggested on the CLiP library website, using the couple of primers *apx2-1\_F*/OMJ944 and *apx2-1\_R*/OMJ913 to map the 3' end and the 5' end of the cassette respectively of the *apx2-1* mutant, primers *apx2-2\_F*/OMJ944 to

map the 3' side of the cassette of the *apx2-2* mutant. Primer sequences are in Supplemental Table S2. Sequencing was made at Eurofins genomics.

#### *4.2.4 Total RNA extraction*

Cultures of wt and *apx2-1* mutant were grown in triplicates in TMP and TMP + 1 nM CuSO<sub>4</sub> under continuous low light 50 μmol photons m<sup>-2</sup> s<sup>-1</sup>. Cultures of TMP + 1 nM CuSO<sub>4</sub> were started by washing the pellets of the pre-cultures grown in TMP-CuSO<sub>4</sub>. The pellets were suspended in TMP-CuSO<sub>4</sub> and the cultures launched in TMP + 1 nM CuSO<sub>4</sub>. After four days, the cultures were refreshed with new TMP + 1 nM CuSO<sub>4</sub> medium until plastocyanin was completely substituted by cytochrome *c*<sub>6</sub>. The cultures were then collected at mid-exponential phase and the pellets were resuspended in 0.5 mL of 2% SDS, 400 mM NaCl, 40 mM EDTA, 100 mM Tris/HCl, pH 8.0, dimethyl pyrocarbonate to lyse the cells and total RNA was extracted using the NucleoSpin® RNA Plant and Fungi kit as described in the Macherey-Nagel protocol (Ref. 740120.50). The concentration and the purity (260/280 ratio 2.0-2.1) of RNA were determined by the NanoDrop (Agilent BioTek Synergy Mx Monochromator-Based Multi-Mode Reader with Time-resolved Fluorescence) and by gel electrophoresis.

#### *4.2.5 Transcriptomic analyses*

##### *Sample collection and preparation*

*Chlamydomonas* wt and *apx2-1* cells were grown in triplicate in the two cultivation conditions (12 samples) and collected for RNA extraction as described in the section Total RNA extraction. The samples were sent for sequencing to the Novogene Company (United Kingdom). Raw data are available at NCBI (BioProject ID: PRJNA994826).

##### *RNA quantification and quality assessment (Novogene Company)*

RNA integrity was assessed using the RNA Nano 6000 Assay Kit of the Bioanalyzer 2100 system (Agilent Technologies, CA, USA).

##### *Library preparation for transcriptome sequencing (Novogene Experimental Department)*

Total RNA was used as input material for the library preparations, which was carried out by using Novogene NGS RNA Library Prep Set (PT042) according



to the manufacturer's protocol. In order to select cDNA fragments of preferentially 370 to 420 bp in length, the library fragments were purified using an AMPure XP system (Beckman Coulter, Beverly, USA). Then, PCR was performed with Phusion High-Fidelity DNA polymerase, Universal PCR primers and Index (X) Primer. At last, PCR products were purified (AMPure XP system) and library quality was assessed on the Agilent Bioanalyzer 2100 system.

#### *Clustering and sequencing (Novogene Experimental Department)*

The clustering of the index-coded samples was performed on a cBot Cluster Generation System using TruSeq PE Cluster Kit v3-cBot-HS (Illumina) according to the manufacturer's instructions. After cluster generation, the library preparations were sequenced on an Illumina Novaseq platform and 150 bp paired-end reads were generated.

#### *Transcriptomic analyses*

Reads were quality trimmed using Trimmomatic software (Bolger et al 2014) removing adapters and bases with the average score lower than 30 over 10bp sliding window. Afterwards they were aligned and counted using Trinity software (Grabherr et al 2011). *Chlamydomonas reinhardtii* v5.5 transcriptome data was downloaded from Phytozome (Goodstein et al 2012) and indexed with bowtie2 (Langmead & Salzberg 2012). Transcripts, including isoforms, abundances were obtained with RSEM (Li & Dewey 2011). The sequencing depth is presented in Dataset2 (section Mapped\_reads). The normalisation and differential expression analysis were performed with DESeq2 R package (Love et al 2014). The reported DE transcripts were obtained by selecting the results with  $\log_2FC > 1$  or  $< -1$  and FDR-adjusted  $p\text{-value} \leq 0.05$ .

#### *4.2.6 Chlorophyll content*

Pigments were extracted from whole cells using methanol, following a protocol adapted from (Emonds-Alt et al 2017). Chlorophyll a and b concentrations were determined by measuring the absorbance at 652, 665 and 750 nm following the equations a) and b) (Ritchie 2006).

a) Chl *a* ( $\mu\text{g/ml}$ ):  $-8.0962 * (\text{Abs}_{652} - \text{Abs}_{750}) + 16.5169 * (\text{Abs}_{665} - \text{Abs}_{750})$

b) Chl *b* ( $\mu\text{g/ml}$ ):  $27.4405 * (\text{Abs}_{652} - \text{Abs}_{750}) - 12.1688 * (\text{Abs}_{665} - \text{Abs}_{750})$

#### 4.2.7 Isolation of soluble and chloroplast enriched fractions

Soluble fractions were prepared as in (Li & Merchant 1992). Cultures of wt and *apx2* mutants were harvested in mid-exponential phase and washed with sodium phosphate buffer 10 mM pH 7.0, 2,000 g for 3 min at room temperature. The pellet was suspended in the same buffer at  $2 \times 10^8$  cells/ml and frozen at  $-80^\circ\text{C}$ . Five cycles of freeze-thaw during 1 h each were performed to extract soluble proteins. After the last cycle the cells were centrifuged for 15 min at  $4^\circ\text{C}$  at 12,000 g, the supernatant and the pellet were collected and the protein content was determined with a Bradford assay, as in (Ernst & Zor 2010). Chloroplast-enriched fractions were isolated according to (Mason et al 2006).

#### 4.2.8 Efficiency of photosystem II

*In vivo* chlorophyll *a* fluorescence was measured in 1 cm microcuvettes by using a Joliot-Type-Spectrophotometer (JTS-10, BioLogic France). A blue-LED probe of 10  $\mu\text{s}$  pulses was used to measure the chlorophyll *a* fluorescence in dark conditions ( $F_0$ ) and after a saturating pulse of red light ( $F_m$ , 3000  $\mu\text{mol photons m}^{-2} \text{s}^{-1}$ ) to reach the maximum PSII quantum yield ( $F_v/F_m = F_m - F_0/F_m$ ). Samples were then acclimated to different photosynthetic photon flux densities (PPFD) for 3 min and fluorescence values were measured ( $F_s$ ). A saturating pulse was then given to fully reduce PSII acceptors and reach the maximal fluorescence yield ( $F_m'$ ). These parameters were used to calculate the PSII quantum yield ( $\Phi_{\text{PSII}} = (F_m' - F_s)/F_m'$ ) and the relative electron transfer rate ( $r\text{ETR} = \Phi_{\text{PSII}} * \text{PPFD}$ ) (Maxwell & Johnson 2000).

#### 4.2.9 Fast fluorescence increase

The fast chlorophyll *a* fluorescence rises in response to a saturating pulse of light of 3000  $\mu\text{mol photons m}^{-2} \text{s}^{-1}$ , was obtained using a HandPea instrument (Hansatech, UK) after a short dark incubation in 1 cm microcuvettes. The chlorophyll *a* fluorescence increases were normalised to variable fluorescence (i.e. between the values of  $F_0$  and  $F_m$ ) (Strasser & Govindjee 1992).

#### 4.2.10 Activity of photosystem I

Photosystem I (PSI) activity was monitored with the Joliot-Type-Spectrophotometer (JTS-10, BioLogic France) by the changes in absorption in the near infra-red region of the P700, the primary electron donor at the PSI

reaction centre. The signal at 705 nm was corrected by the absorption at 725 nm. After a short period of dark incubation, a saturating red actinic light of 3000  $\mu\text{mol photons m}^{-2} \text{s}^{-1}$  was given for one second. The measurements were normalised to the maximum change of absorption due to P700 oxidised in the presence of 10  $\mu\text{M}$  of 3-(3,4-dichlorophenyl)-1,1-dimethylurea (DCMU) and 10  $\mu\text{M}$  of 2,5-dibromo-3-methyl-6-isopropylbenzoquinone (DBMIB). The signal/level of oxidised cytochrome *f* ( $\text{Cyt}f^+$ ) from the cytochrome *b\_6f* complex, was deconvoluted from the signal at 554 nm and a baseline between 546 nm and 573 nm in presence of 10  $\mu\text{M}$  of DCMU and 10  $\mu\text{M}$  DBMIB. The relative abundance of  $\text{Cyt}f^+$  and  $\text{P700}^+$  ( $\text{Cyt}f^+/\text{P700}^+$ ) was calculated from molar extinction coefficients of 18  $\text{mM}^{-1} \text{cm}^{-1}$  at 554 nm for *Cyt**f* (Pierre et al 1995) and of 50  $\text{mM}^{-1} \text{cm}^{-1}$  at 705 nm for P700 (Heinnickel et al 2013). Electron transfer to  $\text{P700}^+$  was monitored after a single-turnover-flash, provided by a Nd-YAG laser (Minilite II, Continuum) generating one charge separation per photosystem. A train of ten consecutive single-turnover-flashes, triggered every 100 ms, was used to oxidise P700 in the presence of DCMU and DBMIB (Drepper et al 1996).

#### 4.2.11 Electrochromic shift assay

The electrochromic shift (ECS), used to monitor the electric field of the thylakoid membranes in response to photosynthetic activity, was measured with the JTS-10. A baseline of absorption in darkness was made, and afterwards a single-turnover-flash was applied. Then the measurements were repeated with the addition of 10  $\mu\text{M}$  DCMU and 1 mM hydroxylamine preventing charge separations at PSII. The change in absorption corresponding to PSII and PSI or only to PSI charge separations were used to calculate the relative abundance of active PSI and PSII (Bailleul et al 2010).

#### 4.2.12 Plastocyanin and cytochrome *c\_6* quantification

Soluble proteins were extracted as described in (Li & Merchant 1992). Cultures of wt and *apx2* mutants were harvested in mid-exponential phase and washed with sodium phosphate buffer 10 mM pH 7.0, 2,000 *g* for 3 min at room temperature. Soluble extracts were prepared as described above. Each sample was split in two, one oxidised with 1 mM potassium ferricyanide and the second one reduced with 1 mM of ascorbic acid. Absorbance was recorded between 400 and 800 nm. The plastocyanin concentration was calculated using a molar extinction coefficient for the oxidised form of 4.9  $\text{mM}^{-1} \text{cm}^{-1}$  at 597 nm (Sommer et al 2002). The actual absorbances of plastocyanin at 597 nm were calculated

by subtracting the absorption value of the reduced sample to the oxidised one (Li & Merchant 1995) and correcting the signal by removing that one at 700 nm.

The cytochrome  $c_6$  concentration was calculated using a molar extinction coefficient for the reduced form of  $20 \text{ mM}^{-1} \text{ cm}^{-1}$  at 552 nm (Sommer et al 2002). The actual absorbances of cytochrome  $c_6$  at 552 nm were calculated by subtracting the absorption value of the oxidised samples to the reduced one (Howe & Merchant 1992) by correcting the signal to that one at 530 nm.

#### *4.2.13 Gel electrophoresis and blotting*

Soluble extracts and chloroplastic fractions were loaded on 10, 12 or 15% Laemmli-SDS-PAGE gel, or Tricine-SDS-PAGE (Schagger 2006) and electroblotted according to standard protocols onto PVDF membranes (Cytiva Amersham Hybond). Detection was performed using a Chemiluminescence Western blotting kit (Roche). The blots were developed using commercially available primary antibodies for CYC6 ( $\alpha$ -CYC6, 1/2000, Agrisera AS06 202) and FNR protein ( $\alpha$ -FNR, 1/5000, Agrisera AS15 2909), or polyclonal antibodies raised in rabbits against recombinant APX2 ( $\alpha$ -APX2, 1/10000, Proteogenix), and plastocyanin ( $\alpha$ -PC, 1/500, Proteogenix). Fluorescence was detected using an iBright FL1000 Imaging System (Invitrogen by Thermo Fisher Scientific).

#### *4.2.14 Proteomic analyses*

Cells were grown in phototrophy under low light conditions until the mid-exponential phase.  $10^8$  cells were harvested by centrifugation for 3 min at 1000 g, at room temperature. The supernatant was discarded and the pellet was suspended in 1 ml of RIPA – like buffer: triethylammonium bicarbonate (TEAB) 100 mM, NaCl 150 mM, octylphenoxypolyethoxyethanol (IGEPAL) 1%, deoxycholic acid sodium salt (DOC) 0.5% sodium dodecyl sulphate (SDS) 0.1%, n-dodecyl- $\beta$ -D-maltoside (DDM) 0.2%, phenylmethylsulfonyl fluoride (PMSF) 0.5 mM EDTA, vortexed for 10 min at room temperature and centrifuged for 10 min at 4°C at 21,000 g. The protein concentration of the supernatant was determined with a BCA assay (Pierce™ BCA Protein Assay Kit). Reduction of 200  $\mu$ l of protein solution at 1.5  $\mu$ g/ $\mu$ l was performed with 10 mM of 1,4-dithiothreitol (DTT) at 45°C for 30 min and the alkylation with 50 mM of chloroacetamide for 30 min in the dark at room temperature. Detergents were removed using the Pierce™ Detergent Removal Spin Column (0.5 ml) and the

protein content was again determined with the BCA assay (Pierce™ BCA Protein Assay Kit). 60 µg of proteins were precipitated overnight at 4°C with trichloroacetic acid (TCA) 20%. The pellet was washed with cold acetone and dried. The pellet was resuspended in 50 mM TEAB and digested overnight at 37°C with trypsin (Pierce™ Trypsin Protease, MS Grade). The digested samples were directly used for TMT-labelling preparation. The TMT-labelling was performed by following the TMTsixplex Label Reagent Set, and the fractionation in 6 fractions was performed with the Pierce High pH Reversed-Phase Peptide Fractionation Kit. Resulting MS/MS data were processed using Sequest HT search engine within Proteome Discoverer 2.5 against a *Chlamydomonas reinhardtii* reference target-decoy database obtained from Uniprot (18 828 forward entries). Trypsin was specified as the cleavage enzyme, allowing up to 2 missed cleavages, 4 modifications per peptide, and up to 3 charges. Mass error was set to 10 ppm for precursor ions and 0.1 Da for fragment ions, and considered dynamic modifications were +15.99 Da for oxidized methionine and +42.011 Da for acetylation of the protein N-term. Fixed modifications were TMT(+229.162Da) for lysine and peptide N-termini and +57.00 for carbamidomethyl cysteine. The false discovery rate (FDR) was calculated using Percolator, and thresholds for protein, peptide, and modification sites were specified at 1%. Relative quantification was performed with the MS2 signal from TMT reporters' ions. Quan value corrections for isotopic impurities was applied and co-isolation threshold was set at 50 for MS2 data. PX Complete: The mass spectrometry proteomics data have been deposited to the ProteomeXchange Consortium (<http://proteomecentral.proteomexchange.org>) via the PRIDE partner repository (Perez-Riverol et al 2022) with the dataset identifier PXD046605 and DOI 10.6019/PXD046605.

### 4.3 Results

#### 4.3.1 The *apx2* mutants display undetectable levels of APX2

The *APX2* gene model (Cre06.g285150) as described in Phytozome (<https://phytozome-next.jgi.doe.gov/>) contains 7 exons and 6 introns, has a length of 3568 bp and codes for a protein of 337 amino acids (**Fig. 1A**). Two insertional mutants of the *APX2* gene, containing the mutagenesis cassette in exon 2 (*apx2-1*, LMJ.RY0402.180063), and exon 1 (*apx2-2*, LMJ.RY0402.095128) have been ordered from the CLiP library (**Fig. 1A**). To confirm the *APX2* gene disruption, we first checked the integration site of the cassette by amplifying the cassette junctions by PCR followed by sequencing of the amplified products (**Table S1**). We were able to map both sides for the *apx2-1* mutant and one side for the *apx2-2* mutant. Polyclonal antibodies were raised against the purified recombinant protein expressed in *E. coli*. Their sensitivity was assessed by a dilution series of the wild type (wt). For that purpose, 30 mg of wt soluble extracts were diluted by a factor two (100%, 50, 25, 12.5, 6.25, 3.125%) and the immunoblot was labelled with the APX2 antibodies. A signal corresponding to the expected size of the mature form (24 kDa, (Caccamo et al 2023)) was detected in wt soluble extracts and absent in the *apx2* mutants. The detection limit was between 12.50 and 6.25%, indicating that the level of APX2 in the *apx2* mutants was below 12.5% of that of wt (**Fig. 1B, Fig. S1A**). Since our previous work demonstrated that APX2 is chloroplast-localized and exhibits a twin arginine motif (TAT signal) for targeting to the lumen of the thylakoids (Caccamo et al 2023), chloroplast fractions of the wt and of one of the *apx2* mutants (the *apx2-1* allele) were isolated and analysed on immunoblot (**Fig 1C, Fig. S1B**). The 24 kDa band was not detected in the chloroplasts of the *apx2-1* mutant while it was clearly visible in the chloroplast fraction of wt.

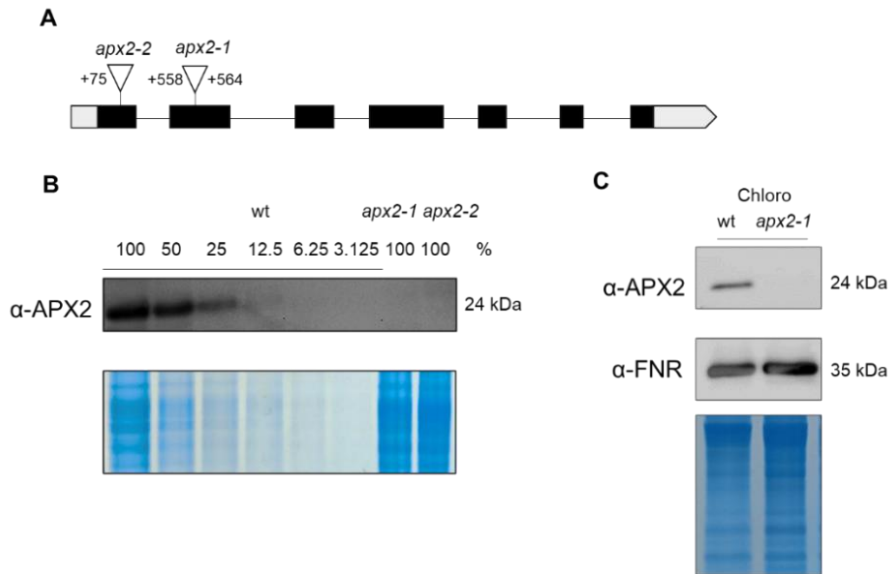


**Figure 1: Mutants of APX2 exhibit levels of the APX2 protein that are beyond detection.**

**A)** Scheme of the *APX2* gene (Cre06.g285150) and position of the paromomycin cassette in the *apx2-1* and *apx2-2* mutants. The numbers indicate the position of the cassette from the ATG start codon. Grey blocks are the 5' UTR and the 3' UTR, black blocks the exons. **B)** Immunoblot using soluble protein extracts with a serial dilution of a factor two for wt (100% is 30  $\mu$ g of loaded extracts, 50% is 15  $\mu$ g, 25% is 7.5  $\mu$ g, 12.5% is 3.25  $\mu$ g, 6.25% is 1.625  $\mu$ g and 3.125% is 0.8125  $\mu$ g) and the two *apx2* mutants (100% with 30  $\mu$ g) labelled with antibodies against APX2. The Coomassie staining of the gel is shown as control of loading. **C)** Immunoblot using chloroplast fractions (15  $\mu$ g per lane) from wt and the *apx2-1* mutant labelled with antibodies against APX2 and FNR (Ferredoxin-NADP reductase) (shown as loading control) together with the Coomassie staining of the gel.

#### 4.3.2 Mutants lacking APX2 do not exhibit a decrease in growth rate or PSII photosynthetic activity

To evaluate the impact of the loss of APX2 on the physiology of *Chlamydomonas*, the growth rates of the *apx2* mutants were determined in phototrophy (minimal medium, low light intensity) and mixotrophy (acetate as organic carbon source, low light intensity). The growth rates of the mutants were similar to those of wt cells except for a minor difference for the *apx2-2* mutant in mixotrophy (**Table 1**). These results suggest that the loss of APX2 is not responsible for physiological modifications that affect growth in low light conditions.

**Table 1.** The growth rate of both wt and *apx2* mutants is comparable. Doubling time (h) of wt and *apx2* mutant cells grown under low light (30  $\mu\text{mol photons m}^{-2} \text{s}^{-1}$ ) in phototrophy and mixotrophy is shown. Values are means of six independent biological replicates with standard deviations. ANOVA One-Way, Dunnett's Test, \* equals  $p < 0.05$ , nothing equals  $p > 0.05$ , relative to the wt.

Cells	Phototrophy	Mixotrophy
	Low light	Low light
wt	37 $\pm$ 4	8 $\pm$ 1
<i>apx2-1</i>	38 $\pm$ 5	9 $\pm$ 1
<i>apx2-2</i>	34 $\pm$ 4	7 $\pm$ 1*

Next, we evaluated the photosynthetic activity of PSII. To maximise the use of photosynthesis, the cells were grown in phototrophy conditions. Under these cultivation conditions, the maximum efficiency of PSII was not affected, except for a small decrease (-8%) for the *apx2-2* mutant (**Fig. 2A**). The initial phases (O to J, **Fig. 2B**) of the rapid rise in chlorophyll *a* fluorescence in PSII, associated with photochemistry (Kitajima & Butler 1975), showed similar trends. Additionally, the relative electron transport rate (rETR) of PSII remained unaffected at low light intensities (**Fig. 2C**). All these results indicated that the PSII activity in low light is barely affected in the *apx2* mutants, aligning with the calculated growth rates (**Table 1**).

Nevertheless, the decline in rETR of PSII in high light conditions (*i.e.* beyond 100  $\mu\text{mol photons m}^{-2} \text{s}^{-1}$ , **Fig. 2C**) was observed in the *apx2* mutants. Besides,



the faster increase in the J to I phase during the analysis of the rapid rise in chlorophyll *a* fluorescence suggested a donor side limitation of PSI (Zivcak et al 2015) (**Fig. 2D**). Lastly, the ratio between the active PSI and PSII centers (PSI/PSII) was lower in the mutants, indicating a potential deficiency of PSI (**Fig. 2E**).

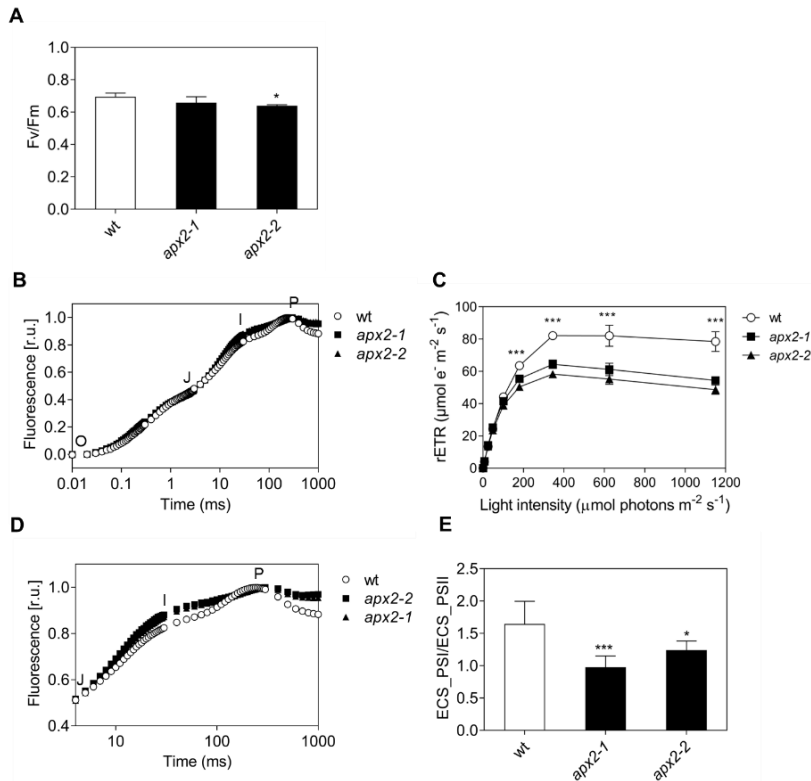


**Figure 2: *apx2* mutants display no defect in PSII activity but in electron transfer around PSI when grown in phototrophic conditions with low light.** **A**) Maximum quantum yield of PSII (Fv/Fm) measured after 1 min of dark incubation (n=6). **B**) Fast chlorophyll *a* fluorescence increase was measured during 1 s of saturating light after 1 min of dark cell incubation. (r.u.: relative unit normalised to maximum fluorescence value and the fluorescence value at 20 ms) (n=6). **C**) Light-response curve of photosynthetic relative electron transfer rate (rETR) at increasing light intensities with measurements of 30 s per each light step (n=3). **D**) Zoom on the JIP phase of the fast chlorophyll *a* fluorescence increase. The faster increase of the J to I phase of the *apx2* mutants indicates a limitation on the PSI donor side. **E**) Ratio between active PSI and PSII centers calculated from ECS measurements in presence of PSII inhibitors (n=9). Values are means with standard deviations calculated with ANOVA-OneWay, Dunnett's Test, \*\*\* equals  $p < 0.001$ , \* equals  $p < 0.05$ , nothing equals  $p > 0.05$ , relative to wt, for panels A, C and E.

#### 4.3.3 Reduced levels of plastocyanin in *apx2* mutants lead to rapid oxidation of P700

To further investigate PSI activity, we monitored P700 oxidation during one second of saturating light (**Fig. 3A**). *apx2* mutants exhibited a more oxidized P700 redox state, during the first 100 ms of the saturating light intensity, indicating a donor side limitation of PSI. To determine the underlying cause of the observed effect in the mutant cells, we conducted a single-turnover-flash experiment to induce a single charge separation of one electron from P700. It is worth mentioning that the electron transfer between plastocyanin and P700<sup>+</sup> occurs rapidly, with time constants of approximately 1-3  $\mu$ s (Drepper et al 1996). Considering this fast electron transfer, the first detection in the P700 monitoring system (200  $\mu$ s after the single-turnover-flash) could not detect the oxidised state in the wt (**Fig. 3B**), but it was surprising to see that *apx2* mutant cells retained the oxidised state for a longer period with a constant time for P700<sup>+</sup> re-reduction of approximately 1 ms (50% of P700<sup>+</sup> re-reduced). Such a difference suggested an impairment at the donor side of PSI.

To assess the size of the PSI electron donor pool (*i.e.* mainly plastocyanin), the P700 redox state in the presence of PSII and Cyt *b<sub>6</sub>f* was monitored *in vivo* in response to a train of ten consecutive single-turnover-flashes. In wt, the oxidation level of P700 was increased with consecutive flashes, indicating a progressive withdrawal of electrons from the plastocyanin pool to PSI. The maximum P700 oxidation level was obtained after seven flashes. In contrast, *apx2* mutant cells required only two flashes to reach the maximum P700 oxidation level (**Fig. 3C**). This result suggests a significant reduction in the size of the plastocyanin pool in the absence of APX2. Spectrophotometric analysis of plastocyanin on soluble protein extracts demonstrated a substantial decrease in plastocyanin abundance in the *apx2* mutants compared to wt cells (**Fig. 3D**). The lower abundance was further confirmed by immunoblots labelled with plastocyanin antibodies, showing that the quantity of plastocyanin in the *apx2* mutants is less than 10% of that in wt cells (**Fig. 3E, Fig. S1C**). In contrast, the molar stoichiometry of Cyt *f*<sup>+</sup> to P700<sup>+</sup> remained consistent between wt and the *apx2* mutants (**Fig. 3F**) as well as the level of Cyt *f*, as indicated by immunoblot analysis (**Fig. 3E**).

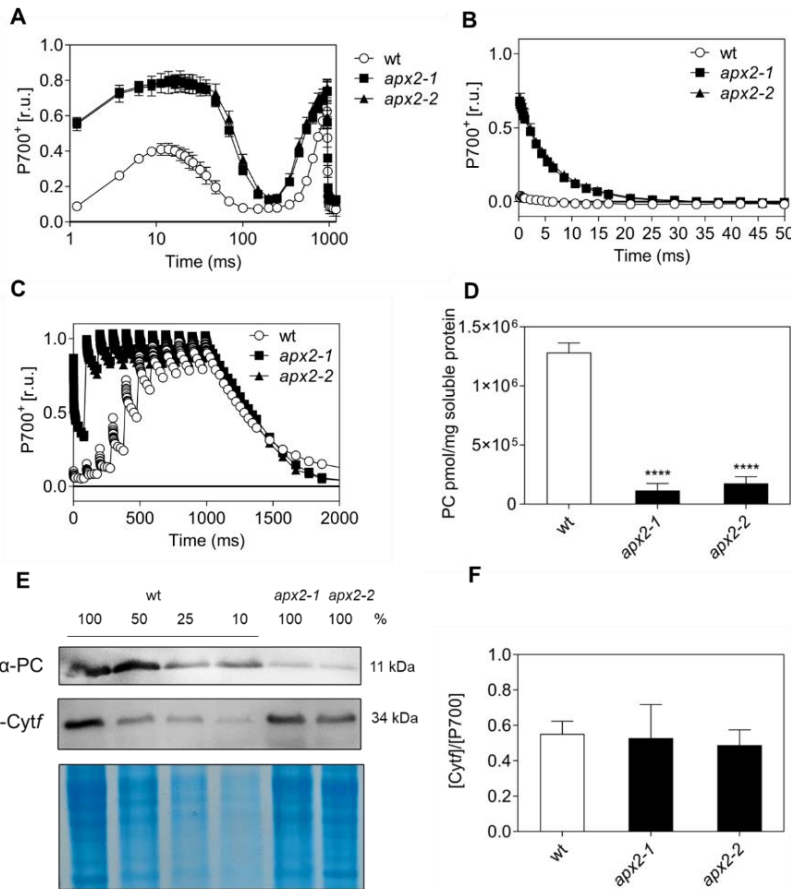


**Figure 3: The electron transfer to P700 was impaired in the *apx2* mutant cells, accompanied by a reduced level of plastocyanin.** **A**) P700 redox kinetics measured during 1 s of saturating light after 1 min of dark incubation. Values are normalised to maximum oxidisable P700 in presence of DCMU and DBMIB, inhibitors of PSII and Cyt *b<sub>6</sub>f* respectively (n=3). **B**) Monitoring of P700 redox state upon a single-turnover-flash on wt and *apx2* mutants (values normalised to the maximum oxidisable value of P700) (n=3). **C**) Monitoring of P700 redox state during a train of ten single-turnover-flashes (every 100 ms) in wt and *apx2* mutants previously incubated in PSII and Cyt *b<sub>6</sub>f* inhibitors (values normalised to the maximum oxidisable value of P700 after adding 10  $\mu$ M DCMU and 10  $\mu$ M DBMIB inhibitors of PSII and Cyt *b<sub>6</sub>f* respectively) (n=3). **D**) Plastocyanin (PC) intracellular level in wt and *apx2* mutants measured with spectroscopic analyses (n=3). **E**) Immunoblot with a serial dilution for wt (100% is 30  $\mu$ g of loaded extracts, 50% is 15  $\mu$ g, 25% is 7.5  $\mu$ g, 10% is 3  $\mu$ g) labelled with antibodies against plastocyanin (PC) and Cyt*f*. Coomassie blue stained gel with the same loadings is shown as control. **F**) Ratio between [Cyt*f*] and [P700] (changes in absorption values calculated considering the respective molar extinction coefficient of 18 mM<sup>-1</sup> cm<sup>-1</sup> at 554 nm for Cyt*f* and of 50 mM<sup>-1</sup> cm<sup>-1</sup> at 705 nm for P700) (n=4). ANOVA-TwoWay, Dunnett's Test indicated by \*\*\*\* equals p<0.0001, ns or nothing equals p>0.05, relative to wt, for panels D and F.

#### 4.3.4 Proteomic analyses of the *apx2-1* mutant validate the reduced abundance of plastocyanin, and uncover deficiencies in PSI subunits, as well as copper-related enzymes

Since plastocyanin represents the major sink of copper in *Chlamydomonas* in phototrophic conditions (Kropat et al 2015), we wanted to investigate the whole proteome to identify any variation of copper-related proteins. For this reason, tandem-mass-tag (TMT) labelling (Zecha et al 2019) was used to semi-quantitatively analyse the whole cell proteome of *Chlamydomonas* in phototrophy for the wt and the *apx2-1* mutant only, since the two *apx2* mutants showed the same phenotype. With this technique we could identify and quantify 2502 and 2255 proteins, respectively (**Dataset 1**, [Dataset 1 final.xlsx](#)). Variations in abundance were considered significant when there was an increase or a decrease of 30% compared to the wt, with an adjusted p-value < 0.05 ( $\log_2$  fold change  $\geq 0.37$  and  $\leq -0.5$ ) (**Dataset 1**, **Fig. 4A**). Twenty-one proteins were found significantly decreased, and 42 were significantly increased. As expected, there was a notable decrease in the quantity of plastocyanin ( $\log_2$  fold change - 1.4). We successfully identified six subunits of PSI, six subunits of cytochrome *b<sub>6</sub>f*, and nine subunits of PSII (**Dataset 1**). No significant differences were observed for these proteins except for some subunits of PSI. Indeed, four PSI core subunits (*i.e.* PsaB, PsaD, PsaF, PsaL) exhibited a significant decrease in abundance. These findings were validated through immunoblot analysis using antibodies specifically targeting PsaF and PsaD subunits (**Fig. 4B**, **Fig. S1D**). These results support the finding of a reduced PSI/PSII ratio and the absence of any PSII defects (**Fig. 2**) in these *apx2* mutants.

Regarding other copper-related proteins beyond plastocyanin, we did observe a significant difference in abundance for two of them, the ferroxidase-like 1 (FOX1) and a cupredoxin multicopper enzyme (Cre12.g537250). FOX1, reported as a multicopper periplasmic oxidase involved in iron uptake (Terzulli & Kosman 2010), showed a  $\log_2$  fold change of -0.7 in absence of APX2 whereas Cre12.g537250 was found to be more abundant in *apx2-1* mutant cells ( $\log_2$  fold change 1.3) (**Fig. 4A**, **Dataset 1**). The higher abundance of this enzyme in the *apx2-1* mutant might suggest a function as a copper storage. However, no information is available about Cre12.g537250 and its localisation, and the hypothesis on its function in this context, remains speculative. The reduction in FOX1 protein was verified through immunoblot analysis for the two *apx2*

mutants (**Fig. 4C, Fig. S1E**). On the contrary, there was no observed alteration in protein levels of several other copper proteins: copper transport CTR1 and CTR3, copper chaperone ATX1 and one of the copper-binding subunits of the mitochondrial cytochrome *c* oxidase (COX2B) (**Fig. 4A, Dataset 1**). Altogether, these findings suggest that the pattern of copper metabolism could be modified in the mutants, although not to a significant extend.

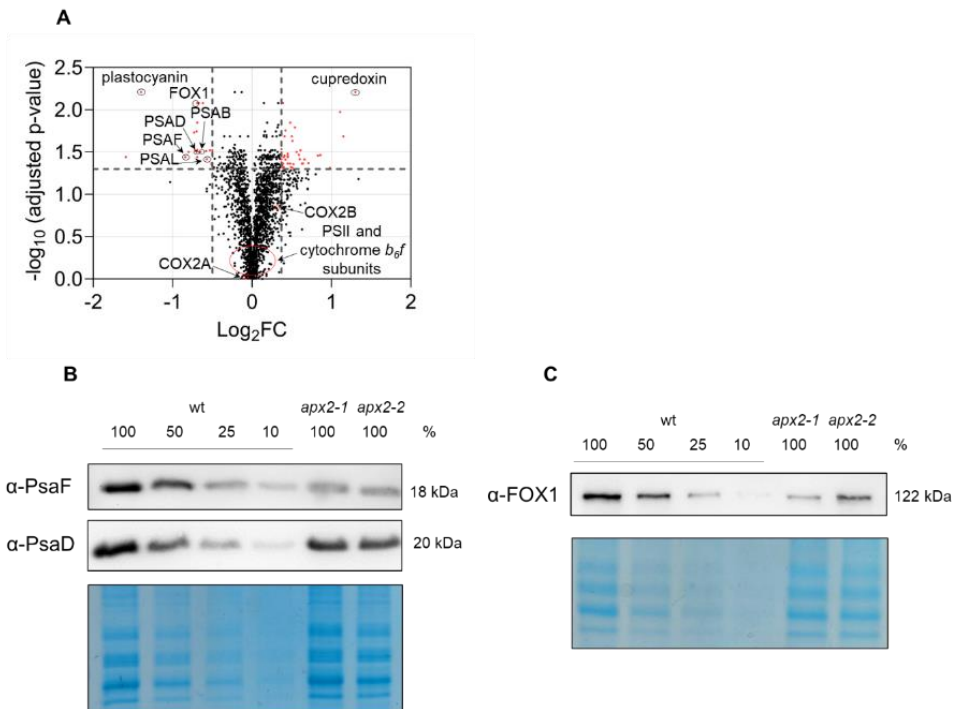


**Figure 4: Comparative proteomic analysis reveals variations in protein levels in the *apx2-1* mutant which are confirmed by immunoblot in both mutants. A)** Volcano plots of the proteomic data. Red dots indicate significantly different proteins in the *apx2-1* mutant compared to wt ( $\log_2$  fold change  $> 0.37$  and  $< -0.5$ ). Black dots indicate the non-significant proteins. In the plot plastocyanin, PSI subunits (PSAB, PSAD, PSAF, PSAL), copper-enzymes (FOX1, cupredoxin), and subunits of the cytochrome *c* oxidase (COX2A, COX2B) are indicated. The PSII and cytochrome *b<sub>6</sub>f* subunits are shown in the non-significant portion of the plot. **B)** Immunoblot with a serial dilution for wt (100% is 30  $\mu\text{g}$  of loaded extracts, 50% is 15  $\mu\text{g}$ , 25% is 7.5  $\mu\text{g}$ , 10% is 3  $\mu\text{g}$ ) labelled with antibodies against PSAF and PSAD. Coomassie blue stained gel with the same loadings is shown as control. **C).** Immunoblot with a serial dilution for wt (100% is 30  $\mu\text{g}$  of loaded extracts, 50% is 15  $\mu\text{g}$ , 25% is 7.5  $\mu\text{g}$ , 10% is 5  $\mu\text{g}$ ) labelled with antibodies against ferroxidase-like 1 (FOX1). Coomassie blue stained gel with the same loadings is shown as control.

#### 4.3.5 *Copper deficiency induces a similar response in wild type and apx2 mutants*

To investigate the impact of *APX2* gene disruption at the level of the PSI electron donor, we evaluated the functional replacement of plastocyanin by cytochrome *c*<sub>6</sub> induced by copper-deficiency (Li & Merchant 1995). Previously, it has been demonstrated that *Chlamydomonas* cells utilise cytochrome *c*<sub>6</sub> (Cre16.g651050) as PSI electron donor below concentrations of 20 nM of copper in the culture medium (Hill & Merchant 1992). Therefore, cells were grown under phototrophic conditions in the presence of 1 nM CuSO<sub>4</sub>. We observed that after ten days of copper-deficiency, cytochrome *c*<sub>6</sub> took over the role of plastocyanin, as evidenced by the quantification of its characteristic absorption peak at 552 nm in soluble protein extracts (**Fig. 5A**) and confirmed by immunodetection using antibodies specific to cytochrome *c*<sub>6</sub> (**Fig. 5B**, **Fig. S1F**). Interestingly, under these conditions, the oxidation level of P700 induced by a series of ten consecutive single-turnover flashes, displayed identical kinetics in both the wt and *apx2* mutant cells (**Fig. 5C**). Additionally, we do not observe any changes in the P700 kinetics between wt and *apx2* mutants (**Fig. 5D**). These observations suggest that the pool of electron donors to PSI becomes comparable between the mutant and the wt cells when copper concentrations are limited. In addition, even if variations in the rETR are observed (**Fig. 5E**), they are very small (between 7 and 14%) indicating that PSII activity is restored even upon high light intensities, contrary to what is observed in the presence of copper (**Fig. 2C**). We concluded that the absence of *APX2* adversely affects plastocyanin, without compromising the ability to substitute plastocyanin with cytochrome *c*<sub>6</sub> during copper deficiency.

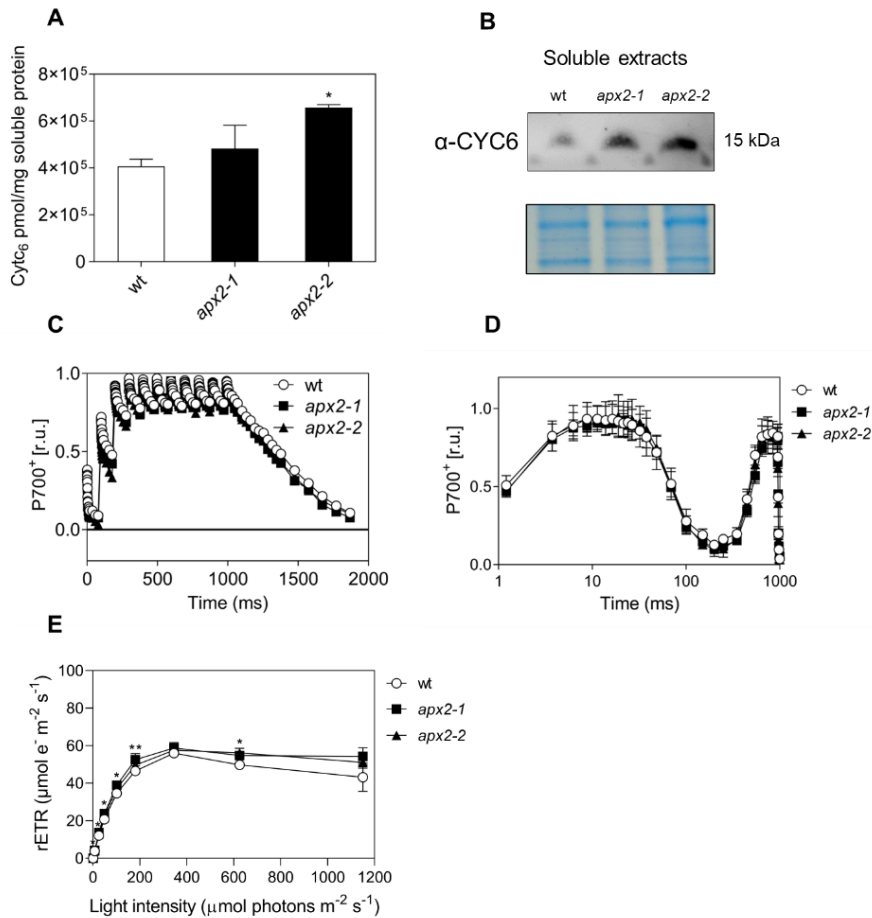


**Figure 5: Induction of cytochrome *c*<sub>6</sub> under copper-deficiency restores a wt phenotype in *apx2* mutants.** **A**) Cytochrome *c*<sub>6</sub> (Cyt*c*<sub>6</sub>) intracellular level in wt and *apx2* mutants measured with spectroscopic analyses (n=3). **B**) Immunoblot labelled with cytochrome *c*<sub>6</sub> (CYC6) antibodies of soluble extracts (10 μg per lane) separated by Tricine gel in presence of 1 nM CuSO<sub>4</sub>. The lower panel shows a gel stained with Coomassie blue for loading control. **C**) wt and *apx2* mutant cells exposed to copper deficiency were subjected to a train of ten consecutive single-turnover-flashes (n=3). **D**) P700 redox kinetics measured during 1 s of saturating light after 1 min of dark incubation. Values are normalised to maximum oxidisable P700 in presence of DCMU and DBMIB, inhibitors of PSII and Cyt *b*<sub>6</sub>*f* respectively (n=3). **E**) Light-response curve of photosynthetic relative electron transfer rate (rETR) at increasing light intensities with measurements of 30 s per each light step (n=3). Significant differences between *apx2-1* and wt are present for several light steps: 7 μmol photons m<sup>-2</sup> s<sup>-1</sup>: +9%; 25 μmol photons m<sup>-2</sup> s<sup>-1</sup>: +13%; 48 μmol photons m<sup>-2</sup> s<sup>-1</sup>: +14%; 101 μmol photons m<sup>-2</sup> s<sup>-1</sup>: +12%; *apx2-2* and wt at 101 μmol photons m<sup>-2</sup> s<sup>-1</sup>: +7%; 180 μmol photons m<sup>-2</sup> s<sup>-1</sup>: +7% and 625 μmol photons m<sup>-2</sup> s<sup>-1</sup>: +13%. Values are means with standard deviations calculated with ANOVA-OneWay, Dunnett's Test indicated by \*\* equals p<0.01, \* equals p<0.05, nothing equals p>0.05, relative to wt, for panels A and E.

#### 4.3.6 Transcriptomics analyses reveal post-transcriptional regulation in copper replete conditions and no modification of the CRR1 targets in copper deficient conditions

From the results above, it can be concluded that the main differences between wt and *apx2* mutants are present in copper replete and not in copper-deficient conditions. To further understand the cellular regulation, a transcriptomics study was undertaken by comparing *apx2-1* and wt cells grown in phototrophy under both copper-replete (6 mM CuSO<sub>4</sub>) and copper-deficient (1 nM CuSO<sub>4</sub>) conditions. To achieve this, RNA was extracted from three biological replicates for each cultivation condition and RNA-seq data were acquired. After quality check, approximately 20 million reads could be uniquely mapped, indicating the high quality of the libraries (**Dataset 2**, [Dataset 2\\_final.xlsx](#)). The generated raw data are available under the project number PRJNA994826.

Differentially expressed genes (DEGs) [adjusted *p* value < 0.05 and log<sub>2</sub> fold change > or <1] were identified in wt and *apx2-1* with standard copper concentration (6 μM) (wt-*apx2*), and wt (wt- wt [1 nM Cu]) and *apx2-1* (*apx2-1* [*apx2-1* [1 nM Cu)]) in copper deficient conditions (**Dataset 2**). **Fig. S2A** presents a heat map of the most up-regulated and the most down-regulated genes in each comparison. Many of these genes encode uncharacterized proteins. Regarding the comparison between wt and *apx2-1* in copper replete conditions (wt-*apx2*), the transcripts encoding the proteins with altered abundance (plastocyanin, PSAD, PSAF, PSAL, FOX1, cupredoxin, **Fig. 4A**) are not differentially expressed, suggesting that the regulation occurs at the post-transcriptional level (**Fig. 6A**).

In copper deficient conditions, both the wt (wt- wt [1 nM Cu]) and the *apx2-1* mutant (*apx2-1* [*apx2-1* [1 nM Cu)]) display higher abundance of some transcripts governed by the CRR1 transcription factor (copper response regulator 1, Cre09.g390023), such as Cyt *c*<sub>6</sub> and FDX5 encoding ferredoxin 5 (**Fig. S2A**). This prompted us to look at the abundance of the 58 target genes of CRR1 (Kropat et al 2015). Out of these targets, one gene was excluded from our analysis (Cre07.g346900) due to insufficient mapped reads. The remaining 57 genes showed consistent differential expression in both strains. However, for some of them, the log<sub>2</sub> fold change was not significant, in contrast to previous observations by Kropat *et al.* (Kropat et al 2015). This discrepancy is likely attributed to variations in growth conditions used in the two studies (**Fig. 6B**). In



conclusion, even though there are differences between wt and *apx2* mutants in copper deficient conditions, they seem not linked to the CRR1 targets and will be complicated to interpret due to the absence of phenotype in these conditions.

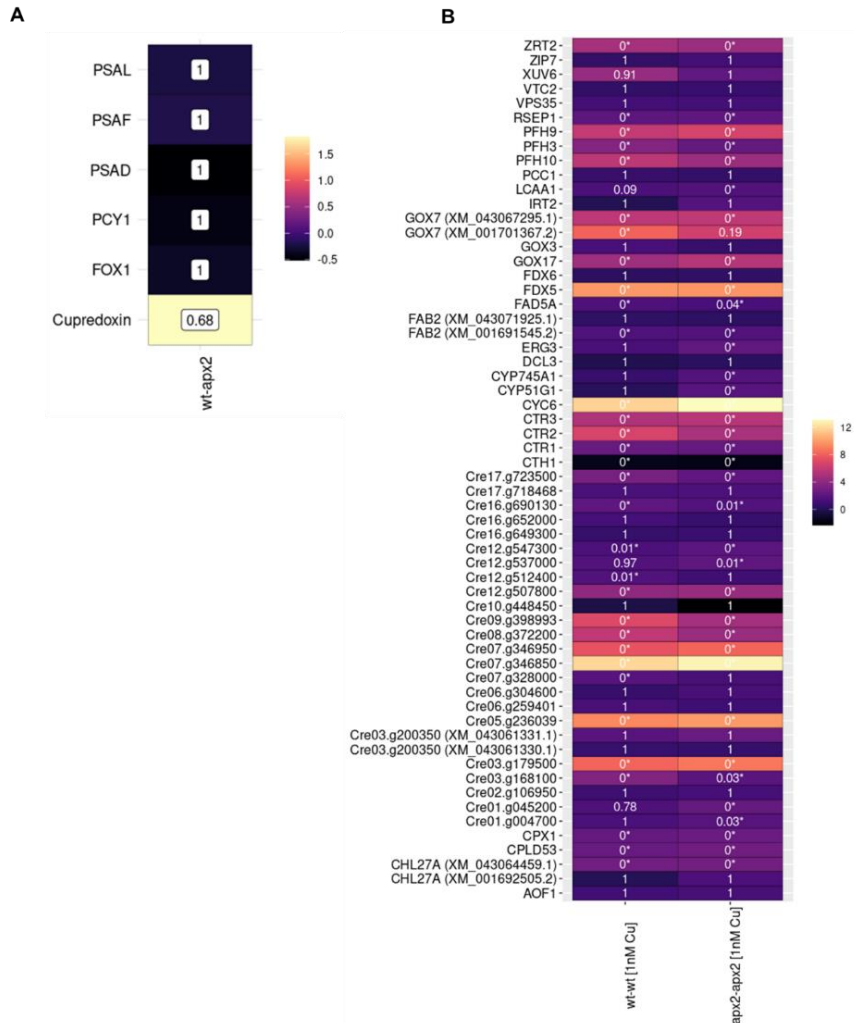


**Figure 6: Transcriptomics analyses reveal post-transcriptional differences between wt and the *apx2-1* mutant in copper replete conditions and similar response to CRR1 master regulator in copper deficient conditions. A) Expression of *PCY1*, *PsaF*, *PsaD*, *PsaL*, *FOX1* and *cupredoxin* is not significantly different between wt and *apx2-1* mutant. The colour code at the right shows the difference in  $\log_2$  fold change. The adjusted p-value is shown in the boxes corresponding to each comparison. B) Comparison between wt and *apx2-1* mutant in response to copper deficient conditions. The colour code at the right shows the difference in  $\log_2$  fold change. The adjusted p-value is shown in the boxes corresponding to each comparison with significantly differential expressed genes indicated with asterisks.**

#### 4.4 Discussion

APX-R enzymes form a recently identified class within the ascorbate peroxidase family, present in the eukaryotic green lineage (Lazzarotto et al., 2015). Previous studies on loss-of-function mutant lines in *Arabidopsis* have suggested that the APX-R enzyme plays a role during stress periods, such as seed maturation, germination, and leaf senescence (Chen et al 2021, Chen et al 2014), although the precise underlying mechanisms remain unknown. Despite the chloroplast localization of APX-R, no interaction with the photosynthetic machinery has been explored in any photosynthetic organism.

Our previous *in vitro* work demonstrated that recombinant APX2 binds copper and that copper-loaded APX2 interferes with the copper binding capabilities of plastocyanin (Caccamo et al 2023). The detailed photosynthetic analysis performed in this study reveals that the main defect of the *apx2* mutants is a significant reduction of plastocyanin levels. Therefore, the relation between plastocyanin and APX2 is confirmed *in vivo* in *Chlamydomonas*.

Despite the diminished plastocyanin content relative to PSI in the *apx2* mutants, the photosynthetic electron transport can still take place. However, two effects were observed: one showing that light acclimated cells are able to perform photosynthetic electron transfer at 80% of the wt rate, and another one showing that dark acclimated cells have a longer re-reduction rate of P700<sup>+</sup> (ca. 1 ms) in comparison to the wt (3 μs) (Hippler et al 1997). Plastocyanin has been shown to be the long-range electron carrier, which diffusion influences the photosynthetic electron transfer rate. Evidence of this was provided by a mutant lacking the curvature thylakoid 1 protein (CURT1) in *Arabidopsis* (Hohner et al 2020). The loss of this protein causes an increase of the grana diameter, which in turn affects the diffusion of plastocyanin between Cyt *b<sub>6</sub>f* and PSI and decrease of 20% the electron flow of the wt. However, this does not affect PSII activity or lateral diffusion of PSII and Cyt *b<sub>6</sub>f* in the thylakoid domains. In our study, we proved that this efficiency is also affected by the relative abundance of plastocyanin to PSI in *Chlamydomonas*. The lower plastocyanin content in *apx2* might reflect a related phenomenon, with longer periods of time to carry out oxidation of Cyt *f* at cytochrome *b<sub>6</sub>f*, and reduction of P700<sup>+</sup> at PSI. This has been shown to be one of the limiting steps of the photosynthetic electron transfer (Drepper et al 1996). Light acclimation has a remarkable effect on the thylakoid structure (Broderson et al 2024, Cruz et al 2001, Farci & Schröder 2023) which

may contribute to improve the diffusion of soluble components of the thylakoid lumen, including plastocyanin (Li et al 2020). This effect might contribute to the comparable electron transfer rates between *apx2* mutant (80%) in comparison to the wt. In plants, such as Arabidopsis, it has been observed a similar effect. In Arabidopsis, there are two genes encoding plastocyanin, *PETE1* and *PETE2* (Abdel-Ghany 2009). *PETE2* is the predominant isoform, *PETE1* is less abundant and substitutes *PETE2* in copper deficient conditions (Abdel-Ghany 2009). Mutants of *pete1* and *pete2* exhibit reduced plastocyanin content, and null *pete2* mutants, with 90% reduction of the plastocyanin content, only show slight effect on growth and photosynthesis (Pesaresi et al 2009). Double mutants are not viable (Weigel et al 2003). Consequently, plastocyanin is not limiting under optimal growth conditions, being growing in day/night cycles, suggesting another role for the protein that remains to be deciphered (Pesaresi et al 2009). Similarly, based on the spectroscopic and immunoblot analyses, the results presented here, show that plastocyanin levels can be reduced to less than 10% without any significant impact on the physiology under low light growth conditions in *Chlamydomonas*. Hence, a similar question about an alternative role for plastocyanin in *Chlamydomonas* may rise, as in Arabidopsis. The low content of plastocyanin in *apx2* mutant raises the question of its association to PSI. In *Chlamydomonas* cells grown in mixotrophic conditions the stoichiometric abundance of plastocyanin and PSI has been reported to be 1:1 (Hippler et al 1997, Nikolova et al 2018). This could explain why in presence of DCMU and DBMIB inhibitors, P700<sup>+</sup> accumulates faster in the *apx2* mutants. However, a question about the preservation of the 1:1 stoichiometry between plastocyanin and PSI in different cultivation conditions (minimal medium vs acetate medium) has not been addressed and may differ. On the contrary, in tobacco plants the stoichiometry of plastocyanin to PSI is 3-4:1 (Burkey et al 1996), even though the photosynthetic efficiency between plants and algae is comparable. In addition, a *Chlamydomonas* mutant lacking the PsaF subunit of PSI, responsible for plastocyanin interaction, it has shown the inability to bind plastocyanin to PSI in the dark, consequently P700 remained largely oxidized upon a light flash (Finazzi et al 2005). This suggests that the prebound of plastocyanin to PSI in the dark in *apx2* mutant, might also be modified either by its low abundance at sub-stoichiometric values of PSI, and by the lower abundance of PsaF subunit, increasing in turn the half-life of PSI turnover.

The capacity of the *apx2* mutants to maintain similar growth rate as the wt, might be also compensated by the increased protein level observed in *apx2-1* of phosphoribulokinase (PRK1, log<sub>2</sub> fold change 0.41, **Table S4**) and sedoheptulose-1,7-bisphosphatase (SEBP1, log<sub>2</sub> fold change 0.5, **Table S4**), involved in the Calvin-Benson-Bassham (CBB) cycle (Brandes et al 1996, Liu et al 2012). Moreover, the thioredoxin f1 (TRXf1, log<sub>2</sub> fold change 0.42, **Table S4**), involved in ferredoxin-thioredoxin (Fd-TRX) system regulating the CBB cycle (Nikkanen et al 2016) interacting with PRK1 (Brandes et al 1996), is also highly abundant in *apx2-1*. Further, peroxiredoxin Q (PRX6, log<sub>2</sub> fold change 1.11, **Table S4**) involved in H<sub>2</sub>O<sub>2</sub> scavenging and PSII protection (Petersson et al 2006, Telman et al 2020) was also found at a higher level. In Arabidopsis this enzyme was shown to reside in the thylakoid membrane (Lamkemeyer et al 2006) or even in the lumen (Petersson et al 2006). However, a recent study proved that luminal localization is unlikely or concerns a minor fraction (Telman et al 2020). Thus, in the *apx2-1* mutant, PRX6 might help to maintain the redox balance in the chloroplast for cell growth and involved in PSII photoprotection. Considering the relation between APX2 and plastocyanin and the lack of information regarding the substrate *in vivo* for APX2, one hypothesis could be that the electron carrier might function as substrate for APX2. Another possibility could be the presence of electron transfer between the copper of plastocyanin and the iron of APX2. Another hypothesis might be related to the involvement of the APX2 protein in controlling plastocyanin level by promoting its degradation. A potential protease candidate, RSEP1, has been recognized as regulated by the copper response regulator 1 (CRR1) during copper deficiency (Castruita et al 2011, Kropat et al 2015). However, the precise mechanism remains unclear. Alternatively, APX2 may play a role in the degradation of plastocyanin under copper conditions where copper relocation is necessary, such as in mitochondria, especially in specific conditions like darkness (Kropat et al 2015). The absence of APX2 and the lower level of plastocyanin in *apx2* mutants, might influence intracellular copper distribution. One possibility could be that copper is stored in another compartment, like the cytosol, where a cupredoxin protein (Cre12.g537250) is putatively localized. Higher levels of this protein have been found in the *apx2-1* mutant. Cupredoxins are proteins which present several copper-binding sites like the ferredoxin-like 1 (FOX1) (Terzulli & Kosman 2010). Unfortunately, as for now, no information regarding this specific protein

(Cre12.g537250) is available. Most probable, the lower abundance of FOX1 in the *apx2-1* mutant, indicates that copper might be necessary in other pathways, considering that the iron uptake by *Chlamydomonas* cells can be exerted by other proteins like IRT1 and IRT2, encoding ZIP-family iron transporters (Chen et al 2008). However, further experiments are necessary to validate these hypotheses. Apart from *Arabidopsis*, other land plants such as poplar, parsley, tobacco, rice, and the moss *Physcomitrella patens* express two plastocyanin isoforms (as described in (Pesaresi et al 2009)). In contrast, green algae and cyanobacteria, such as *Chlamydomonas* and *Synechocystis*, respectively, possess only one plastocyanin gene (Briggs et al 1990, Merchant & Bogorad 1987, Pesaresi et al 2009). This raises the question of whether APX-R (APX6) of *Arabidopsis* would have a similar impact on plastocyanin levels.

The TAT signal motif consists of a twin arginine (RR) followed by a hydrophobic stretch and an AxA cleavage site (Cline 2015). When comparing *Chlamydomonas* and *Arabidopsis* APX-R sequences, the double arginine RR is present but the AxA cleavage site is not found in APX6 (**Fig. S3**). This suggests that APX6, despite being chloroplast-localized (Lazzarotto et al 2021b), might not be directed to the lumen. In addition, APX6 is transcribed in copper replete condition, while in copper deficiency, its transcription is repressed by miR398, regulated SQUAMOSA-promoter-binding protein-like 7 (SPL7), an ortholog of the copper response regulator 1 (CRR1) of *Chlamydomonas* (Chen et al 2021). In *Chlamydomonas*, the transcriptomics analysis presented here shows that APX2 is transcribed in both copper replete and copper-deficient conditions in wt (**Data set 2, Fig. S2B**). Thus, the function of the APX-R might differ between the green algae and the land plants. Nevertheless, both APX-R contain the MxxM motif, typical for metal binding (Caccamo et al 2023) (**Fig. S3**), suggesting that their dependence on copper could be conserved.

In conclusion, this study demonstrates that APX2 regulates plastocyanin levels under standard copper concentration in *Chlamydomonas*. This discovery paves the way for future experiments that could unveil the yet undiscovered mechanisms underlying the relation between APX2 and plastocyanin, and more broadly, the biogenesis of this photosynthetic component.

### *Acknowledgments*

This work was funded by Fonds de la Recherche Scientifique - the Research Foundation Flanders—Excellence of Science project no.30829584 (to C.R., J.M., D.V.) and a VIB-grant (to J.M.); A.C. acknowledges a PhD fellowship of ULiège supported by Fonds de la Recherche Scientifique Excellence of Science project no.30829584. We would like to thank Michèle Radoux for expert technical assistance, Dr. Fabrizio Iacono for helpful discussion about photosynthesis, Dr. Sara M. Esteves for the productive discussion about metal homeostasis and Gaëtan Herinckx for technical support for proteomic analysis.

### *Authors contributions*

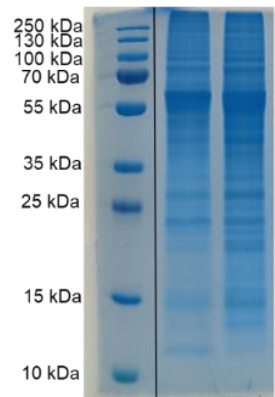
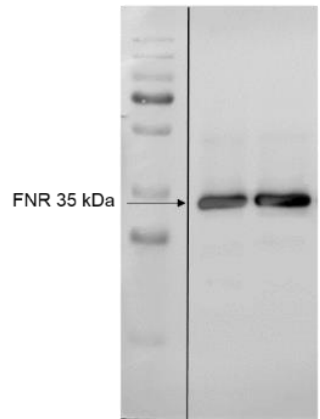
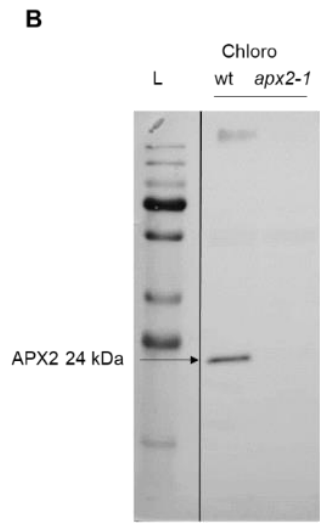
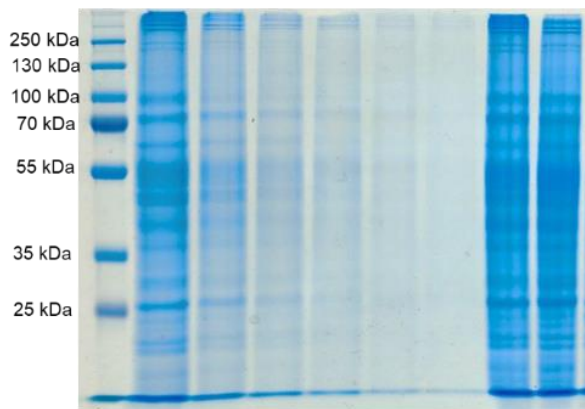
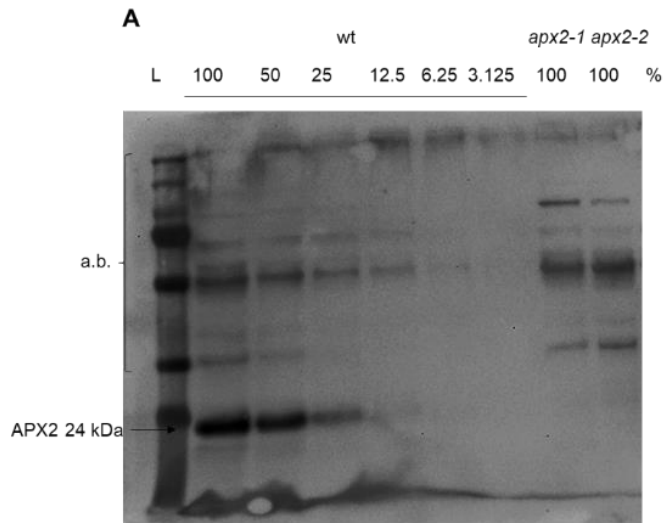
A.C., F.V.L., A.E.M., S.P.R., D.V., P.C., J.M. and C.R. designed the research, performed research and analysed data; A.C., C.R. and J.M. wrote the paper and all authors read and approved the manuscript.

*Funding:* This work was funded by the Research Foundation Flanders—Fonds de la Recherche Scientifique Excellence of Science project no.30829584 (to C.R., D.V., and J.M.) and a VIB-grant (to J.M.); A.C. acknowledges a PhD fellowship of ULiège supported by Fonds de la Recherche Scientifique Excellence of Science project no.30829584; P.C. is senior research associate from Belgian Fonds de la Recherche Scientifique-FNRS, respectively.

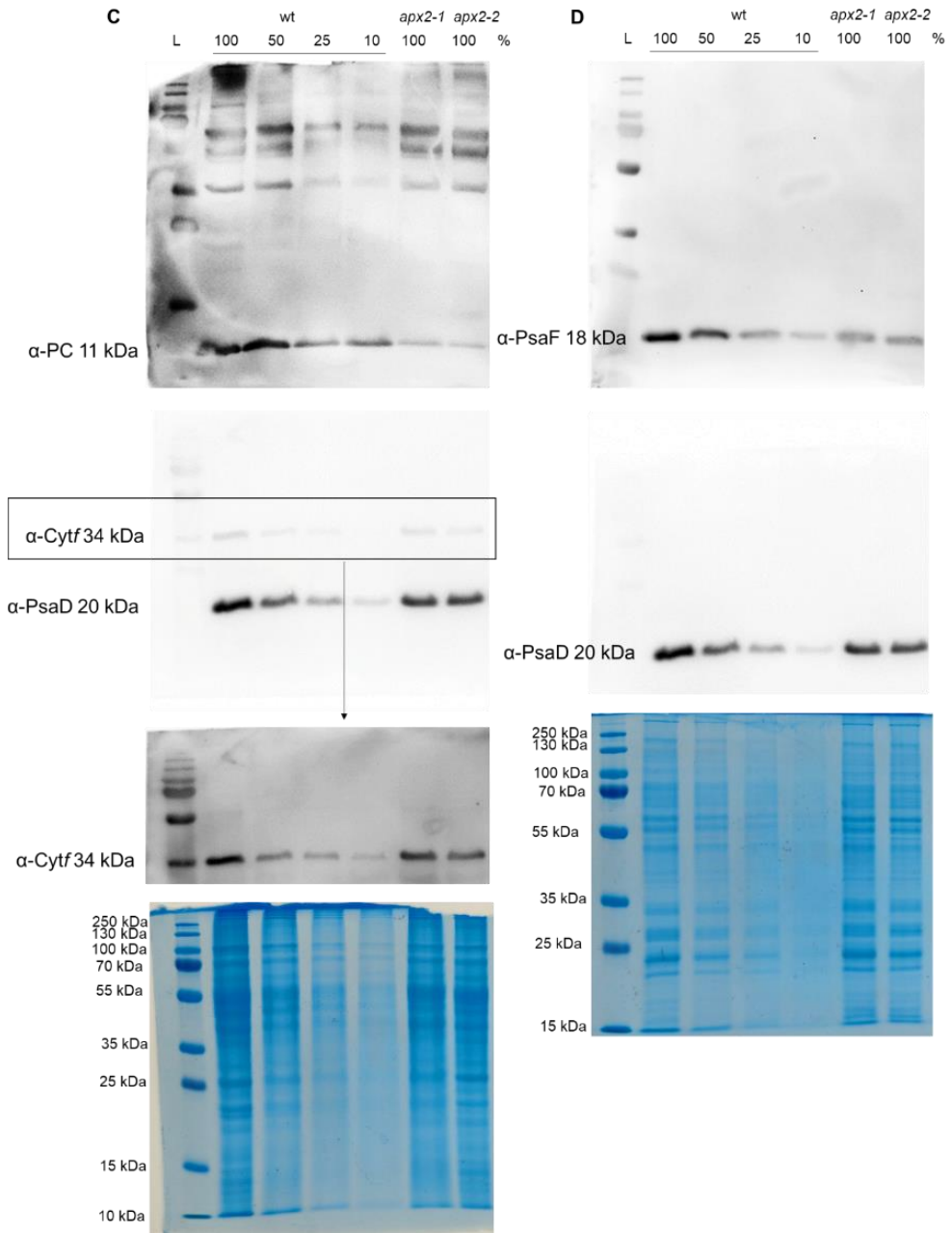
## Supplementary materials

### **Figure S1: Uncropped gel images of the immunoblots showed in Fig. 1.**

**A)** Uncropped immunoblot as shown in **Fig. 1B** depicting a serial dilution of soluble protein extracts fractions of wt compared with the *apx2-1* and *apx2-2* mutants labelled using APX2 antibodies. Coomassie blue staining of the gel serves as control of loading. The 24 kDa band corresponds to APX2. a.b. indicates unspecific bands. **B)** Uncropped immunoblot as shown in **Fig. 1C** of chloroplast fractions of wt and *apx2-1* labelled with APX2 and FNR antibodies. Coomassie blue staining of the gel serves as control of loading. The black line in each of the panels shows the separation on the blot between the ladder and the loadings of wt and *apx2-1*. **C)** Uncropped immunoblot as shown in **Fig. 3E** of serial dilution of soluble protein extracts of wt compared with the *apx2-1* and *apx2-2* mutants labelled with plastocyanin (PC) and cytochrome *f* (Cyt*f*) antibodies. Please note that the Cyt*f* immunoblot is a rehybridization after the PsaD labelling (see panel **D**). Coomassie blue staining of the gel is shown as control of loading. **D)** Uncropped immunoblot as shown in **Fig. 4B** of serial dilution of soluble protein extracts of wt compared with the *apx2-1* and *apx2-2* mutants labelled with PsaF and PsaD antibodies. Coomassie blue staining of the gel is shown as control of loading. **E)** Uncropped immunoblot as shown **Fig. 4C** of serial dilution of soluble protein extracts of wt compared with the *apx2-1* and *apx2-2* mutants labelled with multicopper ferroxidase (FOX1) antibodies. Coomassie blue staining of the gel is shown as control of loading. **F)** Uncropped immunoblot as shown in **Fig. 5B** of soluble protein extracts of wt, *apx2-1* and *apx2-2* mutants labelled with cytochrome *c*<sub>6</sub> (CYC6) antibodies. Coomassie blue staining of the gel is shown as control of loading.







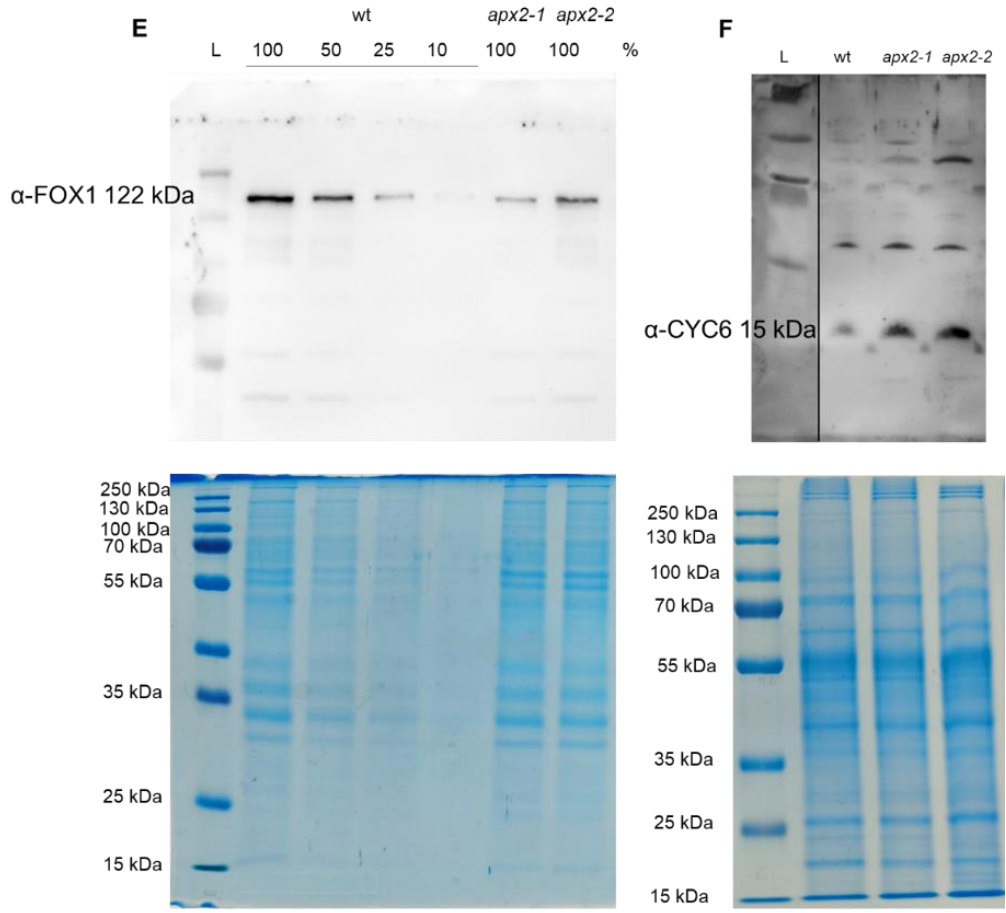
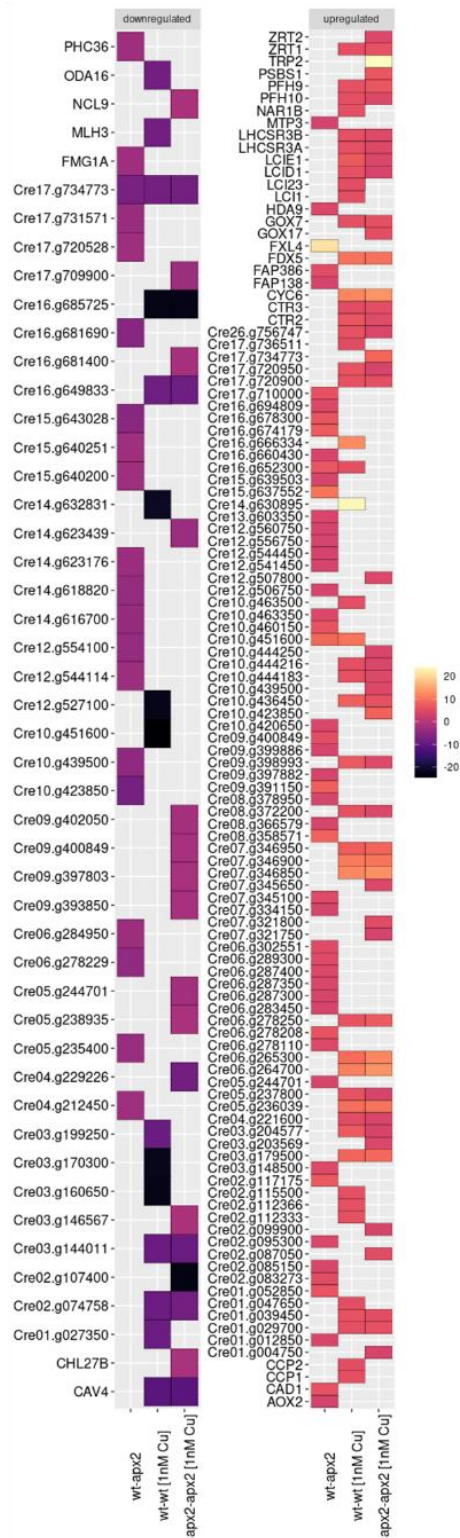


**Figure S2: Wt and *apx2-1* exhibit comparable responses to copper deficiency, and the APX2 transcript remains unchanged in the presence of copper deficiency.**

**A)** The heat map illustrates the 50 most up-regulated genes and the 20 most down-regulated genes in each comparison in both wild type (wt) and *apx2-1* mutants under copper-replete and copper-deficient conditions (1 nM Cu). Variations are observed within the strains. Genes with a log<sub>2</sub> fold change < -1 (range violet – black) represent down-regulated ones, while those with a log<sub>2</sub> fold change > 1 (range pink – cream) signify up-regulated ones, all with a p-value < 0.05, as analysed by DESeq2. Rows are labeled with gene symbols (if available) or gene locus. The three columns represent comparisons: wt vs. *apx2-1* in control conditions with standard copper concentration 6 μM (wt-*apx2*), wt in control vs. copper-deficient conditions (wt-wt [1 nM Cu]), and *apx2-1* in control vs. copper-deficient conditions (*apx2-1*-*apx2-1* [1 nM Cu]). **B)** Normalized reads for the *APX2* transcript demonstrate that gene expression is independent of copper. Three replicates of wt in copper-replete and in copper-deficient conditions are presented.

**A**



**B**

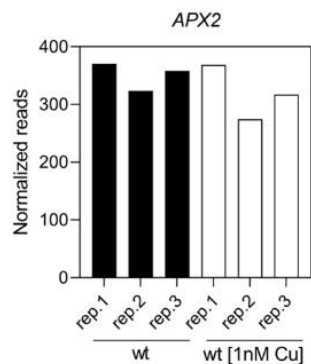


**Figure S3: Alignment of Arabidopsis APX6 and Chlamydomonas APX2 reveals the absence of the AxA cleavage site of the TAT signal in APX6 but confirms the presence of the MxxM motif.**

The double arginine (RR) of the TAT signal is highlighted in pink, and the hydrophobic region in grey. The cleavage site is only found in Chlamydomonas (putative AAA, highlighted in bold). The MxxM motif is in bold orange.

R_At	MTTTTASLVKTFILFRCDSSFSSFKFKCFESPATRLLSPATEKHVVRSSRAWRIRCLSDD	60
R_Cr	--MSTSVLSHRSLSNCTRHGPNRRACRVATHAKL-----RDLSQWRQEGSG--	44
	:* : * : * . * . . . : * : . : ** * . ** . .	
R_At	PGSSHVFA--- <b>SRRKM</b> VVLLSTV-----QLLSHMLPQNGNAE-IYPVMQN	103
R_Cr	--TSEPAVAPEL <b>SRR</b> AVLKLGAALPALAAALAAATPPALLLAPL <b>AAA</b> EGPTLPSPAVAA	102
	:* . ** *** : * :: : * * * . : . * :	
R_At	EIRKVV---TKGKAAGVLRVLFHDAGTFELD-DHGGINGSIAYELERPENIGLKKSLVLA	159
R_Cr	ALDKALAKNIPKTTAVALRLAFHDAATFSAGAKDGLNASIQYELDRPENFGLKRGWRII	162
	: * . : . : * . * * . * * * . * . . . * * . * * * * * * * * * . : :	
R_At	KAK---VK-VDEIQPVSWADMISVAGSEAVSICGGPTIPVVLGRLD--SAQPDPEGKLP	213
R_Cr	EQVRADLKGTAAGVVTADLVALAGAFVRLCGGPAIPLPIGRPVAAAAAQDPPGRMPS	222
	: * . * * : * : * : * : * * : * * * * * : * * : * * * * * :	
R_At	ETLSASGLKECFKRKGFSTQELVALSGAHTIGSKGFGDPTVFDNAYYKILLEKPWTSS-K	272
R_Cr	ENASAAELKANFAAKGLSVQEMVALSGAHTLGSKGFGDPVTFDNAYYVALLQKPWNNTDA	282
	* . * * : * * * * * : * * : * * * * * * * * * * * . * * * * * * * * * :	
R_At	<b>M</b> TSMVGLPSDHALVQDDECLRWVKRYAEDQDKFFEDFTNAYIKLVNSGA-KWNML	326
R_Cr	<b>M</b> ASMIGLPSDHVLPDDPDCLPVIQRYAADQDLFFRDFSAAYIKMCGLVAGWA--	335
	* : * * : * * * * * . * : * : * * : * * * * * * * * * : * * * : . * . *	

Supplemental tables

**Table S1.** Confirmation of the presence of paromomycin cassette in the three *apx2* mutants.

Mutant name	CLiP reference <sup>1</sup>	PCR	Sequencing with	Sequence <sup>2</sup>
<i>apx2-1</i>	LMJ.RY0402.180063	<i>apx2-1_R</i> OMJ913	<i>apx2-1_R</i>	GCACCAATCATGTCAAGCCTCAGCGAGCTGCC ATGGATGGTTCTCTAGCTTGCCCTGACCGGACG CGTGCTGGTA GGAGACGTGTTTCTGACGAGGGCT CGTGACGAAAGGTGCGTGAGAGGGTGCGAGTTAC GAGGACCAAAATTGCAAGGGTGTGCAACAGTGG CGGGTCTACTTGGGGCAGTGGGGGAAGCAGGGC GCAGCGGGTGGGCGAGGCAAGGACGGTGCCACTT TGCGGAGGCACGGCACGGCGCCTCAGGGCCGCG CTGGTGAGTGGTGCCCCCACTCCCGGTCCGGT GTTGGTGATCTGGATGCGGCTCAGTTCGCATGAT GCGCCCGGATGCCCTCTGTGCACCAATTATGAC C
		<i>apx2-1_F</i> OMJ944	<i>apx2-1_F</i>	TTTGACGTTACCAGCACACCTTGTATCATCATCA GCTGCTCTTCCCTGCGCTGCAACACGCCCCGCG CTA GCGCGGTCTGTGCGAACTGCACACTGACGTC GAGCCTTCTGGCAGACTAGTTGCTCTGAGTCCA ACGATGTCTTAGCAAGAGCCTTGCCAAAGCAG CCGCCACGGCCGGAGACGGCAACGTCGGCCCT CGGGCGCGCCGGCAGTGGCCAGCAGCAGCG CCGGCGGGGTGGCCGCGGCCAGAGCCCGCCCA GGCCGGCAGTGGCCGCCAGCTTCAGCACCG CTCGTCGCA AAGCTCCGGAGCTACAGCCGGCT CCGAGGTACCGCTGCCGTGCTTAGTCAAGCGTGA CGCAACCGGATGCCCGGGCGGACCGTGACG GCAGGCAACGACGTACTAGTACTAGCTAT CTAAGAGCTCGCATCCCTGCGCTCGCTCCCTC CGGTGATGCGCCAGTTGCCGGGGGCACTGT GGCCACGGGTACCA TCCGAGGGGTACAGTTAC GCCGAGCTGCGGCCCATCGACATCCGCCACG CACCTCTTGGCGCCACTGTGACAGGTCCC GTAG CTTGGCATGCGTTCGCAACTCTGCACGCTTGGCT TGCCGG
<i>apx2-2</i>	LMJ.RY0402.095128	<i>apx2-2_F</i> OMJ944	OMJ944	TATGACGCTCTTGCCGTGCACAGCCCCGCGC TA TAGCCGCA CCGCTAGTATGGTA ACTGACGTCG AGCCTTCTGGCAGACTAGTTGCTCTGAGTCCAA CTCTGCACGCTGTCGCGGGTGCATGGC GTGT GCAATTCGACAGGGAAACGGTGCGAAAGGACGCT TGACTATGTTGTGACTACGGTGCGAAAAGACGC TTGTAATAAAGGAAAGTCCA TGGTTAACCTGG TTTTGGCCCTGATTTGCGGCA TACAGGGATCG GCGTGACCTCAAGGGCGTGGGTGTGCTTGC TT CGCCCACTCTTCA GTCCGCGTTACGCTTAGCGA GCCTACAGGTGCGTAAAGGGCGAAAGGAAAGCTT GCAAAAAACGCA TGTACCCAGTGCATCTTGT GTATGGCCAGGATTTTTTTTTTGAATATGT

<sup>1</sup> <https://www.chlamylibrary.org/>

<sup>2</sup> yellow: internal bar code of the cassette (<https://www.chlamylibrary.org/>); pink: paromomycin resistant cassette (CIB1, <https://www.chlamylibrary.org/>); grey: APX2 sequence.

**Table S2.** Primers used for sequencing.

Mutants	Primer name	Orientation 5' ->3'
<i>apx2-1</i>	<i>apx2-1_F</i>	TTCCCTGTCTGAATTGCA C
	<i>apx2-1_R</i>	CGAGACCACACATATC AAGG
<i>apx2-2</i>	<i>apx2-2_F</i>	GAGTACAAGCGTCCTTT CGCAC
	<i>apx2-2_R</i>	GGGGATGTTCTTAGCA AGAGCC
cassette	OMJ913	GCACCAATCATGTCAA GCCT
cassette	OMJ944	GACGTTACAGCACACC CTTG

**Table S3. Significantly decreased protein from TMT labeling analysis with a log<sub>2</sub> fold change ≤ -0.5 and p-value < 0.05.** Gene symbols, descriptions of proteins and proteins putative localization (C chloroplast, M mitochondria, SP secretory pathway, O others) were based on Phytozome (<https://phytozome-next.jgi.doe.gov/>). The ones without any description are indicated as uncharacterized proteins.

Proteins decreased – log <sub>2</sub> fold change ≤ -0.5				
Gene identifier	Gene symbol	Description	Putative localization	Log <sub>2</sub> fold change
Cre12.g552200	PHOB1	Starch phosphorylase PhoB	C	-0.5
Cre16.g680250	/	Uncharacterized protein	SP	-0.51
Cre02.g077750	FAP211	Flagellar associated protein 211	SP	-0.51
Cre03.g164600	PMA3 (previous PMH1)	P-type ATPase/cation transporter	O	-0.53
Cre12.g486300	PsaL	Photosystem I reaction center subunit XI	C	-0.57

Cre08.g373100	CYP97C3	Cytochrome P450, CYP97 superfamily	C	-0.58
Cre06.g282800	ICL1	Isocitrate lyase	M	-0.62
CreCp.g802312	PsaB	Photosystem I P700 chlorophyll <i>a</i> apoprotein A2	C	-0.65
Cre12.g485150	GAPC1 (previous GAP1a GAP1b)	Glyceraldehyde-3- phosphate dehydrogenase	C/M	-0.67
Cre09.g393150	FOX1	Ferroxidase-like 1/multicopper ferroxidase	O	-0.69
Cre01.g028850	/	Rhodanese-related sulphurtransferase	SP	-0.7
Cre05.g238332	PsaD	Photosystem I reaction center subunit II	C	-0.7
Cre16.g658800	CDP1	Cysteine domain- containing protein	SP	-0.72
Cre18.g750047	FMG1	Flagella Membrane Glycoprotein 1A	SP	-0.73
Cre07.g315750	/	NADP(+)-dependent D-arabinitol dehydrogenase	C	-0.8
Cre09.g412100	PsaF	Photosystem I reaction center subunit III	C	-0.84
Cre03.g182551	PCY1	Plastocyanin	C	-1.4
Cre02.g095146	/	Predicted protein	O	-1.59



**Table S4. Significantly increased protein from TMT labeling analysis with a log<sub>2</sub> fold change  $\geq$  0.37 and p-value  $<$  0.05.** Gene symbols, descriptions of proteins and proteins putative localization (C chloroplast, M mitochondria, SP secretory pathway, O others) were based on Phytozome (<https://phytozome-next.jgi.doe.gov/>). The ones without any description are indicated as uncharacterized proteins.

Proteins increased – log <sub>2</sub> fold change $\geq$ 0.37				
Gene identifier	Gene symbol	Description	Putative localization	Log <sub>2</sub> fold change
Cre09.g394843	/	C3HC zinc finger-like	C	0.37
Cre11.g479050	FKB15A (previous FKB15-4)	Peptidyl-prolyl cis-trans isomerase	SP	0.37
Cre01.g005050	GLG1, ESL1	Golgi apparatus protein 1	SP	0.37
Cre09.g414200	VPS26	Subunit of retromer complex	O	0.37
Cre03.g151100	SSA15	Cilia-sensing, structure and/or assembly	O	0.38
Cre11.g476550	ADH11	Alcohol dehydrogenase	O	0.39
Cre07.g315150	RBD1	Rubredoxin	C	0.39
Cre04.g223050	CAH2	Carbonic anhydrase	SP	0.39
Cre13.g567600	COX4	Mitochondrial cytochrome c oxidase subunit 4	M	0.4
Cre09.g399250	KIR1	Ketoacid isomerase-like protein	C	0.4
Cre12.g554800	PRK1	Phosphoribulokinase	C	0.41
Cre03.g173900	/	Zinc finger protein, RING-type	C	0.41
Cre03.g175750	/	JmjC domain-containing protein 7	O	0.41
Cre12.g537450	COX13	Mitochondrial cytochrome c oxidase 12 kDa subunit	M	0.41
Cre01.g066552	TRXf1	Thioredoxin f1	C	0.42
Cre02.g143650	/	Uncharacterized protein	C	0.42
Cre06.g308850	EIF3X	hypothetical eIF3-like protein	O	0.45
Cre03.g203850	ATS1	ATP-sulfurylase	C	0.45
Cre11.g474800	OTA1	Ornithine transaminase	M	0.45

Cre02.g097000	DHP1	Dihydropyrimidinase	SP	0.45
Cre08.g360950	/	Uncharacterized protein	C	0.48
Cre17.g734612	MRP2	Putative ABC transporter	O	0.48
Cre06.g278245	/	Pheophorbide a oxygenase-related protein	C	0.49
Cre03.g185550	SEBP1	Sedoheptulose-1,7-bisphosphatase	C	0.5
Cre02.g092350	CYP51G1	Cytochrome P450, CYP51 superfamily	SP	0.51
Cre12.g528700	TRPA1	Tryptophan synthetase alpha subunit	C	0.51
Cre08.g377150	/	Succinyl-CoA--L-malate CoA-transferase	M	0.52
Cre02.g111450	TEF4	Rhodanese-like protein	C	0.54
Cre10.g418450	/	Uncharacterized protein	SP	0.56
CreCp.g802299	rps2	30S ribosomal protein S2	C	0.59
Cre02.g093750	NRX2	Nucleoredoxin 2	O	0.6
Cre07.g315100	/	Pyrimidodiazepine synthase	O	0.61
Cre16.g657750	CCD2	Carotenoid cleavage dioxygenase	M	0.63
Cre05.g245102	CGL3	Conserved in the Green Lineage	O	0.64
Cre02.g095113	TFC-E	Tubulin-folding cofactor subunit	O	0.66
Cre03.g195388	/	Uncharacterized protein	C	0.71
Cre06.g252892	MTA4A	MT+ locus copy of the MTA4 gene	SP	0.83
Cre06.g250902	METH	Cobalamin-independent methionine synthase	O	0.86
Cre17.g726200	/	Uncharacterized protein	M	0.98
Cre10.g422300	PRX6	Peroxiredoxin Q	C	1.11
Cre18.g748297	/	Uncharacterized protein	O	
Cre12.g537250	/	Cupredoxin multicopper oxidase	SP	1.3

## Chapter V

### Ascorbate peroxidase 2 (APX2) of *Chlamydomonas* binds copper and modulates the copper insertion into plastocyanin

Anna Caccamo<sup>1,2,3,4</sup>, Félix Vega de Luna<sup>1</sup>, Khadija Wahni<sup>2,3,4</sup>, Alexander N. Volkov<sup>2,5</sup>, Jonathan Przybyla-Toscano<sup>1,†</sup>, Antonello Amelii<sup>1</sup>, Alexandre Kriznik<sup>6</sup>, Nicolas Rouhier<sup>7</sup>, Joris Messens<sup>2,3,4,\*</sup> and Claire Remacle<sup>1,\*</sup>

<sup>1</sup>Genetics and Physiology of Microalgae, InBios/Phytosystems research unit, University of Liège, 4000 Liège, Belgium; anna.caccamo@uliege.be (A.C.); felix\_vega@comunidad.unam.mx (F.V.d.L.); jonathan.przybyla-toscano@cea.fr (J.P.-T.); antonello.amelii@univr.it (A.A.)

<sup>2</sup>VIB-VUB Center for Structural Biology, 1050 Brussels, Belgium; khadija.wahni@vub.be (K.W.); oleksandr.volkov@vub.be (A.N.V.)

<sup>3</sup>Brussels Center for Redox Biology, 1050 Brussels, Belgium

<sup>4</sup>Structural Biology Brussels, Vrije Universiteit Brussel, 1050 Brussels, Belgium

<sup>5</sup>Jean Jeener NMR Centre, Vrije Universiteit Brussel (VUB), 1050 Brussels, Belgium

<sup>6</sup>CNRS, IMoPA and IBSLor, Université de Lorraine, F-54000 Nancy, France; kriznik5@univ-lorraine.fr

<sup>7</sup>INRAE, IAM, Université de Lorraine, F-54000 Nancy, France; nicolas.rouhier@univ-lorraine.fr

\*Correspondence: joris.messens@vub.be (J.M.); c.remacle@uliege.be (C.R.); Tel.: +32-2-6291992 (J.M.); +32-4-3663812 (C.R.)

†Current address: CEA, INRAE, CNRS, IRIG, LPCV, Université Grenoble Alpes, F-38000 Grenoble, France

In this publication, my involvement encompassed helping on purifying proteins, conducting *in vitro* APX2 activity assays, and performing fluorescence measurements on purified proteins. This work was published in *Antioxidants* in 2023 (<https://doi.org/10.3390/antiox12111946>).

#### Abstract

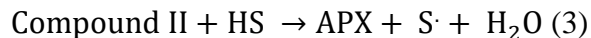
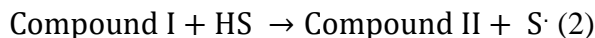
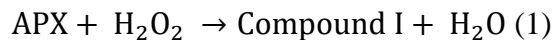
Recent phylogenetic studies have unveiled a novel class of ascorbate peroxidases called “ascorbate peroxidase-related” (APX-R). These enzymes, found in green photosynthetic eukaryotes, lack the amino acids necessary for ascorbate binding. This study focuses on the sole APX-R from *Chlamydomonas reinhardtii* referred to as ascorbate peroxidase 2 (APX2). We used immunoblotting to locate APX2 within the chloroplasts and *in silico* analysis to identify key structural motifs, such as the twin-arginine transport (TAT) motif for lumen translocation and the metal-binding MxxM motif. We also successfully expressed recombinant APX2 in *Escherichia coli*. Our *in vitro* results showed that the peroxidase activity of APX2 was detected with guaiacol but not with ascorbate as an electron donor. Furthermore, APX2 can bind both copper and heme, as evidenced by spectroscopic, and fluorescence experiments. These findings suggest a potential

interaction between APX2 and plastocyanin, the primary copper-containing enzyme within the thylakoid lumen of the chloroplasts. Predictions from structural models and evidence from <sup>1</sup>H-NMR experiments suggest a potential interaction between APX2 and plastocyanin, emphasizing the influence of APX2 on the copper-binding abilities of plastocyanin. In summary, our results propose a significant role for APX2 as a regulator in copper transfer to plastocyanin. This study sheds light on the unique properties of APX-R enzymes and their potential contributions to the complex processes of photosynthesis in green algae.

Keywords: Chlamydomonas; green microalga; ascorbate peroxidase-related; copper-binding motif; peroxidase activity; plastocyanin; structural prediction; <sup>1</sup>H-NMR

### 5.1 Introduction

Ascorbate peroxidases (APXs) (EC 1.11.1.11) are heme b-containing enzymes belonging to class I peroxidases. They catalyze the reduction of H<sub>2</sub>O<sub>2</sub> using ascorbate. This reaction involves the formation of the oxidized Compound I (1), which is subsequently reduced in an intermediate (2) and Compound II (3) by the electron donor ascorbate (Macdonald et al 2006).



In this reaction, HS represents the substrate, and the S is the oxidized form of the substrate. From the crystal structure of the recombinant pea cytosolic APX, it is observed that the heme is bound to the protein through a bond formed between the iron (Fe) and histidine 163 (H163), as well as a hydrogen bond between the 7-propionate and histidine 169 (H169) (view of the active site in the X-ray structure of Ps\_1APX, **Fig. 1 A**). The essential active residues within the distal pocket include arginine 38 (R38), tryptophane 41 (W41), and histidine 42 (H42) (**Fig. 1 A**). On the proximal side, the catalytic triad consists of histidine 163 (H163), aspartate 208 (D208), and tryptophane 179 (W179) (**Fig. 1 A**) (Raven 2003). Ascorbate binding implicates an interaction close to cysteine 32 (C32) and 6-propionate of the heme (Raven 2003). Mutagenesis analyses revealed that arginine 172 (R172) is primarily responsible for ascorbate binding (Burse &

Poulos 2000), with the additional involvement of lysine 30 (K30) in the binding process (Raven 2003) (**Fig. 1 A**).

Organisms capable of oxygenic photosynthesis, such as plants and algae, have multiple versions of APXs encoded within their nuclear genome, each of which is directed to a distinct organelle (Caverzan et al 2012). The chloroplast-localized APX isoforms primarily play a role in supporting photosynthetic activity and protection against oxidative damage (Foyer & Shigeoka 2011, Shigeoka et al 2002). These enzymes play a crucial role in the water–water cycle. The superoxide generated by the Mehler reaction is subsequently converted into H<sub>2</sub>O<sub>2</sub> by superoxide dismutase (SOD) located on the stromal side of the thylakoid membranes (Asada 1999). During H<sub>2</sub>O<sub>2</sub> reduction by APXs, ascorbate is oxidized to monodehydroascorbate, which is then reduced back to ascorbate by NADPH-dependent monodehydroascorbate reductases (Hossain & Asada 1985, Hossain et al 1984). Alternatively, monodehydroascorbate is converted to dehydroascorbate which is then reduced to ascorbate via glutathione-dependent dehydroascorbate reductases (Hossain & Asada 1984).

In addition to these well-known APX enzymes, recent sequence and phylogenetic analyses revealed the existence of two new classes, named Ascorbate Peroxidase-Related (APX-R) and Ascorbate Peroxidase-Like (APX-L). Both types of proteins are targeted to the chloroplasts and lack the amino acids responsible for ascorbate binding. However, APX-R contains the heme b binding residues, while APX-L does not (Lazzarotto et al 2021a, Lazzarotto et al 2011). APX-L (TL-29) of *A. thaliana* has no peroxidase activity and was shown to be associated with photosystem II (PSII) (Granlund et al 2009, Lundberg et al 2011). *In vitro* studies have shown that APX-R (APX6) of *A. thaliana* displays peroxidase activity, but it does not use ascorbate as electron donor (Lazzarotto et al 2021b). So far, most studies on APX-R have focused on their expression in response to stress conditions (Chen et al 2021, Chen et al 2014, Lazzarotto et al 2011, Tyagi et al 2020, Verma et al 2022). In contrast to *A. thaliana*, which possesses eight APXs, including APX6 and TL-29 as cited above, the green alga *Chlamydomonas reinhardtii* (referred to as *Chlamydomonas* hereafter) has only three APXs: one classical (APX1), one APX-R (APX2), and one APX-L (APX4) (Lazzarotto et al 2021a). Kuo et al. showed that APX4 is involved in protecting cells from photodamage caused by high light (Kuo et al 2020a). However, nothing is known about APX2, which is the ortholog of AtAPX6.

Because of the poor characterization of APX-R, we decided to study the APX-R (APX2) from *Chlamydomonas*. The APX2 sequence exhibits two key features that lead us to propose its potential interaction with plastocyanin: the presence of a metal binding motif (MxxM) (Rubino et al 2010) and a twin-arginine transport (TAT) motif (Cline 2015), which is known to direct proteins to the thylakoid lumen. After confirming its localization within chloroplasts and its affinity for binding copper, we propose that APX2 could play a role in regulating the insertion of copper into plastocyanin, the photosynthetic electron carrier which transfers electrons from cytochrome *b<sub>6</sub>f* (Cyt *b<sub>6</sub>f*) to photosystem I (PSI).

## 5.2 Materials and Methods

### 5.2.1 Isolation of chloroplast- and mitochondrion-enriched fractions of wild-type strain

The wt strain (CC-4533 cw15 mt<sup>-</sup>) has been ordered from the *Chlamydomonas* library (<https://www.chlamylibrary.org/>, accessed on 15 September 2023) (Li et al 2019) and used to isolate chloroplastic and mitochondrial protein fractions. Wt cells grown in mixotrophy (light and acetate) were collected at mid-exponential phase and resuspended in various buffer solutions according to (Cardol et al 2002, Mason et al 2006), respectively. After cell breakage, all the steps were carried out on ice to avoid any degradation and the subcellular fractions were separated and collected after centrifugations on Percoll gradients.

### 5.2.2 Gel electrophoresis and blotting

Mitochondrial and chloroplastic protein fractions were loaded on 12 or 15% Laemmli-SDS-PAGE gel and electroblotted onto PVDF membranes (Cytiva Amersham Hybond, Freiburg, Germany) according to standard protocols. Detection was performed using a Chemiluminescence Western blotting kit (Roche, Mannheim, Germany). The blots were developed using commercially available primary antibodies for PsbA1 protein of PSII ( $\alpha$ -D1, 1/10,000, Agrisera AS05 084, Vännäs, Sweden), polyclonal antibodies raised in rabbits against recombinant APX2 ( $\alpha$ -APX2, 1/10,000, Proteogenix, Schiltigheim, France), and alternative oxidase ( $\alpha$ -AOX, 1/27,000, kind gift from Prof S. Merchant). Fluorescence was detected using an iBright FL1000 Imaging System (Invitrogen by Thermo Fisher Scientific, Brussels, Belgium).

### 5.2.3 Expression of recombinant APX2 in *Escherichia coli* and purification

The sequence encoding the putative mature form of APX2 protein (amino acids 97 to 337) was amplified synthetically (Genecust, Boynes, France). Primers (CrAPX2for 5'-CCCCATATGTCTCCGGCCGTGGCGGCTGCG-3' and CrAPX2rev CCGGATCCTCACGCCAGCCCCGCCACGCC) were used to clone the sequence into the NdeI and BamHI restriction sites of a pET15b vector (Merck, Trosly-Breuil, France) in order to express an N-terminal His-tagged recombinant protein (Figure S1a). The introduction of a His-tag and a cleavage sequence for a protease does not alter the APX-R activity as previously shown (Lazzarotto et al 2021b). The APX2 protein was expressed in the *Escherichia coli* BL21(DE3) strain co-transformed with the psBET plasmid allowing expression of the AGA and AGG recognizing tRNA. Expression of APX2 was induced at exponential phase with 100  $\mu$ M of isopropyl 1-thio- $\beta$ -D-galactopyranoside (IPTG). Of note, the LB culture medium was supplemented with 0.25 mM FeCl<sub>3</sub> and 1.5 mM 5-aminolevulinic acid 1 h before induction in order to boost heme synthesis as reported (Sylvestre-Gonon et al 2020). After 4 h induction at 37 °C, bacteria were centrifuged at 6000 $\times$  g for 20 min, and the pellet was resuspended in 30 mM Tris-HCl pH 8.0, 200 mM NaCl lysis buffer containing 10 mM imidazole. Cells were lysed by sonication (three cycles of 1 min, Branson sonifier, 20% amplitude). Insoluble fraction and cellular debris were removed by centrifugation at 40,000 $\times$  g for 25 min. Soluble fraction containing His-tagged APX2 was loaded on a Ni-NTA (Ni<sup>2+</sup>-nitrilotriacetate)-agarose resin equilibrated with 30 mM Tris-HCl pH 8.0, 200 mM NaCl, 10 mM imidazole. After a washing step with 30 mM Tris-HCl pH 8.0, 200 mM NaCl, 10 mM imidazole, His-tagged APX2 was eluted with the same buffer containing 250 mM imidazole. Elution fraction was concentrated using Vivaspin® Turbo columns (10 kDa). Then, a second step of purification by size exclusion chromatography was performed using a HiLoad® 16/600 Superdex® 200 pg column (Cytiva, Marlborough, USA) equilibrated with 30 mM Tris-HCl pH 8.0, 200 mM NaCl. The column was calibrated using the following molecular weight standards: thyroglobulin (670 kDa, 48 mL),  $\beta$ -amylase (200 kDa, 63 mL), bovine serum albumin (66 kDa, 73 mL), and cytochrome c (12.4 kDa, 95 mL). Finally, after a last concentration step, purity and integrity of the purified recombinant protein were analyzed by 15% SDS-PAGE. The concentration of recombinant

His-tagged APX2 protein was determined spectrophotometrically using the theoretical molecular extinction coefficient at 280 nm of  $24,000 \text{ M}^{-1} \text{ cm}^{-1}$ .

#### *5.2.4 Trp fluorescence assay*

Recombinant His-tagged APX2 was used to perform Trp fluorescence analyses using the SpectraMax® iD3 and iD5 Multi-Mode Microplate Readers. His-tagged APX2 was diluted in 20 mM phosphate buffer, pH 6.0 to  $1 \mu\text{M}$  and titrated with increasing concentrations of  $\text{CuSO}_4$  or of  $\text{NiCl}_2 \cdot 6\text{H}_2\text{O}$  dissolved in  $\text{H}_2\text{O}$ . The change in the Trp fluorescence was monitored at  $\lambda_{\text{ex}}$  of 295 nm and following the emission between 335 and 500 nm, with a peak at 350 nm. The dissociation constant ( $K_D$ ) for  $\text{Cu}^{2+}$  binding to APX2 was calculated by fitting the data with the one-site-total-binding equation (GraphPad Prism 9).

#### *5.2.5 Circular dichroism*

Samples for circular dichroism (CD) were prepared at the concentration of 0.2 mg/mL ( $7.265 \mu\text{M}$ ) for His-tagged APX2 in 20 mM phosphate buffer, pH 6.0 and  $50 \mu\text{M}$  of plastocyanin in 20 mM phosphate buffer, pH 6.0 with 50 mM NaF. The measurements were carried out on a Chirascan Plus spectropolarimeter (Applied Photophysics, Ltd., Leatherhead, UK) or on a MOS-500 spectropolarimeter (BioLogic, Seyssinet-Pariset, France). Data were collected at 1 nm intervals in the wavelength range between 180 nm and 260 nm. A cuvette of 0.01 cm with  $30 \mu\text{L}$  of protein sample for Chirascan Plus spectropolarimeter or  $200 \mu\text{L}$  of protein sample for MOS-500 spectropolarimeter was used for all measurements. Measurements were taken in triplicate, averaging three readings per sample, and each sample spectrum was adjusted for the buffer solution.

#### *5.2.6 APX2/ $\text{Cu}^+$ stoichiometry determination*

APX2/ $\text{Cu}^+$  stoichiometry was determined as described in (Blaby-Haas et al 2014). A total of  $10 \mu\text{M}$  of APX2 was incubated with  $20 \mu\text{M}$  of  $\text{CuSO}_4$  in 25 mM MES pH 5.0, 150 mM NaCl in presence of 1 mM DTT to reduce  $\text{Cu}^{2+}$  into  $\text{Cu}^+$  for 10 min at room temperature with gentle agitation. The samples were concentrated with Amicon Ultra SUB1111 and washed once with 25 mM MES pH 5.0, 150 mM NaCl. The APX2 protein concentration was determined spectrophotometrically using the theoretical molecular extinction coefficient at 280 nm of  $24,000 \text{ M}^{-1} \text{ cm}^{-1}$ . The copper binding was confirmed by recording a UV-VIS absorption spectrum from 260 nm to 700 nm. The concentration of  $\text{Cu}^+$



was determined by Rapid Gold BCA assay kit (Pierce, Rockford, USA) with a spectrophotometer (Agilent BioTek Synergy Mx Monochromator-Based Multi-Mode Reader with Time-resolved Fluorescence) at 562 nm. Standard curve was prepared using solutions A and B provided by the BCA assay kit. Solution B (copper sulfate,  $\text{CuSO}_4 \cdot 5\text{H}_2\text{O}$ ) was first prepared in serial dilutions with a factor of two (0, 4.88, 9.77, 19.53, 39.06, 78.13, 156.25, 312.5, 652, 1250, 2500, 5000, 10,000  $\mu\text{M}$ ). Each dilution (10  $\mu\text{L}$ ) was incubated with the alkaline solution A containing bicinchoninic acid (200  $\mu\text{L}$ ) to reduce  $\text{Cu}^{2+}$  in  $\text{Cu}^+$ . The complex formed by  $\text{Cu}^+$  ion chelated with two molecules of bicinchoninic acid was read at 562 nm.

#### *5.2.7 AlphaFold2 prediction for the interaction between APX2 and plastocyanin*

The structural prediction was performed with AlphaFold2, powered by ColabFold. The following script was used for running the structural prediction process: `colabfold_batch --model-type AlphaFold2-multimer-v2 --num-recycle 48 --amber --use-gpu-relax` (Mirdita et al 2022). AlphaFold2-multimer-v2 is a specialized version of the AlphaFold2 model tailored for managing protein complexes or multimers. In the prediction process, 48 recycling steps were employed, serving as iterations where the model fine-tuned its predictions to enhance accuracy. The refinement stage utilized AMBER (Assisted Model Building with Energy Refinement), a force field commonly used in molecular dynamics simulations. Additionally, a relaxation process was implemented, optimizing the predicted structures further to attain more realistic and energetically favorable conformations. Sequences were retrieved from Phytozome (<https://phytozome-next.jgi.doe.gov/>, accessed on 15 September 2023). The copper of plastocyanin and the heme of APX2 were added by superimposition with the 3D structure of a plastocyanin (PDB ID 2PLT) and of the chloroplastic APX from *Nicotiana tabacum* (PDB ID 1IYN), respectively. The approximate distance between the  $\text{Cu}^{2+}$  in plastocyanin and the center of the heme of APX2 was measured using PyMol version 2.5.2.

#### *5.2.8 Recombinant plastocyanin*

Purified plastocyanin was kindly given by Prof. Michael Hippler and Dr. Yuval Milrad (UMunster) and prepared according to (Kuhlgert et al 2012). Apoplastocyanin was obtained by treating holoplastocyanin as described in another study (Ubbink et al 1996) in CHES (N-cyclohexyl-2-

aminoethanesulfonic acid) pH 8.5. Then, 5 mM EDTA, 1 M GdnHCl (guanidinium hydrochloride), and 50  $\mu$ M ascorbate were added, followed by a buffer exchange to 20 mM Na-acetate pH 5.5, 0.2 M NaCl.

### 5.2.9 NMR spectroscopy

All proteins except APX2(Cu) were dialyzed against 20 mM MES pH 5, 150 mM NaCl using slide-a-lyzer cassettes of 3.5 kDa (Pierce, Rockford, USA) at 4°C for 2 h. To avoid precipitation of APX2 during the incorporation of copper, we incubated 10  $\mu$ M APX2 with 20  $\mu$ M CuSO<sub>4</sub> in 25 mM MES pH 5.0, 150 mM NaCl, 1 mM DTT, to reduce Cu<sup>2+</sup> to Cu<sup>+</sup>, by gentle shaking for 10 min. This step was made to be sure that copper would be inserted into APX2, because in these experimental conditions adding directly Cu<sup>2+</sup> led to APX2 precipitation. This was followed by a buffer exchange to the NMR buffer using 5K cut-off concentrators (vivaspın, Sartorius). To ensure the thorough removal of most DTT, this process was repeated three times. The copper binding was confirmed by recording a UV-VIS absorption spectrum recorded from 260 to 700 nm with a kinetics biophotometer (Eppendorf). The quantification of copper was performed using the Rapid Gold BCA assay kit (Pierce) as described in “APX2/Cu<sup>+</sup> stoichiometry determination”.

All NMR experiments were performed at 298 K on a Bruker Avance III HD 800 MHz spectrometer equipped with a TCI cryoprobe for enhanced sensitivity. The samples contained 50–100  $\mu$ M proteins in 20 mM MES pH 5.0, 150 mM NaCl and 6% D<sub>2</sub>O for the lock, and 0.5 mM DSS as the internal standard for chemical shift referencing. The ApX2-bound PC samples were prepared by mixing equal molar concentrations of each protein. A 20 mM buffered stock of CuSO<sub>4</sub> was used for Cu<sup>2+</sup> titrations. The <sup>1</sup>D <sup>1</sup>H spectra were acquired with 16 ppm spectral width, 128 or 256 total number of scans, and water suppression using gradient excitation sculpting (Hwang & Shaka 1995). NMR experiments were conducted under ambient, aerobic conditions. Consequently, both copper bound APX2 and plastocyanin are in the cupric (Cu<sup>2+</sup>) form. The recording, processing, and analysis of these experiments were carried out using TopSpin 3.6 (Bruker, Rheinstetten, Germany).

### 5.2.10 Peroxidase activity assay

Peroxidase activity of recombinant His-tagged APX2 was measured as oxidation of ascorbate or guaiacol in the presence of increasing H<sub>2</sub>O<sub>2</sub> concentrations (0, 0.025 mM, 0.1 mM, 0.3 mM, 0.5 mM, 1 mM). Enzyme concentration was used at 0.2 μM with guaiacol at 10 mM, or 1 μM of enzyme with sodium ascorbate at 0.5 mM, in 20 mM potassium phosphate buffer (pH 6.0) (Lazzarotto et al 2021b). The activity was monitored by recording the changes of absorbance at 470 nm due to formation of tetraguaiacol, or at 290 nm due to consumption of ascorbate (Lazzarotto et al 2021b) in a 1 cm quartz cuvette in a Safas UVmc2-Double Beam spectrophotometer (SAFAS, Monaco, Monaco). The measurements were started with the buffer followed by the addition of guaiacol or ascorbate, of H<sub>2</sub>O<sub>2</sub>, and finally of His-tagged APX2 and followed for two more min. Measurements were repeated twice at each H<sub>2</sub>O<sub>2</sub> concentration. The rates of H<sub>2</sub>O<sub>2</sub> consumption were calculated using molar extinction coefficients of 26.6 mM<sup>-1</sup> cm<sup>-1</sup> at 470 nm for tetraguaiacol (Ogola et al 2009) and of 2.8 mM<sup>-1</sup> cm<sup>-1</sup> at 290 nm for ascorbate (Kumar et al 2004). It was considered that one molecule of formed tetraguaiacol allowed the reduction of two molecules of H<sub>2</sub>O<sub>2</sub>, and one consumed ascorbate allowed the reduction of one molecule of H<sub>2</sub>O<sub>2</sub> in the reaction. Activity was expressed as equivalents of H<sub>2</sub>O<sub>2</sub> (μM) consumed per min in the presence of 1 μM of His-tagged APX2.

### 5.2.11. Structural predictions

The ColabFold interface (Mirdita et al 2022) was used to construct Multiple Sequence Alignments (MSA) for APX2 (Cre06.g285150) (<https://phytozome-next.jgi.doe.gov/>, accessed on 15 September 2023) and plastocyanin PCY1 (Cre03.g182551) (<https://phytozome-next.jgi.doe.gov/>, accessed on 15 September 2023). The following script was used for running the structural prediction process: `colabfold_batch --model-type alphafold2_multimer_v3 --num-recycle 48 --amber --use-gpu-relax`. Visualization was performed using PyMol version 2.5.2 (<https://pymol.org>, accessed on 15 September 2023) (Janson et al 2017).

### 5.3 Results

#### 5.3.1 APX2 resides in chloroplasts, presents a TAT motif for translocation to the thylakoid lumen and a MxxM motif for metal binding

The APX2 gene model (Cre06.g285150) is 3568 bp-long, composed of seven exons and six introns, and codes for a protein of 337 amino acids. According to the Target-P prediction tool (Almagro Armenteros et al 2019), APX2 would be targeted to the chloroplasts. We confirmed this localization by immunoblots on chloroplast- and mitochondrion-enriched fractions (**Fig. 1 B**). The purity of the fractions was assessed with markers typical for chloroplasts (PsbA, a subunit of photosystem II) or for mitochondria (alternative oxidase, AOX), and we showed that APX2 predominantly resides in the chloroplasts. The weak signal observed in the mitochondrial fraction was interpreted as a chloroplast contamination, since PsbA was also weakly detected in this fraction (**Fig. 1 B**). Moreover, Target-P also predicted the existence of a twin-arginine transport (TAT) motif (Cline 2015) (**Fig. 1 C**), which is known to direct proteins to the thylakoid lumen. It consists of a pair of arginine residues (RR) in the N-terminal region, followed by a hydrophobic region and an AxA cleavage sequence at position 90 (**Fig. 1 C**), which would generate a mature protein of 209 amino acids (24 kDa), in accordance with the observed molecular weight on the immunoblot. The TAT-signal sequence present in APX2 is similar to the one present in the oxygen evolving protein PsbQ (Cre08.g372450), an experimentally confirmed luminal protein from *Chlamydomonas* (Mayfield et al 1989). Next, *Chlamydomonas* APX2 was compared with other APX-R and APX from land plants and algae (**Fig. S1 B**). The amino acid sequence alignment showed that the known catalytic residues, arginine (R38) and histidine (H42), present in Ps\_1APX used as a reference, are conserved. The histidine residue at position 163 (H163), which is essential for heme binding, is also conserved in APX-R sequences. However, the arginine residue important for ascorbate binding (R172) is not present in APX-R, supporting previous results indicating that this class of APX does not use ascorbate as electron donor for H<sub>2</sub>O<sub>2</sub> reduction (Lazzarotto et al 2021b). Two specific conserved regions in APX-R sequences were identified. The TAT-signal sequence motif [RR(X...X)A(X)A] mentioned above is found in orthologs from green algae (*Micromonas pusilla* R\_Micp, *Chlorella sorokiniana* R\_Cs, *Chlamydomonas reinhardtii* R\_Cr, *Volvox carterii* R\_Vc, *Chlorokybus atmophyticus* R\_Ca in **Fig. S1C**) and from some land plants (*Azolla filiculoides*

R\_Af, *Salvinia cucullata* R\_Sc, *Marchantia polymorpha* R\_Marp, *Physcomitrium patens* R\_Pp, *Selaginella moellendorffii* R\_Sm, *Oryza sativa* R\_Os, *Zea mays* R\_Zm in **Fig. S1B**). A MxxM or MxxH motif (in the case of *Chlorella sorokiniana* R-Cs and *Micromonas pusilla* R\_Micp), typical for metal-binding proteins, like Cu<sup>+</sup>, is present in all orthologs from green algae and land plants (Rubino et al 2010) except for *Marchantia polymorpha* R\_Marp and *Salvinia cucullata* R\_Sc, both of which exhibit a xxxM motif (**Fig. S1 B**). Previously, it has been shown that several MxxM motifs are required for copper binding in copper transporters and copper resistance proteins of *E. coli* (Jiang et al 2005). However, in another study conducted on yeast and human transporters (Rubino et al 2010), the authors proved that a single motif is sufficient for copper binding, albeit with reduced affinity. These two motifs are not present in APX-R from two diatoms, *Thalassiosira pseudonana* and *Phaeodactylum tricorutum* (**Fig. S1 B, C**). Next, we employed AlphaFold2 (Jumper et al 2021) to predict the structure of APX2. The average predicted local distance difference test (pLDDT) score of the APX2 model was 91.43, which indicates a highly confident residue structure of APX2. The APX2 predicted structure aligned with the X-ray crystal structure of chloroplast APX from *N. tabacum* (PDB ID 1IYN) (**Fig. 1 D**) with an r.m.s.d. value of 0.754 Å. While the fundamental structural fold of APX remains intact, there are significant differences to note. One such distinction is the absence of a loop in APX2, which covers the propionyl tails of the heme group in NtAPX (as illustrated in **Fig. 1 D**). This loop is a consistent feature in other traditional APX structures, as depicted in **Fig. S2 A**. Instead, the conserved MxxM motif is only present in APX2 (depicted in **Fig. 1 D** and **S2 B**). We determined an approximate distance of 16 Å between the MxxM motif for copper binding and the heme of the APX2 (**Fig. 1 E**).

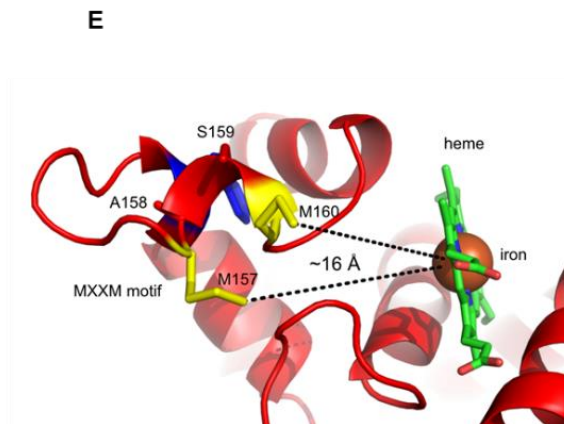
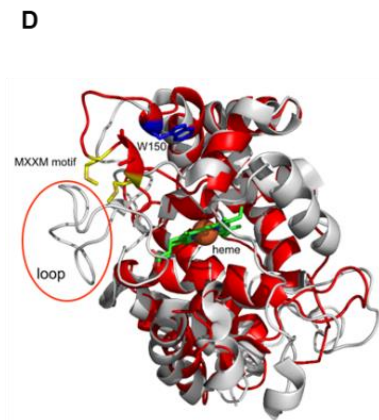
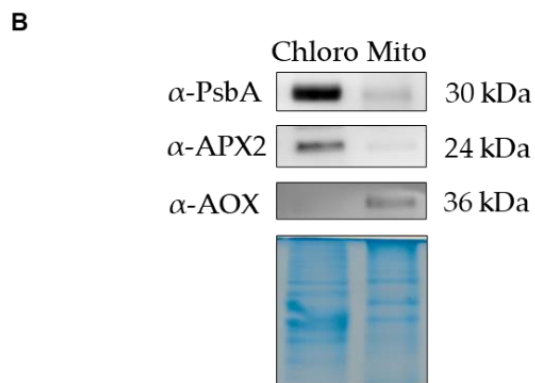
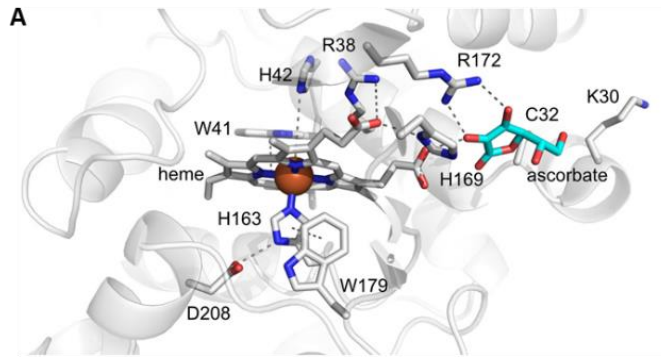


**Figure 1: APX2 is localized in the chloroplasts and present specific conserved motifs typical for lumen targeting and metal binding.** **A)** View of the active site of *Pisum sativum* APX1 (PDB: 1APX). Residues associated with the catalytic activity, ascorbate binding, and heme binding are shown. On the distal side, residues R38, W41, and H42 are crucial for catalytic activity, while on the proximal side, H163, D208, and W179 play essential roles. Ascorbate binding is facilitated by R172, with binding stabilization contributed by C32 and K30. Heme binding is associated with residues H163 and H169. The ascorbate placement in *Pisum sativum* APX1 was guided by the sequence alignment with cytosolic ascorbate peroxidase from *Sorghum bicolor* (PDB: 8DJT), resulting in the light-blue representation. The alignment yielded a r.m.s.d. value of 0.283 Å. **B)** Immunoblots of chloroplast- and mitochondrion-enriched fractions of wt cells (10 µg per lane) developed with antibodies against PsbA, APX2, and alternative oxidase (AOX). Coomassie blue staining of an SDS-PAGE gel was used as loading control. **C)** Highlight of the TAT motif present in the sequences of APX2 (Cre06.g285150) and PsbQ (Cre08.g372450). Blue indicates the RR sequence, yellow indicates the hydrophobic region, arrows indicate the (putative) cleavage in the lumen. Asterisk (\*) indicate fully conserved amino acids, colon (:) indicates conservation between groups of strongly similar properties, period (.) indicates conservation between groups of weakly similar properties. **D)** Superimposition of the APX2 AF2-model (red) and chloroplast NtAPX (PDB code 1IYN) (gray) shows the absence of the loop (circled in red) facing the heme (green) and the presence of a MxxM motif highlighted in yellow in APX2. The Trp150, which is located close to the MxxM sequence motif, is shown in blue. **E)** A closer view focused on the region encompassing the copper-binding site of APX2 (MxxM motif) and the heme, revealing an approximate distance of 16 Å. The distance was determined using PyMOL version 2.5.2.

### 5.3.2 Recombinant APX2 does not use ascorbate as electron donor and binds copper

The observations regarding the lack of the conserved residues for ascorbate binding and the presence of the MxxM sequence motif (**Fig. S1 B**) prompted us to express a recombinant His-tagged APX2. The purification process yielded a homogenous form of APX2 (**Fig. 2 A, B**), existing as a monomer, as confirmed by gel filtration analysis. The calculated molecular weight (27.5 kDa) is in agreement with the migration distance observed on SDS-PAGE gel (**Fig. 2 B**). The UV-visible absorption spectrum showed the presence of the heme (**Fig. 2 A, C**). Analysis by circular dichroism (CD) spectroscopy indicated that APX2 exhibited a characteristic folded protein structure (**Fig. 2 D**).

To evaluate the ability of recombinant APX2 to reduce H<sub>2</sub>O<sub>2</sub>, two different electron donors, ascorbate and guaiacol, were tested. The enzyme demonstrated activity in the presence of guaiacol, a well-known electron donor for peroxidases (Doerge et al 1997) but did not exhibit activity with ascorbate, confirming that

APX2 does not utilize ascorbate as an electron donor for the reduction of H<sub>2</sub>O<sub>2</sub> (**Fig. 2 E** and **S3**).

Finally, the presence of a MxxM sequence motif led us to investigate the binding of Cu<sup>2+</sup> to APX2. We decided to check the effect of Cu<sup>2+</sup> addition on APX2 by evaluating the changes in the secondary structure by CD (**Fig. 2 D**) and by measuring the intrinsic tryptophan fluorescence (**Fig. 2 F**). While alterations in secondary structure were not definitive, a distinct reduction in tryptophan fluorescence, likely stemming from Trp150 in close proximity to the MxxM motif (**Fig. 1 D**), was evident with increasing concentrations of Cu<sup>2+</sup>. We also checked whether the Trp fluorescence change observed after the addition of Cu<sup>2+</sup> was not due to the binding of Cu<sup>2+</sup> to the His-tag of APX2, by doing a similar experiment with Ni<sup>2+</sup>. No Trp fluorescence change was observed in the presence of Ni<sup>2+</sup> (**Fig. 2 F**). From these results, a dissociation constant (K<sub>D</sub>) of 3.6 μM was calculated for the binding of Cu<sup>2+</sup> to APX2. A K<sub>D</sub>-value in the micromolar range hinted in the direction of a copper transfer functionality for APX2. We also determined the copper/APX2 stoichiometry according to (Blaby-Haas et al 2014). Given that copper enters the lumen in Cu<sup>+</sup> redox state (Aguirre & Pilon 2015), we aimed to examine the copper/APX2 ratio using Cu<sup>+</sup>. Hence, APX2 was incubated with CuSO<sub>4</sub> in the presence of the reductant DTT as described in section 5.2.6. We found an APX2/Cu<sup>+</sup> ratio of 1.2 ± 0.1, indicating a one-to-one binding. The copper binding is further evidenced by changes in its UV-vis absorption spectrum (**Fig. 2 G**). In particular, the typical Soret band of the heme-containing protein APX2 underwent a shift from 409 nm to 428 nm upon Cu<sup>+</sup> insertion, indicating alterations in the electronic configuration of the heme. This is likely due to proximity of the heme and Cu-binding sites, as suggested by the predicted structure (**Fig. 1 D, E**).



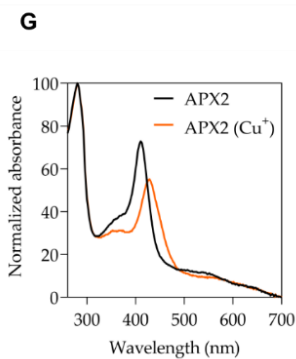
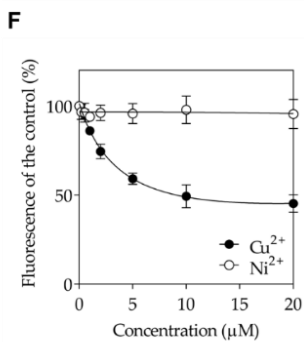
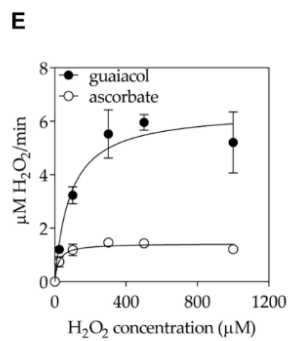
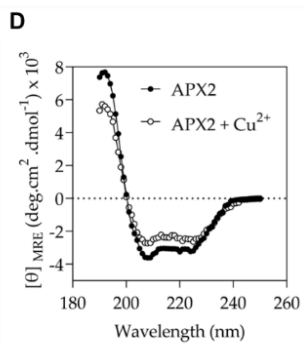
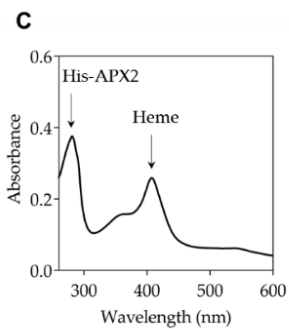
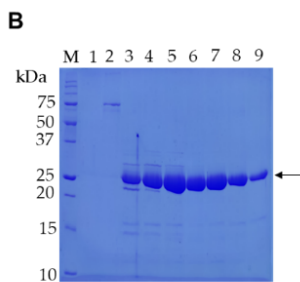
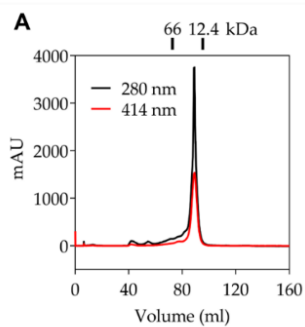


**Figure 2: APX2 peroxidase activity relies on guaiacol instead of ascorbate and APX2 binds copper.** **A)** The heme-containing APX2 eluted as a monomer (elution volume at 89 mL) in size exclusion chromatography (SEC, 16/600 Superdex200®, Cytiva) based on standard calibration. The molecular masses of proteins used as standards and eluted around APX2 have been indicated (details provided in the method section). Absorbance at 414 nm indicates the presence of a heme. **B)** Coomassie blue stained SDS-PAGE gel of the fractions eluted from the SEC column of panel **A**. Arrow indicates purified APX2 (**A**). In addition to the molecular weight marker (Precision Plus Protein Unstained Standards, BioRad), lanes 1 and 2 correspond to two fractions that eluted between 40 and 80 mL, whereas lanes 3 to 9 correspond to fractions under the peak. Based on the purity, fractions 6 to 9 have been pooled for subsequent analyses. **C)** The UV-visible absorption spectrum of APX2 purified protein confirmed the presence of a heme. **D)** Circular dichroism spectra between 190 and 250 nm of recombinant APX2 (7.3  $\mu$ M) with and without 300  $\mu$ M  $\text{CuSO}_4$  in 20 mM phosphate buffer, pH 6.0 are shown. **E)** Peroxidase activity of recombinant His-APX2 was measured by recording the absorbance of oxidized guaiacol at 470 nm or sodium ascorbate at 290 nm as a function of time. Data were fitted with one site specific binding using GraphPad Prism 9 ( $n = 2$  for guaiacol,  $n = 2$  for sodium ascorbate). **F)** Monitoring of the change in tryptophan fluorescence of recombinant His-APX2 with increasing concentrations of  $\text{Cu}^{2+}$  and  $\text{Ni}^{2+}$ . The changes in fluorescence of tryptophan were monitored at  $\lambda_{\text{ex}} = 295$  nm and emission between 335 and 500 nm, with a peak of maximum fluorescence at 350 nm. The percentage (%) of fluorescence change versus the control at  $\lambda_{\text{ex}} = 350$  nm is shown ( $n = 3$ ). Data were fitted with a reverse hyperbolic equation using GraphPad Prism 9. Values are means with standard deviations. **G)** Copper binds at the proximity of the heme site. UV-visible absorption spectra of APX2 and copper-loaded APX2 ( $\text{APX2}(\text{Cu}^+)$ ) are shown.

### 5.3.3 Recombinant APX2 modulates the binding of copper to plastocyanin

Considering the ability of APX2 to bind copper and its putative localization in the lumen, we hypothesized that it might interact with plastocyanin, the main copper sink in *Chlamydomonas* located in the lumen of the chloroplast (Kropat et al 2015). This hypothesis was supported by the fact that transcripts of the two genes were expressed at the start of the day phase, when *Chlamydomonas* cells are subjected to day/night cycles (Strenkert et al 2019) (**Fig. S4 A**). This raised the possibility that both proteins could be present at the same time and therefore could interact. Moreover, given the limited knowledge regarding the players needed for copper insertion into plastocyanin (Merchant et al 2020), we postulated that APX2 might serve as a copper-delivery protein to the apoform of plastocyanin. We utilized AlphaFold2 to predict the interaction between the apoform of plastocyanin and APX2 (as shown in **Fig. 3 A** and **S4 B**). To enhance the accuracy of our model, we incorporated copper and heme into the predicted structures through superposition with known structures from the Protein Data

Bank, specifically using the plastocyanin structure 2PLT for copper and the APX from *N. tabacum* structure 1IYN for heme (as illustrated in **Fig. 3 A**).

To experimentally probe the effect of the APX2-plastocyanin binding on the copper insertion into apoplastocyanin, we have resorted to nuclear magnetic resonance (NMR) spectroscopy (**Fig. 3 B-D**). The upfield region of the 1D  $^1\text{H}$  NMR spectrum contains several well-resolved resonances for apo- and holoplastocyanin. The addition of copper-loaded APX2 to apoplastocyanin yielded a spectrum that was the sum of the NMR spectra of the corresponding individual proteins (cf. green, blue, and orange traces in **Fig. 3 B**), indicating no direct copper transfer from APX2 to plastocyanin under these NMR conditions. This observation suggested that using purified recombinant proteins may not be the most suitable approach for investigating the mechanism of APX2-mediated copper insertion into plastocyanin. Instead, this process likely requires the specific (redox) conditions present in the cellular environment, which may occur simultaneously with plastocyanin folding or involve other cellular factors.

Therefore, in the next experiment, we decided to gradually introduce  $\text{Cu}^{2+}$  ions to apoplastocyanin. This led to an incremental increase in the holoplastocyanin peak and a corresponding decrease in the apoplastocyanin signal (indicated, respectively, by dotted and solid vertical lines in **Fig. 3 C**), consistent with the  $\text{Cu}^{2+}$  binding. Regrettably, we could not achieve saturation in the  $\text{Cu}^{2+}$  titrations due to protein aggregation occurring at higher  $\text{Cu}^{2+}$  concentrations. We observed that in the presence of APX2, apoplastocyanin did also bind  $\text{Cu}^{2+}$ , albeit to a lesser degree than in the absence of APX2 (cf. **Fig. 3 C, D**). In particular, the intensity ratio between the holo- and apo-plastocyanin peaks consistently remained higher in the free plastocyanin titrations, implying a larger equilibrium fraction of the holoplastocyanin in the absence of APX2. It should be noted that the sub-optimal signal-to-noise ratio of the reported NMR experiments could not be improved due to practical limitations. Indeed, much longer spectral acquisition (which would be required for higher-quality spectra) was precluded by a visible sample aggregation, the extent and onset of which depended on the amount of added  $\text{Cu}^{2+}$ . Thus, the limited sample stability has hampered a more comprehensive study of this system by solution NMR spectroscopy.

Altogether, this analysis suggested that the binding site for  $\text{Cu}^{2+}$  in plastocyanin might become obstructed due to the formation of a complex between APX2 and

plastocyanin. The AlphaFold2 model of the plastocyanin-APX2 interaction (as depicted in **Fig. 3 A**) provides insight into the observed inhibitory effect of APX2 on  $\text{Cu}^{2+}$  insertion into apo-plastocyanin. It suggests that APX2 binds in proximity to the Cu-binding site of plastocyanin.

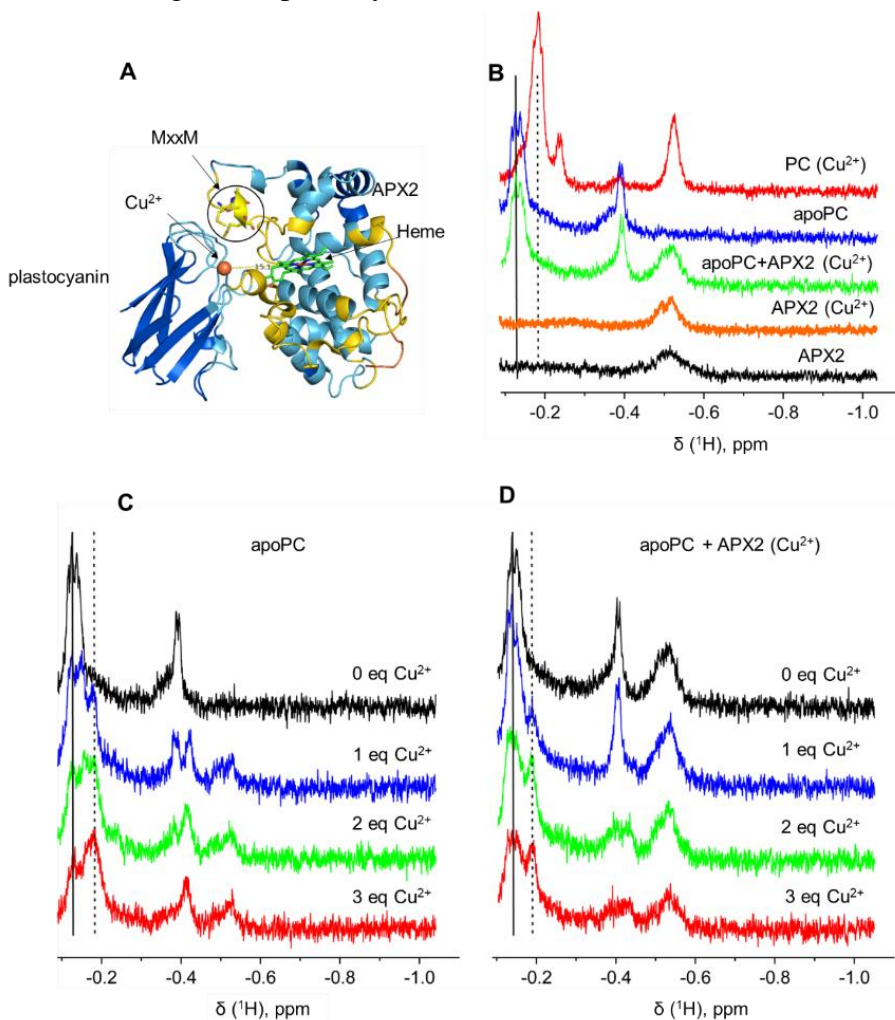


**Figure 3: APX2 modulates copper binding in plastocyanin (PC).** **A**) Prediction of the interaction between APX2 and plastocyanin with AlphaFold2. The copper of plastocyanin and the heme of APX2 were added by superimposition of plastocyanin structure (PDB ID 2PLT) and the chloroplastic APX from *Nicotiana tabacum* (PDB ID 1IYN), respectively. The approximate distance (15.1 Å) between the  $\text{Cu}^{2+}$  in plastocyanin and the center of the heme of APX2 was measured using PyMol2.5.2. **(B-D)** Upfield regions of 1D  $^1\text{H}$  NMR spectra of the studied proteins, with the signals of the apo- and holoPC indicated by the vertical solid and dotted lines, respectively. **(C, D)**  $\text{Cu}^{2+}$  titrations of the free (c) or APX2-bound (D) apoPC.

#### 5.4 Discussion

APX-R enzymes represent a newly identified class of the ascorbate peroxidase family present throughout the eukaryotic green lineage (Lazzarotto et al 2015). We showed that APX2 is a plastid enzyme in *Chlamydomonas* (**Fig. 1 B**) and most probably targeted to the luminal side of the thylakoids (**Fig. 1 C** and **S1 B**), suggesting that its function might be related to photosynthetic processes. We also demonstrated that APX2 still maintains its peroxidase activity but not dependent on ascorbate as electron donor (**Fig. 2 E**), as already shown for the APX6 of *Arabidopsis* (Lazzarotto et al 2021b). Further analyses are required to define the substrate *in vivo*. In addition, APX2 binds copper due to the presence of a MxxM sequence motif (**Fig. 2 D, F, G**). Copper is one of the most important micronutrients in *Chlamydomonas*, playing a vital role in photosynthesis. Within the cell, copper exists in two forms: cupric ( $\text{Cu}^{2+}$ ) and cuprous ( $\text{Cu}^+$ ). Copper, initially in the form of  $\text{Cu}^{2+}$ , undergoes reduction by cupric reductase (Georgatsou et al 1997), resulting in its insertion into the cell as  $\text{Cu}^+$ . The process of copper uptake has been extensively described in *Chlamydomonas* (Hill et al 1996). Given the toxicity of copper and its potential to generate harmful reactive oxygen species (ROS), various Cu-chaperones are present to mitigate oxidative stress. The chaperone antioxidant 1 (ATX1) has been identified (Pham et al 2022). It is localized in the cytosol and plays a role in distributing copper from copper transporters-like (CTR-like) and/or glutathione (GSH) at the plasma membrane to the secretory pathway. Additionally, there are other putative chaperones, such as the plastid copper chaperone (PCC1), structurally similar to ATX1 and down-regulated in copper deficiency (Castruita et al 2011). Another candidate is plastid chaperone 1 (PCH1), derived from an alternative splicing of the copper transporter 2 (CTP2) (Blaby-Haas et al 2014). In *Arabidopsis*, PCH1 has been demonstrated to deliver copper to the  $\text{P}_{1\text{B}}$ -type ATPase PAA1, ortholog of CTP2, of the inner chloroplast membrane (Blaby-Haas et al 2014). The transport of copper to the thylakoid lumen is facilitated by CTP4 (Kropat et al 2015). Plastocyanin enters the thylakoid lumen unfolded via the SEC translocation system (Smeekens et al 1986) and becomes functional in presence of copper (Aguirre & Pilon 2015). However, the mechanism of copper insertion into plastocyanin is not yet defined. Based on the fact that APX2 binds copper and is probably targeted to the thylakoid lumen, we hypothesized that APX2 might participate in copper insertion into plastocyanin. While conclusive proof

remains elusive, our findings strongly indicate that APX2 binds in the vicinity of the Cu-binding site of plastocyanin, thereby influencing the insertion of copper into this protein (**Fig. 3 B-D**).

Phylogenetic analyses carried out on APXs have revealed that the emergence of APX-R occurred in the basal branches of Chlorophyta, resulting from a process of diversification through the deletion and duplication of the APX enzyme (Lazzarotto et al 2021a). The scenario varies in other algal phyla. In red algae, for instance, there is no indication of APX-R (Lazzarotto et al 2021a), and no plastocyanin; instead, they utilize the iron-containing carrier cytochrome *c<sub>6</sub>* (Castell et al 2021). Diatoms, such as *P. tricornutum* and *T. pseudonana*, do possess an APX-R, but our research demonstrates that it lacks the distinctive MxxM or MxxH motif required for metal binding and the TAT motif, which hinders its localization to the lumen (**Fig. S1 B, C**). Interestingly, in these diatoms, plastocyanin does not serve as the electron carrier between Cyt *b<sub>6</sub>f* and PSI; instead, they employ the iron-containing carrier cytochrome *c<sub>6</sub>* (Castell et al 2021). In some diatoms, such as *Thalassiosira oceanica*, a gene encoding plastocyanin exists, although plastocyanin levels are notably lower compared to those present in green algae, plants, and cyanobacteria (Castell et al 2021). In the case of cyanobacteria, APX activity has been observed, yet no gene encoding for an APX has been identified to date (Miyake 1991). Land plants also present APX-R as described in (Dunand et al 2011). Based on the alignment presented in **Fig. S1 C**, the presence of the TAT motif is not definitively evident in some cases, notably in R\_Zm (*Zea mays*). This ambiguity is particularly pronounced within the hydrophobic region located between the double arginine (RR) and the putative cleavage site (AxA), raising questions about their potential luminal localization and any potential association with plastocyanin. However, it is worth noting that they do exhibit the MxxM motif, implying a possible conservation of their interaction with copper or plastocyanin. Nevertheless, to substantiate this hypothesis, additional experiments will be necessary.

Examining APX6 of Arabidopsis, a notable observation is the lack of a complete TAT motif, as illustrated in **Fig. S1 C**. Instead, it exhibits only the double arginine (RR) without the usual cleavage site (AxA). Nevertheless, the presence of the MxxM motif is evident, as demonstrated in the alignment depicted in **Fig. S1 B**. Additionally, structural similarities become evident upon superimposing it with APX2 of Chlamydomonas, as illustrated in **Fig. S4 D**. Arabidopsis APX-R

(APX6) localizes in the chloroplast (Lazzarotto et al 2021b) and was shown to be translocated from the stroma to vesicles identified as plastoglobuli during photomorphogenesis. These organelles act during senescence and thus participate to APX-R degradation. Other studies on *Arabidopsis* *apx6* mutant lines provided evidence of the involvement of this enzyme in the senescence process, proposed to be regulated by copper (Chen et al 2021). These findings align with our results, underscoring the connection between copper and APX-R.

### *Conclusions*

We demonstrated for the first time that the newly classified APX-R enzyme, specifically APX2 of *Chlamydomonas*, has an affinity for copper binding. This would fit with a role of APX2 in regulating copper insertion into plastocyanin, hinting at potential implications in plastocyanin biogenesis and the integrity of the photosynthetic electron transport chain. Additionally, we have confirmed that this enzyme maintains its peroxidase activity for the reduction of H<sub>2</sub>O<sub>2</sub> without relying on ascorbate as an electron donor. These results strongly imply that APX-R may have a function distinct from its conventional redox function. To gain a comprehensive understanding of its *in vivo* function, additional experiments are needed, including the analysis of mutants without APX2 in *Chlamydomonas* to delve into their physiological traits.

### *Acknowledgments*

We would like to thank Michele Radoux for expert technical assistance, Daria Ezeriņa for assisting with the SpectraMax® iD3 and iD5 Multi-Mode Microplate Readers for tryptophan fluorescence experiments, Julia Malo Pueyo for setting-up the CD experiments. We warmly thank Michael Hippler and Yuval Milrad (UMunster, Germany) for kindly providing recombinant plastocyanin.

### *Funding*

This work was funded by Fonds de la Recherche Scientifique-the Research Foundation Flanders—Excellence of Science project no. 30829584 (to C.R. and J.M.) and a VIB-grant (to J.M.); A.C. acknowledges a PhD fellowship of ULiège supported by Fonds de la Recherche Scientifique Excellence of Science project no. 30829584; J.P.T is postdoc from Belgian Fonds de la Recherche Scientifique-FNRS, respectively. The Hubert Curien Tournesol partnership is acknowledged by N.R. and C.R.

## Supplementary materials

### Figure S1: Amino acid sequence alignment of APX and APX-R showing conserved residues in representatives from algae, plants and diatoms.

A) Sequence of recombinant His-tagged APX2 expressed in *E. coli*. The His-tag is underlined in blue and the sequence for cleavage by thrombin in violet. The sequence of APX2 (Cre06.g285150) from Phytozome is also shown and the targeting signal that has been removed in recombinant His-tagged APX2 is in grey.

B) The amino acid sequence alignment of APX-R from selected photosynthetic organisms (green algae, diatoms, plants) was performed using ClustalW ([https://npsa-pbil.ibcp.fr/cgi-bin/npsa\\_automat.pl?page=/NPSA/npsa\\_clustalw.html](https://npsa-pbil.ibcp.fr/cgi-bin/npsa_automat.pl?page=/NPSA/npsa_clustalw.html), accessed on 15 September 2023). The organisms were chosen based on (Dunand et al 2011) and the sequences retrieved from the RedOxiBase (<https://peroxibase.toulouse.inra.fr/>, accessed on 15 September 2023). The sequences for classical APXs were retrieved by blastp analysis using AtAPXs. Double arginine for TAT-motif is highlighted in bold (CrAPX2 as RedoxiBase reference: 56RR57, putative cleavage site is highlighted in yellow). Conserved amino-acid residues are highlighted in bold. The ones of the reference sequence from *Pisum sativum* Ps\_1APX are in blue and bold, however, due to the alignment the exact position of these residues as described in (Raven 2003) in the crystal structure has shifted (the essential active residues are **R38 -> R196**, **W41 -> W199**, **H42 -> H200**, **H163 -> H365**, **W179 -> W416**, **D208 -> D459**; the primary residue responsible for ascorbate binding is **R172 -> R374** together with the contribution of **C32 -> C190** and **K30 -> K185**; **H163 -> H365** and **H169 -> H371** are the heme-binding residues). In grey is highlighted the **MxxM** or **MxxH** motif typical of metal binding.

RedOxiBase Entry ID are the following: **R\_Tp** *Thalassiosira pseudonana* APX-R 2559; **R\_Pt** *Phaeodactylum tricornutum* APX-R 8208; **R\_Micp** *Micromonas pusilla* APX-R 8359; **R\_Cs** *Chlorella sorokiniana* APX-R 15183; **R\_Cr** *Chlamydomonas reinhardtii* APX-R 7433; **R\_Vc** *Volvox carteri* APX-R 8357; **R\_Ca** *Chlorokybus atmophyticus* APX-R 7707; **R\_Af** *Azolla filiculoides* APX-



R 16514; **R\_Sc** *Salvinia cucullate* APX-R 16550; **R\_Marp** *Marchantia polymorpha* APX-R 5764; **R\_Pp** *Physcomitrella patens* APX-R 5761; **R\_Sm** *Selaginella moellendorffii* APX-R 7143; **R\_At** *Arabidopsis thaliana* APX-R 3952; **R\_Os** *Oryza sativa* APX-R 3961; **R\_Zm** *Zea mays* APX-R 5183.

C) ClustalW ([https://npsa-pbil.ibcp.fr/cgi-bin/npsa\\_automat.pl?page=/NPSA/npsa\\_clustalw.html](https://npsa-pbil.ibcp.fr/cgi-bin/npsa_automat.pl?page=/NPSA/npsa_clustalw.html), accessed on 15 September 2023) was used to perform the alignment of the APX-R from selected organisms (green algae, diatoms, plants). Sequences of APX-R were retrieved on RedOxiBase (<https://peroxibase.toulouse.inra.fr/>). Entry ID are the following: **R\_Tp** *Thalassiosira pseudonana* APX-R 2559; **R\_Pt** *Phaeodactylum tricorutum* APX-R 8208; **R\_Micp** *Micromonas pusilla* APX-R 8359; **R\_Cs** *Chlorella sorokiniana* APX-R 15183; **R\_Cr** *Chlamydomonas reinhardtii* APX-R 7433; **R\_Vc** *Volvox carteri* APX-R 8357; **R\_Ca** *Chlorokybus atmophyticus* APX-R 7707; **R\_Af** *Azolla filiculoides* APX-R 16514; **R\_Sc** *Salvinia cucullata* APX-R 16550; **R\_Marp** *Marchantia polymorpha* APX-R 5764; **R\_Pp** *Physcomitrella patens* APX-R 5761; **R\_Sm** *Selaginella moellendorffii* APX-R 7143; **R\_At** *Arabidopsis thaliana* APX-R 3952; **R\_Os** *Oryza sativa* APX-R 3961; **R\_Zm** *Zea mays* APX-R 5183. Putative twin-arginine-translocation motif (TAT) is highlighted: double arginine (RR) for chloroplast translocation is highlighted in bold and the AxA cleavage site for luminal translocation is highlighted in yellow (as checked using TargetP-2.0, <https://services.healthtech.dtu.dk/services/TargetP-2.0/>, accessed on 30 October 2023). The AxA cleavage site is not clear for **R\_Micp**, **R\_Zm**, **R\_Af** and **R\_Pp**, and is lacking for **R\_At**. Differences in the length of the hydrophobic region between the RR and the AxA cleavage site can be noticed between algal and land plant sequences. The members in the two diatoms **R\_Tp** *Thalassiosira pseudonana* and **R\_Pt** *Phaeodactylum tricorutum* do not present the TAT motif.

## A

### Recombinant His-tagged APX2

MGSSHHHHHHSSGLVPRGSHMSPAVAAALDKALAKNIPKTKTAVALLRFAFHDAATFSAGAKDGG  
LNASIQYELDRPENFGLKRGWRIIEQVRADLKGTA AEGVVTADLVALAGAFVRLCGGPAIPLPIGRP  
VAAAARQDPPGRMPSENASAAELKANFAAKGLSVQEMVALSGAHTLGSKGFGDPVTFDNAYYV  
ALLQKPWNNTKDAMASMIGLPSDHVLPDDPDCLPVIQRYAADQDLFFRDFSAAAYIKMCG  
LGVAGWA

### APX2 (Cre06.g285150)

MSTSVLSHRSLSNCTRHGPNRRACRVATHAKLRDLSQWRQEGSGTSEPAVAPELSRRAVLKLGA  
ALPALAAALAAATPPALLLAPLAAAEGPTLSPAVAAALDKALAKNIPKTKTAVALLRFAFHDA  
ATFSAGAKDGG LNASIQYELDRPENFGLKRGWRIIEQVRADLKGTA AEGVVTADLVALAGAF  
VRLCGGPAIPLPIGRPVA AAARQDPPGRMPSENASAAELKANFAAKGLSVQEMVALSGAHT  
LGSKGFGDPVTFDNAYYVALLQKP WNNTKDAMASMIGLPSDHVLPDDPDCLPVIQRYAADQ  
DLFFRDFSAAAYIKMCG LGVAGWA



**Figure S2: Chlamydomonas APX2 lacks the loop that faces the heme, and APX-R contains the MxxM/H sequence motif.** **A)** Structural comparison of classical cytosolic and chloroplastic APXs (respective PDB ID 1APX for *Pisum sativum* APX1; 1IYN for *Nicotiana tabacum* sAPX) with the predicted structure of *Chlamydomonas* APX2 (Jumper et al 2021). The loop covering the heme propionyl tails present in the cytosolic and stromal APX enzymes is absent in CrAPX2, in which there is a solvent-exposed MxxM or MxxH motif. **B)** Partial amino acid sequence alignment showing differences in the secondary structures (including the loop facing the heme or the MxxM or MxxH motif) between cytosolic (C), stromal (S) and luminal (L) isoforms (APX-R). Sequences of cytosolic and stromal isoforms were retrieved by a blastp search using stromal APX from *A. thaliana* (AtsAPX). The sequences of chloroplast APX isoforms used are the same as in **Fig. S1** and they are compared with the cytosolic isoform APX1 of *P. sativum*, from which the helices and loops are defined by crystal structure.

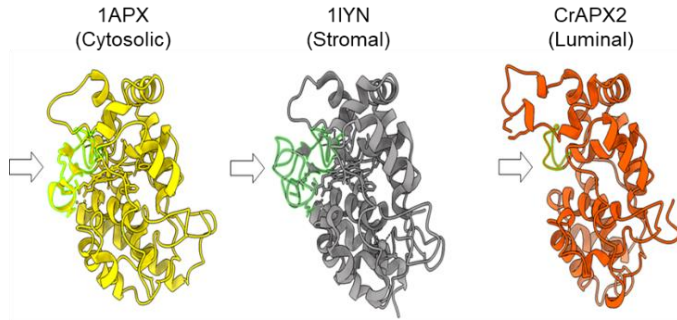
RedOxiBase Entry ID are the following: **R\_Cs** *Chlorella sorokiniana* APX-R 15183; **R\_Cr** *Chlamydomonas reinhardtii* APX-R 7433; **R\_Vc** *Volvox carteri* APX-R 8357; **R\_Ca** *Chlorokybus atmophyticus* APX-R7707; **R\_Af** *Azolla filiculoides* APX-R 16514; **R\_Sc** *Salvinia cucullata* APX-R 16550; **R\_Mp** *Marchantia polymorpha* APX-R 5764; **R\_Pp** *Physcomitrella patens* APX-R 5761; **R\_Sm** *Selaginella moellendorffii* APX-R 7143; **R\_At** *Arabidopsis thaliana* APX-R 3952; **R\_Os** *Oryza sativa* APX-R 3961; **R\_Zm** *Zea mays* APX-R 5183.

GenBank/NCBI accession numbers are as follows: **Ps\_1APX** *Pisum sativum* 1APX XP\_050898393.1; **Ds\_APX1** *Dunaliella salina* APX1 QBY35580; **Vc\_APX1** *Volvox carteri* APX1 XP\_002953608.1;

**Cr\_APX1** *Chlamydomonas reinhardtii* APX1 XP\_001701947.1; **Cd\_APX** *Chlorella desiccata* APXhypot KAG7671850.1; **Cs\_APX** *Coccomyxa subellipsoidea* APX XP\_005643275.1; **Mp\_APX4** *Marchantia polymorpha* APX4 PTQ42354.1; **Pp\_APX2** *Physcomitrella patens* APX2 XP\_024381690.1; **Sm\_APX6** *Selaginella moellendorffii* APX6 XP\_002986232.1; **At\_sAPX** *Arabidopsis thaliana* sAPX NP\_001319883.1; **Nt\_sAPX** *Nicotiana tabacum* sAPX 1IYN\_A; **Os\_APX7** *Oryza sativa*

APX7 NP\_001389298.1; **Zm\_APX7** *Zea mays* APX7 NP\_001132683.1;  
**Zm\_sAPX** *Zea mays* sAPX ONM17334.1.

**A**



**B**

	α-helix	Loop	
C			
Ps_1APX	GSDHLRDFVGKAMGLSDQDIVALSGGHTL	SAHKERSGFE-----	176
Ds_APX1	AADHIRKVFN-RMGINDQEIIVLSSGHTL	ERVRKDRSLGLGVDETKYTKD-GPGLK----	223
Vc_APX1	PAEHLRRVFG-RMGLTDQEIIVLSSGHTL	GRARPERSGFGADTKYTKDVG-GPSTSSASPS	229
Cr_APX1	PAEHLRRVfy-RMGLNDQEIIVLSSGHTL	GRARPERSGFGAEKTKYTKDVG-GPSTTASPS	229
Cd_APX	PAHLRAVfy-RMGLTDKDIVALSGHTL	GRARPERSGFGKASTKYTKAN-GPGNP----	226
Cs_APX	PGDHLRKFVfy-RMGLNDQEIIVLSSGHTL	GRAYFNRSFGFKSTKYTKD-GPGTK----	238
Mp_APX4	PADHLRKFVfy-RMGLNDREIVLSSGHTL	GRSRPERSGWGKTKYTKDVG-GANIGAP----	276
Pp_APX2	PADHLRKFVfy-RMGLNDQEIIVLSSGHTL	GRVHPERSGFGQKTKYTKRNG-GPGKP----	281
Sm_APX6	PSEHLRKFVfy-RMGLDDKDIVALSGHTL	GRSRPERSGWGKTKYTKDVG-GPGAP----	260
At_sAPX	PATHLRVfy-RMGLDDKDIVALSGHTL	GRSRPERSGWGKTKYTKRNG-GPGAP----	289
Nt_sAPX	PAQHLRDFVfy-RMGLNDKEIVLSSGHTL	GRSRPDRSGWGKTKYTKDVG-GPGAP----	190
Os_APX7	PADHLRKFVfy-RMGLNDKEIVLSSGHTL	GRSRPERSGWGKTKYTKRNG-GPGAP----	274
Zm_APX7	PADHLRDFVfy-RMGLNDKEIVLSSGHTL	GRSRPERSGWGKTKYTKRNG-GPGAP----	254
Zm_sAPX	PADHLRDFVfy-RMGLNDKEIVLSSGHTL	GRSRPERSGWGKTKYTKRNG-GPGAP----	190
R_Cs	SAEQLLDNFA-AKGLSARELIVLSSGSH-LGSK----	GYG-----	240
R_Cr	SAEELKANFA-AKGLSVQEMVALSGHTL	LGSK----GFG-----	259
R_Vc	TAEQKANFA-AKGLSVQEMVALSGHTL	LGSK----GFG-----	247
R_Ca	TAQQLKSHFA-AQGFSTRELVALGHTL	IGFK----GYG-----	288
R_Af	DASNLKKNFL-ARGFTSELVALSGHTL	LGSK----GFG-----	284
R_Sc	DVLSLKKNFI-ARGFTSELVALSGHTL	LGSK----GFG-----	249
R_Mp	TGSQLREAFQ-ARGFSTQELVALSGHTL	VGSK----GFG-----	255
R_Pp	TASELKRTFQ-SKGFSTQEMVALSGHTL	IGNK----GFG-----	273
R_Sm	NAVALKKIFQ-SKGFSTQEMVALSGHTL	LGSK----GFG-----	216
R_At	SASGLKECFK-RKGFSTQELVALSGHTL	IGSK----GFG-----	250
R_Os	DATALKTLFS-KKGFSTQEMVALSGHTL	IGSK----GFG-----	251
R_Zm	DAASLKTLS-KKGFSAQELVALSGHTL	IGSK----GFG-----	256

	Loop	α-helix	MxxM/H motif		
C					
Ps_1APX	-----GPWTSNPLIFD	NSYFTELLETK	SEKD-----	GLLQLPSDKA 210	
Ds_APX1	-----GGTSWTPDWLNF	NSYFTELKARRDA	-----	DLVIMTDC 259	
Vc_APX1	GGSPDRPVTPKFVGLG	TSWTANWLEFNS	YFTEVKARRDA	-----	DLLVLPTDC 279
Cr_APX1	GATDRPVTPKFVGGQ	TSWTWNWLEFNS	YFKELKARRDS	-----	DLLVLPTDC 279
Cd_APX	-----GGSSWTVEWLQ	FNSYFTDIKEK	KDE-----	ELLVLPTDAA 262	
Cs_APX	-----GGSSWTFEWLQ	FNSYFYIKDQ	FDS-----	ELLVLETDV 274	
Mp_APX4	-----GGQSWTAEWLRF	NSYFRDIKQ	QSDS-----	DLLVLPTDKV 312	
Pp_APX2	-----GGSSWTFEWLRF	NSYFREIKER	RDA-----	DLVVLPTDAV 317	
Sm_APX6	-----GGQSWTFEWLRF	NSYFKDIKE	KRDE-----	DLLVLPTDAV 296	
At_sAPX	-----GGQSWTFEWLRF	NSYFKDIKE	KRDE-----	DLLVLPTDAA 325	
Nt_sAPX	-----GGQSWTAQWLRF	NSYFKDIKE	KRDE-----	DLLVLPTDAA 226	
Os_APX7	-----GGQSWTAEWLRF	NSYFKDIKE	KRDQ-----	DLLVLPTDAA 310	
Zm_APX7	-----GGQSWTFEWLRF	NSYFKDIKE	KRDQ-----	DLLVLPTDAA 290	
Zm_sAPX	-----GGQSWTFEWLRF	NSYFKDIKE	KRDQ-----	DLLVLPTDAA 226	
R_Cs	-----DPVTFDNTYYKTL	LLEKFWER	-----VSAKMAA	GIPTDHW 276	
R_Cr	-----DPVTFDNTYYKTL	LLEKFWPN	-----T-DMA	MASMLGLPSDHV 294	
R_Vc	-----DPTRFDNTYYR	LLEKFWFTN	-----FNDSMASM	GLPSDHV 283	
R_Ca	-----MPDVFDNTYYKTL	LLEKFWPN	-----SKDMAYM	GIPIDHA 324	
R_Af	-----NPLVFDNSYFKIL	LLEKFWTQ	-----IDNMGSM	GLPSDRT 320	
R_Sc	-----NPLVFDNSYFKIL	LLEKFWTQ	-----TDNIGSM	GLPTDRA 285	
R_Mp	-----DPYTFDNTYYKTL	LLEKFWL	-----KENETKM	GLDSRA 290	
R_Pp	-----NPNLFDNSYFQILL	LLEKFWKI	-----GPDDMTSM	GLATDRA 310	
R_Sm	-----NPTVFDNSYFQILL	LLEKFWSD	-----DNRMASM	GLPSDRV 251	
R_At	-----DPTVFDNTYYKTL	LLEKFWT	-----SSRMTSM	GLPSDHA 284	
R_Os	-----NPNLFDNSYFKV	LLEKFWP	-----SSCMFAM	GLRTDWA 295	
R_Zm	-----SPVYFDNTYFKV	LLEKFWP	-----NRPPTSS	TGMLGLRTDWA 295	

**Figure S3: APX2 utilizes guaiacol, but not ascorbate, as electron donor.** Peroxidase activity progress curves are shown. **A)** Oxidation of guaiacol monitored at 470 nm as a function of time in the presence of recombinant APX2 and increasing  $\text{H}_2\text{O}_2$  concentrations and **B)** Oxidation of sodium ascorbate followed at 290 nm as a function of time in the presence of recombinant APX2 and increasing  $\text{H}_2\text{O}_2$  concentrations. Arrows pointing at the position where guaiacol, ascorbate,  $\text{H}_2\text{O}_2$ , and His-tagged APX2 were added.

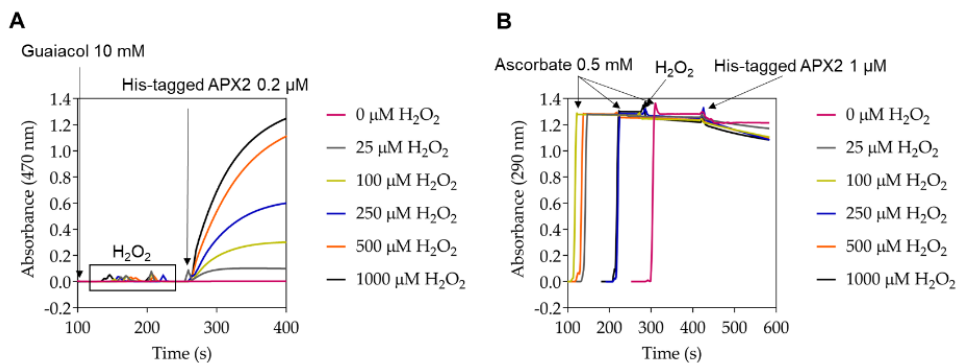
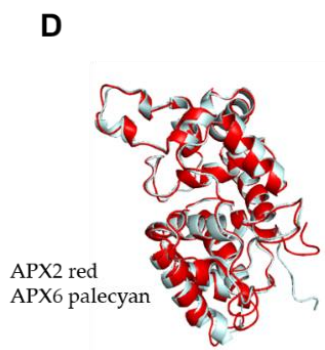
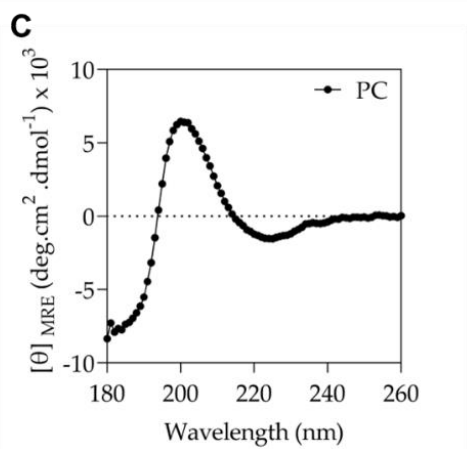
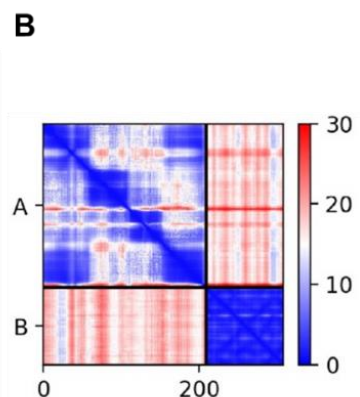
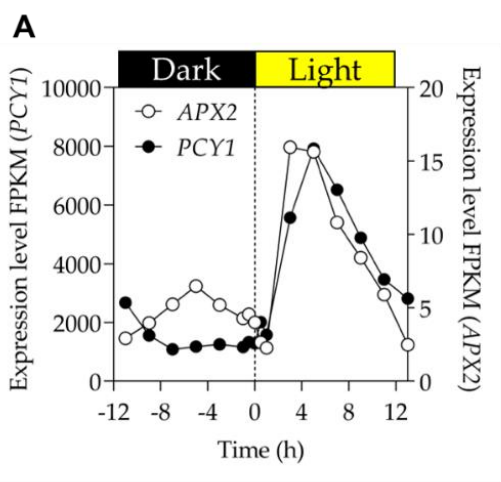


**Figure S4: Further analyses of APX2 and plastocyanin.** **A)** Transcript levels of APX2 and plastocyanin (PCY1) in *Chlamydomonas* present similar dynamics changes in the light phase of asynchronized day-night culture. The time points -11 to 0 correspond to the dark phase, the time points 0 to 12 corresponds to the light phase, time points 12 to 13 correspond to the next dark phase. The data are retrieved from (Strenkert et al 2019). **B)** AlphaFold2\_multimer pairwise alignment diagram for the interaction of APX2 with apoplastocyanin. A represents all the residues of APX2 and B represents all the residues of apoplastocyanin. AF2 predicted five models and only the one ranked as number one is shown. The first quadrant shows the prediction error on the interactions within APX2 and the fourth quadrant the internal interaction error within apoplastocyanin. The blue color indicates high confidence, while the red color indicates low confidence (or high flexibility). The blue line marks in the second and third quadrant of the diagram show specific well predicted interactions between both proteins. **C)** Circular dichroism spectrum of the recombinant plastocyanin. Circular dichroism between 180 and 260 nm of recombinant plastocyanin (PC, 50  $\mu$ M) in 20 mM phosphate buffer, pH 7.4 + 100 mM NaF shows the characteristic folded structure (recombinant plastocyanin was a kind gift from M. Hippler and Yuval Milrad (UMunster)). **D)** Superimposition of predicted structure of APX2 of *Chlamydomonas* (red) and APX6 of *Arabidopsis* (palecyan) (predicted with AlphaFold2 powered by ColabFold) reveals that the two proteins are similar. The r.m.s.d. is 0.407 Å.





# Chapter VI

## Refinement of the methodology for capturing cysteine-modified proteins: protocol and encountered challenges

Anna Caccamo<sup>1,2,3,4</sup>, Sébastien Pyr dit Ruys<sup>5,6</sup>, Gaetan Herinckx<sup>5</sup>, Didier Vertommen<sup>5</sup>, Joris Messens<sup>2,3,4</sup>, Claire Remacle<sup>1</sup>

<sup>1</sup>Genetics and Physiology of Microalgae, InBios/Phytosystems, University of Liège, Liège, Belgium

<sup>2</sup>VIB-VUB Center for Structural Biology, Brussels, Belgium

<sup>3</sup>Brussels Center for Redox Biology, Brussels, Belgium

<sup>4</sup>Structural Biology Brussels, Vrije Universiteit Brussel, Brussels

<sup>5</sup>SSS/DDUV/PHOS, Faculty of Medicine and Duve Institute, Catholic University of Louvain, Brussels, Belgium

<sup>6</sup>SSS/LDRI/PMGK, Faculty of Pharmacy and Louvain Drug Research Institute, Catholic University of Louvain, Brussels, Belgium

My contribution to this part covered the *in vivo* BTD labelling of *Chlamydomonas* cells, protein extraction, validation by immunoblot and preparation of samples to identify modified cysteines by mass spectrometry. This part of the project was in close collaboration with the lab of Didier Vertommen and his team from UCLouvain.

### *Abstract*

This section describes the second objective of my thesis, the identification of the sulfenylated proteins modified in their cysteine residues in *Chlamydomonas* cells, with and without addition of H<sub>2</sub>O<sub>2</sub>. To do so, we first proceeded with the optimisation of the protocol on wt strains of *Chlamydomonas* before applying the assay to mutants of interest. We followed the procedures outlined in (Huang et al 2019) and (Fu et al 2019) as references for verifying protein labelling and identifying modified proteins, respectively. The protocol optimization was quite challenging and the issues we faced were critical for the total protein yield. Selecting the appropriate strain for effective protein labelling and employing protein precipitation to minimize interference from chlorophyll molecules in subsequent steps were crucial decisions. We succeeded in labelling modified proteins and confirmed them by immunoblot analyses. However, we encountered quite a lot of issues during the workflow for sample preparation for mass spectrometry analyses. Despite numerous trials, we only managed to detect a limited number of modified cysteines. In this section, I detail the comprehensive

protocol refined for protein labelling in *Chlamydomonas*. Additionally, I provide an overview of the encountered challenges and our successful approach to identifying cysteine residues.

## *6.1 Introduction*

Sulfenylation (-SOH) is one of the post translational modifications (PTMs) in protein cysteine residues, mediated by H<sub>2</sub>O<sub>2</sub>. An efficient probe that traps sulfenylated cysteines is the benzothiazine-based chemoselective probe (BTD) (Gupta and Carroll, 2016). This probe is not commercially available and it was kindly provided by our collaborator Kate Carroll from UFlorida (Scripps research, USA). The BTD probe was used to identify sulfenylated proteins in mammalian and plant cells (Fu et al., 2019; Huang et al., 2019). In this part of the project, we used BTD to trap sulfenylated proteins in *Chlamydomonas*, to better define the H<sub>2</sub>O<sub>2</sub>-cellular signaling and to identify new H<sub>2</sub>O<sub>2</sub>-related proteins. This would provide additional information on the pattern of H<sub>2</sub>O<sub>2</sub>-dependent proteins in *Chlamydomonas* (i.g. glutathionylation and nitrosylation, section 1.3, **chapter I**)

## *6.2 Material and Methods*

### *6.2.1 Trapping assay with BTD probe*

#### *6.2.1.1 Lysis buffer and protein extraction*

Labelled modified proteins with a benzothiazine-based probe BTD were lysate with lysis buffer 1X containing 1.5 % sodium dodecyl sulphate (SDS), 75 mM sodium chloride (NaCl), 50 mM tetraethylammonium bromide (TEAB) pH 7.6, 200 U/mL catalase, 0.25 mM phenylmethylsulfonyl fluoride, 10 mM N-ethylmaleimide (NEM). At the end of the labelling process and subsequent washing of the cells with fresh medium, the resulting cell pellets were resuspended in 2 ml of lysis buffer 1X and kept on ice for a period of 20 min. Then, the samples were vortexed for 20 min at 1000 rpm at room temperature and centrifuged for 30 min at 21,000 g at 4°C. The supernatant was retained and protein content was measured using the BCA assay (Thermo Scientific™ Pierce™, 23225).

### 6.2.1.2 BCA quantification protein assay

Protein extracts were quantified by using BCA protein assay kit (Thermo Scientific™ Pierce™, 23225). Standard curve was prepared from a stock of 10 mg/ml of albumin with serial dilutions. Unknown samples and blank were prepared in triplicate, vortexed and spinned down. 5 µl of each standard curve sample, unknown samples and blank were added to 1 ml of working solution from the kit, vortexed, spinned down and incubated for 30 min at 37°C. At the end of the incubation time, all the samples were vortexed, spinned down and placed on ice to stop the reaction. Protein content was determined by taking 200 µl of each vial into 96-well microplates (BRANDplates®, 781602) and reading the absorbance at 562 nm using the Gen5 software (SynergyMX, BioTek).

### 6.2.1.3 Protocols for checking labelling and identifying modified cysteine residues using streptavidin beads

The capture was performed by following the protocol as in (Fu et al 2019), using streptavidin-sepharose beads (GE-Healthcare, 17-5113-01). To ensure the accuracy of western blotting exposure signals, a labelling check was conducted to remove any interference from endogenous biotinylated proteins present in the extracts. Based on the recommendation by Fu *et al.*, the proportion of beads to protein extracts was maintained at 1:10. Accordingly, 20 µl of beads slurry was pre-washed three times with 0.5 ml of lysis buffer 1X for a duration of 3 min at 1,700 g and 25°C. The beads were then resuspended in the same lysis buffer and added to the protein extracts. The mixture was incubated for 30 min at 4°C before being centrifuged for 3 minutes at 1,700 g and 25°C. The supernatant was collected for the subsequent steps.

To identify modified cysteines, the streptavidin binding beads were used to capture modified peptides, which were subsequently released using UV-light. The same bead-to-peptide proportion as described above was maintained, and the beads slurry was pre-washed twice with 1 ml of streptavidin binding buffer (83 mM sodium acetate in 1 L of HPLC-grade H<sub>2</sub>O, pH 4.5 with acetic acid). The beads were then resuspended in the same buffer and added to the clicked (3.5.2.1.4) and cleaned (3.5.2.1.8.) samples, followed by incubation for 2 h at 25°C in the dark. After incubation, the beads were washed twice with 10 ml of streptavidin washing buffer (2 M sodium chloride in 250 ml of streptavidin

binding buffer) and once with 10 ml of H<sub>2</sub>O, for a duration of 5 min at 1700 g and 25°C. The streptavidin beads were then resuspended in 0.5 ml of 25 mM ammonium bicarbonate for the subsequent steps.

#### 6.2.1.4 Copper(I)-catalyzed Azide-Alkyne Cycloaddition (CuAAC)

The Copper(I)-catalyzed Azide-Alkyne Cycloaddition (CuAAC), also known as “click-reaction”(Gonzalez-Lainez et al 2022), is a copper-catalysed reaction between an azide and an alkyne to form a five-membered heteroatom ring (Fu et al 2019). For labelling checking we used the protocol as described in (Huang et al 2019). After precipitation, protein pellets were resuspended by sonication in 20 µl in phosphate buffered saline with 2% sodium dodecyl sulphate. After resuspension, 80 µl were added to reach the final concentration of sodium dodecyl sulphate at 0.4%. Resuspended proteins were quantified as described in section 3.5.2.1.2 and 80 µg total sample were incubated with click-reaction reagents by following the proportion indicated as follows.

	Final concentration	Stock	volume for 100 µl
Biotin-azide	0.1 mM	5 mM	2 µl
Copper sulfate	0.25 mM	12.5 mM	2 µl
BTTP	0.5 mM	10 mM	5 µl
Sodium ascorbate	2.5mM	125 mM	2 µl

Biotin-azide (KeraFast, EVU101) was dissolved in dimethyl sulfoxide (stored at -80°C); copper sulphate is freshly prepared in H<sub>2</sub>O; BTTP (Click Chemistry Tool, 1334179-85-9), 3-(4-((bis((1-(tert-butyl)-1H-1,2,3-triazol-4-yl)methyl)amino)methyl)-1H-1,2,3-triazol-1-yl)propan-1-ol was dissolved in dimethyl sulfoxide (stored at -80°C); sodium ascorbate is freshly prepared in H<sub>2</sub>O.

The samples and reagents were incubated with rotation for 1 h at 25°C in the dark. To stop the reaction, 1 mM of ethylenediaminetetraacetic acid was added, and the samples were kept for SDS-PAGE and western blot analysis. We followed the modified cysteine identification protocol described in (Fu et al 2019). The modified peptides were sonicated in 20 µl of HPLC-grade H<sub>2</sub>O and

10  $\mu$ l of HPLC-grade acetonitrile, and they were quantified as described in section 3.5.2.1.7. The pH of the mixture was checked using pH indicator strips and adjusted to approximately 6 by adding formic acid or ammonium hydroxide, if necessary. For each sample containing 1 mg of total peptides, 10  $\mu$ l of the reagent mix was added. The proportions of the click-reaction reagents were determined based on 1-2 mg of total peptides, and the volumes were adjusted accordingly to the peptides we had (2.5 mg).

	Final concentration	Stock	volume for 40 $\mu$ l
UV-biotin-azide	1 mM	40 mM	1 $\mu$ l
Sodium ascorbate	10 mM	100 mM	4 $\mu$ l
TBTA	1.25 mM	50 mM	1 $\mu$ l
Copper sulfate	10 mM	100 mM	4 $\mu$ l

15.6 mg UV-biotin-azide (KeraFast, EVU102) were dissolved in 50  $\mu$ l dimethyl sulfoxide and 450  $\mu$ l of HPLC-grade acetonitrile (stored at  $-80^{\circ}\text{C}$ ); sodium ascorbate was freshly prepared in HPLC-grade  $\text{H}_2\text{O}$ ; 13 mg TBTA, Tris((1-benzyl-4-triazolyl)methyl)amine (Roth, 7814.4) were dissolved in 50  $\mu$ l dimethyl sulfoxide and 450  $\mu$ l of HPLC-grade acetonitrile (stored at  $-80^{\circ}\text{C}$ ).

The samples were then incubated for 2 h in the dark at  $25^{\circ}\text{C}$ . To stop the reaction 3 volumes of the strong cation exchange (SCX) columns loading buffer were added, samples were centrifuged for 5 min at 20,000 g at  $25^{\circ}\text{C}$  and the supernatant saved to be used for the next step of removing excess click reagents with strong cation exchange columns.

#### 6.2.1.5 SDS-PAGE and immunoblotting

SDS-PAGE and immunoblot analysis were used to evaluate labelled protein signals with and without  $\text{H}_2\text{O}_2$ . Clicked samples were prepared by mixing protein with loading buffer 4X (trisaminomethane - chloridric acid 0.250 M pH 6.8 (Tris-HCl), 8% sodium dodecyl sulfate (SDS), 40% glycerol, 0.2% blue bromophenol). The mixtures were then vortexed, boiled for 5 min at  $95^{\circ}\text{C}$ , centrifuged for 5 min at a max speed of 21,000 g at  $25^{\circ}\text{C}$  and transferred on ice. 13.5  $\mu$ g of total protein was loaded onto. The 12% SDS-PAGE gels. After the

run, one gel was used for western blot analysis and the second one for Coomassie staining. The blotted gel was transferred to a PVDF (Poly(vinylidene fluoride), Cytiva, 1060029) membrane during 1 h at 4°C at 100 V constant. After that, the membrane was rinsed in TBS (50 mM Tris-HCl, 150 mM NaCl, pH 7.5) protein blocked with blocking solution 1% for 1 h with gentle shaking (50 rpm) at 25°C. The membrane was then washed 3 times for 5 min with TBST and incubated for 2 h at 25°C with anti-streptavidin-HRP antibody diluted 1:10000 in TBST (TBS plus Tween-20, 1000:1) with gentle shaking (50 rpm). Membrane was washed again 3 times for 5 min with TBST and incubated for few seconds with revelation mix solution A (AgriserECL Bright Western Blot Detection reagent A) and solution B (AgriserECL Bright Western Blot Detection reagent B) prepared with 1:1 ratio before reveal the signal with iBright FL1000 Imaging System (Invitrogen by Thermo Fisher Scientific). The gel for control loading was washed 3 times for 5 min with H<sub>2</sub>O and incubated O/N with Coomassie (ThermoScientific, 24620).

#### *6.2.1.6 Desalting peptides samples*

Peptides samples in 50 mM ammonium bicarbonate were processed through 60 mg HLB SPE (Hydrophilic-Lipophilic-Balanced, Solid-Phase-Extraction, Waters, cat. no. WAT094226) cartridge columns. HLB SPE columns were conditioned with 1 ml HPLC-grade acetonitrile by gravity flow 2 times and equilibrated with 2 ml HPLC-grade by gravity flow. Samples were loaded on the column by gravity flow. Cartridges were washed with 1 ml HPLC-grade H<sub>2</sub>O, peptides eluted with HLB solvent A 80% acetonitrile and 10% methanol and dried with SpeedVac. Dried pellet was resuspended in HPLC-grade water and acetonitrile by sonication and used for next steps (3.5.2.1.4).

#### *6.2.1.7 Peptides assay quantification*

Peptides were quantified using Thermo Scientific™ Pierce™ Quantitative Colorimetric Peptide Assay, 23275. Standard curve was prepared with the high-quality peptide digest reference standard of 1 mg/ml stock in 20 µl of H<sub>2</sub>O to a final concentration 1 µg/µl. From that, serial dilutions were prepared and 16 µl of each dilution was pipetted into 96-well microplates (BRANDplates®, 781602). The unknown samples were prepared by mixing 2 µl of each sample with 14 µl of buffer solution to make a final volume of 16 µl per well. A blank

sample was also prepared by adding 16  $\mu$ l of buffer solution. Next, 144  $\mu$ l of working reagent from the kit was added to each well and the mixture was allowed to react for 10 min at 25°C. After the reaction time, the absorbance of each sample was measured at 480 nm.

#### *6.2.1.8 Cleaning of the click samples*

The clicked samples were subjected to strong cation exchange columns for removal of excess reagents. The procedure was carried out according to the Pierce SCX Spin Columns Mini (ThermoFisher, 90008). Before proceeding with sample processing, MiniSpin SCX columns were placed into 2 ml microcentrifuge tubes, equilibrated with 0.4 ml purification buffer 25 mM sodium acetate, pH 5.5 and centrifuged for 5 min at 2,000  $g$  at 25°C. Samples were then loaded on the MiniSpin SCX columns and centrifuged for 5 min at 2,000  $g$  at 25°C. Columns were washed two times with 0.4 ml purification buffer for 5 min at 2,000  $g$  at 25°C. Collecting tubes were removed and the columns were placed in new Eppendorf tubes of 1.5 ml. 150  $\mu$ l of elution buffer 25 mM sodium acetate pH 5.5 with 0.5 M sodium chloride were added and the samples centrifuged for 5 min at 2000  $g$  at 25°C. The flowthrough was collected, and the process was repeated once more. The collected flowthrough was pooled and transferred into a 15 ml tube containing 10 ml of streptavidin binding buffer solution (consisting of 83 mM sodium acetate in 1 L of HPLC-grade H<sub>2</sub>O, pH 4.5 with acetic acid) for the binding on streptavidin-Sepharose beads (GE-Healthcare, 17-5113-01) (as described in section 3.5.2.1.3).

## 6.3 Results

### 6.3.1 Final version of the complete protocol

The final version of the whole adapted assay for *Chlamydomonas* is described in **Fig. 1**. Culture of wt strain was launched and grown in mixotrophy under continuous low light intensity and the cells collected at mid-exponential phase ( $2 \times 10^8$  total cells) in triplicate. The pellet was resuspended in 2 ml of fresh medium with 400  $\mu$ M BTD for *in vivo* labelling. After 5 min of dark rotating incubation, 100  $\mu$ M  $H_2O_2$  were added in one of each replicate to compare modified proteins under stress condition with control samples (400  $\mu$ M BTD only) (**Fig. 1 A, B**). Samples were incubated for 15 min with  $H_2O_2$ . After the incubation step, 200 U/ml of catalase were added to remove  $H_2O_2$ , and cells were washed twice with fresh medium to remove the excess of catalase (**Fig. 1 C**). Finally, the cells were lysed by adding 2 ml of lysis buffer 1X (section 6.2.1.1) and the protein content was determined with a BCA assay (ThermoFisher) (section 6.2.1.2). Before proceeding to protein extraction for mass spectrometric sample analysis, we first checked the labelling on immunoblot. Therefore, 200  $\mu$ g of total protein were reduced with 10 mM dithiothreitol to avoid any false positive modification and incubated for 30 min in the dark at 56°C. Then, reduced thiol residues were alkylated with 50 mM chloroacetamide and incubated in the dark for 30 min at 25°C. At this point, endogenous biotinylated proteins were removed on streptavidin beads (section 6.2.1.3) as the following step required a click-addition-reaction (Gonzalez-Lainez et al 2022) with a biotin-azide molecule for immunoblotting analyses using streptavidin antibodies. To do so, we followed the protocol described in Fu *et al.*, 2019. Protein extracts were incubated for 30 min at 4°C and the supernatant collected by 2 min centrifuge at 1700 *g* at 25°C for following steps. Cleaned samples were precipitated with cold acetone overnight, resuspended in phosphate-buffered saline (PBS) + 0.4% SDS and used for click reaction (section 6.2.1.4) as shown in the scheme in **Fig. 1** where the biotin-azide molecule is linked to BTD probe (**Fig. 1 C**). The increase of protein sulfenylation by  $H_2O_2$  treatment was checked on western blot with anti-strep antibodies (**Fig. 1 D**) (section 6.2.1.5). Once checked the labelling and the difference of signal between the control and  $H_2O_2$  treated samples, proteins were prepared for mass spectrometry (**Fig. 1 D, E**). 3-4 mg of total extract was reduced, alkylated, and precipitated with cold acetone



/overnight as described above. The pellet was then resuspended in 0.5 ml 50 mM ammonium bicarbonate, trypsinized O/N at 37°C and desalted with HLB SPE (Hydrophilic-Lipophilic-Balanced, Solid-Phase-Extraction, Waters, cat. no. WAT094226) column (section 6.2.1.6). Peptides were dried in a SpeedVac instrument and resuspended in a solution with water and acetonitrile, quantified (section 6.2.1.7) and used for next steps of click-reaction, cleaned from the excess of reagents with strong cation exchange column (SCX) (section 6.2.1.8) and bound to the streptavidin beads (section 6.2.1.3). For mass spectrometry, click-reaction was performed by using UV-sensitive biotin moiety to be linked to BTB. The UV-sensitive biotin molecule has a special tag for UV light at 365 nm which would release the bond between the BTB and biotin molecule, making it easier to collect the modified peptides trapped on the streptavidin beads. Beads with peptides were placed under UV-light with 4 cycles of 15 min spaced out with 5 min on ice. Peptide release was completed after 1 h incubation at 37°C and the supernatant collected with centrifugation for 5 min at 20,000 x g at room temperature. Samples were quantified and prepared for mass spectrometry injection (**Fig. 16 E**). Mass spectrometry analyses were performed by Didier Vertommen, UCLouvain, Brussels, Belgium.

Before reaching the final version of the trapping assay, we faced quite some problems at the beginning of the procedure which are described in the following sections.

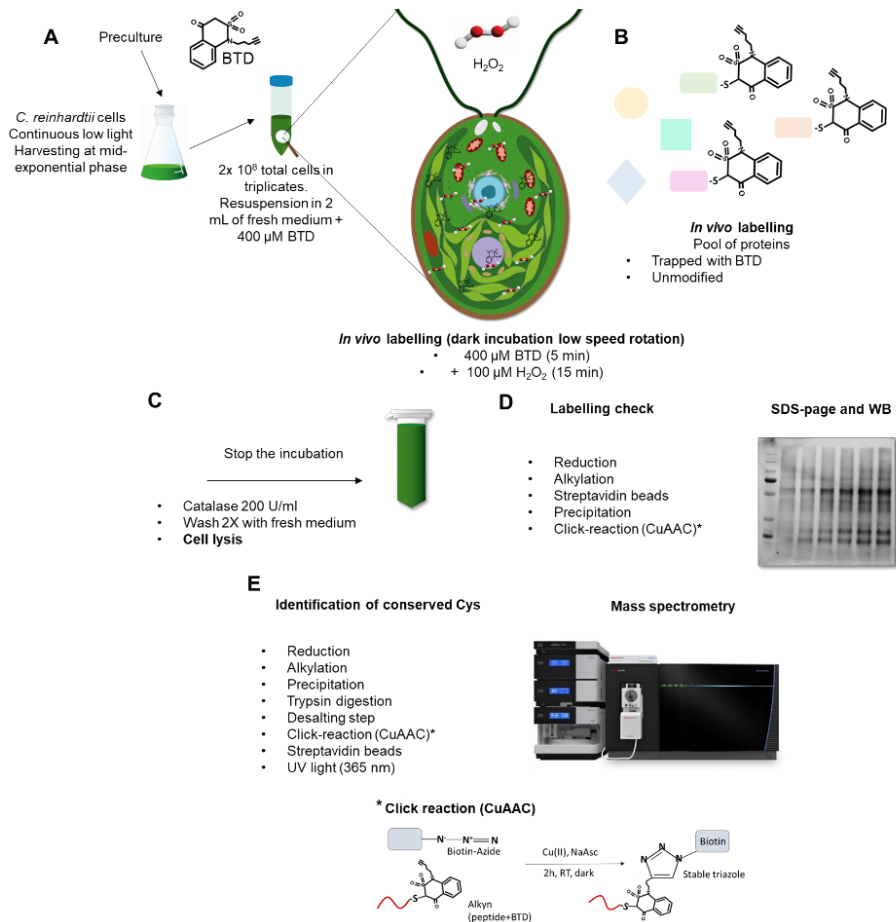


**Figure 1: Schematic overview depicting the complete protocol for capturing modified cysteine residues.** **A, B)** Cell collection and labelling *in vivo* with 400 μM BTD probe for control condition and with addition of 100 μM H<sub>2</sub>O<sub>2</sub> for stress condition. **C)** Stop the labelling and the H<sub>2</sub>O<sub>2</sub> action with 200 U/ml catalase and lysate the cells to extract proteins. **D)** Labelling check with WB analysis. Reduce, alkylate, and clean protein extracts from endogenous biotinylated proteins with streptavidin beads. Precipitate protein extracts, resuspend the pellet and add biotin molecule to BTD probe by click-reaction (CuAAC)\*. Check labelling by SDS-PAGE and immunoblot with anti-streptavidin antibodies. **E)** Identification of conserved cysteine residues. Reduce, alkylate and precipitate protein extracts. Digest protein with trypsin, desalt the samples and add UV-biotin molecule to BTD probe by click-reaction (CuAAC)\*. Remove the excess of click reagents with SCX columns and elute modified peptides. Incubate peptides with streptavidin beads and release them by UV-light at 365 nm. Quantify peptides and prepare the samples for mass spectrometry injection.

### 6.3.2 Selection of the strain

First trials of labelling were performed with CC-4533 *cw15* mt<sup>-</sup> wt strain from the CLiP library where the cells seemed to be stressed already without any H<sub>2</sub>O<sub>2</sub> addition. One of the trials, is shown in **Fig. 2 A** where the signal between the control and treated cells is not so evident and not consistent between the three replicates. One possible explanation for the absence of a signal increase could be the potential overoxidation of cysteine residues, leading to sulfinylation (-SO<sub>2</sub>H) or sulfonylation (-SO<sub>3</sub>H), which may render the method less suitable for capturing sulfenylated cysteines (-SOH). Consequently, the observed signal might be similar to that of the control sample. To address this issue, which may have been caused by the absence of the cell wall and its impact on the cell physiology during labelling, we utilised the wt strain wt137C from the laboratory collection that retains its cell wall. A gradient of increasing H<sub>2</sub>O<sub>2</sub> concentrations was tested to evaluate the differences in the signal. The signal variations observed at increasing H<sub>2</sub>O<sub>2</sub> concentrations, as presented in **Fig. 2 B**, led us to conclude that pursuing work on cell-wall-plus-strain would be the way to proceed. Among the several attempts conducted, the most relevant are reported.

### 6.3.3 BTD probe and cell concentrations are important

The concentration of 400 µM BTD was chosen according to (Huang et al 2019). We tested different cell concentrations incubated with the same concentration of probe, in order to standardize the conditions (**Fig. 3**). From **Fig. 3**, we decided to label 10<sup>8</sup> cells with 400 µM BTD because the difference between untreated and H<sub>2</sub>O<sub>2</sub>-treated cells can be seen. However, considering the variable efficiency of the BTD probe, a check on cell concentration and BTD concentration would be required each time an experiment is performed.

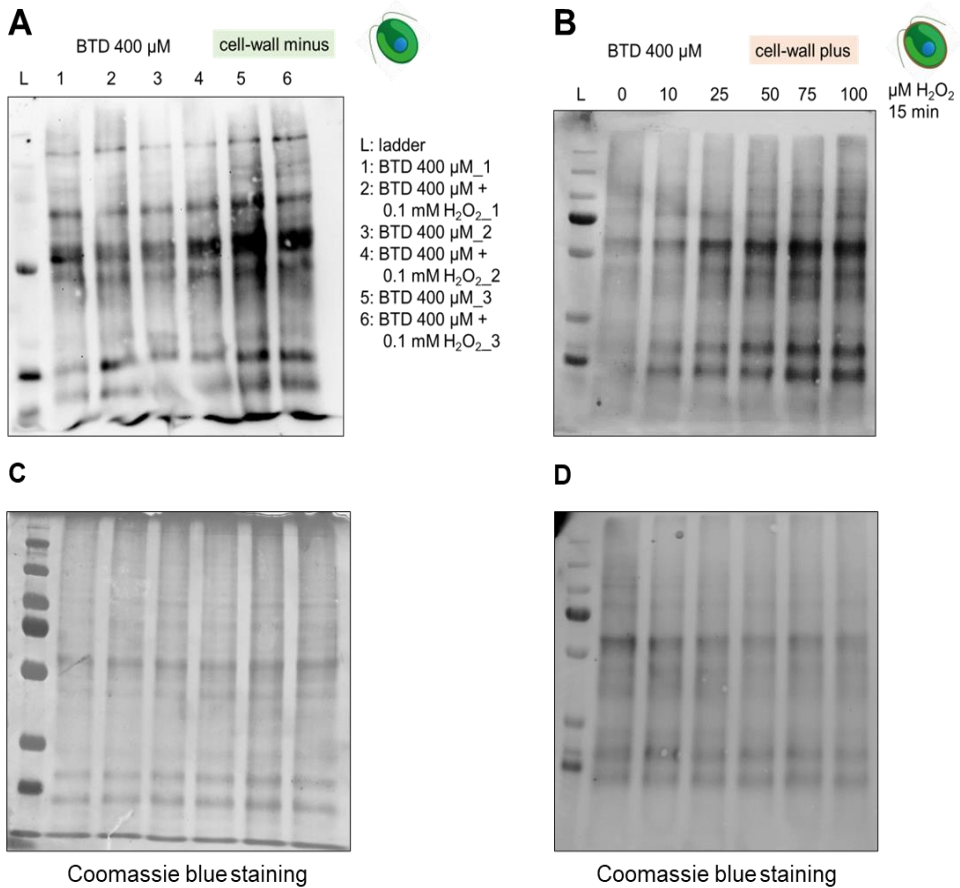


**Figure 2: Immunoblot analysis shows that the cell-wall-plus-strain is suitable for labelling Cys-modified proteins.** **A)** Labelled proteins of cell-wall less *Chlamydomonas* strain. Lanes are triplicate of control + treated sample. **B)** Labelled proteins of cell-wall plus *Chlamydomonas* strain with increasing  $\text{H}_2\text{O}_2$  concentration. Control sample has been incubated with BTD for 20 min, treated samples were incubated with BTD for 5 min + 15 min with  $\text{H}_2\text{O}_2$ . 13.5  $\mu\text{g}/\text{well}$  loaded, anti-streptavidin antibody dilution 1/10000. **C)** and **D)** are the Coomassie blue staining of **A)** and **B)** respectively.

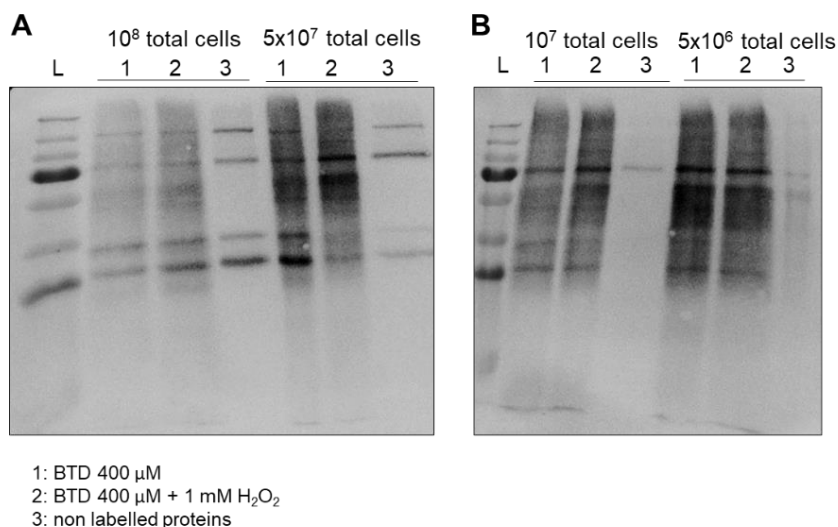


**Figure 3: Immunoblot analyses show that cell and BTD concentrations are important for protein labelling.** A) and B) Labelled protein of cell-wall-plus-strain wt 137C with different cell concentration incubated with 400  $\mu$ M BTD. Control samples have been incubated with BTD for 20 min in the dark, treated samples were incubated with BTD for 5 min + 15 min with H<sub>2</sub>O<sub>2</sub> in the dark. 6  $\mu$ g/well loaded, anti-streptavidin-HRP antibody dilution 1/10000.

#### 6.3.4 Elimination of chlorophyll

Another issue we faced was related to the presence of chlorophyll in the protein extract which caused problems during the desalting step with the HLB SPE (Hydrophilic-Lipophilic-Balanced, Solid-Phase-Extraction) column. To limit the interference of the chlorophyll in the desalting process, we compared two different ways of precipitation. Initially, we attempted the methanol/chloroform technique (outlined in the "Methods" section) following the approach outlined in (Fu et al 2019). However, the challenge we encountered was not present in the investigations carried out by Fu et al. and Huang et al., as they respectively focused on mammalian cells and plant cell suspensions. With the methanol/chloroform method we could remove a bit of chlorophyll, but still it was not enough to completely recover the yield of the starting material. We tried to solve this problem by simply using cold acetone precipitation overnight and washing the pellet once with cold acetone. With this method we could recover at least 80% of the starting material contrary to the previous method with which we recovered less than 50%. Consequently, we opted for cold acetone precipitation.

### 6.3.5 UV incubation for peptide release

Another important step was the release of peptides from the streptavidin beads. The UV-biotin-azide used in the click-reaction harbours a UV-tag released at 365 nm. In Fu et al., this step is performed by incubating biotinylated BTD-trapped peptides for 2 h in the dark under UV-light, at room temperature, with shaking, to avoid any beads precipitation that could compromise the photo-release. Using this procedure, we could not identify any peptide and modified cysteines by mass spectrometry. Furthermore, due to the strong UV-light used, the temperature of the tube containing the samples, increased. Therefore, we tried to reduce the time from 2 h to 20 min, to avoid any damage to the peptide due to the temperature. We have tried to expose the samples with one or two cycles of 20 min each, to compare the number of peptides released. For those samples submitted to two cycles of 20 min, we could identify 27, 16 and 7 peptides, in the three replicates of wt 137C strain without any addition of H<sub>2</sub>O<sub>2</sub>. Two peptides were found in common between the three replicates: one corresponding to three of the light harvesting complexes of PSII (LHCBM2, LHCBM3 and LHCBM5) and one corresponding to an ADP, ATP carrier protein (AAA1) predicted in the chloroplast. The samples exposed for only one cycle of 20 min under the UV-light were those ones of wt137C treated with 0.1 mM H<sub>2</sub>O<sub>2</sub> or 1 mM H<sub>2</sub>O<sub>2</sub>. Only one replicate was analyzed and we could not perform any statistics. We could identify 4 and 10 peptides respectively (**Table 1**, 0.1 mM H<sub>2</sub>O<sub>2</sub> and **Table 2**, 1 mM H<sub>2</sub>O<sub>2</sub>). From these results, we concluded that the best option for future experiments is to perform two cycles of UV-light incubation to increase the number of peptides released.

### 6.3.6 Sulfenylated peptides

One of the peptides identified in the three replicates of wt137C strain in control condition without H<sub>2</sub>O<sub>2</sub>, is common to LHCBM3, LHCBM5 and LHCBM2 (Takahashi et al 2006) involved in the mechanism of state transition (discussed in section 1.1.3.3 of the “Introduction” **Chapter I**, 3.1.3.4 and 3.1.3.5 of the “Results” **Chapter III**) (highlighted in bold, **Fig. 4 A**). Those proteins are members of the major light harvesting complex of PSII. The alignment of those sequences with other CrLHCBM proteins and their orthologs in Arabidopsis (Umate 2010) shows that the identified cysteine, highlighted in red (**Fig. 4 A**) is conserved. The sulfenylated cysteine is located within the hydrophobic region of

an alpha-helix of the protein (**Fig. 4 B**). So far, this is the first time that sulfenylation in the LCHBM proteins is reported and further investigation should be conducted to define the biological significance. However, we can suggest that the sulfenylated cysteine which might be involved in the LCHBMs regulation. LHCBM2 and LHCBM3, are two of the most abundant antennas of *Chlamydomonas* and they were found associated with the PSII supercomplexes (Drop et al., 2014). LHCBM5 has not be found associated with the PSII (Drop et al., 2014), but all of them have been suggested to participate in the state transition (Takahashi et al 2006). Sulfenylation of cysteine might help the regulation of the LCHBM movement together with phosphorylation. Moreover, sulfenylation might have also been involved in the functional and structural organization of the supercomplexes.

The second peptide identified corresponds to the ADP, ATP carrier protein 1 (AAA1, Cre08.g358526) predicted in the chloroplast. Three ADP, ATP carrier proteins (two chloroplastic and one mitochondrial), were also identified in the analysis of the sulfenome of *Arabidopsis* (Huang et al 2019), however, none of them is the ortholog of the one of *Chlamydomonas*. The AAA1 transporter is involved in the import of the ATP into the chloroplast for metabolic process like the Calvin-Benson-Bassham cycle (CBB) (Johnson & Alric 2013).

**A**

```

AtLHCB3      -----FAKNRALEVIHGRWAMLGAFGCITPEVLQKWVRVDFKEPVWFKAGSQIFSEGGLD 143
AtLHCB1.5    -----FARNRELEVIHSRWAMLGALGCVFPELLARN-GVKFGEAVWFKAGSQIFSDGGLD 143
AtLHCB1.4    -----FARNRELEVIHSRWAMLGALGCVFPELLARN-GVKFGEAVWFKAGSQIFSDGGLD 144
AtLHCB2.1    -----FAKNRELEVIHSRWAMLGALGCTFPEILSKN-GVKFGEAVWFKAGSQIFSEGGLD 144
AtLHCB2.2    -----FAKNRELEVIHSRWAMLGALGCTFPEILSKN-GVKFGEAVWFKAGSQIFSEGGLD 144
AtLHCB2.4    -----FAKNRELEVIHSRWAMLGALGCTFPEILSKN-GVKFGEAVWFKAGSQIFSEGGLD 177
CrLHCBM5    -----FKRYRELELIHARWAMLGALGCITPELLAKN-GTPIVEPVWFKAGAQIFAEGGLD 147
CrLHCBM1     -----FKRYRELELIHARWAMLGALGCIFPELLGSY-GVPFGEAVWFKAGAQIFQEGGLD 136
CrLHCBM2    -----FKRYRELELIHARWAMLGALGCITPELLAKN-GIPFGEAVWFKAGAQIFAEGGLN 128
CrLHCBM7     -----FKRYRELELIHARWAMLGALGCITPELLAKN-GIPFGEAVWFKAGAQIFAEGGLN 128
CrLHCBM3    -----FKRYRELELIHARWAMLGALGCITPELLAKS-GTQFGEAVWFKAGAQIFSEGGLD 136
CrLHCBM4     -----FKRYRELELIHARWAMLGALGCLTPELLAKN-GTKFGEAVWFKAGAQIFSEGGLD 133
CrLHCBM8     -----FKRYRELELIHARWAMLGALGCLTPELLAKS-GTKFGEAVWFKAGAQIFSEGGLD 133
CrLHCBM6     -----FKRYRELELIHARWAMLGALGCLTPELLAKS-GTKFGEAVWFKAGAQIFSEGGLD 132
  
```

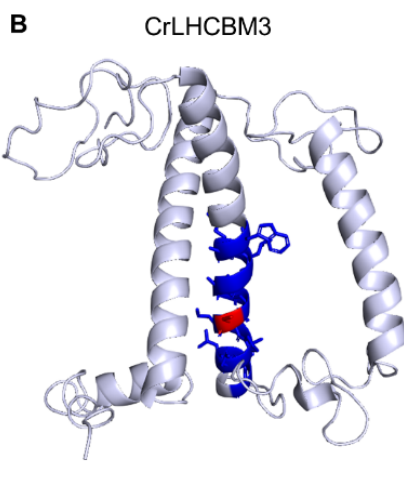


**Figure 4: Analysis of the identified peptides shows the conserved Cys. A)** Alignment of AtLHCB proteins with CrLHCB and CrLHCBM proteins. Identified proteins are highlighted in bold, the identified peptides with MS are highlighted in bold and blue and the modified cysteine is highlighted in bold and red. Peptides and cysteine are conserved in some of the protein sequences. **B)** Structure of monomeric CrLHCBM3 protein (PDB code: 6KAF, (Shen et al 2019). In blue the identified peptide is highlighted, in red the modified cysteine.



**Table 1.** Identified peptides with conserved sulfenylated cysteines of wt137C sample treated with 0.1 mM H<sub>2</sub>O<sub>2</sub>.

Annotation number	Gene symbol	Description	Putative localization	Peptide and modified cysteine identified
Cre16.g663900	PBGD1	Porphobilinogen deaminase	Chloroplast	AFLTALDGS CR
Cre01.g012150	MSRA4	Peptide methionine-S-sulfoxide reductase, msrA-type	Mitochondria	ATFAAGCF WGPELAFQ R
Cre02.g120100	RBCS-1	Ribulose bisphosphate carboxylase small chain 1	Chloroplast	LPMFGCR
Cre12.g542250	TUB1	Tubulin beta chain	Other	NMMCAADP R

**Table 2.** Identified peptides with conserved sulfenylated cysteines of wt137C sample treated with 1 mM H<sub>2</sub>O<sub>2</sub>.

Annotation number	Gene symbol	Description	Putative localization	Peptide and modified cysteine identified
Cre12.g516200	EFG2	Elongation factor 2	Other	TVL <b>C</b> MGR
Cre16.g663900	PBGD1	Porphobilinogen deaminase	Chloroplast	AFLTALDGS <b>C</b> R
Cre12.g542250	TUB1	Tubulin beta chain	Other	EIVHIQGGQ <b>C</b> GNQIGAK
Cre02.g080900	PRX4	Peroxiredoxin type II	Mitochondria	VILVGFPGG P <b>V</b> C <b>V</b> EK
<i>Chloroplastic gene</i>	PsaA	Photosystem I P700 chlorophyll <i>a</i> apoprotein A1	Chloroplast	F <b>P</b> <b>C</b> DGPGR
CreCp.g802313	rbcL	Ribulose biphosphate carboxylase large chain	Chloroplast	AVYE <b>C</b> LR
Cre01.g012150	MSRA4	Peptidylprolyl isomerase	Mitochondria	ATFAAG <b>C</b> F WGPELAFQ R
Cre03.g180750	METE1	Cobalamin-independent methionine synthase	Other	IWVNP <b>D</b> CGL K
Cre05.g234550	FBA3	Fructose-1,6-biphosphate aldolase 1	Chloroplast	VMFEGILLK PAMVTPGA <b>D</b> C <b>K</b>
Cre12.g542250	TUB1	Tubulin beta chain	Other	NMM <b>C</b> AADP R

## 6.4 Discussion

As already mentioned above, unfortunately we could not succeed in defining a proper and reproducible workflow for BTB labelling in *Chlamydomonas* cells. However, despite the difficulties faced during the optimization of the protocol, we could identify a few modified peptides and most importantly, define the main steps that still need to be improved to make the whole assay reproducible.

Selecting the appropriate strain was one of the primary challenges we addressed. Previous studies (Fu et al 2019, Huang et al 2019) were conducted with BTB labelling after cell lysis, which avoided the problem of over-stressing the cells during *in vivo* labelling. We could observe that the presence of the cell-wall protects the cell from over-oxidation, as noticed from immunoblotting analyses. To further limit protein oxidation, performing the labelling step in anaerobic condition would be an option. This will avoid any contact with oxygen even though we introduce catalase during the washing step to remove excess of H<sub>2</sub>O<sub>2</sub> and during lysis step. Moreover, it would be useful to check different probe concentrations to have a basal signal in a control sample in contrast with a higher signal in treated samples. Regrettably, our ability to work with various probe concentrations was limited due to low probe availability. To overcome this hurdle, we experimented varying cell numbers while maintaining a constant probe concentration. This approach aimed to identify the optimal combination that yielded both a satisfactory protein yield and a desirable signal. Through experimentation, we determined that using 10<sup>8</sup> total cells with 400 µM BTB yielded the most favourable signal.

The second and more challenging problem we faced was the chlorophyll content in the protein extract which interfered with the column for desalting steps. After testing several methods of protein precipitation with methanol:chloroform and acetone, we found that the best option was acetone precipitation to reduce the chlorophyll content as much as possible. However, in our scenario, this proved insufficient, leading to significant material loss. To circumvent this challenge, one could consider altering the chromatographic column, opting for an alternative procedure, or refining this particular step, as outlined in the work by (McConnell et al 2018). Unfortunately, for our specific situation, sidestepping this issue prior to initiating the click reaction wasn't feasible due to the necessity of resuspending the samples in ammonium bicarbonate for trypsin digestion. The presence of ammonium bicarbonate, although it is volatile and can be removed

through SpeedVac, would have disrupted the desired pH level (around 6) for the ensuing click reaction step.

Even though the chlorophyll removal is still challenging, another possibility would be optimising the click reaction as described in (Berg & Straub 2013) to increase the percentage of labelling of BTD-modified-peptide complexes with biotin. Notwithstanding these challenges, especially the presence of chlorophyll, we managed to successfully identify a small set of proteins associated with photosynthesis. Notably, we identified a peptide of the light-harvesting complexes (LHCBMs), crucial for light capture and state transitions. This process aims to harmonize energy distribution between photosystem II and photosystem I. One of the LHCBMs, namely LHCBM3, has been previously observed to undergo nitrosylation (Morisse et al 2014). The identified peptide underlined in **Fig. 4 A** (WAMLGALGCITPELLAK) is widely conserved among all the LHCBM proteins of *Chlamydomonas* and some of the LHCB proteins of *Arabidopsis*. The fact that we could detect modified cysteine in photosynthetic proteins is promising, and could open a deep study on the sulfenylation process during photosynthesis. Moreover, it is also important considering that the study in *Arabidopsis* was conducted on cell suspension and no photosynthetic related proteins have been identified (Huang et al 2019).

## Chapter VII: General discussion and perspectives

In photosynthetic organisms, chloroplasts are one of the main sources of reactive oxygen species (ROS). In the past, ROS were viewed as harmful to cells, causing the oxidation of proteins, lipids, or nucleic acids and leading to cell death. However, current perspectives recognize their dual role. ROS can now be seen as signaling molecules facilitating communication between organelles. They play a part in both anterograde signaling (from the nucleus to mitochondria and chloroplasts) and retrograde signaling (from mitochondria and chloroplasts to the nucleus) (Jung & Chory 2010). ROS produced during photosynthesis are superoxide anion ( $O_2^-$ ), singlet oxygen ( $^1O_2$ ), hydrogen peroxide ( $H_2O_2$ ) and hydroxyl radical ( $\cdot OH$ ) (Asada 2006). In this project, I focused on  $H_2O_2$  due to its longest half-life and capability to migrate over longer distances (Mittler 2017).  $H_2O_2$  can modify proteins in their cysteine residues into their sulfenylated form ( $-SH \rightarrow -SOH$ ) (Lo Conte & Carroll 2013). This post-translational modification leads proteins to change their conformation and function, assisting the cell in adapting to various stress stimuli (Mukherjee 2021).

The aim of my project was to identify the pattern of proteins that are sulfenylated at the cysteine residues, referred to as sulfenome, in the model organism green alga *Chlamydomonas reinhardtii*. This investigation sought to define  $H_2O_2$ -dependent redox signaling. Our strategies involved (i) a molecular, genetic, and physiological analysis of mutants affected in  $H_2O_2$ -scavenging enzymes under diverse stress conditions (inducing endogenous  $H_2O_2$  production or by adding  $H_2O_2$ ); (ii) a proteomic approach to trap and identify sulfenylated protein using a chemical BTD probe.

### 7.1 General discussion

#### 7.1.1 Exploring the phenotype of mutants affected in $H_2O_2$ -scavenging enzymes revealed complex effects of gene disruption

A molecular, genetic, and physiological characterization of selected mutants (**Table 1, chapter III**) has been described in **chapter III**. A variety of mutants affected in genes involved in ROS and more specifically in  $H_2O_2$  scavenging, was chosen to have a wide spectrum of possible cell responses: mutants with disruption in genes coding for enzymes directly (ascorbate peroxidase APX, catalase CAT, glutathione peroxidase GPX) or indirectly [nucleoredoxin 1

(NRX1), nucleoredoxin 2 (NRX2), sulfiredoxin 2 (SRX2)] involved in the H<sub>2</sub>O<sub>2</sub> detoxification or influencing/interacting with ROS molecules [glutathione-S-transferase 13 (GST13), truncated hemoglobin 5 (THB5), respiratory burst oxidase 1 (RBOL1), ATP-ase-AAA (LCA1)].

The phenotypical exploration conducted by drop tests on agar media in different conditions, did not show any differences in growth between the mutants and the wt (some examples are reported in **Fig. 4, chapter III**). This was probably due to the capacity of the mutant cells to respond to stress stimuli (*i.e.* growth under continuous high light) with compensatory mechanisms, or due to a low ROS cellular production under the high light stress condition. A study conducted on the *Chlamydomonas* mutant lacking the glutathione peroxidase 5 (GPX5) enzyme, showed cell growth by drop test in stress condition in the presence of the photosensitizer Rose Bengal (RB) which leads to <sup>1</sup>O<sub>2</sub> production. The effect of stress depicted by drop tests, is more pronounced in the mutant compared to the wt strain (Ma et al 2020a). In this study, transcriptional analyses were conducted using RNASeq and qRT-PCR in the wt and the *gpx5* mutant with and without RB treatment. Among the up-regulated enzymes found in the *gpx5* mutant under control condition there were *NRX2*, *NRX3* and *SRX2*. In RB treated samples, up-regulated *APX1*, *SRX2* have been found in both wt and *gpx5*. Increase of *SRX2* and *NRX2* transcripts was also observed in another study, in which transcriptomic analyses were performed in *Chlamydomonas* wt strain in the presence of H<sub>2</sub>O<sub>2</sub> or RB (Blaby et al 2015). This supports the hypothesis that under our experimental conditions with *Chlamydomonas* mutants, additional antioxidant enzymes may undergo up-regulation to mitigate the impact of ROS production. Moreover, it suggests that the potential cellular signaling does not adversely affect cell growth.

In photosynthetic organisms, a way to evaluate the fitness of the cell, is monitoring photosynthetic parameters by measuring *in vivo* fluorescence of chlorophyll *a*, originated at the photosystem II (PSII). A common parameter that can be monitored, is the maximum efficiency of PSII (also referred to as Fv/Fm). This measurement has demonstrated to be very sensitive to the functioning of the photosynthetic machinery (Maxwell & Johnson 2000). In the above-mentioned study of (Blaby et al 2015), the authors showed that the addition of 1 mM H<sub>2</sub>O<sub>2</sub> affects the maximum efficiency of PSII by decreasing the Fv/Fm value after 30 min. On the contrary, in our measurements the addition of 1 mM H<sub>2</sub>O<sub>2</sub>,

led to a slight increase of the Fv/Fm value in some of the mutants after 15 min or 30 min exposure to H<sub>2</sub>O<sub>2</sub> compared to control condition without H<sub>2</sub>O<sub>2</sub> (**Table 3** and **Table 4, chapter III**). The increase of Fv/Fm that we observed, might be explained as a consequence of the redox state of plastoquinone (PQ), which might be oxidized by plastoquinol terminal oxidase (PTOX), localized at the level of PSII in the photosynthetic chain. In condition of dark acclimation, PTOX uses PQ as electron donor to reduce O<sub>2</sub> into H<sub>2</sub>O (Joet et al 2002). The oxidation of PQ can influence minimal chlorophyll fluorescence, leading to an augmentation of variable fluorescence (Fm-Fo). Consequently, this contributes to an elevation in the Fv/Fm value (Hohmann-Marriott et al 2010). It is conceivable that in mutants exhibiting elevated Fv/Fm values, the dark incubation preceding the measurements could enhance PTOX activity, facilitating the oxidation of PQ. This, in turn, leads to an increase in Fv/Fm, while H<sub>2</sub>O<sub>2</sub> is scavenged by the thioredoxin system within the chloroplast (Nikkanen & Rintamäki 2019). Another hypothesis is that plastoquinol is directly oxidized by the H<sub>2</sub>O<sub>2</sub>. Moreover, variations in Fv/Fm values among cells under treatment and control conditions may have also been influenced by technical factors, such as non-standardized measurement conditions (e.g., chlorophyll content or cell numbers).

### *7.1.2 Mutants of APX2 and SRX2 enzymes displayed different photosynthetic activities*

Among the mutants screened, we selected *apx2* and *srx2* mutants. Both mutants are affected in genes coding for enzymes putatively localized in the chloroplast and directly and indirectly involved in H<sub>2</sub>O<sub>2</sub> scavenging respectively. APX2 falls into a novel class of ascorbate peroxidase-related (APX-R) enzymes, capable of converting H<sub>2</sub>O<sub>2</sub> into H<sub>2</sub>O without relying on ascorbate as an electron donor (Caccamo et al 2023, Lazzarotto et al 2021b) (**Fig. 1 A**). SRX2, sulfiredoxin 2, is a member of the class of thioredoxins. It regulates the redox state of 2-Cys PRX, reducing the oxidized form of 2-Cys PRX-SO<sub>2</sub>H to 2-Cys PRX-SOH. This 2-Cys PRX then directly reduces H<sub>2</sub>O<sub>2</sub> (**Fig. 1 B**) (Dietz 2011).

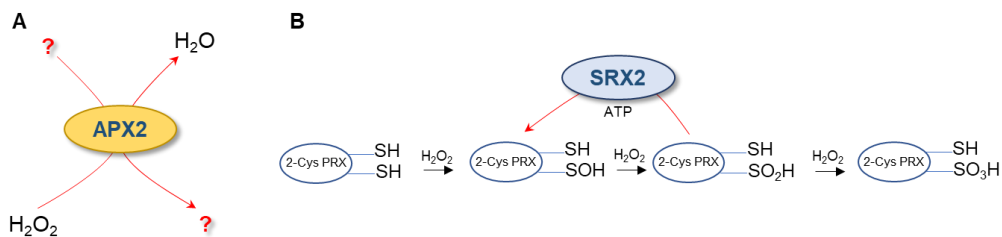


**Figure 1: Schemes of APX2 and SRX2 catalytic reaction mechanisms.** **A)** APX2 can scavenge  $\text{H}_2\text{O}_2$  into  $\text{H}_2\text{O}$ , but it does not use ascorbate as reductant and the substrate *in vivo* is still unknown. **B)** SRX2 catalyzes the conversion of the sulfinic acid of 2-Cys PRX ( $-\text{SO}_2\text{H}$ ) into its sulfenic form ( $-\text{SOH}$ ) using ATP. In over-stressing conditions, sulfinic form of 2-Cys PRX ( $-\text{SO}_2\text{H}$ ) undergoes to over-oxidation into its sulfonic form ( $-\text{SO}_3\text{H}$ ), which cannot be reduced by the SRX enzyme.

When evaluating cell fitness through measurements of *in vivo* fluorescence of chlorophyll *a*, both *apx2* and *srx2* mutants showed similar PSII activity ( $F_v/F_m$ ) as the wt (**Fig. 5A, 8A, chapter III**). However, we could highlight distinctions between mutants and wt by analyzing the relative electron transport rate (rETR) in control and stress condition by the addition of  $\text{H}_2\text{O}_2$ . The *srx2* mutant displayed higher rETR than wt in control conditions and in presence of  $\text{H}_2\text{O}_2$  after 1 h and 6 h incubation, in light intensity above  $100 \mu\text{mol photons m}^{-2} \text{s}^{-1}$  (**Fig. 5 C, 5 E, chapter III**). Similarly, Arabidopsis *srx1* mutant lines (ortholog of SRX2 in Chlamydomonas) subjected to high light and cold temperature, presented less stress effect than the wt (reduced leaf bleaching, increasing photosynthetic activity and decreased lipid oxidation) (Rey et al 2007). In addition, the authors also observed an increase of the sulfinylated ( $-\text{SO}_2\text{H}$ ) form of 2-Cys PRX (substrate of SRX1) indicative of the function of the SRX1 enzyme to reduce the sulfinylated form of the 2-Cys PRX in its sulfenylated form (Rey et al 2007). The authors proposed that the low levels of sulfinylated 2-Cys-PRX present in AtSRX1 mutant lines in mild stress conditions, to which plant can adapt, act as a ROS sensor that would trigger antioxidant defenses. We can then hypothesize a similar scenario in the Chlamydomonas *srx2* mutant, in which the addition of 1.5 mM  $\text{H}_2\text{O}_2$  constitute a mild stress environment as Chlamydomonas can tolerate up to 2 mM  $\text{H}_2\text{O}_2$  (Shao et al 2008). Therefore, increase of sulfinylated form of 2-Cys PRX might help to protect the cells from the oxidative stress. This would explain the increase of the rETR in the *srx2* mutant, especially in the presence of  $\text{H}_2\text{O}_2$  (**Fig. 5 E, chapter III**).



On the contrary, *apx2* mutant displayed lower rETR than the wt, especially after 6 h of H<sub>2</sub>O<sub>2</sub> incubation (**Fig. 5 F, chapter III**). The reduced rETR may be attributed to damage in PSII, to the up-regulation of non-photochemical quenching (NPQ), to a slowdown of the electron transport reactions beyond PSII, or to the impaired state transitions (which balance antenna sizes between PSII and PSI in low light conditions) (Hohner et al 2020). Considering that the PSII activity of the *apx2* mutant remains intact, other possibilities reside among the above-mentioned ones.

In general, no decrease of rETR has been observed between control and H<sub>2</sub>O<sub>2</sub> conditions within wt, *apx2* and *srx2* mutants (**Fig. 5, chapter III**). This was probably related to the H<sub>2</sub>O<sub>2</sub> concentration, which was in the range of tolerance for *Chlamydomonas* (Shao et al 2008). Therefore, to increase the susceptibility to oxidative stress and the response to H<sub>2</sub>O<sub>2</sub>, the double mutant *dl* was generated by crossing *srx2* and *apx2* mutants. Interestingly, we noticed an increased PSII activity in the *dl* mutant (**Fig. 8 A and 8 B, chapter III**) when compared to the wt, as well as the *srx2* and *apx2* mutants. This could be attributed to the presence of overoxidized 2-Cys PRX (-SO<sub>2</sub>H) in the *dl* mutant, as it lacks SRX2. The absence of SRX2 could contribute to the elevation of PSII activity. Additionally, since *dl* also lacks APX2, the increased PSII activity might be linked to other mechanisms that warrant further exploration for identification.

Further investigations on the possibility of the lower rETR of the *apx2* mutant, were carried out by measuring non-photochemical quenching (NPQ), as indication of PSII photoprotection capacity, induced by high light incubation. Measurements were conducted on wt, the three mutants *apx2*, *srx2*, *dl*, and a mutant of the serine/threonine kinase (STT7) involved in state transition (qT) (Depege et al 2003). qT is a constituent of NPQ associated with PSII-antenna state transitions, a process in which the light-harvesting complexes (LHCII) shift between PSII and PSI (**chapter I, 1.1.3.3**). The migration of LHCII from PSII to PSI is facilitated by phosphorylation, a process dependent on the kinase STT7 in *Chlamydomonas* (Fleischmann et al 1999). No differences in the NPQ induction are observed in the *apx2* mutant compared to the wt, ruling out the possibility that NPQ was responsible for the reduced rETR. Similar NPQ induction is observed in *srx2* and *dl* mutants, except for *dl* in low-light cells in which the induction was faster as well as in the *stt7* mutant. Indeed, *stt7* displays faster induction of NPQ (Girolomoni et al 2019). However, the qT fraction was lower

in *apx2* and *d1* mutants, similarly to *stt7*, compared to the wt in low-light cells. This might suggest that state transition might be impaired in the *apx2* mutant, causing lower rETR, as also observed in *d1* mutant (**Fig. 8 C, chapter III**). One explanation might be related to the H<sub>2</sub>O<sub>2</sub>-dependent activity of the STT7. It has been proposed that the activity of the STT7, which presents two cysteine residues at the luminal side (Lemeille et al 2009), depends on H<sub>2</sub>O<sub>2</sub>. The oxidation of the cysteines, would lower the STT7 activity, preventing the phosphorylation and in turn, the migration of LHCII (Puthiyaveetil 2011, Roach et al 2015). One hypothesis could be that the low fraction of qT observed in the *apx2* and *d1* mutants, might depend on H<sub>2</sub>O<sub>2</sub>.

However, assessments of chlorophyll fluorescence emission at 77 K originating from PSI and PSII revealed that the *apx2* mutant, similar to the *d1* mutant, is capable of transitioning to state II (**Fig. 9 F, chapter III**). Notably, the *apx2* mutant exhibits a more pronounced shift compared to the wild type and other mutants. Further, in the condition we tested to induce state I transition (far-red light incubation), *apx2* mutant could not reach a full state I (**Fig. 9 E, chapter III**) suggesting that a portion of the LHCII antenna cannot shift from PSI to PSII. However, this shift may be constrained by PQ kept in reducing state.

Due to this interesting phenotype, we decided to continue working on the *apx2* mutant to study the role of APX2 during photosynthesis. We did not further explore the phenotype of the *srx2* and the *d1* mutants, which indeed would be interesting to investigate considering their photosynthetic performance.

### *7.1.3 The apx2 mutant exhibits a distinct photosynthetic poise compared to the wild type*

The capacity to perform state transition in the *apx2* mutant was assessed by chemically induction of state I and state II with DCMU and FCCP, respectively. In the presence of those chemicals, wt and *apx2* mutant presented a similar profile, confirming that the tendency of the *apx2* mutant to be in state II depends on reduced PQ (PQH<sub>2</sub>). This raised the question about the electron transport downstream PSII, leading us to investigate the redox state of the primary electron donor of PSI, P700. We observed a faster oxidation of P700 upon increasing light intensities (**Fig. 11 C, chapter III**) and a lower re-reduction rate (**Fig. 11 D, chapter III**), especially in low-light *apx2* cells.

We then hypothesized a limitation of the donor side of PSI, which could involve either the cytochrome *b<sub>6</sub>f* (Cyt *b<sub>6</sub>f*) or the electron carrier plastocyanin. Measurements of the redox state of Cyt *b<sub>6</sub>f* showed no differences between wt and *apx2* mutant (**Fig. 12, chapter III**). With these results obtained, we excluded that Cyt *b<sub>6</sub>f* is responsible of the redox state of P700 in the *apx2* mutants. Our focus shifted then to the evaluation of the plastocyanin-pool size. One method to gather information about the plastocyanin level, is by studying the electrochromic shift (**chapter III, 3.2.2.4**) in presence of the PSII inhibitor DCMU, at various times of light exposure. This provides an indication of the cyclic electron flow capacity. This cyclic electron flow is defined as the process where electrons return from ferredoxin, which is reduced by PSI activity, to the cytochrome *b<sub>6</sub>f* and plastocyanin (**chapter I, 1.1.3.2**). In the *apx2* mutant, we observed a reduced initial photosynthetic rate of electrons per PSI (**Fig. 13, chapter III**), drawing attention to the limitation of the plastocyanin pool, which might explain the possible reduced state of PQ. Indeed, we confirmed this hypothesis and we found that the levels of the electron carrier plastocyanin were reduced in the *apx2* mutant. Faster P700 oxidation was also observed in a study conducted on a mutant line of Arabidopsis lacking the Curvature Thylakoid 1 (CURT1) protein, which controls the tight membrane bending of the margins of the grana (Hohner et al 2020). In this mutant, the grana of the thylakoid are unstacked and plastocyanin requires more time than in the stacked grana thylakoid to deliver electrons to PSI. This underscores the importance of the electron carrier plastocyanin in sustaining long-range electron transport. Additional insights on this subject are detailed and discussed in the publication(s) in **chapter IV** and **chapter V**.

We have also assessed the growth in fluctuating light, to test the acclimation of the *apx2* mutant to fast changes of light. Indeed, we could observe that under fluctuating light conditions, the growth of *apx2* was reduced (**Fig. 14 B, chapter III**). In addition, the PSII activity was damaged, as shown by Fv/Fm and maximum rETR values, which could not be recovered after 4 days of fluctuating light (**Fig. 14 C, 14 D, chapter III**). Likely, the *apx2* mutant cannot afford early light acclimation, most probably due to the lower level of the plastocyanin pool. In conditions of fluctuating light, reduced growth and a limited electron donor for PSI were observed in the mutant lacking the proton gradient regulation 5-like photosynthetic phenotype 1 (PGRL1) (Jokel et al 2018). As for the *pgrr1* mutant,

the *apx2* mutant is than unable to balance the electron transport via PSI. Therefore, APX2 might be considered as an important player for the survival of *Chlamydomonas* under fluctuating light, along with other proteins already documented (Jokel et al 2018).

Further, ROS production was measured in wt and the *apx2* mutant when transferred from low light to high light for 1 h (**Fig. 15, chapter III**). No significant increase of ROS production was observed in the *apx2* mutant compared to the wt. This effect might be dependent on the limitation of the plastocyanin pool, so that the acceptor side of PSI, which is the major H<sub>2</sub>O<sub>2</sub> production site, does not get over-reduced and the electrons are not accepted by O<sub>2</sub> to form superoxide. However, ROS production was not measured in other conditions, such as fluctuating light, where the *apx2* mutant showed an increased sensitivity (**Fig. 14 B, chapter III**). The role of APX2 in the presence of H<sub>2</sub>O<sub>2</sub> remains unanswered. We proved *in vitro* that APX2 exhibits peroxidase activity, as described and discussed in (Caccamo et al 2023), in which we also demonstrated that the enzyme binds copper. However, being an APX-R, APX2 does not utilize ascorbate as reductant, and the *in vivo* electron donor is still unidentified. In (Caccamo et al., PCP, submitted), we speculated that plastocyanin could potentially serve as a substrate for APX2. The involvement of both H<sub>2</sub>O<sub>2</sub> and copper in the activity, or solely H<sub>2</sub>O<sub>2</sub>, remains uncertain. In the former case, a Fenton-like reaction could occur, leading to the formation of the intermediate hydroxyl radical ( $\cdot\text{OH}$ ). *In vitro* measurements, following the procedure outlined in (Pham et al 2013), could be conducted by incubating APX2 and plastocyanin with H<sub>2</sub>O<sub>2</sub> and copper, and measuring their respective concentrations. Some pertinent questions arising from this are: Can APX2 and H<sub>2</sub>O<sub>2</sub> contribute to maintaining a stable copper redox state in plastocyanin? Are they involved in H<sub>2</sub>O<sub>2</sub> scavenging? Exploring these questions could shed light on the observed effects in the photosynthetic machinery and provide new insights into photosynthetic processes.

## 7.2 Perspectives

### 7.2.1 Looking beyond the APX2 model system

A proposed model for APX2 function in *Chlamydomonas* and its relation with copper and plastocyanin and highlighting the differences between wt and the *apx2* mutant, is illustrated in **Fig. 2**.

Additional experiments to study copper homeostasis in *apx2* mutants might be helpful to understand the destiny of intracellular copper ion. Measurement of copper with inductively coupled plasma mass spectrometry (ICP-MS) (Nouet et al 2015) in different cellular compartments (soluble cellular fractions, total membrane fractions and extracts enriched in thylakoid fractions) might be useful to better understand copper distribution inside *apx2* mutants (Kropat et al 2015). Indeed, from our proteomic data, we could observe an increase of a cupredoxin (Cre12.g537250,  $\log_2$  fold change 1.3, **Table S4, chapter IV**) that is putatively localized in the cytosol (according to Phytozome) and might exerts a role in copper storage. On the other hand, we also found that the protein level of ferroxidase-like 1 (FOX1), which is also a plasma membrane cupredoxin involved in iron uptake, is decreased ( $\log_2$  fold change -0.69, **Table S3, chapter IV**). This might suggest a new pathway where the uncharacterized cupredoxin (Cre12.g537250) is involved and requires copper redistribution. Based on this hypothesis, we could expect a decrease of the copper content inside the thylakoid fraction of the *apx2* mutants, considering that plastocyanin is one of the most abundant copper-containing proteins (Kropat et al 2015). Preliminary data have shown no differences in total copper content between wt and *apx2-1*, while higher content has been observed in *apx2-2* mutant. However, further measurements are required to reach a conclusive understanding of the underlying cause for this discrepancy. Moreover, copper uptake can be measured through radioisotope of copper ( $^{64}\text{Cu}$ ) (Hill et al 1996) and can give additional information on copper metabolism. In addition, as FOX1 is highly expressed in iron deficiency conditions (Chen et al 2008), growth experiments in iron limited conditions might be performed and give other information on copper intracellular distribution. Another hypothesis of the relation between plastocyanin and APX2, might be related to the involvement of the APX2 in the plastocyanin degradation process. Indeed, in *Arabidopsis* it has been found that copper is involved in the dark-induced senescence process, regulated by the

module plantacyanin/senescence-associated genes (PCY-SAG14) (Hao et al 2022). The PCY-SAG14 module was found repressed by the conserved microRNA, miR408, which is in turn repressed by the phytochrome interacting factor 3/4/5 (PIF3/4/5), the transcription factor that promotes dark-induced senescence. The authors observed that during light, copper is kept in plastocyanin for the photosynthetic electron transport, while miR408 represses PCY-SAG14. In dark prolonged conditions, PIF3/4/5 represses miR408, activating PCY-SAG14, which promote the degradation of plastocyanin for copper relocation. Moreover, it has been also proposed that APX6, ortholog of the APX2 in Arabidopsis, is involved in the senescence process through regulation mediated by abscisic acid (ABA) (Chen et al 2021). The authors suggested that prolonged darkness, plant age, and water stress would prompt the activation of the abscisic acid insensitive 5 (ABI5) transcription factor by ABA. Consequently, ABI5 would then trigger the expression of APX6. This process is expected to occur under copper-replete conditions, whereas in the case of copper deficiency, this mechanism would be suppressed. Senescence is not occurring in *Chlamydomonas*, but plastocyanin degradation for copper redistribution might occur in specific conditions (*e.g.* light to dark growing conditions). In this case, APX2 might be involved in copper chelation and relocation, by taking copper from degraded plastocyanin. To investigate this hypothesis, conducting experiments such as cultivating cells in a minimal medium to maximize photosynthesis, followed by transferring them to an acetate medium and employing <sup>35</sup>S radiolabeling could be beneficial (Merchant & Bogorad 1986). In mixotrophy condition, copper is indeed repositioned within mitochondria for the respiratory process. Moreover, this would be followed by transfer of the cell into the dark. Under these various conditions, it is possible to measure copper concentrations in different compartments and plastocyanin. This approach can assist in addressing the proposed hypothesis. In our study we have also shown that APX2 presents peroxidase activity *in vitro* (Caccamo et al 2023). Considering that one of the hypotheses is that APX2 may play a role as chaperone for plastocyanin, one could wonder how both activities of peroxidase and chaperone may exist. Recently, to such proteins that possess peroxidase and chaperone activities, has been given a name of “chaperedoxin” (Goemans et al 2018). In this study the authors found that the *Escherichia coli* CnoX (YbbN), is a folding factor that works as an holdase upon activation through chlorination

mediated by hypochlorous acid (HOCl) and prevents protein aggregation. Moreover, it can protect itself from overoxidation by forming disulfide bonds during HOCl stress. Therefore, APX2 could potentially function as a "chaperedoxin," aiding in the folding process of plastocyanin by facilitating copper insertion as a chaperone. Its peroxidase activity evidently reflects its redox function.

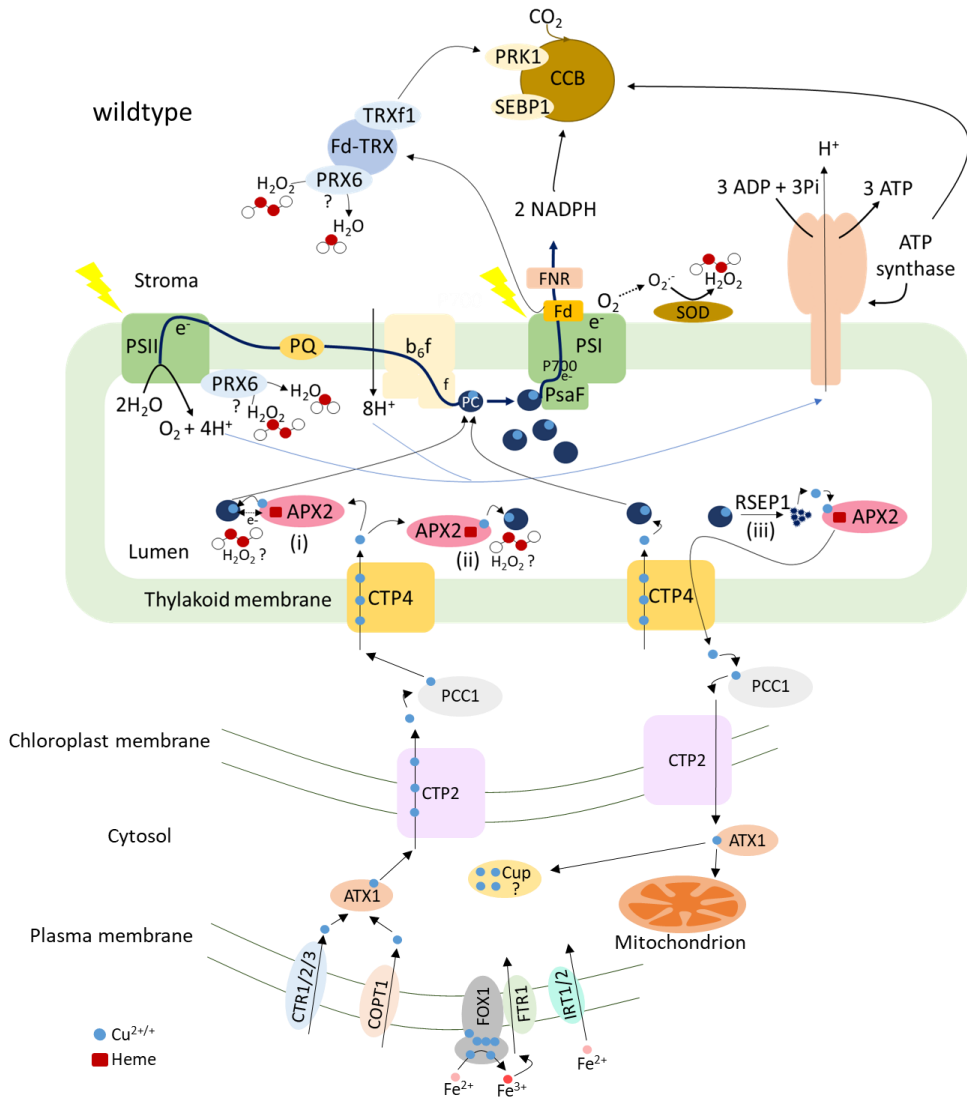
Peroxidase proteins that present both activities have been already described. For example, APX1 of Arabidopsis and APX2 of rice can be function as chaperone under heat stress conditions (Hong et al 2018, Kaur et al 2021) and 2-Cys PRX under overoxidation conditions (Kim et al 2009a, Muthuramalingam et al 2009). However, the activity of these proteins switches according to the environmental stress condition, so that another possibility would be that the activity of APX2 might be regulated according to specific conditions that still need to be identified. We have already shown through fluorescent probes that in the *apx2-1* mutant no increase of ROS has been observed when the cells are transferred to high light for one hour (**Fig. 15, chapter III**). It might be that the high light stress condition is not the one that might trigger APX2 activity. On the contrary, fluctuating light might be an option (**Fig. 14, chapter III**). Indeed, monitoring H<sub>2</sub>O<sub>2</sub> in real-time using recently developed H<sub>2</sub>O<sub>2</sub>-sensors like the pH-stable HyPer7 could help to understand where H<sub>2</sub>O<sub>2</sub> is mostly generated (Pak et al 2020). Real-time H<sub>2</sub>O<sub>2</sub> monitoring has been already assessed in *Chlamydomonas* using roGFP<sub>2</sub>-Tsa2ΔC<sub>R</sub> (Niemeyer et al 2021). These sensors might help to better investigate the H<sub>2</sub>O<sub>2</sub>-stress mediated in *apx2* mutants and might give useful information on the possible activity of APX2 as peroxidase. In addition, it is possible to mutate the H155 of APX2 that should bind the heme and perform similar photosynthetic measurements as described in chapter IV coupled with H<sub>2</sub>O<sub>2</sub> measurements. If no changes will be detected compared to the wt, then we could hypothesize that APX2 might not work as peroxidase *in vivo*. Further, by mutating the MxxM motif to LxxL we could confirm through *in vitro* experiments that the well conserved motif is responsible for copper binding. *In vivo* experiments in cells expressing APX2 with LxxL, might also be useful to better understand the relation between plastocyanin and APX2 protein. Additional analyses on the AlphaFold2 predicted structural model of the APX2 and plastocyanin complex presented in chapter V would also help to confirm the model. We have tried some techniques such as pull down, yeast-two-hybrid and

Bio-Layer interferometry (BLI), however, we did not observe any clear interaction. The absence of a clear interaction strongly suggests that the potential interaction within the predicted structural model of the complex is either weak or transient. To substantiate and establish the proposed interaction, it becomes imperative to explore methodologies aimed at stabilizing the complex. One promising avenue involves the generation and selection of nanobodies, which are small antibody fragments known for their ability to specifically bind and stabilize transient protein complexes (Beghein & Gettemans 2017, Kohler et al 2018, Uchanski et al 2020). In addition to the nanobody approach, an alternative strategy involves the use of chemical linkers to establish a covalent connection between the proteins, thereby forming a stable protein-protein complex. This method can be particularly effective in situations where traditional interaction assays may not capture transient interactions. Notable examples of successful implementation of chemical linkers can be found in studies such as (some examples in (Buchert et al 2018, Luo et al 2021, Nguyen et al 2020, Ozawa et al 2018)). Exploring these avenues could significantly contribute to unraveling the dynamics of the APX2 and plastocyanin complex interaction predicted by the AlphaFold2 structural model.

Shed light on this relation, would be useful to elucidate the role of the APX-R in the green photosynthetic eukaryotes. In fact, this new class of APX is not found in other organisms like fungi or bacteria (Lazzarotto et al 2015). In (Lazzarotto et al 2015), the authors proposed that this new class might have diverged after the second event of endosymbiosis from which chloroplast originated. Later, different subclasses of class I of APX have diverged into classic APX, APX-R (APX-Related) and APX-L (APX-Like). Some works have been done on the APX-R class in plants, although no investigations on the photosynthetic machinery have been performed (Chen et al 2021, Chen et al 2014, Lazzarotto et al 2021a, Lazzarotto et al 2011, Tyagi et al 2020, Verma et al 2022) It has been found that the APX-R of rice is upregulated in aluminum stress, water deficiency and 24-cold stress. The *APX-R* genes of *Triticum aestivum* are upregulated during heat stress, drought stress, salt stress and combination of heat and drought stresses. The *APX-R* genes in *Brassica rapa* and *Brassica juncea* are responsive to heat and draught stress. In the contents of crop plants, it might be interesting working on the enhancement of the *APX-R* gene expression, although it is known that the *APX-R* is a single-copy gene and not duplicable



(Dunand et al 2011). Indeed, it has been already shown in Arabidopsis that excess of APX-R gene in overexpressing lines is degraded (Lazzarotto et al 2021b). In rice, preliminary tests on overexpressing APX-R lines did not show any alterations in the phenotype (Lazzarotto et al 2011). The authors suggested that there might appear in wild conditions or different laboratory conditions. However, considering the new findings in Arabidopsis, it might be possible that the same scenario occurs in rice. In general, taking into account the results on the APX-R in Chlamydomonas and Arabidopsis and the presence of the conserved MxxM motif, we may think that the APX-R is implicated in intracellular copper homeostasis. Nevertheless, the exact role of the APX-R might be different between algae and plants, considering that in most of the plant APX-R sequence a truncated twin arginine translocator (TAT) motif typical of luminal protein is present. However, the subcellular localization in the lumen of the APX2 in Chlamydomonas still need to be confirmed. Moreover, information related to photosynthetic measurements on plant APX-R is required to better hypothesize whether the function of the APX-R is conserved between plant algae.



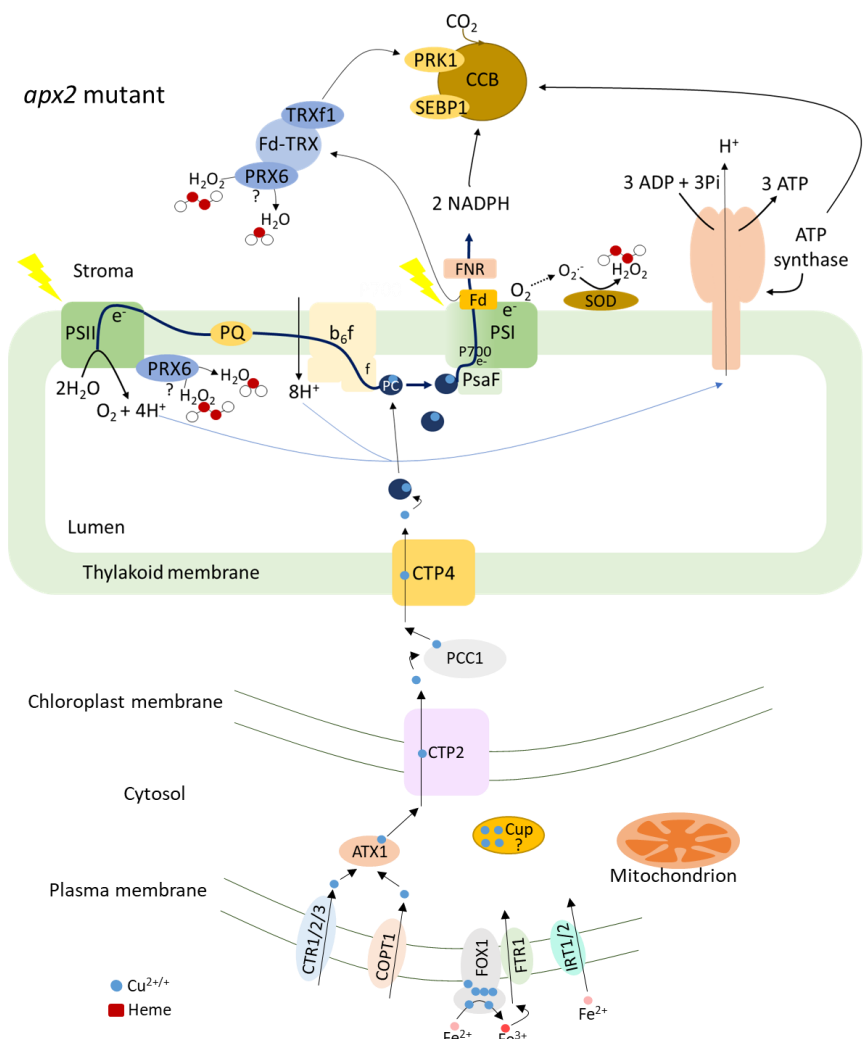


**Figure 2: Model depicting hypotheses regarding the role of APX2, highlighting distinctions between the wildtype (wt) and *apx2* mutant.** In the wildtype, copper enters the cells through copper transporters (CTR1/2/3, COPT1). The antioxidant 1 (ATX1) copper chaperone delivers copper to the chloroplast membrane copper transporter 2 (CTP2). Plastid copper chaperone 1 (PCC1) transfers copper to the copper transporter 4 (CTP4) of the thylakoid membrane. Copper is then delivered to the electron carrier plastocyanin (PC), which transports electrons from the cytochrome *b<sub>6</sub>f* complex (b<sub>6</sub>f) through cytochrome *f* (f) and PSI, involving the PsaF subunit. These electrons then reduce the primary electron donor of PSI, P700, culminating in the generation of NADPH for the Calvin-Benson-Bassham (CBB) cycle. Several hypotheses illustrate the role of the APX2 protein: (i) APX2 might extract copper from CTP4, acting as a chaperone to deliver copper to apoplastocyanin, forming holoplastocyanin. In this scenario, electron transfer might occur between the copper of plastocyanin and the iron in the heme of APX2; (ii) plastocyanin might serve as a substrate for APX2 to scavenge H<sub>2</sub>O<sub>2</sub> (“chaperedoxin”); (iii) APX2 might be involved in plastocyanin degradation and copper redistribution to the cytosol (multicopper cupredoxin, Cup) and mitochondria. In the *apx2 mutant*, plastocyanin levels decrease, leading to reduced electron transfer to PSI and accumulation of P700<sup>+</sup>. Moreover, certain subunits of PSI, like PsaF and PsaD exhibit decreased levels compared to the wildtype. The higher level of the uncharacterized multicopper cupredoxin (Cup) and lower level of ferredoxin-like 1 (FOX1) suggest that most of the intracellular copper is stored in the cytosol, potentially aiding compensatory mechanisms. Iron uptake may occur through IRT1/2 iron transporters, and increased growth might compensate for the electron transport by enhanced enzymes involved in the ferredoxin-thioredoxin (Fd-TRX) system, controlling phosphoribulokinase 1 (PRK1) of the the Calvin-Benson-Bassham (CBB) cycle. Sedoheptulose-1,7-bisphosphatase (SEBP1) of the CBB cycle is also found to be increased. Upon light stress, H<sub>2</sub>O<sub>2</sub> levels do not show an increase.

The used abbreviations include: APX2, ascorbate peroxidase 2; ATX1, antioxidant 1; b<sub>6</sub>f, cytochrome *b<sub>6</sub>f* complex; f, cytochrome *f*; CBB, Calvin-Benson-Bassham cycle; CTP2/4, copper transporter 2/4; COPT1, copper transporter 1; CTR1/2/3, copper transporter 1/2/3; Cup, cupredoxin; Fd, ferredoxin; Fd-TRX, ferredoxin-thioredoxin system; FNR, ferredoxin-NADP<sup>+</sup> reductase; FTR1, iron permease; IRT1/2, ZIP-family iron transporters 1/2; PCC1, plastid copper chaperone 1; PQ, plastoquinone pool; PRK1, phosphoribulokinase 1; PRX6, peroxiredoxin Q; PSI, photosystem I; PSII, photosystem II; RSEP1, regulator of sigma-E protease; SEBP1, sedoheptulose-1,7-bisphosphatase; SOD, superoxide dismutase; TRXf1, thioredoxin f1.

### 7.2.2 Additional future experiments to uncover APX2 function in *Chlamydomonas*

In **chapter III** there are described our new findings on the function of the APX2, the newly classified APX-R in *Chlamydomonas*. With our results, we concluded that the APX2 binds copper and modulates copper insertion into plastocyanin, the electron carrier from Cyt *b<sub>6</sub>f* and PSI. Moreover, we also found that the absence of APX2 influences the level of plastocyanin, resulting in a faster oxidation and a slower re-reduction of the primary electron donor of PSI, P700. Extended discussion on the results related to the role of the APX2 as possible chaperone for plastocyanin, is reported in the two publications in **chapter III**. Nevertheless, there are still unanswered questions that need to be addressed to uncover the function of this enzyme.

First, the possibility of APX2 to act as copper chaperone for plastocyanin remains to be confirmed. Indeed, additional measurements with <sup>1</sup>H-NMR would probably answer the question. We have shown that in presence of Cu<sup>2+</sup>-bound APX2 and apoplastocyanin, no copper insertion is observed. However, when we titrated apoplastocyanin with copper, we do notice the formation of the holoplastocyanin. In presence of copper-bound APX2, this mechanism still occurs, but at a slower extent. Given the lack of information regarding the *in vivo* redox state of copper when it is incorporated into plastocyanin, another possibility would be to carry out these measurements in presence of Cu<sup>+</sup> bound to APX2. To do so, all the measurement should be performed in absence of oxygen, to avoid oxidation of Cu<sup>+</sup> into Cu<sup>2+</sup>.

Concerning cell physiology, further experiments in different copper or iron concentration, would be interesting to explore in the mutants. For example, conducting experiments with higher copper concentrations than standard concentration of 6 μM, would give information about plastocyanin and other copper related proteins. Moreover, considering that in *Chlamydomonas* exists a copper-dependent iron assimilation (La Fontaine et al 2002), varying iron concentrations may provide additional insights into the function of APX2.

Other growth conditions worth testing includes anoxia. It has been demonstrated that oxygen- and copper- deficiency, share signal transduction components (Quinn et al 2002). We have shown that *apx2* mutant responds to copper deficiency as the wt (Caccamo et al., PCP, in revision). However, both oxygen-

and copper- deficiency responses are not identical, as the one to oxygen-deficiency requires an additional regulator. Moreover, it has been shown that cyclic electron flow (CEF) around PSI is important for cell survival in oxygen limitation environment (Godaux et al 2015). Considering the low level of plastocyanin and the low initial photosynthetic rate of CEF in the *apx2* mutant (**Fig. 13, chapter III**), testing anoxia condition would provide additional information of the role of APX2 in distinct cellular responses.

In addition, another interesting point for *apx2* physiology, would be comparing *apx2* mutant strains with over-expressing APX2 lines. As already described in (Dunand et al 2011), APX-R is encoded by a single copy gene and present at low level. In Arabidopsis, over-expressing lines of the ortholog APX6, showed that the enzyme accumulates at the early stage of seeds maturation promoting seeds metabolism and germination (Lazzarotto et al 2021b). Moreover, in that work, the enzyme was found in plastids, stomata, and roots. This implies that the stability of APX6 may be significantly influenced by the specific accumulation site or developmental context. APX6 over-expressing lines also showed that the protein was located in other compartments, plastoglobuli, and subjected to degradation (Lazzarotto et al 2021b). Considering the differences in the sequences between the APX2 and APX6 that would target them in different cell compartments (Caccamo et al 2023) (Caccamo et al., in revision), Chlamydomonas APX2 over-expressing lines, would provide additional clues on the function of the APX-R of the green algae. Moreover, the conditions where APX2 is required at higher level remain questioning. Knowing those conditions where APX2 might be necessary and comparing mutants and over-expressing lines, would provide us with clear information on the protein function, especially not related to plastocyanin.

Furthermore, considering the impairment in some photosynthetic processes described above (sections 7.1.2 and 7.1.3), the *apx2* mutant might serve as a tool to investigate state transition and cyclic electron flow. Investigation of these processes could bring additional interesting information on the side effects of the absence of the APX2 and the lower plastocyanin-pool size, causing new energetic balances in the photosynthetic electron transport. Moreover, exploring deeply the photosynthetic machinery of the *apx2* mutant in cells grown under high light and fluctuating light, would help to explain the differences we observed in the energy distribution and photoprotection mechanisms.

Overall, our findings have raised new and challenging questions regarding the role of the APX2 enzyme, and more broadly, the APX-R class. Several aspects still require investigation. Considering the possible dual function of the APX2, serving as both chaperone and peroxidase, the study of this protein holds appeal for both the photosynthetic and the redox biology communities.

### 7.2.3 Other candidate strains to study *Chlamydomonas* H<sub>2</sub>O<sub>2</sub> signaling

In addition to the *apx2*, *srx2* and *d1* mutants, two other mutant strains, identified as ‘clean’ mutants (**chapter III**, section 3.3.1), lacking glutathione peroxidase 3 (GPX3, *gpx3-1* mutant) and an ATP-ase AAA (LCA1, *lca1-2* mutant), would be intriguing choices for studying redox signaling in *Chlamydomonas*.

The putative localization of the GPX3 enzyme in *Chlamydomonas* varies depending on the prediction tool used, with Predalgo suggesting chloroplast localization and TargetP indicating mitochondrial localization. The Arabidopsis orthologue of *Chlamydomonas* GPX3 is implicated in H<sub>2</sub>O<sub>2</sub> homeostasis and protection from drought stress (Miao et al 2006), implying a potential role in abiotic stress protection for *Chlamydomonas* GPX3 as well. To address the uncertainty of GPX3 localization, immunoblotting on isolated chloroplast and mitochondria fractions or, alternatively, a YFP tag fused to the GPX3 protein could be employed. Subsequently, the investigation would involve assessing the growth of the mutants under various abiotic stress conditions (e.g., cold temperature, plate agar with limited water percentage, pH variations) and correlating this with measurements of photosynthetic parameters or respiration to understand the impact of GPX3 disruption under stress. Additionally, transcriptomic and proteomic analyses would be valuable in identifying stress-related genes and proteins responding to the absence of GPX3.

The other mutant that can be used to study *Chlamydomonas* signaling, is the *lca1-2*. LCA1 is an AAA-Type ATPase most probably located in the outer membrane of mitochondria. Details about mutant lines of this protein are accessible in Arabidopsis (Zhang et al 2014a). The protein known as AtOM66 (ortholog of LCA1 of *Chlamydomonas*), has been reported to be regulated by WKRY transcription factors (Van Aken et al 2016). AtOM66 acts in response to abiotic and biotic stress and is especially involved in touch-stress response, mediating retrograde signaling from mitochondria (Van Aken et al 2016, Xu et al 2019, Zhang et al 2014a). Therefore, it would be interesting to submit the *lca1-*

2 mutant of *Chlamydomonas* to abiotic stress (*e.g.* cold stress, high temperature, hypersalinity...) and focus on the effect by measuring respiration. Additionally, integrating measurements of photosynthetic parameters would offer a more comprehensive insight into the entire cellular system. Finally, leveraging transcriptomic and proteomic data could aid in identifying genes and proteins potentially involved in retrograde signaling (from mitochondria to the nucleus) in the *lca1-2* mutant.

#### *7.2.4 Modified proteins trapping assay to uncover sulfenome patterns in specific mutants*

Additionally, considering the importance of protein modifications mediated by H<sub>2</sub>O<sub>2</sub> in cell physiology, we have also tried to define the sulfenome pattern in *Chlamydomonas*. We applied a chemical approach, utilizing the BTD probe, to discover novel redox regulators. Despite several attempts, we were unable to validate a reliable protocol, indicating the need for further optimization (full description of issues encountered and ideas are described in **chapter VI**). Once achieving this objective, the assay could be applied to the abovementioned strains of interest (*srx2*, *apx2*, *dl*, *gpx3-1*, *lca1-2*) subjected to a specific stress condition. This would help to provide a clear picture of the stress effect, specifically focused on the one mediated by H<sub>2</sub>O<sub>2</sub>. Further, trapping modified proteins with the BTD probe could serve as supplementary information to define the sulfenome pattern associated with each disrupted gene. If successful, the prospect of identifying sulfenylated proteins implicated in photosynthesis could present intriguing new avenues for exploration.



# Acknowledgments

I would like to thank all the people that have helped me during these years. Thanks to my supervisors Claire Remacle and Joris Messens for welcoming me in their labs and giving me the opportunity to work in their team. Thanks for your constant encouragement, support, tutoring and for guiding me along these years to improve myself humanly and professionally.

I would like to thank all the jury members for their feedbacks, comments, suggestions and the fruitful discussion on my PhD work.

I would also like to thank collaborators who contributed to the project. Thanks to Pierre Cardol for his expert support on photosynthesis. Thanks to Didier Vertommen for welcoming me in his lab and his expert support on proteomic analysis. Thanks to Nicolas Rouhier for welcoming me in his lab and for his expert support on biochemistry. Thanks to Alexander N. Volkov and to Alexandre Kriznik for their expert support on biophysics. I would like to thank the technical staff for helping me during this journey. Thanks to Michèle Radoux and to Nadine Coosemans for their constant help on the ULiège and lab administrative stuff and their technical assistance to my experiments. Thanks to Khadija Wahni for performing the last experiments for the manuscript, for VUB and lab administrative stuff and the organization of the private defense. Thanks to Gaëtan Herinckx for his technical assistance for proteomic experiments. I would like to thank my colleagues and researchers that helped me during this journey. Thanks to Félix Vega de Luna for the constant help and support during my PhD thesis. Thanks for the fruitful discussions, for teaching me techniques to measure photosynthetic parameters and for the work we have been doing together. Thanks to Fabrizio Iacono for helpful discussions about photosynthesis and for teaching me techniques to measure photosynthetic parameters and the experiments we performed together. Thanks to Sara M. Cardoso Esteves for helpful discussions about metal homeostasis and for teaching me cells metal extraction. Thanks to Jonathan Przybyla-Toscano for helpful discussions, for purifying proteins and teaching me about protein purification and techniques for protein interaction. Thanks to Agnieszka E. Misztak for analysing RNASeq data. Thanks to Daria Ezeriņa for helping me with the SpectraMax® iD3 and iD5 Multi-Mode Microplate Readers for tryptophan fluorescence experiments. Thanks to Julia Malo Pueyo for helping me with the set-up of the CD

experiments. Thanks to Sébastien Pyr dit Ruys for teaching and assisting me on proteomic experiments. Thanks to my student Antonello Amelii for helping me with the preparation of constructs for recombinant proteins.

My PhD fellowship of ULiège was supported by Fonds de la Recherche Scientifique Excellence of Science project no. 30829584.

## References

- Abdel-Ghany SE. 2009. Contribution of plastocyanin isoforms to photosynthesis and copper homeostasis in *Arabidopsis thaliana* grown at different copper regimes. *Planta* 229: 767-79
- Abdel-Ghany SE, Muller-Moule P, Niyogi KK, Pilon M, Shikanai T. 2005. Two P-type ATPases are required for copper delivery in *Arabidopsis thaliana* chloroplasts. *Plant Cell* 17: 1233-51
- Aguirre G, Pilon M. 2015. Copper Delivery to Chloroplast Proteins and its Regulation. *Front Plant Sci* 6: 1250
- Akter S, Huang J, Bodra N, De Smet B, Wahni K, et al. 2015. DYn-2 Based Identification of *Arabidopsis* Sulfenomes. *Mol Cell Proteomics* 14: 1183-200
- Almagro Armenteros JJ, Salvatore M, Emanuelsson O, Winther O, von Heijne G, et al. 2019. Detecting sequence signals in targeting peptides using deep learning. *Life Sci Alliance* 2
- Alric J. 2010. Cyclic electron flow around photosystem I in unicellular green algae. *Photosynth Res* 106: 47-56
- Andrizhiyevskaya EG, Chojnicka A, Bautista JA, Diner BA, van Grondelle R, Dekker JP. 2005. Origin of the F685 and F695 fluorescence in photosystem II. *Photosynth Res* 84: 173-80
- Aro EM, Virgin I, Andersson B. 1993. Photoinhibition of Photosystem II. Inactivation, protein damage and turnover. *Biochim Biophys Acta* 1143: 113-34
- Arts IS, Vertommen D, Baldin F, Laloux G, Collet JF. 2016. Comprehensively Characterizing the Thioredoxin Interactome In Vivo Highlights the Central Role Played by This Ubiquitous Oxidoreductase in Redox Control. *Mol Cell Proteomics* 15: 2125-40
- Asada K. 1999. THE WATER-WATER CYCLE IN CHLOROPLASTS: Scavenging of Active Oxygens and Dissipation of Excess Photons. *Annu Rev Plant Physiol Plant Mol Biol* 50: 601-39
- Asada K. 2006. Production and scavenging of reactive oxygen species in chloroplasts and their functions. *Plant Physiol* 141: 391-6
- Bailleul B, Cardol P, Breyton C, Finazzi G. 2010. Electrochromism: a useful probe to study algal photosynthesis. *Photosynth Res* 106: 179-89

- Barber J. 2012. Photosystem II: the water-splitting enzyme of photosynthesis. *Cold Spring Harb Symp Quant Biol* 77: 295-307
- Beghein E, Gettemans J. 2017. Nanobody Technology: A Versatile Toolkit for Microscopic Imaging, Protein-Protein Interaction Analysis, and Protein Function Exploration. *Front Immunol* 8: 771
- Behrenfeld MJ, Halsey KH, Milligan AJ. 2008. Evolved physiological responses of phytoplankton to their integrated growth environment. *Philos Trans R Soc Lond B Biol Sci* 363: 2687-703
- Bennett RR, Golestanian R. 2015. A steering mechanism for phototaxis in *Chlamydomonas*. *J R Soc Interface* 12: 20141164
- Berg R, Straub BF. 2013. Advancements in the mechanistic understanding of the copper-catalyzed azide-alkyne cycloaddition. *Beilstein J Org Chem* 9: 2715-50
- Berthold P, Schmitt R, Mages W. 2002. An engineered *Streptomyces hygrosopicus* aph 7" gene mediates dominant resistance against hygromycin B in *Chlamydomonas reinhardtii*. *Protist* 153: 401-12
- Blaby-Haas CE, Merchant SS. 2012. The ins and outs of algal metal transport. *Biochim Biophys Acta* 1823: 1531-52
- Blaby-Haas CE, Padilla-Benavides T, Stube R, Arguello JM, Merchant SS. 2014. Evolution of a plant-specific copper chaperone family for chloroplast copper homeostasis. *Proc Natl Acad Sci U S A* 111: E5480-7
- Blaby IK, Blaby-Haas CE, Perez-Perez ME, Schmollinger S, Fitz-Gibbon S, et al. 2015. Genome-wide analysis on *Chlamydomonas reinhardtii* reveals the impact of hydrogen peroxide on protein stress responses and overlap with other stress transcriptomes. *Plant J* 84: 974-88
- Blaby IK, Blaby-Haas CE, Tourasse N, Hom EF, Lopez D, et al. 2014. The *Chlamydomonas* genome project: a decade on. *Trends Plant Sci* 19: 672-80
- Bolger AM, Lohse M, Usadel B. 2014. Trimmomatic: a flexible trimmer for Illumina sequence data. *Bioinformatics* 30: 2114-20
- Bonente G, Ballottari M, Truong TB, Morosinotto T, Ahn TK, et al. 2011. Analysis of LhcSR3, a protein essential for feedback de-excitation in the green alga *Chlamydomonas reinhardtii*. *PLoS Biol* 9: e1000577

- Bonente G, Pippa S, Castellano S, Bassi R, Ballottari M. 2012. Acclimation of *Chlamydomonas reinhardtii* to different growth irradiances. *J Biol Chem* 287: 5833-47
- Boutigny S, Sautron E, Finazzi G, Rivasseau C, Frelet-Barrand A, et al. 2014. HMA1 and PAA1, two chloroplast-envelope PIB-ATPases, play distinct roles in chloroplast copper homeostasis. *Journal of Experimental Botany* 65: 1529-40
- Boynton JE, Gillham NW, Harris EH, Hosler JP, Johnson AM, et al. 1988. Chloroplast transformation in *Chlamydomonas* with high velocity microprojectiles. *Science* 240: 1534-8
- Brandes HK, Larimer FW, Hartman FC. 1996. The molecular pathway for the regulation of phosphoribulokinase by thioredoxin f. *J Biol Chem* 271: 3333-5
- Briggs LM, Pecoraro VL, McIntosh L. 1990. Copper-induced expression, cloning, and regulatory studies of the plastocyanin gene from the cyanobacterium *Synechocystis* sp. PCC 6803. *Plant Mol Biol* 15: 633-42
- Broderson M, Niyogi KK, Iwai M. 2024. Macroscale structural changes of thylakoid architecture during high light acclimation in *Chlamydomonas reinhardtii*. *Photosynth Res*
- Buchert F, Hamon M, Gabelein P, Scholz M, Hippler M, Wollman FA. 2018. The labile interactions of cyclic electron flow effector proteins. *J Biol Chem* 293: 17559-73
- Buchert F, Mosebach L, Gäbelein P, Hippler M. 2020. PGR5 is required for efficient Q cycle in the cytochrome b6f complex during cyclic electron flow. *Biochemical Journal* 477: 1631-50
- Buchert F, Scholz M, Hippler M. 2022. Electron transfer via cytochrome b6f complex displays sensitivity to antimycin A upon STT7 kinase activation. *Biochemical Journal* 479: 111-27
- Burkey KO, Gizlice Z, Carter TE, Jr. 1996. Genetic variation in soybean photosynthetic electron transport capacity is related to plastocyanin concentration in the chloroplast. *Photosynth Res* 49: 141-9
- Burse EH, Poulos TL. 2000. Two substrate binding sites in ascorbate peroxidase: the role of arginine 172. *Biochemistry* 39: 7374-9
- Caccamo A, Vega de Luna F, Wahni K, Volkov AN, Przybyla-Toscano J, et al. 2023. Ascorbate Peroxidase 2 (APX2) of *Chlamydomonas* Binds Copper and Modulates the Copper Insertion into Plastocyanin. *Antioxidants* 12

- Cardol P, Forti G, Finazzi G. 2011. Regulation of electron transport in microalgae. *Biochim Biophys Acta* 1807: 912-8
- Cardol P, Matagne RF, Remacle C. 2002. Impact of mutations affecting ND mitochondria-encoded subunits on the activity and assembly of complex I in *Chlamydomonas*. Implication for the structural organization of the enzyme. *J Mol Biol* 319: 1211-21
- Caspy I, Fadeeva M, Kuhlert S, Borovikova-Sheinker A, Klaiman D, et al. 2021. Structure of plant photosystem I-plastocyanin complex reveals strong hydrophobic interactions. *Biochem J* 478: 2371-84
- Castell C, Rodriguez-Lumbreras LA, Hervas M, Fernandez-Recio J, Navarro JA. 2021. New Insights into the Evolution of the Electron Transfer from Cytochrome f to Photosystem I in the Green and Red Branches of Photosynthetic Eukaryotes. *Plant Cell Physiol* 62: 1082-93
- Castruita M, Casero D, Karpowicz SJ, Kropat J, Vieler A, et al. 2011. Systems biology approach in *Chlamydomonas* reveals connections between copper nutrition and multiple metabolic steps. *Plant Cell* 23: 1273-92
- Caverzan A, Passaia G, Rosa SB, Ribeiro CW, Lazzarotto F, Margis-Pinheiro M. 2012. Plant responses to stresses: Role of ascorbate peroxidase in the antioxidant protection. *Genet Mol Biol* 35: 1011-9
- Cha JY, Ahn G, Jeong SY, Shin GI, Ali I, et al. 2022. Nucleoredoxin 1 positively regulates heat stress tolerance by enhancing the transcription of antioxidants and heat-shock proteins in tomato. *Biochem Biophys Res Commun* 635: 12-18
- Charoenwattanasatien R, Zinzius K, Scholz M, Wicke S, Tanaka H, et al. 2020. Calcium sensing via EF-hand 4 enables thioredoxin activity in the sensor-responder protein calredoxin in the green alga *Chlamydomonas reinhardtii*. *J Biol Chem* 295: 170-80
- Chatzikonstantinou M, Vlachakis D, Chronopoulou E, Papageorgiou L, Papageorgiou AC, Labrou NE. 2017. The glutathione transferase family of *Chlamydomonas reinhardtii*: Identification and characterization of novel sigma class-like enzymes. *Algal Research* 24: 237-50
- Chaux F, Burlacot A, Mekhalfi M, Auroy P, Blangy S, et al. 2017. Flavodiiron Proteins Promote Fast and Transient O(2) Photoreduction in *Chlamydomonas*. *Plant Physiol* 174: 1825-36

- Chen C, Galon Y, Rahmati Ishka M, Malihi S, Shimanovsky V, et al. 2021. ASCORBATE PEROXIDASE6 delays the onset of age-dependent leaf senescence. *Plant Physiol* 185: 441-56
- Chen C, Letnik I, Hacham Y, Dobrev P, Ben-Daniel BH, et al. 2014. ASCORBATE PEROXIDASE6 protects Arabidopsis desiccating and germinating seeds from stress and mediates cross talk between reactive oxygen species, abscisic acid, and auxin. *Plant Physiol* 166: 370-83
- Chen JC, Hsieh SI, Kropat J, Merchant SS. 2008. A ferroxidase encoded by FOX1 contributes to iron assimilation under conditions of poor iron nutrition in *Chlamydomonas*. *Eukaryot Cell* 7: 541-5
- Chibani K, Pucker B, Dietz KJ, Cavanagh A. 2021. Genome-wide analysis and transcriptional regulation of the typical and atypical thioredoxins in *Arabidopsis thaliana*. *FEBS Lett* 595: 2715-30
- Cline K. 2015. Mechanistic Aspects of Folded Protein Transport by the Twin Arginine Translocase (Tat). *J Biol Chem* 290: 16530-8
- Corpas FJ, Gonzalez-Gordo S, Rodriguez-Ruiz M, Munoz-Vargas MA, Palma JM. 2022. Thiol-based Oxidative Posttranslational Modifications (OxiPTMs) of Plant Proteins. *Plant Cell Physiol* 63: 889-900
- Craig RJ, Gallaher SD, Shu S, Salome PA, Jenkins JW, et al. 2023. The *Chlamydomonas* Genome Project, version 6: Reference assemblies for mating-type plus and minus strains reveal extensive structural mutation in the laboratory. *Plant Cell* 35: 644-72
- Cross FR, Umen JG. 2015. The *Chlamydomonas* cell cycle. *Plant J* 82: 370-92
- Cruz JA, Salbilla BA, Kanazawa A, Kramer DM. 2001. Inhibition of Plastocyanin to P700 +Electron Transfer in *Chlamydomonas reinhardtii* by Hyperosmotic Stress. *Plant Physiology* 127: 1167-79
- Curien G, Flori S, Villanova V, Magneschi L, Giustini C, et al. 2016. The Water to Water Cycles in Microalgae. *Plant Cell Physiol* 57: 1354-63
- DalCorso G, Pesaresi P, Masiero S, Aseeva E, Schunemann D, et al. 2008. A complex containing PGRL1 and PGR5 is involved in the switch between linear and cyclic electron flow in *Arabidopsis*. *Cell* 132: 273-85
- Davies J, Wright GD. 1997. Bacterial resistance to aminoglycoside antibiotics. *Trends Microbiol* 5: 234-40

- Dayer R, Fischer BB, Eggen RI, Lemaire SD. 2008. The peroxiredoxin and glutathione peroxidase families in *Chlamydomonas reinhardtii*. *Genetics* 179: 41-57
- De Smet B, Willems P, Fernandez-Fernandez AD, Alseekh S, Fernie AR, et al. 2019. In vivo detection of protein cysteine sulfenylation in plastids. *Plant J* 97: 765-78
- Delaunay A, Pflieger D, Barrault MB, Vinh J, Toledano MB. 2002. A thiol peroxidase is an H<sub>2</sub>O<sub>2</sub> receptor and redox-transducer in gene activation. *Cell* 111: 471-81
- Depege N, Bellafiore S, Rochaix JD. 2003. Role of chloroplast protein kinase Stt7 in LHCII phosphorylation and state transition in *Chlamydomonas*. *Science* 299: 1572-5
- Dhokane D, Bhadra B, Dasgupta S. 2020. CRISPR based targeted genome editing of *Chlamydomonas reinhardtii* using programmed Cas9-gRNA ribonucleoprotein. *Mol Biol Rep* 47: 8747-55
- Dietz KJ. 2011. Peroxiredoxins in plants and cyanobacteria. *Antioxid Redox Signal* 15: 1129-59
- Dietz KJ. 2016. Thiol-Based Peroxidases and Ascorbate Peroxidases: Why Plants Rely on Multiple Peroxidase Systems in the Photosynthesizing Chloroplast? *Mol Cells* 39: 20-5
- Dixon DP, Skipsey M, Grundy NM, Edwards R. 2005. Stress-induced protein S-glutathionylation in Arabidopsis. *Plant Physiol* 138: 2233-44
- Doerge DR, Divi RL, Churchwell MI. 1997. Identification of the colored guaiacol oxidation product produced by peroxidases. *Anal Biochem* 250: 10-7
- Dogra V, Rochaix JD, Kim C. 2018. Singlet oxygen-triggered chloroplast-to-nucleus retrograde signalling pathways: An emerging perspective. *Plant Cell Environ* 41: 1727-38
- Drepper F, Hippler M, Nitschke W, Haehnel W. 1996. Binding dynamics and electron transfer between plastocyanin and photosystem I. *Biochemistry* 35: 1282-95
- Dunand C, Mathe C, Lazzarotto F, Margis R, Margis-Pinheiro M. 2011. Ascorbate peroxidase-related (APx-R) is not a duplicable gene. *Plant Signal Behav* 6: 1908-13
- Durante L, Hubner W, Lauersen KJ, Remacle C. 2019. Characterization of the GPR1/FUN34/YaaH protein family in the green microalga *Chlamydomonas* suggests their role as intracellular membrane acetate channels. *Plant Direct* 3: e00148



- Dutcher SK. 2020. Asymmetries in the cilia of *Chlamydomonas*. *Philos Trans R Soc Lond B Biol Sci* 375: 20190153
- Dutcher SK, O'Toole ET. 2016. The basal bodies of *Chlamydomonas reinhardtii*. *Cilia* 5: 18
- Eberhard S, Finazzi G, Wollman FA. 2008. The dynamics of photosynthesis. *Annu Rev Genet* 42: 463-515
- Ebersold WT. 1956. Crossing Over in *Chlamydomonas reinhardtii*. *American Journal of Botany* 43: 408-10
- El-Sheekh MM, Almutairi AW, Touliabah HE. 2019. Construction of a novel vector for the nuclear transformation of the unicellular green alga *Chlamydomonas reinhardtii* and its stable expression. *Journal of Taibah University for Science* 13: 529-35
- El Meskini R, Culotta VC, Mains RE, Eipper BA. 2003. Supplying copper to the cuproenzyme peptidylglycine alpha-amidating monooxygenase. *J Biol Chem* 278: 12278-84
- Emonds-Alt B, Coosemans N, Gerards T, Remacle C, Cardol P. 2017. Isolation and characterization of mutants corresponding to the MENA, MENB, MENC and MENE enzymatic steps of 5'-monohydroxyphyllloquinone biosynthesis in *Chlamydomonas reinhardtii*. *Plant J* 89: 141-54
- Erickson E, Wakao S, Niyogi KK. 2015. Light stress and photoprotection in *Chlamydomonas reinhardtii*. *Plant J* 82: 449-65
- Ernst O, Zor T. 2010. Linearization of the Bradford protein assay. *J Vis Exp*
- Exposito-Rodriguez M, Laissue PP, Yvon-Durocher G, Smirnoff N, Mullineaux PM. 2017. Photosynthesis-dependent H<sub>2</sub>O<sub>2</sub> transfer from chloroplasts to nuclei provides a high-light signalling mechanism. *Nat Commun* 8: 49
- Farci D, Schröder WP. 2023. Thylakoid Lumen; from “proton bag” to photosynthetic functionally important compartment. *Frontiers in Plant Physiology* 1
- Farnese FS, Menezes-Silva PE, Gusman GS, Oliveira JA. 2016. When Bad Guys Become Good Ones: The Key Role of Reactive Oxygen Species and Nitric Oxide in the Plant Responses to Abiotic Stress. *Front Plant Sci* 7: 471
- Finazzi G, Furia A, Barbagallo RP, Forti G. 1999. State transitions, cyclic and linear electron transport and photophosphorylation in *Chlamydomonas reinhardtii*. *Biochim Biophys Acta* 1413: 117-29

- Finazzi G, Moreau H, Bowler C. 2010. Genomic insights into photosynthesis in eukaryotic phytoplankton. *Trends Plant Sci* 15: 565-72
- Finazzi G, Sommer F, Hippler M. 2005. Release of oxidized plastocyanin from photosystem I limits electron transfer between photosystem I and cytochrome b6f complex in vivo. *Proc Natl Acad Sci U S A* 102: 7031-6
- Fleischmann MM, Ravanel S, Delosme R, Olive J, Zito F, et al. 1999. Isolation and characterization of photoautotrophic mutants of *Chlamydomonas reinhardtii* deficient in state transition. *J Biol Chem* 274: 30987-94
- Foyer CH. 2018. Reactive oxygen species, oxidative signaling and the regulation of photosynthesis. *Environ Exp Bot* 154: 134-42
- Foyer CH, Halliwell B. 1976. The presence of glutathione and glutathione reductase in chloroplasts: A proposed role in ascorbic acid metabolism. *Planta* 133: 21-5
- Foyer CH, Hanke G. 2022. ROS production and signalling in chloroplasts: cornerstones and evolving concepts. *Plant J* 111: 642-61
- Foyer CH, Noctor G. 2011. Ascorbate and glutathione: the heart of the redox hub. *Plant Physiol* 155: 2-18
- Foyer CH, Shigeoka S. 2011. Understanding oxidative stress and antioxidant functions to enhance photosynthesis. *Plant Physiol* 155: 93-100
- Fu L, Liu K, Ferreira RB, Carroll KS, Yang J. 2019. Proteome-Wide Analysis of Cysteine S-Sulfenylation Using a Benzothiazine-Based Probe. *Curr Protoc Protein Sci* 95: e76
- Gäbelein P, Mosebach L, Hippler M. 2017. Bioenergetic Pathways in the Chloroplast: Photosynthetic Electron Transfer. In *Chlamydomonas: Molecular Genetics and Physiology*, ed. M Hippler, pp. 97-134: Springer Cham
- Gallaher SD, Fitz-Gibbon ST, Glaesener AG, Pellegrini M, Merchant SS. 2015. *Chlamydomonas* Genome Resource for Laboratory Strains Reveals a Mosaic of Sequence Variation, Identifies True Strain Histories, and Enables Strain-Specific Studies. *Plant Cell* 27: 2335-52
- Galvan A, Gonzalez-Ballester D, Fernandez E. 2007. Insertional mutagenesis as a tool to study genes/functions in *Chlamydomonas*. *Adv Exp Med Biol* 616: 77-89
- Georgatsou E, Mavrogiannis LA, Fragiadakis GS, Alexandraki D. 1997. The yeast Fre1p/Fre2p cupric reductases facilitate copper uptake and are regulated by the copper-modulated Mac1p activator. *J Biol Chem* 272: 13786-92

- Giraud E, Ho LH, Clifton R, Carroll A, Estavillo G, et al. 2008. The absence of ALTERNATIVE OXIDASE1a in Arabidopsis results in acute sensitivity to combined light and drought stress. *Plant Physiol* 147: 595-610
- Girolomoni L, Cazzaniga S, Pinnola A, Perozeni F, Ballottari M, Bassi R. 2019. LHCSR3 is a nonphotochemical quencher of both photosystems in *Chlamydomonas reinhardtii*. *Proc Natl Acad Sci U S A* 116: 4212-17
- Godaux D, Bailleul B, Berne N, Cardol P. 2015. Induction of Photosynthetic Carbon Fixation in Anoxia Relies on Hydrogenase Activity and Proton-Gradient Regulation-Like1-Mediated Cyclic Electron Flow in *Chlamydomonas reinhardtii*. *Plant Physiol* 168: 648-58
- Goemans CV, Vertommen D, Agrebi R, Collet JF. 2018. CnoX Is a Chaperedoxin: A Holdase that Protects Its Substrates from Irreversible Oxidation. *Mol Cell* 70: 614-27 e7
- Gonzalez-Ballester D, Pootakham W, Mus F, Yang W, Catalanotti C, et al. 2011. Reverse genetics in *Chlamydomonas*: a platform for isolating insertional mutants. *Plant Methods* 7: 24
- Gonzalez-Lainez M, Gallegos M, Munarriz J, Azpiroz R, Passarelli V, et al. 2022. Copper-Catalyzed Azide-Alkyne Cycloaddition (CuAAC) by Functionalized NHC-Based Polynuclear Catalysts: Scope and Mechanistic Insights. *Organometallics* 41: 2154-69
- Goodenough U, Lin H, Lee JH. 2007. Sex determination in *Chlamydomonas*. *Semin Cell Dev Biol* 18: 350-61
- Goodstein DM, Shu S, Howson R, Neupane R, Hayes RD, et al. 2012. Phytozome: a comparative platform for green plant genomics. *Nucleic Acids Res* 40: D1178-86
- Grabherr MG, Haas BJ, Yassour M, Levin JZ, Thompson DA, et al. 2011. Full-length transcriptome assembly from RNA-Seq data without a reference genome. *Nature Biotechnology* 29: 644-52
- Granlund I, Storm P, Schubert M, Garcia-Cerdan JG, Funk C, Schroder WP. 2009. The TL29 protein is lumen located, associated with PSII and not an ascorbate peroxidase. *Plant Cell Physiol* 50: 1898-910
- Grossman A, Sanz-Luque E, Yi H, Yang W. 2019. Building the GreenCut2 suite of proteins to unmask photosynthetic function and regulation. *Microbiology (Reading)* 165: 697-718

- Gupta V, Carroll KS. 2016. Profiling the Reactivity of Cyclic C-Nucleophiles towards Electrophilic Sulfur in Cysteine Sulfenic Acid. *Chem Sci* 7: 400-15
- Gupta V, Yang J, Liebler DC, Carroll KS. 2017. Diverse Redoxome Reactivity Profiles of Carbon Nucleophiles. *J Am Chem Soc* 139: 5588-95
- Hagglund P, Bunkenborg J, Maeda K, Finnie C, Svensson B. 2014. Identification of thioredoxin target disulfides using isotope-coded affinity tags. *Methods Mol Biol* 1072: 677-85
- Hagglund P, Bunkenborg J, Maeda K, Svensson B. 2008. Identification of thioredoxin disulfide targets using a quantitative proteomics approach based on isotope-coded affinity tags. *J Proteome Res* 7: 5270-6
- Hahn A, Vonck J, Mills DJ, Meier T, Kuhlbrandt W. 2018. Structure, mechanism, and regulation of the chloroplast ATP synthase. *Science* 360
- Hamel PP, Salinas-Giegé T, Przybyla-Toscano J, Caccamo A, Subrahmanian N, et al. 2022. The mitochondrion: from genome to proteome In *The Chlamydomonas Sourcebook*, pp. 369-412
- Hanikenne M, Kramer U, Demoulin V, Baurain D. 2005. A comparative inventory of metal transporters in the green alga *Chlamydomonas reinhardtii* and the red alga *Cyanidioschyzon merolae*. *Plant Physiol* 137: 428-46
- Hao C, Yang Y, Du J, Deng XW, Li L. 2022. The PCY-SAG14 phytoeyanin module regulated by PIFs and miR408 promotes dark-induced leaf senescence in *Arabidopsis*. *Proc Natl Acad Sci U S A* 119
- Hao G, Derakhshan B, Shi L, Campagne F, Gross SS. 2006. SNOSID, a proteomic method for identification of cysteine S-nitrosylation sites in complex protein mixtures. *Proc Natl Acad Sci U S A* 103: 1012-7
- Harris EH. 2001. *Chlamydomonas* as a Model Organism. *Annu Rev Plant Physiol Plant Mol Biol* 52: 363-406
- Harris EH. 2009. Chapter 8 - *Chlamydomonas* in the Laboratory. *The Chlamydomonas Sourcebook* Second Edition: 241-302
- He L, Ma H, Song W, Zhou Z, Ma C, Zhang H. 2023. *Arabidopsis* COPT1 copper transporter uses a single histidine to regulate transport activity and protein stability. *Int J Biol Macromol* 241: 124404

- Heinrickel M, Kim RG, Wittkopp TM, Yang W, Walters KA, et al. 2016. Tetratricopeptide repeat protein protects photosystem I from oxidative disruption during assembly. *Proc Natl Acad Sci U S A* 113: 2774-9
- Heinrickel ML, Alric J, Wittkopp T, Yang W, Catalanotti C, et al. 2013. Novel thylakoid membrane GreenCut protein CPLD38 impacts accumulation of the cytochrome b6f complex and associated regulatory processes. *J Biol Chem* 288: 7024-36
- Heinrickel ML, Grossman AR. 2013. The GreenCut: re-evaluation of physiological role of previously studied proteins and potential novel protein functions. *Photosynth Res* 116: 427-36
- Hemschemeier A, Duner M, Casero D, Merchant SS, Winkler M, Happe T. 2013. Hypoxic survival requires a 2-on-2 hemoglobin in a process involving nitric oxide. *Proc Natl Acad Sci U S A* 110: 10854-9
- Hertle AP, Blunder T, Wunder T, Pesaresi P, Pribil M, et al. 2013. PGRL1 is the elusive ferredoxin-plastoquinone reductase in photosynthetic cyclic electron flow. *Mol Cell* 49: 511-23
- Hill KL, Hassett R, Kosman D, Merchant S. 1996. Regulated copper uptake in *Chlamydomonas reinhardtii* in response to copper availability. *Plant Physiol* 112: 697-704
- Hill KL, Merchant S. 1992. In Vivo Competition between Plastocyanin and a Copper-Dependent Regulator of the *Chlamydomonas reinhardtii* Cytochrome c(6) Gene. *Plant Physiol* 100: 319-26
- Hippler M, Drepper F, Farah J, Rochaix JD. 1997. Fast electron transfer from cytochrome c6 and plastocyanin to photosystem I of *Chlamydomonas reinhardtii* requires PsaF. *Biochemistry* 36: 6343-9
- Hippler M, Drepper F, Haehnel W, Rochaix JD. 1998. The N-terminal domain of PsaF: precise recognition site for binding and fast electron transfer from cytochrome c6 and plastocyanin to photosystem I of *Chlamydomonas reinhardtii*. *Proc Natl Acad Sci U S A* 95: 7339-44
- Hisabori T, Sunamura E, Kim Y, Konno H. 2013. The chloroplast ATP synthase features the characteristic redox regulation machinery. *Antioxid Redox Signal* 19: 1846-54
- Hochmal AK, Zinzius K, Charoenwattanasatien R, Gabelein P, Mutoh R, et al. 2016. Calredoxin represents a novel type of calcium-dependent sensor-responder connected to redox regulation in the chloroplast. *Nat Commun* 7: 11847

- Hohmann-Marriott MF, Takizawa K, Eaton-Rye JJ, Mets L, Minagawa J. 2010. The redox state of the plastoquinone pool directly modulates minimum chlorophyll fluorescence yield in *Chlamydomonas reinhardtii*. *FEBS Lett* 584: 1021-6
- Hohner R, Pribil M, Herbstova M, Lopez LS, Kunz HH, et al. 2020. Plastocyanin is the long-range electron carrier between photosystem II and photosystem I in plants. *Proc Natl Acad Sci U S A* 117: 15354-62
- Hong SH, Tripathi BN, Chung MS, Cho C, Lee S, et al. 2018. Functional switching of ascorbate peroxidase 2 of rice (OsAPX2) between peroxidase and molecular chaperone. *Sci Rep* 8: 9171
- Hossain MA, Asada K. 1984. Purification of Dehydroascorbate Reductase from Spinach and Its Characterization as a Thiol Enzyme. *Plant and Cell Physiology* 25: 85-92
- Hossain MA, Asada K. 1985. Monodehydroascorbate reductase from cucumber is a flavin adenine dinucleotide enzyme. *Journal of Biological Chemistry* 260: 12920-26
- Hossain MA, Nakano Y, Asada K. 1984. Monodehydroascorbate Reductase in Spinach Chloroplasts and Its Participation in Regeneration of Ascorbate for Scavenging Hydrogen Peroxide. *Plant and Cell Physiology* 25: 385-95
- Howe G, Merchant S. 1992. The biosynthesis of membrane and soluble plastidic c-type cytochromes of *Chlamydomonas reinhardtii* is dependent on multiple common gene products. *EMBO J* 11: 2789-801
- Huang J, Willems P, Van Breusegem F, Messens J. 2018. Pathways crossing mammalian and plant sulfenomic landscapes. *Free Radic Biol Med* 122: 193-201
- Huang J, Willems P, Wei B, Tian C, Ferreira RB, et al. 2019. Mining for protein S-sulfenylation in Arabidopsis uncovers redox-sensitive sites. *Proc Natl Acad Sci U S A* 116: 21256-61
- Hutner SH, Provasoli L, Schatz A, Haskins C. 1950. Some approaches to the study of the role of metals in the metabolism of microorganisms. *Proceedings of the American Philosophical Society* 94: 152-70
- Hwang T-L, Shaka AJ. 1995. Water Suppression That Works. Excitation Sculpting Using Arbitrary Wave-Forms and Pulsed-Field Gradients. *Journal of Magnetic Resonance, Series A* 112: 275-79

- Iacono F. 2023. *Photosynthetic variation within Chlamydomonas reinhardtii: a multidisciplinary approach to learn from biodiversity*. Research thesis. University of Liège. 209 pp.
- Innami R, Miyamura S, Okoshi M, Nagumo T, Ichihara K, et al. 2022. Gamete dimorphism of the isogamous green alga (*Chlamydomonas reinhardtii*), is regulated by the mating type-determining gene, MID. *Commun Biol* 5: 1333
- Ito H, Iwabuchi M, Ogawa K. 2003. The sugar-metabolic enzymes aldolase and triose-phosphate isomerase are targets of glutathionylation in *Arabidopsis thaliana*: detection using biotinylated glutathione. *Plant Cell Physiol* 44: 655-60
- Jaffrey SR, Snyder SH. 2001. The biotin switch method for the detection of S-nitrosylated proteins. *Sci STKE* 2001: p11
- Jans F, Mignolet E, Houyoux P-A, Cardol P, Ghysels B, et al. 2008. A type II NAD(P)H dehydrogenase mediates light-independent plastoquinone reduction in the chloroplast of *Chlamydomonas*. *Proceedings of the National Academy of Sciences* 105: 20546-51
- Janson G, Zhang C, Prado MG, Paiardini A. 2017. PyMod 2.0: improvements in protein sequence-structure analysis and homology modeling within PyMOL. *Bioinformatics* 33: 444-46
- Jeanneret R, Contino M, Polin M. 2016. A brief introduction to the model microswimmer *Chlamydomonas reinhardtii*. *The European Physical Journal Special Topics* 225: 2141-56
- Jiang J, Nadas IA, Kim MA, Franz KJ. 2005. A Mets motif peptide found in copper transport proteins selectively binds Cu(I) with methionine-only coordination. *Inorg Chem* 44: 9787-94
- Jiang W, Brueggeman AJ, Horken KM, Plucinak TM, Weeks DP. 2014. Successful transient expression of Cas9 and single guide RNA genes in *Chlamydomonas reinhardtii*. *Eukaryot Cell* 13: 1465-9
- Jiang X, Stern D. 2009. Mating and tetrad separation of *Chlamydomonas reinhardtii* for genetic analysis. *J Vis Exp*
- Joet T, Genty B, Josse EM, Kuntz M, Cournac L, Peltier G. 2002. Involvement of a plastid terminal oxidase in plastoquinone oxidation as evidenced by expression of the *Arabidopsis thaliana* enzyme in tobacco. *J Biol Chem* 277: 31623-30

- Johnson X, Alric J. 2013. Central carbon metabolism and electron transport in *Chlamydomonas reinhardtii*: metabolic constraints for carbon partitioning between oil and starch. *Eukaryot Cell* 12: 776-93
- Johnson X, Vandystadt G, Bujaldon S, Wollman FA, Dubois R, et al. 2009. A new setup for in vivo fluorescence imaging of photosynthetic activity. *Photosynth Res* 102: 85-93
- Jokel M, Johnson X, Peltier G, Aro EM, Allahverdiyeva Y. 2018. Hunting the main player enabling *Chlamydomonas reinhardtii* growth under fluctuating light. *Plant J* 94: 822-35
- Josef K, Saranak J, Foster KW. 2006. Linear systems analysis of the ciliary steering behavior associated with negative-phototaxis in *Chlamydomonas reinhardtii*. *Cell Motil Cytoskeleton* 63: 758-77
- Jumper J, Evans R, Pritzel A, Green T, Figurnov M, et al. 2021. Highly accurate protein structure prediction with AlphaFold. *Nature* 596: 583-89
- Jung HS, Chory J. 2010. Signaling between chloroplasts and the nucleus: can a systems biology approach bring clarity to a complex and highly regulated pathway? *Plant Physiol* 152: 453-9
- Kanazawa A, Chattopadhyay A, Kuhlert S, Tuitupou H, Maiti T, Kramer DM. 2021. Light potentials of photosynthetic energy storage in the field: what limits the ability to use or dissipate rapidly increased light energy? *R Soc Open Sci* 8: 211102
- Kang CH, Park JH, Lee ES, Paeng SK, Chae HB, et al. 2020. Redox-Dependent Structural Modification of Nucleoredoxin Triggers Defense Responses against *Alternaria brassicicola* in *Arabidopsis*. *Int J Mol Sci* 21
- Kato N, Nelson G, Lauersen KJ. 2021. Subcellular Localizations of Catalase and Exogenously Added Fatty Acid in *Chlamydomonas reinhardtii*. *Cells* 10
- Kaur S, Prakash P, Bak DH, Hong SH, Cho C, et al. 2021. Regulation of Dual Activity of Ascorbate Peroxidase 1 From *Arabidopsis thaliana* by Conformational Changes and Posttranslational Modifications. *Front Plant Sci* 12: 678111
- Keeling PJ. 2010. The endosymbiotic origin, diversification and fate of plastids. *Philos Trans R Soc Lond B Biol Sci* 365: 729-48
- Kehr S, Jortzik E, Delahunty C, Yates JR, 3rd, Rahlfs S, Becker K. 2011. Protein S-glutathionylation in malaria parasites. *Antioxid Redox Signal* 15: 2855-65



- Kelterborn S, Boehning F, Sizova I, Baidukova O, Evers H, Hegemann P. 2022. Gene Editing in Green Alga *Chlamydomonas reinhardtii* via CRISPR-Cas9 Ribonucleoproteins. *Methods Mol Biol* 2379: 45-65
- Kim J, Lee S, Baek K, Jin E. 2020. Site-Specific Gene Knock-Out and On-Site Heterologous Gene Overexpression in *Chlamydomonas reinhardtii* via a CRISPR-Cas9-Mediated Knock-in Method. *Front Plant Sci* 11: 306
- Kim SY, Jang HH, Lee JR, Sung NR, Lee HB, et al. 2009a. Oligomerization and chaperone activity of a plant 2-Cys peroxiredoxin in response to oxidative stress. *Plant Science* 177: 227-32
- Kim YY, Choi H, Segami S, Cho HT, Martinoia E, et al. 2009b. AtHMA1 contributes to the detoxification of excess Zn(II) in Arabidopsis. *Plant J* 58: 737-53
- Kindle KL. 1990. High-frequency nuclear transformation of *Chlamydomonas reinhardtii*. *Proc Natl Acad Sci U S A* 87: 1228-32
- Kitajima M, Butler WL. 1975. Quenching of chlorophyll fluorescence and primary photochemistry in chloroplasts by dibromothymoquinone. *Biochim Biophys Acta* 376: 105-15
- Kneeshaw S, Keyani R, Delorme-Hinoux V, Imrie L, Loake GJ, et al. 2017. Nucleoredoxin guards against oxidative stress by protecting antioxidant enzymes. *Proc Natl Acad Sci U S A* 114: 8414-19
- Kohler M, Neff C, Perez C, Brunner C, Pardon E, et al. 2018. Binding Specificities of Nanobody\*Membrane Protein Complexes Obtained from Chemical Cross-Linking and High-Mass MALDI Mass Spectrometry. *Anal Chem* 90: 5306-13
- Kohzuma K, Froehlich JE, Davis GA, Temple JA, Minhas D, et al. 2017. The Role of Light-Dark Regulation of the Chloroplast ATP Synthase. *Front Plant Sci* 8: 1248
- Koide S, Dyson HJ, Wright PE. 1993. Characterization of a folding intermediate of apoplastocyanin trapped by proline isomerization. *Biochemistry* 32: 12299-310
- Kolb HC, Finn MG, Sharpless KB. 2001. Click Chemistry: Diverse Chemical Function from a Few Good Reactions. *Angew Chem Int Ed Engl* 40: 2004-21
- Komsic-Buchmann K, Wostehoff L, Becker B. 2014. The contractile vacuole as a key regulator of cellular water flow in *Chlamydomonas reinhardtii*. *Eukaryot Cell* 13: 1421-30

- Kong F, Liang Y, Legeret B, Beyly-Adriano A, Blangy S, et al. 2017. Chlamydomonas carries out fatty acid beta-oxidation in ancestral peroxisomes using a bona fide acyl-CoA oxidase. *Plant J* 90: 358-71
- Krieger-Liszkay A, Feilke K. 2015. The Dual Role of the Plastid Terminal Oxidase PTOX: Between a Protective and a Pro-oxidant Function. *Front Plant Sci* 6: 1147
- Kropat J, Gallaher SD, Urzica EI, Nakamoto SS, Strenkert D, et al. 2015. Copper economy in Chlamydomonas: prioritized allocation and reallocation of copper to respiration vs. photosynthesis. *Proc Natl Acad Sci U S A* 112: 2644-51
- Kropat J, Tottey S, Birkenbihl RP, Depege N, Huijser P, Merchant S. 2005. A regulator of nutritional copper signaling in Chlamydomonas is an SBP domain protein that recognizes the GTAC core of copper response element. *Proc Natl Acad Sci U S A* 102: 18730-5
- Kuhlgert S, Drepper F, Fufezan C, Sommer F, Hippler M. 2012. Residues PsaB Asp612 and PsaB Glu613 of photosystem I confer pH-dependent binding of plastocyanin and cytochrome c(6). *Biochemistry* 51: 7297-303
- Kumar SV, Misquitta RW, Reddy VS, Rao BJ, Rajam MV. 2004. Genetic transformation of the green alga—Chlamydomonas reinhardtii by Agrobacterium tumefaciens. *Plant Science* 166: 731-38
- Kuo EY, Cai MS, Lee TM. 2020a. Ascorbate peroxidase 4 plays a role in the tolerance of Chlamydomonas reinhardtii to photo-oxidative stress. *Sci Rep* 10: 13287
- Kuo EY, Chien Y-L, Dai W-C, Huang MJ-H, Lee T-M. 2020b. *The Acclimation Mechanisms of Chlamydomonas reinhardtii against Nitrosative Stress: A Role of NADPH Oxidase (RBOL2) in the Regulation of Nitric Oxide-Mediated ER Stress and Glutathione Redox State*. Presented at The 1st International Electronic Conference on Plant Science,
- Kurisu G, Kusunoki M, Katoh E, Yamazaki T, Teshima K, et al. 2001. Structure of the electron transfer complex between ferredoxin and ferredoxin-NADP(+) reductase. *Nat Struct Biol* 8: 117-21
- La Fontaine S, Quinn JM, Nakamoto SS, Page MD, Gohre V, et al. 2002. Copper-dependent iron assimilation pathway in the model photosynthetic eukaryote Chlamydomonas reinhardtii. *Eukaryot Cell* 1: 736-57
- Labs M, Ruhle T, Leister D. 2016. The antimycin A-sensitive pathway of cyclic electron flow: from 1963 to 2015. *Photosynth Res* 129: 231-8

- Lamkemeyer P, Laxa M, Collin V, Li W, Finkemeier I, et al. 2006. Peroxiredoxin Q of *Arabidopsis thaliana* is attached to the thylakoids and functions in context of photosynthesis. *Plant J* 45: 968-81
- Langmead B, Salzberg SL. 2012. Fast gapped-read alignment with Bowtie 2. *Nat Methods* 9: 357-9
- Lauersen KJ, Willamme R, Coosemans N, Joris M, Kruse O, Remacle C. 2016. Peroxisomal microbodies are at the crossroads of acetate assimilation in the green microalga *Chlamydomonas reinhardtii*. *Algal Research* 16: 266-74
- Laurent TC, Moore EC, Reichard P. 1964. Enzymatic Synthesis of Deoxyribonucleotides. Iv. Isolation and Characterization of Thioredoxin, the Hydrogen Donor from *Escherichia Coli* B. *J Biol Chem* 239: 3436-44
- Lazarotto F, Menguer PK, Del-Bem LE, Zamocky M, Margis-Pinheiro M. 2021a. Ascorbate Peroxidase Neofunctionalization at the Origin of APX-R and APX-L: Evidence from Basal Archaeplastida. *Antioxidants (Basel)* 10
- Lazarotto F, Teixeira FK, Rosa SB, Dunand C, Fernandes CL, et al. 2011. Ascorbate peroxidase-related (APx-R) is a new heme-containing protein functionally associated with ascorbate peroxidase but evolutionarily divergent. *New Phytol* 191: 234-50
- Lazarotto F, Turchetto-Zolet AC, Margis-Pinheiro M. 2015. Revisiting the Non-Animal Peroxidase Superfamily. *Trends Plant Sci* 20: 807-13
- Lazarotto F, Wahni K, Piovesana M, Maraschin F, Messens J, Margis-Pinheiro M. 2021b. Arabidopsis APx-R Is a Plastidial Ascorbate-Independent Peroxidase Regulated by Photomorphogenesis. *Antioxidants (Basel)* 10
- Le Moigne T, Boisset ND, de Carpentier F, Crozet P, Danon A, et al. 2023. Photoproduction of reducing power and the Calvin-Benson cycle In *The Chlamydomonas Sourcebook*, pp. 273-315
- Leliaert F, Smith DR, Moreau H, Herron MD, Verbruggen H, et al. 2012. Phylogeny and Molecular Evolution of the Green Algae. *Critical Reviews in Plant Sciences* 31: 1-46
- Leliaert F, Verbruggen H, Zechman FW. 2011. Into the deep: new discoveries at the base of the green plant phylogeny. *Bioessays* 33: 683-92
- Lemaire SD, Miginiac-Maslow M. 2004. The thioredoxin superfamily in *Chlamydomonas reinhardtii*. *Photosynth Res* 82: 203-20

- Lemeille S, Rochaix JD. 2010. State transitions at the crossroad of thylakoid signalling pathways. *Photosynth Res* 106: 33-46
- Lemeille S, Willig A, Depege-Fargeix N, Delessert C, Bassi R, Rochaix JD. 2009. Analysis of the chloroplast protein kinase Stt7 during state transitions. *PLoS Biol* 7: e45
- Li B, Dewey CN. 2011. RSEM: accurate transcript quantification from RNA-Seq data with or without a reference genome. *BMC Bioinformatics* 12: 323
- Li HH, Merchant S. 1992. Two metal-dependent steps in the biosynthesis of *Scenedesmus obliquus* plastocyanin. Differential mRNA accumulation and holoprotein formation. *Journal of Biological Chemistry* 267: 9368-75
- Li HH, Merchant S. 1995. Degradation of plastocyanin in copper-deficient *Chlamydomonas reinhardtii*. Evidence for a protease-susceptible conformation of the apoprotein and regulated proteolysis. *J Biol Chem* 270: 23504-10
- Li M, Kim C. 2022. Chloroplast ROS and stress signaling. *Plant Commun* 3: 100264
- Li M, Mukhopadhyay R, Svoboda V, Oung HMO, Mullendore DL, Kirchhoff H. 2020. Measuring the dynamic response of the thylakoid architecture in plant leaves by electron microscopy. *Plant Direct* 4: e00280
- Li X, Patena W, Fauser F, Jinkerson RE, Saroussi S, et al. 2019. A genome-wide algal mutant library and functional screen identifies genes required for eukaryotic photosynthesis. *Nat Genet* 51: 627-35
- Li X, Zhang R, Patena W, Gang SS, Blum SR, et al. 2016. An Indexed, Mapped Mutant Library Enables Reverse Genetics Studies of Biological Processes in *Chlamydomonas reinhardtii*. *Plant Cell* 28: 367-87
- Li X, Zhang T, Day NJ, Feng S, Gaffrey MJ, Qian WJ. 2022. Defining the S-Glutathionylation Proteome by Biochemical and Mass Spectrometric Approaches. *Antioxidants (Basel)* 11
- Lima-Melo Y, Kilic M, Aro EM, Gollan PJ. 2021. Photosystem I Inhibition, Protection and Signalling: Knowns and Unknowns. *Front Plant Sci* 12: 791124
- Liu L, Hausladen A, Zeng M, Que L, Heitman J, Stamler JS. 2001. A metabolic enzyme for S-nitrosothiol conserved from bacteria to humans. *Nature* 410: 490-4
- Liu XL, Yu HD, Guan Y, Li JK, Guo FQ. 2012. Carbonylation and loss-of-function analyses of SBPase reveal its metabolic interface role in oxidative stress, carbon

- assimilation, and multiple aspects of growth and development in Arabidopsis. *Mol Plant* 5: 1082-99
- Liu XP, Liu XY, Zhang J, Xia ZL, Liu X, et al. 2006. Molecular and functional characterization of sulfiredoxin homologs from higher plants. *Cell Res* 16: 287-96
- Liu Y, He C. 2017. A review of redox signaling and the control of MAP kinase pathway in plants. *Redox Biol* 11: 192-204
- Lo Conte M, Carroll KS. 2013. The redox biochemistry of protein sulfenylation and sulfinylation. *J Biol Chem* 288: 26480-8
- Love MI, Huber W, Anders S. 2014. Moderated estimation of fold change and dispersion for RNA-seq data with DESeq2. *Genome Biol* 15: 550
- Lundberg E, Storm P, Schroder WP, Funk C. 2011. Crystal structure of the TL29 protein from Arabidopsis thaliana: an APX homolog without peroxidase activity. *J Struct Biol* 176: 24-31
- Luo T, Pueyo JM, Wahni K, Yvanoff C, Lazar T, et al. 2021. Thiol-disulphide independent in-cell trapping for the identification of peroxiredoxin 2 interactors. *Redox Biol* 46: 102066
- Ma X, Wei H, Zhang Y, Duan Y, Zhang W, et al. 2020a. Glutathione peroxidase 5 deficiency induces lipid metabolism regulated by reactive oxygen species in Chlamydomonas reinhardtii. *Microb Pathog* 147: 104358
- Ma X, Zhang B, Miao R, Deng X, Duan Y, et al. 2020b. Transcriptomic and Physiological Responses to Oxidative Stress in a Chlamydomonas reinhardtii Glutathione Peroxidase Mutant. *Genes (Basel)* 11
- Macdonald IK, Badyal SK, Ghamsari L, Moody PC, Raven EL. 2006. Interaction of ascorbate peroxidase with substrates: a mechanistic and structural analysis. *Biochemistry* 45: 7808-17
- Mackinder LC, Meyer MT, Mettler-Altmann T, Chen VK, Mitchell MC, et al. 2016. A repeat protein links Rubisco to form the eukaryotic carbon-concentrating organelle. *Proc Natl Acad Sci U S A* 113: 5958-63
- Malnoe A, Wollman FA, de Vitry C, Rappaport F. 2011. Photosynthetic growth despite a broken Q-cycle. *Nat Commun* 2: 301

- Malone LA, Proctor MS, Hitchcock A, Hunter CN, Johnson MP. 2021. Cytochrome b(6)f - Orchestrator of photosynthetic electron transfer. *Biochim Biophys Acta Bioenerg* 1862: 148380
- Martinez SE, Huang D, Szczepaniak A, Cramer WA, Smith JL. 1994. Crystal structure of chloroplast cytochrome freveals a novel cytochrome fold and unexpected heme ligation. *Structure* 2: 95-105
- Maruta T, Tanouchi A, Tamoi M, Yabuta Y, Yoshimura K, et al. 2009. Arabidopsis Chloroplastic Ascorbate Peroxidase Isoenzymes Play a Dual Role in Photoprotection and Gene Regulation under Photooxidative Stress. *Plant and Cell Physiology* 51: 190-200
- Mason CB, Bricker TM, Moroney JV. 2006. A rapid method for chloroplast isolation from the green alga *Chlamydomonas reinhardtii*. *Nat Protoc* 1: 2227-30
- Massoz S, Cardol P., González-Halphen, D., Remacle, C. 2017. Mitochondrial Bioenergetics Pathways in *Chlamydomonas*. *Chlamydomonas: Molecular Genetics and Physiology* 30: 59-95
- Maul JE, Lilly JW, Cui L, dePamphilis CW, Miller W, et al. 2002. The *Chlamydomonas reinhardtii* plastid chromosome: islands of genes in a sea of repeats. *Plant Cell* 14: 2659-79
- Maxwell K, Johnson GN. 2000. Chlorophyll fluorescence--a practical guide. *J Exp Bot* 51: 659-68
- Mayfield SP, Schirmer-Rahire M, Frank G, Zuber H, Rochaix JD. 1989. Analysis of the genes of the OEE1 and OEE3 proteins of the photosystem II complex from *Chlamydomonas reinhardtii*. *Plant Mol Biol* 12: 683-93
- Mbadinga Mbadinga DL, Li Q, Ranocha P, Martinez Y, Dunand C. 2020. Global analysis of non-animal peroxidases provides insights into the evolution of this gene family in the green lineage. *J Exp Bot* 71: 3350-60
- McConnell EW, Werth EG, Hicks LM. 2018. The phosphorylated redox proteome of *Chlamydomonas reinhardtii*: Revealing novel means for regulation of protein structure and function. *Redox Biol* 17: 35-46
- Mehler AH. 1951. Studies on reactions of illuminated chloroplasts. I. Mechanism of the reduction of oxygen and other Hill reagents. *Arch Biochem Biophys* 33: 65-77
- Merchant S, Bogorad L. 1986. Rapid degradation of apoplastocyanin in Cu(II)-deficient cells of *Chlamydomonas reinhardtii*. *J Biol Chem* 261: 15850-3

- Merchant S, Bogorad L. 1987. The Cu(II)-repressible plastidic cytochrome c. Cloning and sequence of a complementary DNA for the pre-apoprotein. *J Biol Chem* 262: 9062-7
- Merchant SS, Prochnik SE, Vallon O, Harris EH, Karpowicz SJ, et al. 2007. The *Chlamydomonas* genome reveals the evolution of key animal and plant functions. *Science* 318: 245-50
- Merchant SS, Schmollinger S, Strenkert D, Moseley JL, Blaby-Haas CE. 2020. From economy to luxury: Copper homeostasis in *Chlamydomonas* and other algae. *Biochim Biophys Acta Mol Cell Res* 1867: 118822
- Miao Y, Lv D, Wang P, Wang XC, Chen J, et al. 2006. An *Arabidopsis* glutathione peroxidase functions as both a redox transducer and a scavenger in abscisic acid and drought stress responses. *Plant Cell* 18: 2749-66
- Michelet L, Zaffagnini M, Vanacker H, Le Marechal P, Marchand C, et al. 2008. In vivo targets of S-thiolation in *Chlamydomonas reinhardtii*. *J Biol Chem* 283: 21571-8
- Minagawa J. 2013. Dynamic reorganization of photosynthetic supercomplexes during environmental acclimation of photosynthesis. *Front Plant Sci* 4: 513
- Mirdita M, Schutze K, Moriwaki Y, Heo L, Ovchinnikov S, Steinegger M. 2022. ColabFold: making protein folding accessible to all. *Nat Methods* 19: 679-82
- Mittler R. 2017. ROS Are Good. *Trends Plant Sci* 22: 11-19
- Miyagawa Y, Tamoi M, Shigeoka S. 2000. Evaluation of the defense system in chloroplasts to photooxidative stress caused by paraquat using transgenic tobacco plants expressing catalase from *Escherichia coli*. *Plant Cell Physiol* 41: 311-20
- Miyake C, Michihata, F., Asada, K. 1991. Scavenging of Hydrogen Peroxide in Prokaryotic and Eukaryotic Algae: Acquisition of Ascorbate Peroxidase during the Evolution of Cyanobacteria. *Plant and Cell Physiology* 32: 33 - 43
- Molnar A, Bassett A, Thuenemann E, Schwach F, Karkare S, et al. 2009. Highly specific gene silencing by artificial microRNAs in the unicellular alga *Chlamydomonas reinhardtii*. *Plant J* 58: 165-74
- Moreno I, Norambuena L, Maturana D, Toro M, Vergara C, et al. 2008. AtHMA1 is a thapsigargin-sensitive Ca<sup>2+</sup>/heavy metal pump. *J Biol Chem* 283: 9633-41

- Morisse S, Zaffagnini M, Gao XH, Lemaire SD, Marchand CH. 2014. Insight into protein S-nitrosylation in *Chlamydomonas reinhardtii*. *Antioxid Redox Signal* 21: 1271-84
- Moss DA, Bendall DS. 1984. Cyclic electron transport in chloroplasts. The Q-cycle and the site of action of antimycin. *Biochimica et Biophysica Acta (BBA) - Bioenergetics* 767: 389-95
- Mukherjee S. 2021. Cysteine modifications (oxPTM) and protein sulphenylation-mediated sulfenome expression in plants: evolutionary conserved signaling networks? *Plant Signal Behav* 16: 1831792
- Muller P, Li XP, Niyogi KK. 2001. Non-photochemical quenching. A response to excess light energy. *Plant Physiol* 125: 1558-66
- Munekage Y, Hojo M, Meurer J, Endo T, Tasaka M, Shikanai T. 2002. PGR5 is involved in cyclic electron flow around photosystem I and is essential for photoprotection in *Arabidopsis*. *Cell* 110: 361-71
- Murik O, Elboher A, Kaplan A. 2014. Dehydroascorbate: a possible surveillance molecule of oxidative stress and programmed cell death in the green alga *Chlamydomonas reinhardtii*. *New Phytol* 202: 471-84
- Muthuramalingam M, Seidel T, Laxa M, Nunes de Miranda SM, Gartner F, et al. 2009. Multiple redox and non-redox interactions define 2-Cys peroxiredoxin as a regulatory hub in the chloroplast. *Mol Plant* 2: 1273-88
- Nawrocki WJ, Bailleul B, Cardol P, Rappaport F, Wollman FA, Joliot P. 2019a. Maximal cyclic electron flow rate is independent of PGRL1 in *Chlamydomonas*. *Biochim Biophys Acta Bioenerg* 1860: 425-32
- Nawrocki WJ, Bailleul B, Picot D, Cardol P, Rappaport F, et al. 2019b. The mechanism of cyclic electron flow. *Biochim Biophys Acta Bioenerg* 1860: 433-38
- Nawrocki WJ, Liu X, Raber B, Hu C, de Vitry C, et al. 2021. Molecular origins of induction and loss of photoinhibition-related energy dissipation q(I). *Sci Adv* 7: eabj0055
- Newman SM, Boynton JE, Gillham NW, Randolph-Anderson BL, Johnson AM, Harris EH. 1990. Transformation of chloroplast ribosomal RNA genes in *Chlamydomonas*: molecular and genetic characterization of integration events. *Genetics* 126: 875-88



- Nguyen PN, Tossounian MA, Kovacs DS, Thu TT, Stijlemans B, et al. 2020. Dehydrin ERD14 activates glutathione transferase Phi9 in *Arabidopsis thaliana* under osmotic stress. *Biochim Biophys Acta Gen Subj* 1864: 129506
- Niemeyer J, Scheuring D, Oestreicher J, Morgan B, Schroda M. 2021. Real-time monitoring of subcellular H<sub>2</sub>O<sub>2</sub> distribution in *Chlamydomonas reinhardtii*. *The Plant Cell* 33: 2935-49
- Nikkanen L, Rintamäki E. 2019. Chloroplast thioredoxin systems dynamically regulate photosynthesis in plants. *Biochemical Journal* 476: 1159-72
- Nikkanen L, Toivola J, Rintamaki E. 2016. Crosstalk between chloroplast thioredoxin systems in regulation of photosynthesis. *Plant Cell Environ* 39: 1691-705
- Nikolova D, Heilmann C, Hawat S, Gabelein P, Hippler M. 2018. Absolute quantification of selected photosynthetic electron transfer proteins in *Chlamydomonas reinhardtii* in the presence and absence of oxygen. *Photosynth Res* 137: 281-93
- Nouet C, Charlier JB, Carnol M, Bosman B, Farnir F, et al. 2015. Functional analysis of the three HMA4 copies of the metal hyperaccumulator *Arabidopsis halleri*. *J Exp Bot* 66: 5783-95
- Ogola HJ, Kamiike T, Hashimoto N, Ashida H, Ishikawa T, et al. 2009. Molecular characterization of a novel peroxidase from the cyanobacterium *Anabaena* sp. strain PCC 7120. *Appl Environ Microbiol* 75: 7509-18
- Ozawa S-I, Bald T, Onishi T, Xue H, Matsumura T, et al. 2018. Configuration of Ten Light-Harvesting Chlorophyll a/b Complex I Subunits in *Chlamydomonas reinhardtii* Photosystem I. *Plant Physiology* 178: 583-95
- Page MD, Allen MD, Kropat J, Urzica EI, Karpowicz SJ, et al. 2012. Fe sparing and Fe recycling contribute to increased superoxide dismutase capacity in iron-starved *Chlamydomonas reinhardtii*. *Plant Cell* 24: 2649-65
- Page MD, Kropat J, Hamel PP, Merchant SS. 2009. Two *Chlamydomonas* CTR copper transporters with a novel cys-met motif are localized to the plasma membrane and function in copper assimilation. *Plant Cell* 21: 928-43
- Pak VV, Ezerina D, Lyublinskaya OG, Pedre B, Tyurin-Kuzmin PA, et al. 2020. Ultrasensitive Genetically Encoded Indicator for Hydrogen Peroxide Identifies Roles for the Oxidant in Cell Migration and Mitochondrial Function. *Cell Metab* 31: 642-53 e6

- Pascual MB, Mata-Cabana A, Florencio FJ, Lindahl M, Cejudo FJ. 2011. A comparative analysis of the NADPH thioredoxin reductase C-2-Cys peroxiredoxin system from plants and cyanobacteria. *Plant Physiol* 155: 1806-16
- Peltier G, Aro EM, Shikanai T. 2016. NDH-1 and NDH-2 Plastoquinone Reductases in Oxygenic Photosynthesis. *Annu Rev Plant Biol* 67: 55-80
- Perez-Perez ME, Mauries A, Maes A, Tourasse NJ, Hamon M, et al. 2017. The Deep Thioredoxome in *Chlamydomonas reinhardtii*: New Insights into Redox Regulation. *Mol Plant* 10: 1107-25
- Perez-Riverol Y, Bai J, Bandla C, Garcia-Seisdedos D, Hewapathirana S, et al. 2022. The PRIDE database resources in 2022: a hub for mass spectrometry-based proteomics evidences. *Nucleic Acids Res* 50: D543-D52
- Pesaresi P, Scharfenberg M, Weigel M, Granlund I, Schroder WP, et al. 2009. Mutants, overexpressors, and interactors of Arabidopsis plastocyanin isoforms: revised roles of plastocyanin in photosynthetic electron flow and thylakoid redox state. *Mol Plant* 2: 236-48
- Petersson UA, Kieselbach T, Garcia-Cerdan JG, Schroder WP. 2006. The Prx Q protein of Arabidopsis thaliana is a member of the luminal chloroplast proteome. *FEBS Lett* 580: 6055-61
- Pham AN, Xing G, Miller CJ, Waite TD. 2013. Fenton-like copper redox chemistry revisited: Hydrogen peroxide and superoxide mediation of copper-catalyzed oxidant production. *Journal of Catalysis* 301: 54-64
- Pham KLJ, Schmollinger S, Merchant SS, Strenkert D. 2022. *Chlamydomonas* ATX1 is essential for Cu distribution to multiple cupro-enzymes and maintenance of biomass in conditions demanding cupro-enzyme-dependent metabolic pathways. *Plant Direct* 6: e383
- Pierre Y, Breyton C, Kramer D, Popot JL. 1995. Purification and characterization of the cytochrome b6 f complex from *Chlamydomonas reinhardtii*. *J Biol Chem* 270: 29342-9
- Plancke C, Vigeolas H, Hohner R, Roberty S, Emonds-Alt B, et al. 2014. Lack of isocitrate lyase in *Chlamydomonas* leads to changes in carbon metabolism and in the response to oxidative stress under mixotrophic growth. *Plant J* 77: 404-17
- Pootakham W, Gonzalez-Ballester D, Grossman AR. 2010. Identification and regulation of plasma membrane sulfate transporters in *Chlamydomonas*. *Plant Physiol* 153: 1653-68

- Pospisil P. 2016. Production of Reactive Oxygen Species by Photosystem II as a Response to Light and Temperature Stress. *Front Plant Sci* 7: 1950
- Pulido P, Spinola MC, Kirchsteiger K, Guinea M, Pascual MB, et al. 2010. Functional analysis of the pathways for 2-Cys peroxiredoxin reduction in *Arabidopsis thaliana* chloroplasts. *J Exp Bot* 61: 4043-54
- Puthiyaveetil S. 2011. A mechanism for regulation of chloroplast LHC II kinase by plastoquinol and thioredoxin. *FEBS Lett* 585: 1717-21
- Quinn JM, Eriksson M, Moseley JL, Merchant S. 2002. Oxygen deficiency responsive gene expression in *Chlamydomonas reinhardtii* through a copper-sensing signal transduction pathway. *Plant Physiol* 128: 463-71
- Quinn JM, Merchant S. 1995. Two copper-responsive elements associated with the *Chlamydomonas* Cyc6 gene function as targets for transcriptional activators. *Plant Cell* 7: 623-8
- Raven EL. 2003. Understanding functional diversity and substrate specificity in haem peroxidases: what can we learn from ascorbate peroxidase? *Nat Prod Rep* 20: 367-81
- Redekop P, Rothhausen N, Rothhausen N, Melzer M, Mosebach L, et al. 2020. PsbS contributes to photoprotection in *Chlamydomonas reinhardtii* independently of energy dissipation. *Biochim Biophys Acta Bioenerg* 1861: 148183
- Remacle C, Cardol P, Coosemans N, Gaisne M, Bonnefoy N. 2006. High-efficiency biolistic transformation of *Chlamydomonas* mitochondria can be used to insert mutations in complex I genes. *Proc Natl Acad Sci U S A* 103: 4771-6
- Rey P, Becuwe N, Barrault MB, Rumeau D, Havaux M, et al. 2007. The *Arabidopsis thaliana* sulfiredoxin is a plastidic cysteine-sulfinic acid reductase involved in the photooxidative stress response. *Plant J* 49: 505-14
- Ritchie RJ. 2006. Consistent sets of spectrophotometric chlorophyll equations for acetone, methanol and ethanol solvents. *Photosynth Res* 89: 27-41
- Roach T, Na CS. 2017. LHCSR3 affects de-coupling and re-coupling of LHCI to PSII during state transitions in *Chlamydomonas reinhardtii*. *Sci Rep* 7: 43145
- Roach T, Na CS, Krieger-Liszkay A. 2015. High light-induced hydrogen peroxide production in *Chlamydomonas reinhardtii* is increased by high CO<sub>2</sub> availability. *Plant J* 81: 759-66

- Rochaix JD. 1995. Chlamydomonas reinhardtii as the photosynthetic yeast. *Annu Rev Genet* 29: 209-30
- Roos G, Messens J. 2011. Protein sulfenic acid formation: from cellular damage to redox regulation. *Free Radic Biol Med* 51: 314-26
- Rouhier N, Lemaire SD, Jacquot JP. 2008. The role of glutathione in photosynthetic organisms: emerging functions for glutaredoxins and glutathionylation. *Annu Rev Plant Biol* 59: 143-66
- Rubino JT, Riggs-Gelasco P, Franz KJ. 2010. Methionine motifs of copper transport proteins provide general and flexible thioether-only binding sites for Cu(I) and Ag(I). *J Biol Inorg Chem* 15: 1033-49
- Sager R. 1955. Inheritance in the Green Alga Chlamydomonas Reinhardi. *Genetics* 40: 476-89
- Sager R, Granick S. 1953. Nutritional studies with Chlamydomonas reinhardi. *Ann NY Acad Sci* 56: 831-8
- Sasso S, Stibor H, Mittag M, Grossman AR. 2018. From molecular manipulation of domesticated Chlamydomonas reinhardtii to survival in nature. *Elife* 7
- Schagger H. 2006. Tricine-SDS-PAGE. *Nat Protoc* 1: 16-22
- Schurmann P, Buchanan BB. 2008. The ferredoxin/thioredoxin system of oxygenic photosynthesis. *Antioxid Redox Signal* 10: 1235-74
- Seigneurin-Berny D, Gravot A, Auroy P, Mazard C, Kraut A, et al. 2006. HMA1, a new Cu-ATPase of the chloroplast envelope, is essential for growth under adverse light conditions. *J Biol Chem* 281: 2882-92
- Serrato AJ, Perez-Ruiz JM, Spinola MC, Cejudo FJ. 2004. A novel NADPH thioredoxin reductase, localized in the chloroplast, which deficiency causes hypersensitivity to abiotic stress in Arabidopsis thaliana. *J Biol Chem* 279: 43821-7
- Shao N, Beck CF, Lemaire SD, Krieger-Liszczay A. 2008. Photosynthetic electron flow affects H<sub>2</sub>O<sub>2</sub> signaling by inactivation of catalase in Chlamydomonas reinhardtii. *Planta* 228: 1055-66
- Shcolnick S, Keren N. 2006. Metal homeostasis in cyanobacteria and chloroplasts. Balancing benefits and risks to the photosynthetic apparatus. *Plant Physiol* 141: 805-10

- Shen L, Huang Z, Chang S, Wang W, Wang J, et al. 2019. Structure of a C(2)S(2)M(2)N(2)-type PSII-LHCII supercomplex from the green alga *Chlamydomonas reinhardtii*. *Proc Natl Acad Sci U S A* 116: 21246-55
- Shi Y, Fu L, Yang J, Carroll KS. 2021. Wittig reagents for chemoselective sulfenic acid ligation enables global site stoichiometry analysis and redox-controlled mitochondrial targeting. *Nat Chem* 13: 1140-50
- Shigeoka S, Ishikawa T, Tamoi M, Miyagawa Y, Takeda T, et al. 2002. Regulation and function of ascorbate peroxidase isoenzymes. *Journal of Experimental Botany* 53: 1305-19
- Shimakawa G, Miyake C. 2018. Oxidation of P700 Ensures Robust Photosynthesis. *Front Plant Sci* 9: 1617
- Shimogawara K, Fujiwara S, Grossman A, Usuda H. 1998. High-efficiency transformation of *Chlamydomonas reinhardtii* by electroporation. *Genetics* 148: 1821-8
- Sizova I, Greiner A, Awasthi M, Kateriya S, Hegemann P. 2013. Nuclear gene targeting in *Chlamydomonas* using engineered zinc-finger nucleases. *Plant J* 73: 873-82
- Slaninová M, Hroššová D, Vlček D, Mages W. 2008. Is it possible to improve homologous recombination in *Chlamydomonas reinhardtii*? *Biologia* 63: 941-46
- Smeekens S, Bauerle C, Hageman J, Keegstra K, Weisbeek P. 1986. The role of the transit peptide in the routing of precursors toward different chloroplast compartments. *Cell* 46: 365-75
- Smith GM. 1946. The nature of sexuality in *Chlamydomonas*. *Am J Bot* 33: 625-30
- Smith GM, Regnery DC. 1950. Inheritance of Sexuality in *Chlamydomonas Reinhardtii*. *Proc Natl Acad Sci U S A* 36: 246-8
- Sommer F, Drepper F, Hippler M. 2002. The luminal helix I of PsaB is essential for recognition of plastocyanin or cytochrome c6 and fast electron transfer to photosystem I in *Chlamydomonas reinhardtii*. *J Biol Chem* 277: 6573-81
- Sommer F, Kropat J, Malasarn D, Grosseohme NE, Chen X, et al. 2010. The CRR1 nutritional copper sensor in *Chlamydomonas* contains two distinct metal-responsive domains. *Plant Cell* 22: 4098-113
- Sousa RHV, Carvalho FEL, Lima-Melo Y, Alencar VTCB, Daloso DM, et al. 2018. Impairment of peroxisomal APX and CAT activities increases protection of

photosynthesis under oxidative stress. *Journal of Experimental Botany* 70: 627-39

- Strand DD, Fisher N, Davis GA, Kramer DM. 2016. Redox regulation of the antimycin A sensitive pathway of cyclic electron flow around photosystem I in higher plant thylakoids. *Biochim Biophys Acta* 1857: 1-6
- Strand DD, Fisher N, Kramer DM. 2017. The higher plant plastid NAD(P)H dehydrogenase-like complex (NDH) is a high efficiency proton pump that increases ATP production by cyclic electron flow. *J Biol Chem* 292: 11850-60
- Strand DD, Livingston AK, Satoh-Cruz M, Froehlich JE, Maurino VG, Kramer DM. 2015. Activation of cyclic electron flow by hydrogen peroxide in vivo. *Proc Natl Acad Sci U S A* 112: 5539-44
- Strasser RJ, Govindjee. 1992. The Fo and the O-J-I-P Fluorescence Rise in Higher Plants and Algae In *Regulation of Chloroplast Biogenesis*, pp. 423-26
- Strenkert D, Schmollinger S, Gallaher SD, Salome PA, Purvine SO, et al. 2019. Multiomics resolution of molecular events during a day in the life of *Chlamydomonas*. *Proc Natl Acad Sci U S A* 116: 2374-83
- Sylvestre-Gonon E, Schwartz M, Girardet JM, Hecker A, Rouhier N. 2020. Is there a role for tau glutathione transferases in tetrapyrrole metabolism and retrograde signalling in plants? *Philos Trans R Soc Lond B Biol Sci* 375: 20190404
- Takahashi H, Iwai M, Takahashi Y, Minagawa J. 2006. Identification of the mobile light-harvesting complex II polypeptides for state transitions in *Chlamydomonas reinhardtii*. *Proc Natl Acad Sci U S A* 103: 477-82
- Takanishi CL, Ma LH, Wood MJ. 2007. A genetically encoded probe for cysteine sulfenic acid protein modification in vivo. *Biochemistry* 46: 14725-32
- Tardif M, Atteia A, Specht M, Cogne G, Rolland N, et al. 2012. PredAlgo: a new subcellular localization prediction tool dedicated to green algae. *Mol Biol Evol* 29: 3625-39
- Telman W, Liebthal M, Dietz KJ. 2020. Redox regulation by peroxiredoxins is linked to their thioredoxin-dependent oxidase function. *Photosynth Res* 145: 31-41
- Terzulli A, Kosman DJ. 2010. Analysis of the high-affinity iron uptake system at the *Chlamydomonas reinhardtii* plasma membrane. *Eukaryot Cell* 9: 815-26
- Thompson MD, Mittelmeier, T.M., Dieckmann, C.L. . 2017. *Chlamydomonas*: The Eyespot. *Springer* 30: 257-81

- Tikkanen M, Mekala NR, Aro EM. 2014. Photosystem II photoinhibition-repair cycle protects Photosystem I from irreversible damage. *Biochim Biophys Acta* 1837: 210-5
- Tyagi S, Shumayla, Verma PC, Singh K, Upadhyay SK. 2020. Molecular characterization of ascorbate peroxidase (APX) and APX-related (APX-R) genes in *Triticum aestivum* L. *Genomics* 112: 4208-23
- Ubbink M, Lian LY, Modi S, Evans PA, Bendall DS. 1996. Analysis of the <sup>1</sup>H-NMR chemical shifts of Cu(I)-, Cu(II)- and Cd-substituted pea plastocyanin. Metal-dependent differences in the hydrogen-bond network around the copper site. *Eur J Biochem* 242: 132-47
- Uchanski T, Pardon E, Steyaert J. 2020. Nanobodies to study protein conformational states. *Curr Opin Struct Biol* 60: 117-23
- Umate P. 2010. Genome-wide analysis of the family of light-harvesting chlorophyll a/b-binding proteins in *Arabidopsis* and rice. *Plant Signal Behav* 5: 1537-42
- Vahrenholz C, Riemen G, Pratje E, Dujon B, Michaelis G. 1993. Mitochondrial DNA of *Chlamydomonas reinhardtii*: the structure of the ends of the linear 15.8-kb genome suggests mechanisms for DNA replication. *Curr Genet* 24: 241-7
- Van Aken O, De Clercq I, Ivanova A, Law SR, Van Breusegem F, et al. 2016. Mitochondrial and Chloroplast Stress Responses Are Modulated in Distinct Touch and Chemical Inhibition Phases. *Plant Physiol* 171: 2150-65
- Van Leene J, Witters E, Inze D, De Jaeger G. 2008. Boosting tandem affinity purification of plant protein complexes. *Trends Plant Sci* 13: 517-20
- Verdoucq L, Vignols F, Jacquot JP, Chartier Y, Meyer Y. 1999. In vivo characterization of a thioredoxin h target protein defines a new peroxiredoxin family. *J Biol Chem* 274: 19714-22
- Verma D, Upadhyay SK, Singh K. 2022. Characterization of APX and APX-R gene family in *Brassica juncea* and *B. rapa* for tolerance against abiotic stresses. *Plant Cell Rep* 41: 571-92
- Vinyard DJ, Ananyev GM, Dismukes GC. 2013. Photosystem II: the reaction center of oxygenic photosynthesis. *Annu Rev Biochem* 82: 577-606
- Wakao S, Niyogi KK. 2021. *Chlamydomonas* as a model for reactive oxygen species signaling and thiol redox regulation in the green lineage. *Plant Physiol* 187: 687-98

- Wang L, Jonikas MC. 2020. The pyrenoid. *Curr Biol* 30: R456-R58
- Waszczak C, Akter S, Eeckhout D, Persiau G, Wahni K, et al. 2014. Sulfenome mining in *Arabidopsis thaliana*. *Proc Natl Acad Sci U S A* 111: 11545-50
- Wei B, Willems P, Huang J, Tian C, Yang J, et al. 2020. Identification of Sulfenylated Cysteines in *Arabidopsis thaliana* Proteins Using a Disulfide-Linked Peptide Reporter. *Front Plant Sci* 11: 777
- Weigel M, Varotto C, Pesaresi P, Finazzi G, Rappaport F, et al. 2003. Plastocyanin is indispensable for photosynthetic electron flow in *Arabidopsis thaliana*. *J Biol Chem* 278: 31286-9
- Woessner JP, Goodenough, U.W. 1994. Volvocine cell walls and their constituent glycoproteins: An evolutionary perspective. *Protoplasma* 181: 245–58
- Wu C, Jain MR, Li Q, Oka S, Li W, et al. 2014. Identification of novel nuclear targets of human thioredoxin 1. *Mol Cell Proteomics* 13: 3507-18
- Xu Y, Berkowitz O, Narsai R, De Clercq I, Hooi M, et al. 2019. Mitochondrial function modulates touch signalling in *Arabidopsis thaliana*. *Plant J* 97: 623-45
- Zaffagnini M, Bedhomme M, Groni H, Marchand CH, Puppo C, et al. 2012. Glutathionylation in the photosynthetic model organism *Chlamydomonas reinhardtii*: a proteomic survey. *Mol Cell Proteomics* 11: M111 014142
- Zecha J, Satpathy S, Kanashova T, Avanesian SC, Kane MH, et al. 2019. TMT Labeling for the Masses: A Robust and Cost-efficient, In-solution Labeling Approach. *Mol Cell Proteomics* 18: 1468-78
- Zhang B, Van Aken O, Thatcher L, De Clercq I, Duncan O, et al. 2014a. The mitochondrial outer membrane AAA ATPase AtOM66 affects cell death and pathogen resistance in *Arabidopsis thaliana*. *Plant J* 80: 709-27
- Zhang MP, Wang M, Wang C. 2021. Nuclear transformation of *Chlamydomonas reinhardtii*: A review. *Biochimie* 181: 1-11
- Zhang R, Patena W, Armbruster U, Gang SS, Blum SR, Jonikas MC. 2014b. High-Throughput Genotyping of Green Algal Mutants Reveals Random Distribution of Mutagenic Insertion Sites and Endonucleolytic Cleavage of Transforming DNA. *Plant Cell* 26: 1398-409
- Zhang S, Zou B, Cao P, Su X, Xie F, et al. 2023. Structural insights into photosynthetic cyclic electron transport. *Mol Plant* 16: 187-205




- Zhang T, Zhu M, Zhu N, Strul JM, Dufresne CP, et al. 2016. Identification of thioredoxin targets in guard cell enriched epidermal peels using cystTMT proteomics. *J Proteomics* 133: 48-53
- Zhao T, Wang W, Bai X, Qi Y. 2009. Gene silencing by artificial microRNAs in *Chlamydomonas*. *Plant J* 58: 157-64
- Zinzius K, Marchetti GM, Fischer R, Milrad Y, Oltmanns A, et al. 2023. Calredoxin regulates the chloroplast NADPH-dependent thioredoxin reductase in *Chlamydomonas reinhardtii*. *Plant Physiol* 193: 2122-40
- Zivcak M, Brestic M, Kunderlikova K, Olsovska K, Allakhverdiev SI. 2015. Effect of photosystem I inactivation on chlorophyll a fluorescence induction in wheat leaves: Does activity of photosystem I play any role in OJIP rise? *J Photochem Photobiol B* 152: 318-24

# Curriculum vitae

## Personal information

---

<b>Name</b>	Anna Caccamo	
<b>Date of Birth</b>	10/February/1991	
<b>Nationality</b>	Italian	
<b>Language</b>	English (fluent), Italian (native)	
<b>Telephone</b>	(+32) 4 56181053	
<b>Email</b>	anna.caccamo@uliege.be anna.caccamo@vub.be	
<b>Address</b>	Génétique et physiologie des microalgues, Institut de Botanique – B22, Chemine de la Vallée, 4, Université de Liège. B-4000, Liège, Belgium	

## Education

---

<b>2018 – present</b>	<b>ULiège Génétique et physiologie des microalgues and VIB-VUB Center for Structural Biology (CSB), Belgium</b> Joint PhD candidate in Doctoral Program of Biochimie, Biologie moléculaire et cellulaire, Bioinformatique et modélisation and Bio-engineering Sciences
<b>2014 – 2017</b>	<b>University of Turin (UniTO), Italy</b> Master programme of Plant Biotechnology
<b>2011 – 2014</b>	<b>University of Turin (UniTO), Italy</b> Bachelor of Science

## Key expertise

---

### Cell culture

- Algal cell cultures (*C. reinhardtii*)

### Molecular biology techniques

- DNA and RNA extractions, PCR, RT-PCR
- Algal crossing for genetic studies
- Algal transformation

- DNA cloning tools including restriction enzyme-based cloning

### **Physiological techniques**

- Algal growth rate analyses
- Photosynthetic measurements to evaluate algal fitness (*in vivo* analysis)

### **Biophysical or biochemical techniques**

- Protein gel analysis (SDS-PAGE)
- Immunoblotting
- Spectroscopic measurements (Joliot Type Spectrophotometer, JTS-10, Beambio, France)

### **Bioinformatic software tools**

- NCBI database
- SnapGene
- PyMol

## Research experience

---

<b>PhD thesis</b>	<p><b>ULiège Génétique et physiologie des microalgues - VIB-VUB Center for Structural Biology (CSB), Belgium</b></p> <p>Topic: Redox signalling in the green alga <i>Chlamydomonas reinhardtii</i>: a study of the role of ascorbate peroxidase 2 and protein cysteine post translational modifications</p> <p>July 2018- Present</p>
<b>Master thesis</b>	<p><b>Biological and Chemical Sciences, National University of Ireland, Galway (NUIG), Ireland</b></p> <p>Topic: Investigating the impact of digestion on the nutraceutical properties of algal polysaccharide-rich extracts.</p> <p>Mar 2016 – Sep 2016</p>
<b>Bachelor thesis</b>	<p><b>Neuroscience Institute Cavaliere Ottolenghi (NICO), Turin, Italy</b></p> <p>Topic: Study of the phosphatase and tensin homolog deleted on chromosome 10 (PTEN) protein and mTOR pathway and rapamycin effects in murine autism models.</p>

Mar 2014 - May 2014

**Others (Internships) Botanical garden, University of Turin (UniTO), Italy**

Topic: Arbuscular mycorrhiza on roots of *Medicago truncatula*

June 2014

**Department of Agronomic Microbiology, University of Turin (UniTO), Italy**

Topic: Soil bacteria evaluation for mais and wheat crops  
Oct 2016 – Dec 2016

## Academic activities

---

2023

**The 20<sup>th</sup> International Conference on the Cell and Molecular Biology of Chlamydomonas, Princeton, NJ, (USA)**

**(Short talk)**

Topic: Ascorbate peroxidase-related binds copper and controls the level of plastocyanin in the chloroplast of *Chlamydomonas*

4 June 2023 – 9 June 2023

2022

**Plant Oxygen Group (POG) within the Joint SFRR-E/POG “Redox Biology Congress 2022”, Oude Vismijn, Ghent, Belgium**

**(Short talk)**

Topic: Ascorbate peroxidase 2 of *Chlamydomonas reinhardtii* is involved in the regulation of the plastocyanin levels

**(Poster presentation)**

Topic: Optimizing the trapping and identification of sulfenylated proteins in the green microalga *Chlamydomonas reinhardtii*

24 Aug 2022 – 26 Aug 2022

**Biosensor Brussels “Tuning the fluorescence of a  $\beta$ -barrel”, Brussels, Belgium**

**(Participant)**

22 Aug 2022

**Spring School “Molecular and biophysical bases of photosynthesis”, Venice, Italy**

**(Short talk)**

Topic: The ascorbate peroxidase 2 (an APX-R) of the green microalga *Chlamydomonas reinhardtii*

9 May 2022 – 13 May 2022

**Workshop on proteomics “A proteomics perspective on protein function in space and time”, Liège, Belgium**

**(Participant)**

3 May 2022

**13th Spring symposium redox biology, Gent, Belgium**

**(Talk)**

**Topic:** The ascorbate peroxidase 2 (an APX-R) of the green microalga *Chlamydomonas reinhardtii*

26 Apr 2022

**Supervising an Erasmus master student, Antonello Amelii, University of Verona (UniVr), Italy**

Topic: Biophysical and biochemical characterization of APX2 in *Chlamydomonas reinhardtii*

Feb 2022 – July 2022

**2021**

**Online conference: GFB, Groupe Français de Bioénergétique**

**(Short talk)**

Topic: In *Chlamydomonas reinhardtii* APX2 exerts photoprotection to sudden increases of light intensity

21 Sep 2021 – 24 Sep 2021

**19th International Conference on the Cell and Molecular Biology of Chlamydomonas, Six-Fours-les-Plages (France)**

**(Poster presentation)**

Topic: The photoprotective role of APX2 in  
*Chlamydomonas reinhardtii*  
29 Aug 2021 – 03 Sep 2021

**Online conference: Sfphi2021, Journées de la Société  
Française de Photosynthèse  
(Flash talk, poster presentation)**

Topic: Characterization of the *apx2* mutant in  
*Chlamydomonas*  
8 Apr 2021 – 9 Apr 2021

**Supervising an Erasmus master student, Ilaria  
Ragnoli, University of Verona (UniVr), Italy**

Topic: Physiological and molecular characterization of  
*nfu1* and *hcf101* mutants in *Chlamydomonas reinhardtii*  
March 2021 – July 2021

**Online conference: I-BE-C, International Bioenergy  
and Environment conference  
(Flash talk, poster presentation)**

Topic: Characterization of the *apx2* mutant in  
*Chlamydomonas*  
16 Feb 2021 – 18 Feb 2021

**2019**

**12<sup>th</sup> Annual Brussels centre for Redox Biology,  
Fall Symposium, Brussels, Belgium  
(Flash talk)**

Topic: H<sub>2</sub>O<sub>2</sub> signalling from chloroplast to nucleus in  
*Chlamydomonas*

**(Poster presentation)**

H<sub>2</sub>O<sub>2</sub> signalling from mitochondria and chloroplast to the  
nucleus in the green microalga *Chlamydomonas*: *in vivo*  
and *in vitro* approaches

7 Dec 2019 – 8 Dec 2019

**Photosynthesis and Symbiosis Day, Liège, Belgium  
(Short talk)**

Topic: H<sub>2</sub>O<sub>2</sub> signalling from chloroplast to nucleus in  
*Chlamydomonas*  
15 Nov 2019

**SPP 1710 workshop: THIOL-BASED SWITCHES AND REDOX-REGULATION - FROM MICROBES TO MEN, San Felui, Spain**

**(Short talk)**

Topic: H<sub>2</sub>O<sub>2</sub> signalling from chloroplast to nucleus in *Chlamydomonas*

**(Poster presentation)**

Topic: H<sub>2</sub>O<sub>2</sub> signalling from mitochondria and chloroplast to the nucleus in the green microalga *Chlamydomonas*: *in vivo* and *in vitro* approaches  
15 Sep 2019 - 20 Sep 2019

**14th international conference on reactive oxygen and nitrogen species in plants, POG meeting, Munich, Germany**

**(Poster presentation)**

Topic: Defining phenotypes of *Chlamydomonas reinhardtii* mutants affected in H<sub>2</sub>O<sub>2</sub> scavenging  
10 July 2019 – 12 July 2019

**3<sup>rd</sup> InBios Day, Liège, Belgium**

**(Flash talk)**

Topic: Analysis of *Chlamydomonas* mutants implicated in H<sub>2</sub>O<sub>2</sub> scavenging  
7 Feb 2019

## Scholarships and prizes

---

**PhD funding**

EOS Project No. 30829584